NASA TECHNICAL TRANSLATION NASA TT F-15,768

ASTROMETRICS AND ASTROPHYSICS, NUMBER 1

I. K. Koval', Editor

Translation of: "Astrometriya i Astrofizika, 17,"
"Naukova Dumka" Press, Kiev, pp. 1-128.

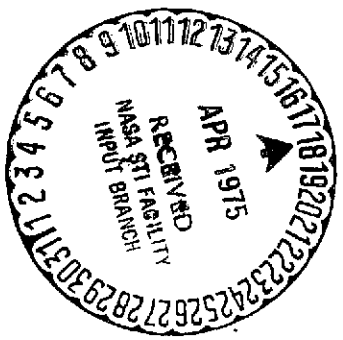

(NASA-TT-F-15768) ASTROMETRICS AND ASTROPHYSICS, NO. 17 (Techtran Corp.) 151 p HC $6.25 CSCL 03B

N75-21164
THRU
N75-21173
Unclas
G3/88 18218

NATIONAL AERONAUTICS AND SPACE ADMINISTRATION
WASHINGTON, D.C. 20546 DECEMBER 1974

STANDARD TITLE PAGE

1. Report No. NASA TT F-15,768	2. Government Accession No.	3. Recipient's Catalog No.
4. Title and Subtitle ASTROMETRICS AND ASTROPHYSICS, NUMBER 17		5. Report Date DECEMBER 1974 6. Performing Organization Code
7. Author(s) I. K. Koval', Editor		8. Performing Organization Report No. 10. Work Unit No.
9. Performing Organization Name and Address Techtran Corporation P.O. Box 729 Glen Burnie, Maryland 21061		11. Contract or Grant No. NASw-2485 13. Type of Report and Period Covered Translation
12. Sponsoring Agency Name and Address National Aeronautics and Space Administration Washington, D. C. 20546		14. Sponsoring Agency Code

15. Supplementary Notes

Translation of: "Astrometriya i Astrofizika, 17," "Naukova Dumka" Press, Kiev, 1972, pp. 1-128.

16. Abstract

Each article contains its own abstract.

17. Key Words (Selected by Author(s))	18. Distribution Statement
	Unclassified-Unlimited

19. Security Classif. (of this report)	20. Security Classif. (of this page)	21. No. of Pages	22. Price
Unclassified	Unclassified	150	

NASA-HQ

TABLE OF CONTENTS

I. STELLAR PHYSICS

ON THE THEORY OF THERMAL RUNAWAY IN THE HYDROGEN ENVELOPE OF A WHITE DWARF

Yu. N. Redkoborodyy

ABSTRACT. An evolutionary sequence was calculated for a white dwarf on which a hydrogen rich envelope is assumed to increase with time. The stellar models were computed by integrating numerically the system of stellar structure equations by means of the Henyey method. The accretion of matter was assumed to be quasi-static. Near the point of the chemical discontinuity, a temperature maximum is shown to arise, then hydrogen ignites, a thin shell energy source being formed. The new shell source is thermally unstable. The resulting thermal runaway was investigated numerically and by means of a simple approximation based on the energy balance in the hydrogen burning shell source.

1. Introduction

Considerable interest attaches to a study of the evolution of the white dwarfs containing hydrogen in their envelopes. Views regarding the possible instability of such stars were advanced in 1950 in papers by Ledoux [1] and Lee [2]. Somewhat later Mestel [3] suggested that thermal instability exists in the external strata of a white dwarf when hydrogen accretion is present, and proposed a simplified model of the development of this instability. Mestel's idea was not widely accepted at that time and was not duly developed. Interest in this hypothesis was renewed in recent years in connection with studies of the reasons for the variability in close binary systems. However, in the majority of papers on accretion of hydrogen by a white dwarf [4-8], the majority of authors followed Mestel [3] in adopting a highly simplified approach to the problem: the structure of the star in the region of the shell source of energy is obtained by "matching" of the isothermal core and the radiant envelope; use is made of approximate Kramers formulas for the absorption coefficient, the power function of nuclear energy release versus temperature, and of zero boundary conditions on the surface of the star; the thermal problem is considered separately from the hydrostatic one, as is done in the case of entirely degenerate configurations. The possibility of development of thermal instability in the burning of hydrogen on the periphery of a white dwarf ultimately depends on the relationship between the local heating rate and the cooling rate due both to heat removal (which increases sharply on appreciable degeneration of matter, owing to the electron thermal conductivity) and to possible expansion of the envelope (in the event of insufficient degeneration). Since the physical

*Numbers in the margin indicate pagination in the foreign text.

parameters of matter in the external layers of a white dwarf change with extreme rapidity with depth, the course of evolution of a star must depend substantially on the precise location of the shell source of energy. The introduction of the simplifying assumptions indicated above, which are justified in consideration of a star "as a whole," in this particular case result in such excessive "coarsening" of the structure of the external layers of a white dwarf that the theoretical conclusion regarding the presence of thermal instability may prove to be unfounded.

Thus it seems to us that the very possibility of thermal runaway (to say nothing of its development in time) may be established only if a rigorous approach is applied to solving the problem of the hydrogen accretion on a white dwarf, through direct solution of a system of equations for the internal structure of the star using precise expressions for energy release [9, 10] and the most recent data on the absorption coefficients [11] and electron screening in thermonuclear reactions [12, 13, 14]. It is necessary also to abandon the other assumptions insofar as possible, ones such as utilization of zero boundary conditions, since the shell source of energy is situated far from the surface of the star. Giannone and Weigert [4] have come the closest to realizing this program, but the use of zero boundary conditions and allowance for the /4
screening effect on the basis of the approximate Salpeter formulas [15] are serious deficiencies of their work. In addition, the results obtained in [4] are rendered largely valueless by the fact that in their work use was made of the original version of the Cox tables and so forth for opacities [16], a version which has been found to be erroneous [17], and the latest refinements of the proton-proton reaction rate values are not taken into account [18].

In the present paper a method is presented of calculating the sequence of evolution of models for a white dwarf on the surface of which accretion of matter rich in hydrogen takes place, and the results are presented of calculations made by this method of the evolution of a white dwarf having a helium core and an initial mass of $M = 0.5\ M_\odot$ in the event $M = 10^{-9}\ M_\odot$/year. Unlike the methods applied in [4-8], the method described here is based on numerical solution of the initial system of equations of the internal structure of a star with nonzero boundary conditions and with much more precise allowance made for all heat release and heat removal effects.

In addition to the usual assumptions made in calculations for spherically symmetrical star models, we make use of the following simplifying assumptions:

1. It is assumed that the layers of hydrogen acquired by the star are optically thin, so that the kinetic energy of matter falling onto the star undergoes dissipation and is reradiated outward (for example, in the x-ray range [5]). In this instance we are concerned with quasistatic accretion, that is, the velocity of the matter at the time it is added to the star may be assumed to equal zero, so that in the uppermost layers of the envelope $L \cong \text{const}$. It is shown by estimation that even at low accretion rates ($10^{-9} M_\odot$/year) the flux of kinetic energy to the surface of a white dwarf reaches a considerable value, but the "slow" accretion approximation is justified by the

fact that precise allowance for the share of "reradiated" kinetic energy is a highly complex problem. On the other hand, this proposal is in agreement with the universally accepted quasistatic approximation in the theory of the internal structure of stars, in which the dynamic term in the hydrostatic equilibrium equation is assumed to equal zero.

2. According to [4, 8] the time interval over which thermal instability may develop is represented by the quantity $\tau \sim 10^6$ years. It can easily be ascertained by means of the well-known relation $(\Delta Z)^2 \sim D\tau$ (D being the diffusion coefficient) that width ΔZ of diffusion "blurring" of the H-He boundary in time τ is much smaller than the thickness of the nondegenerated envelope, that is, abrupt variation in chemical composition on the boundary between the substance of a star and the hydrogen accumulated on it as a result of accretion is a good approximation.

3. The fact that the value of τ is small in comparison to the time of "nuclear" evolution of stars in the main sequence makes it possible to disregard the variation in chemical composition resulting from depletion of the hydrogen. As a matter of fact, as may be seen from the results given in what follows, throughout the calculations the specific rate of energy release ε at any point satisfies statement of inequality

$$\varepsilon \ll \frac{E_*}{\Delta t}, \tag{1}$$

in which Δt is the time step separating a particular model from the foregoing one; E_* is the quantity of energy released on complete conversion of 1 g of hydrogen to helium. Consequently, the variation in hydrogen concentration is

$$|\Delta X| \sim \frac{\varepsilon}{E_*} \cdot \Delta t \ll 1.$$

2. Basic Equations. Physical Conditions in a White Dwarf /5

If we employ mass variable ξ (as the Legrange variable) as an independent variable, the system of equations of the structure of a star assumes the following form [19]:

$$\frac{\partial P}{\partial \xi} + \frac{Gm\rho}{r^2} \cdot \frac{\partial r}{\partial \xi} = 0; \tag{2}$$

$$\frac{dm}{d\xi} - 4\pi r^2 \rho \frac{\partial r}{\partial \xi} = 0; \tag{3}$$

$$\frac{\partial l}{\partial \xi} - \frac{dm}{d\xi}\left[\varepsilon - \frac{\partial E}{\partial t} - P\frac{\partial}{\partial t}\left(\frac{1}{\rho}\right)\right] = 0; \tag{4}$$

$$\left.\begin{aligned} &\frac{\partial T}{\partial \xi} + \frac{3\varkappa\rho l}{64\pi\sigma T^3 r^3}\frac{\partial r}{\partial \xi} = 0 \quad \text{when } \nabla < \nabla_{cr} \\ &\frac{\partial E}{\partial \xi} + P\frac{\partial}{\partial \xi}\left(\frac{1}{\rho}\right) = 0 \quad \text{when } \nabla \geqslant \nabla_{cr} \end{aligned}\right\}, \tag{5}$$

in which $m(\xi)$, $l(\xi, t)$ and $r(\xi, t)$ are the mass, luminosity, and radius of a sphere corresponding to a certain value ξ (unlike M, L, and R — the mass, luminosity, and radius of a star as a whole); P is pressure; T is temperature; r is density; ε is the specific rate of energy release due to nuclear reaction; and κ is the effective absorption coefficient.

Choice of one of two possible expressions (5) for the fourth equation depends on the relationship between the quantities [20]

$$\nabla = \frac{3}{64\pi\sigma G} \cdot \frac{\varkappa l P}{m T^4} \tag{6}$$

and

$$\nabla_{cr} = \nabla_{ad} + \left(\frac{\partial \ln T}{\partial \ln \mu}\right)_{P,\rho} \frac{\partial \ln \mu}{\partial m} \cdot \frac{4\pi r^4 P}{Gm}. \tag{7}$$

The star considered in this paper consists of two chemically homogeneous regions, and consequently $\partial l n \mu / \partial m = 0$ and

$$\nabla_{cr} = \nabla_{ad}, \tag{8}$$

in which ∇_{ad} is the adiabatic gradient (see Section 5).

Quantities P, E, κ and ε in (2)-(5) are functions of ρ, T, and the chemical composition, so that this system of equations (together with the initial and the boundary conditions) determines the relationships $r(\xi, t)$, $l(\xi, t)$, $L(\xi, t)$, and $\rho(\xi, t)$ (as was pointed out in the foregoing section, quantities X, Y, ... are assumed not to depend on time). Let us consider the form of functions $P(\rho, T, X_i)$, and so forth in greater detail for the conditions of a white dwarf.

Equation of State

Estimates show that the relative role of radiation pressure is entirely negligible in all the regions of a white dwarf, that is,

$$P = P_i + P_e,$$

in which P_i and P_e are respectively the partial pressures of the cores (ions) and electrons. The gas of the cores is far from degeneration [21], so that

$$P_i = \frac{k}{m_H} \cdot \frac{\rho T}{\mu_i},$$

in which m_H is the mass of the proton; $\mu_i = \dfrac{1}{X + \frac{1}{4} Y}$ is the mean "nuclear" molecular weight [21]. The state of the electron gas on a white star varies continuously from completely undegenerated to entirely degenerated (in the deep layers of a star it is also necessary to allow for the possibility of relativistic degeneration). As we know, in this case the density of matter ρ and the electron gas pressure P_e are analytical functions of degeneration factor ξ [21]. Thus for quantity P we have

/6

$$P=\begin{cases}\dfrac{k}{m_H}\cdot\dfrac{\rho T}{\mu} & \text{when } \psi<\psi_1; \quad (9)\\ \dfrac{8\pi}{3h^3}(2m_e kT)^{3/2}kTF_{3/2}(\psi)+\dfrac{k}{m_H}\cdot\dfrac{\rho T}{\mu_e} & \text{when } \psi_1\leqslant\psi\leqslant\psi_2; \quad (10)\\ \dfrac{\pi m_e^4c^5}{3h^3}\left[x(2x^2-3)\sqrt{x^2+1}+3\ln\left(x+\sqrt{x^2+1}\right)\right]+\dfrac{k}{m_H}\dfrac{\rho T}{\mu_e} & \text{when } \psi>\psi_2. \quad (11)\end{cases}$$

in which $F^{3/2}(\psi)$ is one of the Fermi-Dirac functions:

$$F_s(\psi)=\int_0^\infty\frac{u^s\,du}{1+\exp(u-\psi)}; \quad (12)$$

μ is the mean molecular weight [21]:

$$\mu=\frac{1}{2X+\frac{3}{4}Y+\frac{1}{2}Z}; \quad (13)$$

x is the maximum value of the dimensionless electron pulse [22]:

$$x=\frac{h}{m_e c}\left[\frac{3(1+X)\rho}{16\pi m_H}\right]^{1/3}, \quad (14)$$

parameter ψ is the root of the equation [21, 22]

$$\rho=\frac{4\pi}{h^3}\mu_e m_H(2m_e kT)^{3/2}F_{3/2}(\psi),\qquad \mu_e=\frac{2}{1+X}, \quad (15)$$

which together with (9)-(14) determines the dependence of P on ρ, T, and the chemical composition of the matter.

The criterion of total absence of degeneration, as we know [22], is the statement of inequality

$$\exp(\psi)\ll 1;$$

otherwise, if $\exp(\psi) \gg 1$, the electron gas is entirely degenerated. For this reason choice of the values of ψ_1 and ψ_2 in (9)-(11) is determined by the conditions

$$\exp(\psi_1)\ll 1,\quad \exp(\psi_2)\gg 1;$$

in addition, ψ_2 must be such that when $\psi \leqslant \psi_2$ the role of relativistic effects is still insignificant. It has been established by numerical calculations that for a typical white dwarf ($M \cong 0.5\ M_\odot$, $T_c \cong 2\cdot 10^7$°K) expressions such as (9)- /7
(11) for P and other physical parameters yield a sufficiently "smooth" relation if

$$\psi_1=-5;\quad \psi_2=12. \quad (16)$$

Relations (9)-(16) fully determine the equation of state of matter employed in the present paper in construction of white dwarf models.

Internal Energy

When electron degeneration is entirely absent, for specific internal energy E we have

$$E=\frac{3}{2}\cdot\frac{k}{m_H}\cdot\frac{T}{\mu}, \tag{17}$$

in which μ is determined from (13). In the nonrelativistic degenerated case quantity E is unambiguously connected to pressure and density by the relation

$$E=\frac{3}{2}\cdot\frac{P}{\rho}, \tag{18}$$

which is valid for any degree of degeneration of an electron gas [22].

The expression for E becomes somewhat more complicated when STO effects play an appreciable role in the electron gas. In this case

$$E=E_i+E_e, \tag{19}$$

in which the core gas energy is

$$E_i=\frac{3}{2}\cdot\frac{k}{m_H}\cdot\frac{T}{\mu_i}; \tag{20}$$

$$\mu_i=\frac{1}{X+\frac{1}{4}Y}; \tag{21}$$

and, in the well-known expression for E_e as a function of x (see (14)) [22], it is necessary to exclude the electron rest energy

$$m_e c^2\frac{n_e}{\rho}=\frac{m_e c^2}{2m_H}(1+X). \tag{22}$$

Thus in accordance with (17)-(22) we have

$$E=\begin{cases}\dfrac{3}{2}\cdot\dfrac{k}{m_H}\cdot\dfrac{T}{\mu} & \text{when } \psi<\psi_1; \quad (23)\\ \dfrac{3}{2}\cdot\dfrac{P}{\rho} & \text{when } \psi_1\leqslant\psi\leqslant\psi_2; \quad (24)\\ \dfrac{3m_e c^2}{16m_H}(1+X)\left[\dfrac{3}{8}\cdot\dfrac{x(2x^2+1)\sqrt{x^2+1}-\ln(x+\sqrt{x^2+1})}{x^3}-1\right]+ & \\ \quad+\dfrac{3k}{2m_H}\cdot\dfrac{T}{\mu_i} & \text{when } \psi>\psi_2, \quad (25)\end{cases}$$

in which μ and μ_i are assigned in accordance with (13) and (21), x in accordance with (14), ψ_1 and ψ_2 in accordance with (16), and P by means of (9)-(11).

Nuclear Reactions

In the temperature range with which we are concerned, $T = 10^7$-10^8° K, energy release ε is determined by the hydrogen combustion reactions [21]:

$$\varepsilon = \varepsilon_{pp} + \varepsilon_{CNO}. \tag{26}$$

The value of ε_{pp} corresponding to the proton-proton cycle is defined by the expression

$$\varepsilon_{pp} = 2{,}51 \cdot 10^6 X^2 \rho T^{-2/3} f_{pp} \exp\left(-\frac{33{,}804}{T_6^{1/3}}\right), \tag{27}$$

in which, in accordance with [9], the numerical coefficient is increased by 12.5% in comparison to that customarily employed [10], and f_{pp} is the screening multiplication factor [12-14]:

$$f_{pp} = \exp\left\{\frac{5\sqrt{2}e^{3/2}}{4k}\left(\frac{\pi m_e}{h^2 m_H}\right)^{1/2} \cdot \frac{\rho^{1/2}(1+X)^{1/2}}{T}\right\}. \tag{28}$$

For reactions of the carbon-hydrogen cycle [10]

$$\varepsilon_{CNO} = 8 \cdot 10^{27} \cdot X X_N \rho T_8^{-2/3} f_N \exp\left(-\frac{152{,}28}{T_6^{1/3}}\right), \tag{29}$$

in which X_N is the concentration of isotope N^{14} (by mass), and for f_N we have [14]

$$f_N = f_{pp}^7. \tag{30}$$

Opacity

Electron degeneration also substantially alters the process of heat removal in a white dwarf. The sharp increase in electron thermal conductivity has the result that, despite a reduced opacity of the degenerated gas [23], transfer of energy by thermal conductivity comes to be of the order of radiative transfer, and in the interior of the star much greater than the latter. To allow for the role of thermal conductivity, it is necessary to replace the customary absorption coefficient, κ_r, corresponding to radiative transfer with the effective absorption coefficient

$$\varkappa = \left(\frac{1}{\varkappa_r} + \frac{1}{\varkappa_e}\right)^{-1}, \tag{31}$$

in which [2]

$$\varkappa_e = \frac{16\sigma T^3}{3\rho\lambda_e}, \tag{32}$$

λ_e is the thermal conductivity of the electron gas (the thermal conductivity of the core gas may be disregarded). The values of functions $\kappa_r = \kappa_r(\rho, T, X_i)$ were calculated by using the Cox-Stewart tables [11] by two-dimensional linear interpolation of lg κ_r relative to lg ρ and lg T. In view of the fact

that λ_e increases sharply when degeneration begins, the interpolation procedure for κ_e entails considerable errors, and for this reason κ_e was determined directly with (32). To calculate $\lambda_e = \lambda_e(\rho, T, X_i)$, we made use of the relations cited in [2] and obtained by means of the Boltzmann equation in the binary collision approximation.

3. Boundary Conditions

Equations (2)-(5) should be supplemented by boundary conditions. The conditions in the center are obvious:

$$r(\xi_0)=0;\ l(\xi_0)=0, \tag{33}$$

in which ξ_0 corresponds to the center of the star ($m(\xi_0) = 0$). The selection of /9 boundary conditions on the surface is determined by the fact that equation (5) is no longer applicable in the atmosphere of a star and must be replaced by a more complex one. Consequently, if ξ_J corresponds to the surface ($m(\xi_J) = M$), the external boundary conditions for equations (2)-(5) must be assigned at a certain value ξ_{J-1} corresponding to the deeper layers of the star ($m(\xi_{J-1}) < M$), where equation (5) is valid. In solving system (2)-(5) by the relaxation method [24], it is advisable to assign the boundary conditions in the following form [19]:

$$r(\xi_{J-1})=\varphi_1(R, L); \tag{34}$$

$$l(\xi_{J-1})=\varphi_2(R, L); \tag{35}$$

$$T(\xi_{J-1})=\varphi_3(R, L); \tag{36}$$

$$\rho(\xi_{J-1})=\varphi_4(R, L), \tag{37}$$

in which R and L are the radius and luminosity of the star[1]; ξ_{J-1} is the Legrange coordinate, which corresponds to the optical depth for which equation (5) is valid. Precise determination of functions $\varphi_i(R, L)$ is a problem of the theory of stellar atmospheres. In the calculation of star models, the most convenient method in practice is preliminary calculation of the values of φ_i at specific points of plane (R, L) followed by interpolation to obtain $\varphi_i(R, L)$ at the required point of (R, L) [19].

To obtain functions $\varphi_i(R, L)$ we have used the results of the work by A. Kolesov [25] on the theory of the hydrogen atmospheres of white dwarfs. As is

[1]Functions φ_1 also depend on the mass of the star M and the chemical composition of the atmosphere, but these quantities are assumed to be constant.

demonstrated in [25], at sufficiently large values of T_0 (the temperature on the surface of the star) and small values of g (the acceleration of gravity on the surface), the condition of hydrostatic equilibrium is approximated with good accuracy by a simpler equation, the numerical integration of which (at an assigned value of T_0) makes it possible to obtain a model of the hydrogen atmosphere of a white dwarf in the following form

$$P(\tau) = \sqrt{g}\,\eta_1(\tau); \tag{38}$$

$$\rho(\tau) = \sqrt{g}\,\eta_2(\tau); \tag{39}$$

$$T(\tau) = T_e\left[\frac{3}{4}(q(\tau)+\tau)\right]^{1/4}, \tag{40}$$

in which τ is the mean optical depth; $q(\tau)$ is the Hopf function; $g = \frac{GM}{R^2}$ is the acceleration of gravity on the surface of the star.

Tables of functions $\eta_1(\tau)$ and $\eta_2(\tau)$ with τ = 0-10 were derived in [25] for three surface temperature values: T_0 = 12,000, 15,000, and 20,000°K. The lower boundary of the hydrogen atmosphere corresponding to τ = 10 was selected as the layer in which boundary conditions (34)-(37) are assigned. Function φ_1 (R, L) was obtained as follows. The layer of the atmosphere in which

$$T(\tau_e) = T_e$$

was adopted as the outer surface of the star. It can be found by means of (40) that τ_e = 0.64 (26). Then the geometric height H of the atmosphere, as follows from the condition of hydrostatic equilibrium, equals

$$H = \int_0^H dh = \frac{1}{g}\int_{P(\tau_e)}^{P(10,0)} \frac{dP}{\rho} = \frac{R^2}{GM}\int_{P(\tau_e)}^{P(10,0)} \frac{dP}{\rho}. \tag{41}$$

The integral in (41) was found by the numerical method by use of the tables for /10 $\eta_1(\tau)$ and $\eta_2(\tau)$ [25]; as is evident from (38), (39), the values of the integral depend only on the value of T_0, which is unambiguously connected to effective temperature T_e [26], the latter obviously being expressed by R, L. Consequently, H = H(R, L) and

$$\varphi_1(R, L) = R - H(R, L), \tag{42}$$

in which H(R, L) are determined by means of relation (41).

Since L = const with good accuracy within the limits of the atmosphere, for function φ_2 = (R, L) we have

$$\varphi_2(R, L) = L. \tag{43}$$

Function $\varphi_3(R, L)$ also is fairly simple in form. As a matter of fact, by using (40) and the relation

$$L = 4\pi R^2 \sigma T_e^4$$

we obtain

$$\varphi_3(R, L) = \left[\frac{3(q(10.0) + (10.0))}{16\pi\sigma}\right]^{1/4} L^{1/4} R^{-1/2}. \tag{44}$$

According to (39), for function $\varphi_4(R, L)$, which represents the density "at the bottom" of the atmosphere, we may write

$$\varphi_4(R, L) = (GM)^{1/2} \eta_2^{-1}(10.0) R^{-1}. \tag{45}$$

Thus functions $\varphi_2(R, L)$ and $\varphi_3(R, L)$ are assigned by analytical means. As regards function $\varphi_1(R, L)$ and $\varphi_4(R, L)$, by using the quantities $\int \frac{dP}{\rho}$ and $\eta_2(10)$ for the three values of T_0 and varying R, by means of (41), (42), and (45), we can plot on plane (R, L) a network of values of φ_1 and φ_4 on which $\varphi_1(R, L)$ and $\varphi_4(R, L)$ are found by means of two-dimensional interpolation.

4. Calculation Method

We follow [4] in introducing independent variable ξ by means of the conversion

$$\xi = \ln\left(1{,}00001 - \frac{M_r}{M}\right), \tag{46}$$

from which we obtain

$$m(\xi) = M[1.00001 - \exp(\xi)], \tag{47}$$

in which M is the mass of the star. Thus $m(\xi)$ is a monotonic function of ξ; for

$$-11.512 \cong \xi_J \leqslant \xi \leqslant \xi_0 \cong 1 \cdot 10^{-5} \tag{48}$$

we have

$$0 = m(\xi_0) \leqslant m(\xi) \leqslant m(\xi_J) = M.$$

The ranges of variation in P, ρ, and l are too large in terms of the volume of the star, and for this reason it is convenient to use in place of these quantities the artificial variables [19]

$$p \equiv P^{1/4}; \quad q \equiv \rho^{1/3}; \quad F \equiv \frac{l}{\xi^2}. \tag{49}$$

Then equations (2)-(5) are converted to the form[2] /11

[2]The variables $r^* = 10^{-8} r$, $E^* = 10^{-10} E$, and $F^* = 10^{-31} F$ were used in the numerical calculations on the computer in place of r, E, and F, but to avoid making the formulas too unwieldy this conversion is not used in the following operations.

$$\frac{\partial p}{\partial \xi} + \frac{Gmq^3}{4p^3 r^3} \cdot \frac{\partial r}{\partial \xi} = 0; \tag{50}$$

$$m' - 4\pi r^2 q^3 \frac{\partial r}{\partial \xi} = 0; \tag{51}$$

$$\xi^3 \frac{\partial F}{\partial \xi} + 2\xi F - m' \left(\varepsilon - \frac{\partial E}{\partial t} + \frac{3p^4}{q^4} \cdot \frac{\partial q}{\partial t} \right) = 0; \tag{52}$$

$$\begin{aligned} &\frac{\partial T}{\partial \xi} - \frac{16 K \xi^2 F}{m} \cdot \frac{\partial p}{\partial \xi} = 0 \quad \text{when} \nabla < \nabla_{cr}; \\ &\frac{\partial E}{\partial \xi} - \frac{3p^4}{q^4} \cdot \frac{\partial q}{\partial \xi} = 0 \qquad \text{when} \quad \nabla > \nabla_{cr}, \end{aligned} \tag{53}$$

in which m' is the derivative found with (47) of function $m(\xi)$; ∇ and ∇_{cr} are determined with (6), (8), and (49), and the "pseudo-opacity" [19, 24] is

$$K \equiv \frac{3\varkappa p^3}{256 \pi G \sigma T^3}. \tag{54}$$

We then select a certain subdivision of interval (ξ_0, ξ_J):

$$0 = m(\xi_0) < m(\xi_1) < \ldots < m(\xi_{J-1}) < m(\xi_J) = M,$$

this corresponding to subdivision of the star into J thin spherical layers (J = 80-150), and we shift from equations (50)-(53) to a system of four J equations in finite differences [19], which, together with boundary conditions (34)-(37) represents a complete system of equations relative to the variables (by means of (49) in (34)-(37) it is easy to shift from variables r, l, T, and ρ, to variables r, F, T, q):

$$r_0, \ldots, r_J, F_0, \ldots, F_J, T_0, \ldots, T_J, q_0, \ldots, q_J \tag{55}$$

(as was demonstrated earlier, variables p, E, K, and ε are known functions of T and q).

To solve the system of equations in finite differences, use is made of the relaxation method [24], often termed the Chenier method [19] (after the name of the author who participated the most actively in developing it) and representing a generalization of the well-known method of Newtonian tangents to the four J-dimensional case. The Chenier method essentially consists of the following. If the approximation of the solution of

$$r_0^{(0)}, \ldots, r_J^{(0)}, F_0^{(0)}, \ldots, F_J^{(0)}, T_0^{(0)}, \ldots, T_J^{(0)}, q_0^{(0)}, \ldots, q_J^{(0)}$$

is known, the next, more precise approximation

$$r_j^{(1)} = r_j^{(0)} + \delta r_j; \quad F_j^{(1)} = F_j^{(0)} + \delta F_j \quad \text{etc.}, (j = 0, 1, \ldots J) \tag{56}$$

and the system of equations relative to the variables of (55) are converted to a system of linear equations relative to δr_j, δF_j, δT_j, δq_j (j = 0, 1, ..., J)

with coefficients depending on $r_j^{(0)}$, $F_j^{(0)}$, and so forth. Solution of the system of equations relative to corrections δr_j, δF_j, δT_j, and δa_j obtained in this manner is found by successive exclusion of the unknowns, after which the new approximation, $r_j^{(1)}$, $F_j^{(1)}$, $T_j^{(1)}$, and $q_j^{(1)}$ may again be used as the initial approximation, and so forth until the corrections become sufficiently small. /12

All the necessary calculations were performed using the "Minsk-22" computer at the Institute of Cybernetics of the Academy of Sciences of the Ukrainian SSR. A block diagram of the program of automatic calculation of white dwarf models is given in Figure 1. Calculation of a successive model begins with selection of a new time step Δt determining increase in the mass of the star $\Delta M = M\Delta t$, in which M is the accretion rate. Step Δt is selected as a function of the convergence of the preceding model; in addition, Δt obviously must not exceed the value

$$\tau = \frac{E}{\varepsilon},$$

in which E and ε correspond to the region of the shell source of energy (see below). The time derivatives in equation (52) are approximated as follows:

$$\left(\frac{\partial E}{\partial t}\right)_j = \frac{E_j - \bar{E}_j}{\Delta t}; \qquad \left(\frac{\partial q}{\partial t}\right)_j = \frac{q_j - \bar{q}_j}{\Delta t}, \tag{57}$$

in which the values $\bar{E}_0$, ..., $\bar{E}_J$, $\bar{q}_0$, ..., $\bar{q}_J$ are taken from the previous star model stored in the external memory of the computer.

Since M figures in expression (46) for ξ, increase in the mass of a star requires reorganization of the system of points $\{\xi_j\}$ accomplishing the subdivision of interval (ξ_J, ξ_0):

$$J \to J' = J + \Delta J; \tag{58}$$

$$\xi_j \to \xi_{j'} \quad (j = 0, \ldots, J, \ldots, J'). \tag{59}$$

In all calculations it was assumed that

$$\xi'_{J'} = \xi_J, \ \xi'_0 = \xi_0,$$

but to the previous layers, in which (59) is of the form (M being the mass of the new model)

$$\xi_{j'} = \ln\left\{1{,}00001 - \frac{M - \Delta M}{M}\left[1{,}00001 - \exp(\xi_j)\right]\right\}, \tag{60}$$

$(0 < j \leqslant J)$, there are added $\Delta J = 10$ new points ξ'_{J+1}; ..., $\xi'_{J'-1}$, contained between ξ'_J and $\xi'_{J'}$.

The number of iterations required to obtain a sufficiently precise solution of the system of equations in finite differences may be greatly reduced by sufficiently correct selection of the zero approximation. The extrapolation on /13 the basis of two models preceding in time that is usually recommended for this purpose [19] is not applicable in this particular case, since this method may result in the appearance of false maxima for variables F and T, which vary sharply in the vicinity of a shell source of energy [20]. Fairly effective improvement in the convergence of the iteration process was achieved in this project as follows. The values of $r_j^{(0)}$, $F_j^{(0)}$, $T_j^{(0)}$, and $q_j^{(0)}$ at point ξ_j, ($j = 0.1, \ldots, J'$) were calculated by quadratic interpolation of functions $r(\xi)$, $F(\xi)$, $T(\xi)$, and $q(\xi)$ provided by the previous model toward point ξ_j, that is, the preceding model is used as the zero approximation, but one "converted" to the new values of mass variable ξ_J', which vary within the same limits as ξ_J[3].

Since the physical conditions in the accreted matter are unknown, we followed [4] in excluding from the recently added layers the second and third terms in parenthesis in equation (52), introducing ahead of these terms the factor[4]

$$\theta(j)=\begin{cases}1 \text{ when} 0 \leqslant j \leqslant J;\\ 0 \text{ when} J < j \leqslant J'.\end{cases}$$

Then on the basis of the values adopted for r, F, T, and q, calculation is made of the values of functions T, E, K, and ε and of their derivatives relative to T and q in each of the J' layers of the star. As regards the chemical composition, it is assumed to be stationary (see above) and depends only on the layer number, that is,

$$X=\begin{cases}X_1 \text{ when } j < j_0;\\ X_2 \text{ when } j \geqslant j_0 \text{ etc.},\end{cases}$$

in which j_0 corresponds to the boundary between the core and the hydrogen envelope. It is to be noted that the convergence of the iteration process is appreciably impaired and may even be altogether absent if the expressions for functions P, E, K, and ε are appreciably discontinuous on transition from one analytical relation to another. A series of control calculations of the functions indicated above and their derivatives with different values of ψ_1 and ψ_2 demonstrated that the values of (16) are the optimum ones.

The extremely laborious calculation of functions $F_\nu(\psi)$ directly from (12), which takes too much computer time, was at $-4 \leqslant \psi \leqslant 20$ replaced by quadratic

---

[3]This procedure sometimes (at large values of Δt) leads to shifting of the discontinuity position of variable q (which latter is caused by change in the chemical composition), and for this reason a special "correction unit" was provided in the program, one which restores the previous density discontinuity position.

[4]Exclusion makes up the last stages of calculation (see below), when Δt decreases to the extent that one is to assume M = const, that is, $\Delta J = 0$.

interpolation based on tables of $F_\nu(\psi)$ [10]; for the remaining values of ψ we use the asymptotic expressions:

$$F_\nu(\psi) \cong \sqrt{\pi} \cdot \frac{1}{2} \cdot \frac{3}{2} \ldots \nu \exp(\psi) \text{ when } \psi < -4;$$

$$F_\nu(\psi) \cong \frac{1}{\nu+1} \psi^{\nu+1} \text{ when } \psi > 20,$$

which can easily be derived from (12) respectively at $\psi \ll -1$ and at $\psi \ll 1$.

Since a part of the boundary conditions on the star surface is based on interpolation (see Section 3), before solving the equation system for corrections δr_j, etc., it is necessary to prepare a network of appropriate reference values (see Figure 1).

The iteration is completed by calculating the relative corrections[5] /14

$$\varepsilon_r = \max_{1<j<J'} \left\{ \left| \frac{\delta r_j}{r_j} \right| \right\}; \quad \varepsilon_F = \left| \frac{\delta F_{J'}}{F_{J'}} \right|; \tag{61}$$

$$\varepsilon_T = \max_{0<j<J'} \left\{ \left| \frac{\delta T_j}{T_j} \right| \right\}; \quad \varepsilon_q = \max_{0<j<J'} \left\{ \left| \frac{\delta q_j}{q_j} \right| \right\},$$

and the cycle of calculations is repeated (see Figure 1) until these values are smaller than a certain limit:

$$\max\{\varepsilon_r, \varepsilon_F, \varepsilon_T, \varepsilon_q\} < \varepsilon_{\max}. \tag{62}$$

After (62) has been reached, the next approximation is assumed to be the definitive one and on the basis of the values obtained for r_j, F_j, T_j, and q_j, one calculates the values of the physical quantities in various star layers. In all the calculations it was assumed that $\varepsilon_{\max} = 2 \cdot 10^{-4}$; accuracy such as this was generally achieved after 3-4 iterations. Depending on the number of layers J', which ranged from 80 to 150, one iteration on the "Minsk-22" computer required 16 to 30 minutes.

In some instances when iterations are performed, the errors decrease to a certain value and then remain approximately constant or even begin to increase again. Generally speaking, despite the obvious advantages of the relaxation method, it has the disadvantage that the region of convergence of variables r, F, T, and q in space is greatly restricted when this method is employed. The convergence region is widened somewhat if the value of the corrections is artificially reduced when the next approximation is obtained [20], if relations (56) are replaced by

$$r_j^{(1)} = r_j^{(0)} + \alpha r_j, \quad F_j^{(1)} = F_j^{(0)} + \alpha \delta F_j \quad \text{etc.},$$

[5]For variable F the value of $\delta F_j / F_j$ is calculated only at j = J', since when j < J' it may be found that $F_j = 0$.

in which $0 < \alpha < 1$. There was a special unit for this purpose in the computer program; the values 0.5 and 0.25 were generally used for α. However, the absence of convergence mostly indicates too large a value of step δt, and the convergence is restored if the process of constructing the model is begun again from the very beginning but with a smaller step δt.

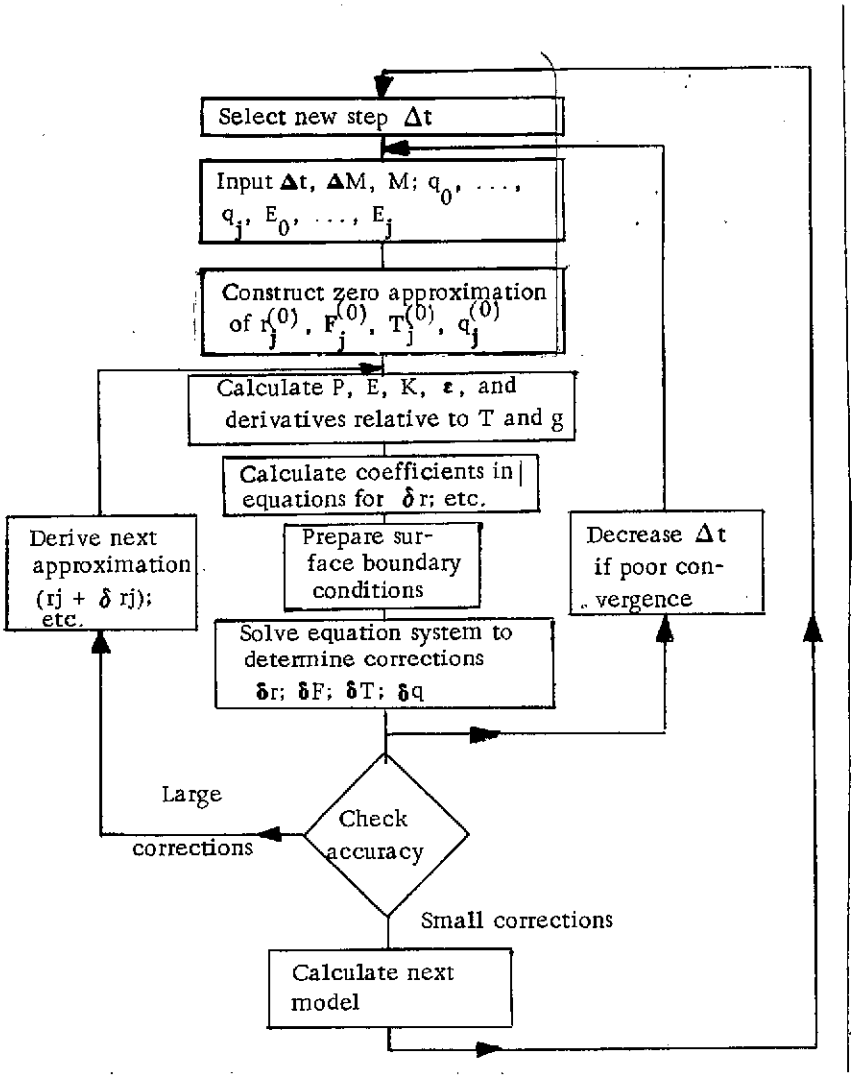

Figure 1.

5. Initial Model

A special situation arises in plotting of the initial model, since in this instance the algorithm described in the foregoing is obviously inapplicable [20]. An exception is represented by the chemical composition of the interior of the star, since the white dwarf considered in this paper has a very simple prehistory (trivial cooling of a homogeneous star). Another substantial simplification results from the fact that the chemical composition of the

hydrogen envelope of a white dwarf arising at time t = 0 may also be regarded as unchanged in calculations (see above). Thus the star is represented as consisting of two homogeneous parts, the "core" and the "envelope," as the chemical composition of which we selected respectively the mixtures CS MIX X and CS MIX VI [11]:

$$\boxed{\begin{array}{l} X_1=0.000;\ Y_1=0.996;\ Z_1=0.004; \\ X_2=0.996;\ Y_2=0.000;\ Z_2=0.004. \end{array}} \qquad (63)$$

The difficulties in calculating the remaining quantities derive from the fact that, at the beginning of the calculations, there is no information whatever regarding the values of $\partial E/\partial t$ and $\partial q/\partial t$ in equation (52) (the values of E_j, q_j /15 are unknown); on the other hand, since at this time $\varepsilon \equiv 0$, the approximation $\frac{\partial E}{\partial t} = \frac{\partial q}{\partial t} \cong 0$ is entirely inapplicable. The brilliant method of obtaining an initial model of a white dwarf used in [4] consists in beginning calculations with a stationary helium star ($\varepsilon \neq 0$) and then formally excluding the helium combustion reactions from model to model. As a result of such a fictitious evolution, the star is cooled to the state of the white dwarf, a state which may be used as the initial one in subsequent calculations [4, 20]. One of the series of homogeneous models obtained in this manner in [4] (model No. 26, see [4], page 49) characterized by a "growth" of $t = 1.43 \cdot 10^8$ years (counting from the time of total elimination of helium combustion) was adopted by us as the basis in construction of the initial model in this particular project. The table given in [4] is not "detailed" enough, and the number of layers was increased (approximately six-fold) by cubic interpolation. In addition, the boundary conditions on the surface of the star assume the presence of an atmosphere of pure hydrogen, and so an appropriate hydrogen atmosphere was added to the star by means of relations (34)-(37). The mass of the atmosphere, the value of which may be estimated if pressure P at level $\tau = 10.0$ is known (see (38)), represents a negligible part of the mass of the star ($q < 10^{-15}$); hence $\xi_{J-1} = \xi_J$ was adopted for all the subsequently calculated models. To eliminate the errors introduced in interpolation and so forth, smoothing of such a model was carried out, this smoothing consisting of taking five time steps of a total duration of $6.3 \cdot 10^7$ years by the method described in Section 4, but at $\Delta M = 0$. The slightly "cooled" model obtained in this manner was ultimately adopted as the initial one. This model, which has the following basic parameters.

$$\boxed{M=0.5\,M_\odot;\ L=1.0337\cdot 10^{32}\,\text{erg/cm};\ \lg T_e=4.2805;\ R=1.0580\cdot 10^9\,\text{cm},} \qquad (64)$$

is shown in Table I (see Appendix) and differs from that given in [4] in higher density and lower temperature in the center[6].

Despite the fact that the mass of the hydrogen envelope of the model of (64) is very small, the introduction of an atmosphere of hydrogen eliminates

[6]This difference is apparently due to the appreciable disparity at high values P and ρ between the old data [16] (used in [4]) and the new data on opacity [11], and to the lower heavy element content than that given in [4].

the possibility of a convective zone in the vicinity of the surface due to incomplete helium ionization. As a matter of fact, as may be seen from Table 1, the temperature "under the atmosphere" is such that the helium may be considered to be completely ionized [27]. This makes it possible to effect maximum simplification of calculation of the adiabatic gradient, that is, to assume[7]

$$\nabla_{ad} = 0.4 \tag{65}$$

6. Results of Calculations

In this section the results are presented of calculations of the evolution of a white dwarf having an initial mass of $M_0 = 0.5\ M_\odot$ in the state of quasistatic hydrogen accretion. We have followed [4] in deriving the basic series of 84 models on the assumption that the growth rate of the hydrogen envelope is constant and equals[8]

$$M = 10^{-9} M_0/\text{years}. \tag{66}$$

Nine of the models calculated in this manner, which correspond to the most typical evolution times, are presented in Tables II-X (see Appendix). The values of r, $L_r \equiv l$, lg, T, lg ρ, and so forth are tabulated as a function of the value of M_r/M ($M_r \equiv m$). Since the mass of the star M increases with time, for each particular layer the value of M_r/M decreases from model to model, only the number jth layer (counting from the center) being "preserved" with time[9]. The basic parameters of the models, including age t counting from the time accretion begins t = 0, are given in Table 1(t_ζ, ρ_ζ, and ψ_ζ are respectively the temperature, density, and degeneration parameter in the lower part of the hydrogen envelope). /16

As is evident from Table 1, the calculations cover a period of $T \sim 0.8 \cdot 10^6$ years, which is negligible in comparison to time τ of cooling of a star as a whole ($\sim 10^8$ years). On the other hand, according to (66) the total change in the mass of a star in time T is $\Delta M \approx 0.8 \cdot 10^{-3} M_\odot \ll M_\odot$. Hence the disturbances in the structure of the deep interior of a star are found to be very slight. For example, the changes in density and temperature in the center (see Tables I and X) are only

---

[7]An additional argument in favor of (65) is that in hot main sequence stars incomplete helium ionization does not at all lead to convection, and the convective zone of incomplete HeII ionization is quite insignificant [28].

[8]AS has been demonstrated in [29, 30], the typical value of quantity M in half-divided systems in the so-called stage of slow mass exchange is $M = 10^{-8}$-10^{-9} $M_\odot$/year.

[9]An exception is represented by layers with j > 33 (see Appendix), since after $J_{max} = 150$ has been reached, part of these layers have been removed and the remaining layers have been renumbered.

$$\frac{\Delta\rho_c}{\rho_c} \sim 1\ \%,\ \frac{\Delta T_c}{T_c} \sim 0{,}1\ \%;$$

the variation in P and ψ is just as small (see Appendix). This by no means applies to the outer layers of the stars, which is the basic subject of our study.

TABLE 1.

Model no.	$t \cdot 10^{-6}$, year	$M/M_\odot$	$\lg T_l$	$\lg \rho_l$	ψ_l	$L \cdot 10^{-31}$	$\lg T_e$
0	0	0,5000000	4,5040	—6,3227	—	10,337	4,2805
1	0,10	0,5001000	7,0395	+2,5053	0,468	12,739	4,2643
3	0,30	0,5003000	7,1348	2,9738	1,630	30,074	4,3524
22	0,49940	0,5004994	7,2060	3,1419	1,887	67,472	4,4332
31	0,59940	0,5005994	7,2470	3,1853	1,809	92,820	4,4584
32	0,60940	0,5006094	7,2515	3,1884	1,794	95,933	4,4607
50	0,73690	0,5007369	7,3135	3,2124	1,512	201,940	4,5144
63	0,80590	0,5008059	7,3921	3,1777	0,945	346,530	4,5706
69	0,81130	0,5008113	7,4342	3,1382	0,600	488,511	4,5945
76	0,812380	0,5008124	7,4837	3,0891	0,213	527,815	4,6085
79	0,812585	0,5008124	7,5060	3,0671	0,049	509,875	4,6079
82	0,812665	0,5008124	7,5365	3,0368	—0,169	496,536	4,6065
84	0,812698	0,5008124	7,5748	2,9981	—0,439	489,194	4,6052

Commas indicate decimal points.

Formation of the Shell Energy Source

As may be seen from Tables I-X, accretion leads to considerable increase in the dimensions of a white dwarf. The total increase in radius R of the star amounts to $\approx$ 55% in comparison to the initial model, or $\approx$ 35% in comparison to model one. However, in the inner layers of a star, the variations in r are not as significant; moreover, even at a short distance from the surface $\frac{dr}{dt} < 0$. This apparently is to be ascribed to compression of the matter of the star under the influence of the hydrogen added $\left(\frac{d\rho}{dt} > 0\right)$. The compression effect, which is quite negligible in the central regions, is especially noticeable on the periphery, and this determines the course of further evolution. It may be seen from Figure 2, which illustrates the change with time of radius r_l of the /17
lower boundary of the hydrogen envelope, that even in the first stages of accretion the He-H boundary is rapidly displaced into the interior, into the region of the higher values ρ and P. Figure 3 shows the temperature distribution in the outer part of the star in different stages of evolution (the figures indicate the model number, and the vertical line designates the location of the He-H boundary). As may be seen from Figures 2 and 3, the growing hydrogen envelope performs the function of a "piston" effecting compression and heating of the outer layers of a white dwarf. As a result of such a process, the interior of the star ($M_r/M \lesssim 0.995$) becomes increasingly isometric, and relation $T(M_r/M)$ soon ceases to be monotonic (see Figure 3). The temperature distribution maximum occurring in model 32 ($t = 0.6094 \cdot 10^6$ years) at $(M_r/M)_m =$

= 0.9988709 ($\lg T_m = 7.2515$, $\lg \rho_m = 3.1884$, $\psi_m = 1.794$) is situated slightly above the lower hydrogen boundary $(M_r/M)_z = 0.9988318$.

To study the evolution of the outer layers of a white dwarf, it is convenient to consider relation $T_z(\rho_z)$ shown in Figure 4[10] (T_z, ρ_z are the temperature and density at the "bottom" of the hydrogen envelope); the figures indicate the model number (see Table 1). It can easily be seen that between models 3 and 31 the compression of the matter near the He-H boundary is quasi-adiabatic [4]; as a matter of fact, the slope of the corresponding portion of curve $T_z(\rho_z)$ is very near the typical adiabat value $(\partial \lg T/\partial \lg \rho)_{ad} = \gamma - 1 \cong$ /18
$\cong 0.67$. As a result of formation of the temperature maximum, the usual flow of energy toward the surface ($L > 0$) is accompanied by the occurrence of an energy flux into the interior of the star ($L_r < 0$). However, the decisive role in this stage of evolution is played by the circumstance that a substantial rise in temperature is observed in the region characterized by slight degeneration ($\psi \lesssim \lesssim 2$), in which the electron thermal conductivity is not so great as to impede further elevation of the temperature. Although the influence of electron thermal conductivity becomes increasingly appreciable as the hydrogen descends into the interior of the star (as can be seen from Figure 3, the temperature maximum is gradually displaced from the He-H boundary in the direction of the less degenerated layers), the temperature reached is nevertheless sufficient to initiate thermonuclear reactions in the lower part of the hydrogen envelope.

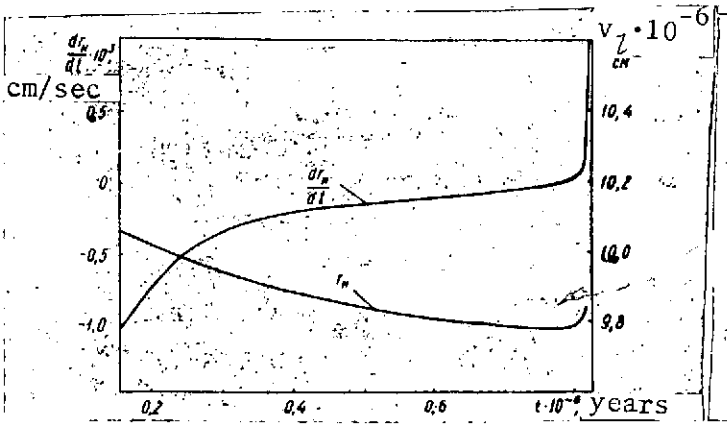

Figure 2.

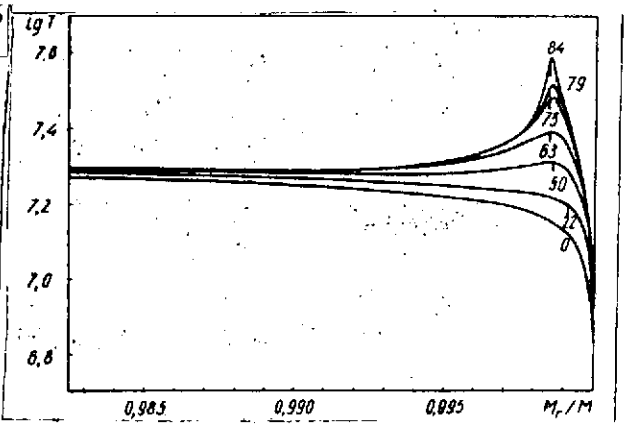

Figure 3.

The sharp increase in energy release ε in this part of the star results in even more abrupt growth of T_z (Figure 4), and the heating is accelerated. The region of intensive energy release is very narrow — its "half-width" (in terms of ε) in model 32 is only 1% of the radius and less than 0.05% of the mass of the star — and, as may be seen from Figure 3, has a tendency to become even more localized in subsequent models. Hence soon after formation of the temperature distribution maximum, one may speak of the formation of a layer energy source

[10]The broken line in Figure 4 corresponds to the results obtained in [4].

situated in the lower part of the hydrogen envelope and corresponding to $\rho \sim 10^3$ g/cm^3. As can be seen from Tables I-X, the temperature and energy release maximum is situated in the immediate vicinity of the He-H boundary, so that the values used by us of temperature T_z and density ρ_z in the lowest hydrogen layer characterize with a fair degree of accuracy the physical conditions in the layer source of energy.

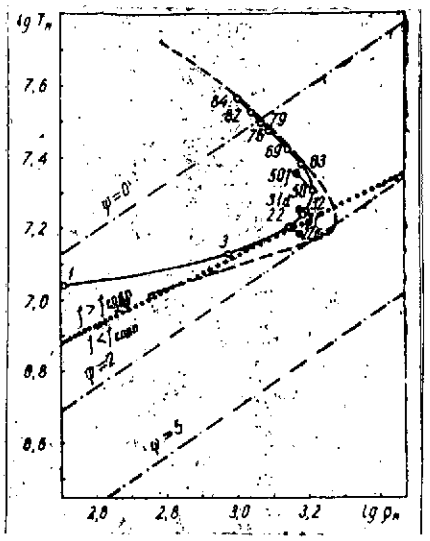

Figure 4.

Thermal Instability in the Outer Layers of a White Dwarf

As is known [4, 31], the nature of thermal instability in a shell source of energy depends on the degree of degeneration of matter. Instability of the flare type ($\dot{T} > 0$, $\dot{\rho} \approx 0$) is observed in the limiting case of extensive degeneration. If the degeneration is not extensive enough, the temperature rise is accompanied by decrease in density ($\dot{T} > 0$, $\rho > 0$); when specific conditions are satisfied [4, 31], instability of such a type as this may also develop in an entirely undegenerated gas.

Since in this particular case the degree of degeneration in the shell source of energy is slight ($\psi_z < 2$), instability of the flare type is of very brief duration — density ρ_z reaches its maximum value of $\lg \rho_z = 3.2131$ and remains at this value (within a few decimal points) approximately for models 50-57, this corresponding to $\Delta t \approx 0.25 \cdot 10^5$ years. By convention the term "flare" may be applied to the period of evolution of model 31 to 63, which is characterized by abrupt rise in temperature and slight variation in density (see Figure 4)[11]. The length of this period is $\Delta t \approx 0.2 \cdot 10^6$ years, a length 3 times shorter than that of the entire preceding evolution after the beginning of accretion (see Table 1); the flare nevertheless leads to sharp increase in energy release — $\varepsilon \approx 1.500$ erg/g·sec in model 31 to $\varepsilon \approx 15{,}000$ erg/g·sec in model 63. The increase in local values of luminosity L_r on the outside of the shells energy source (see Tables IV-VI) now outstrips the increase in the luminosity of the star L. It follows that a large part of the energy released in thermonuclear reactions is accumulated in the layers of matter directly above the shell energy source, and this in turn contributes greatly to acceleration of the heating, that is, to the development of thermal instability. /19

Significant increase in T, provided that $\rho \approx$ const, leads to further elimination of degeneration, and as a consequence to expansion of the heating

[11] In certain instances, whenever it does not result in misunderstanding, we construe the term "hydrogen flare" to mean the entire process studied of thermal instability in the accretion of hydrogen in white dwarfs.

layers: by the end of the flare ψ_l decreases by almost one-half in comparison to the value of ψ_l in model 31; owing to the fact

$$\rho_l < 0, \tag{67}$$

it is precisely the movement of point (ρ_l, T_l) in Figure 4 representing the star that fosters the most rapid decrease in ψ_l (the "track" in Figure 4 becomes perpendicular to the lines ψ = const). However, when expansion of the envelope begins increase in temperature T_l not only does not stop, but on the contrary becomes even more accelerated (see Tables 1 and VI-X). Thus, we may follow the authors of [4] in drawing the conclusion that a flare has as its direct continuation the instability of the second type (see above) first studied by Schwarzschild and Haerm [31]. The origination of such instability is favored by the slight width of the layer energy source arising during a flare. Further evolution leads to even greater localization of the thermal instability (see Figure 3). The development of instability is also facilitated by the fact that when lg T > 7.3 the main role in energy release shifts from pp-reactions to reactions of the carbon-nitrogen cycle, which are much more sensitive to temperature rise and are more greatly subject to the screening effect [12-14]. In addition, the removal of degeneration, and thus the somewhat "damping" instability, nevertheless indirectly favors the development of thermal runaway, since the decrease in electron thermal conductivity reduces the role of heat removal L_r into the interior of the star; it is characteristic that the temperature maximum, which is initially displaced in the direction of the lower densities, subsequently approaches the hydrogen-helium boundary again (see Figure 3 and Tables VI-X).

A highly important feature of the developing thermal runaway lies in the circumstance that the rate of energy release in the hydrogen combustion layer consistently exceeds the heat removal, including that in the direction of the surface of the star, despite the fact that the local luminosity L_r^+ on the outside of the shell source of energy increases very rapidly — in the last of the models calculated the value of L_r^+ is nearly 20 times greater than the luminosity of the star L (see Table X). As a result temperature increase T_l is accelerated at a very fast pace in time: the quantity

$$\tau = T_l / \dot{T}_l \tag{68}$$

ranges from $\tau \approx 10^6$ years in model 31 to $\tau \approx 10^5$ years in model 63 and equals $\tau \approx 250$ years in model 84 (the time step for these models was taken as equalling respectively 10^4; $0.5 \cdot 10^4$; and 13 years). Starting with model 75 the time step /20 is $\Delta t < 100$ years, so that by virtue of (66) $\Delta M < 10^{-7} M_\odot$. Since the calculations were performed on a Minsk-22 computer (one word equals 7 decimal points), M = = const was assumed in the calculation of models 75-84. Comparison of the models for $\Delta t \gtrsim 100$ years calculated at $\Delta M = \dot{M} \Delta t$ and at $\Delta M = 0$ shows that such formal exclusion of accretion in the last stage of calculation apparently has no effect on the accuracy of calculation of thermal runaway in the lower part of the

hydrogen envelope[12], and even permits more correct allowances for all the physical processes in the vicinity of the surface of the star.

As a result of the accelerated heating with time the mean value of energy release ε in the hydrogen combustion layer proves to be very small, since despite the fact that by the end of the calculations ε reaches values of $\sim 10^7$ erg/g·sec (see Table X), for the greater part of the total evolution time the values of ε are small. This has the result firstly that the mean value of energy flux into the interior of the star is also insignificant and, as has already been noted, thermal runaway on the surface of the core of a white dwarf induces only small disturbances in the interior of the star. Secondly, the small value of $\bar{\varepsilon}$ indicates that the burnout of hydrogen in the shell energy source may be disregarded and that the chemical composition may be assumed not to depend on time, and this we have assumed in the calculations.

Let us consider the displacement of the He-H boundary in greater detail. As may be seen from Figure 2, which shows radius r_l and rate $\frac{dr_l}{dt}$ of the lower H-envelope boundary as a function of time, the initial stages of accretion are accompanied by fairly rapid movement of the hydrogen toward the center of the white dwarf — rate $\frac{dr_l}{dt} < 0$ and decreases slowly with time from $\approx -1 \cdot 10^{-5}$ cm/sec in models 1 and 2 to $\approx -1 \cdot 10^{-6}$ cm/sec in model 50. Subsequently r_l reaches a minimum value; rate $\frac{dr_l}{dt} \approx 0$ in model 55 and development of instability of the second type ($\rho < 0$) is accompanied by accelerated expansion, which, it is true, does not manage greatly to exceed r_l (see Figure 2).

Since the calculation of the evolution of a white dwarf was performed on the basis of the customary quasistatic approach to the equations of the structure of the star, after each model had been obtained estimates were made of the term $\rho\frac{d^2r}{dt^2}$ in the Eulerian equation. It was found that the dynamic effects are extremely small in all stages of the calculations. Even in the last stages of calculation, when the rate of envelope expansion increases (see Figure 2), the relative value of the dynamic term represents no more than 10^{-8}. The calculations were discontinued for model 84, not because of an increase in the dynamic effects (as was assumed at the beginning of the calculations), but rather because of difficulties of a numerical nature associated with the fact that in terms of the form $(E_j - \bar{E}_j)/\Delta t$ and $(q_j - \bar{q}_j)/\Delta t$ in equation (52) (see (57)) the rounding errors become substantial, inasmuch as at small values Δt the values of E_j and q_j are very near those of $\bar{E}_j$ and $\bar{q}_j$. This results in disruption of the regularity in relation $L_r(M_r/M)$, and after several steps in substantial deterioration of the convergence.

---

[12]This does not apply to the outermost layers of the star.

As a result of the sharp increase in temperature near the He-H boundary, the temperature gradient in the envelope of the star is very large in the last stages of calculation, and starting with model 76 there arises on the outer surface of /21
the shell source of energy a zone of convective equilibrium which rapidly decreases in size to involve parts of the star increasingly remote from the center (see Tables VII-X; the convective layers are designated by an asterisk in the last column).

As may be seen from Table 1, the hydrogen accretion results in very appreciable increase in the luminosity L and effective temperature T_e of a white dwarf, the maximum variation in which in the calculation process amounts to

$$\Delta \lg L \cong 1.71; \quad \Delta \lg T_e \cong 0.328,$$

values which considerably exceed the corresponding values of 0.945 and 0.203 obtained for the analogous case in [4]. The slight decrease in L and T_e in the very last stages of calculation (after model 76), which is also characteristic of the models of Giannone and Weigert [4], may be ascribed to a certain amount of incorrectness in the vicinity of the star of the approximation $\Delta M = 0$ used at small values Δt.

Generally speaking, in view of the simplifying assumptions in the outermost layers of a white dwarf, the introduction of which is due to the lack of information on the state of the matter added to the star, the accuracy of the values obtained for L and T_e, as well as of the remaining quantities on the surface of the star, should not be overestimated. In particular, as can readily be demonstrated, when $\dot{M} = 10^{-9} M_\odot$/year the flux of kinetic energy on the surface of the star $\dot{E}_k \sim L_\odot$ [4], that is, at any rate is of the order of the luminosity L of a white dwarf (see Table 1). The role of $\dot{E}_k$ may be substantial, especially in the vicinity of the surface, since the actual values of T_e and L may be determined not only by the flux of energy from the interior of a star but also by the necessity of reradiation to the outside of the kinetic energy of the matter falling onto the star. In a very rough approximation it may be assumed that the observed luminosity value simply equals $L' = L + \dot{E}_k$ [4]. On the other hand, certain additional studies conducted by us in the process of performing the calculations show convincingly that the changes on the surface of the star, as well as the variations in the specific form of the simplifications in the outer layers and in the boundary conditions, have a very slight effect on the course of evolution of the lower part of the hydrogen envelope, that is, the introduction of simplifying assumptions at $r \approx R$ has hardly any effect on the accuracy of calculation of thermal instability near the He-H boundary.

In conclusion we may note that the considerable increase in the radius of the star in the accretion process — ratio $\frac{\Delta \ln R}{\Delta \ln M}$ in our case is ≈ 205 (counting

from model 1), in contrast to ≈ 100 in [4]— may be compared to the observational data: as we know, for Sirius B observation yields for R values almost twice as large as the theoretical (Chandrasekhar) values [23].

The Approximation $\dot{P}_l = 0$

The subsequent evolution of the star (after model 84) is highly interesting. The alternative proposed by Giannone and Weigert [4] consists in the following:

A. Gradual disappearance of thermal instability, as a result of excessive increase in the width of the hydrogen combustion shell [31]. This solution is favored by a certain decrease in the inclination of curve $T_l(\rho_l)$ in the last stages of calculation in [4] (see Figure 4). It is highly probable in this case that flares of this kind will be repeated periodically and "thermal pulsations" will occur [32, 33] which it is natural to associate with the observed activity in certain close binary systems, which include the white dwarf [34]. /22

B. It is possible that the thermal runaway in the vicinity of the He-H boundary will have much more catastrophic consequences. The temperature on the lower boundary of the shell energy source reaches very high values, ones fairly close to the ignition temperature of the reaction $3He^4 \rightarrow C^{12}$ [21]. The hydrogen runaway may consequently prove to be a trigger mechanism which includes a much more powerful explosion in the helium core of a white dwarf, an explosion comparable to the phenomenon of the novas or even supernovas.

The results of the calculations presented in the foregoing do not allow us to infer that the thermal instability is overcome (see Figure 4), although it is possible that this is associated with the still fairly large value of step Δt when model 84 is obtained. As may be seen from Figure 3, conclusion B is also favored by the tendency of the shell energy source towards greater localization, as well as by the obvious approach of the temperature maximum toward the surface of the helium core.

A certain amount of progress in resolving this dilemna may be achieved by means of the following simple approximation, which permits extrapolation of relation $T_n(t)$ presented in Table 1 to later time intervals. We write the energy balance for 1 g of hydrogen in the vicinity of the chemical composition discontinutity:

$$\varepsilon_l - \left(\frac{\partial L_r}{\partial M_r}\right)_l = \frac{d}{dt} E_l + P_l \frac{d}{dt}\left(\frac{1}{\rho_l}\right). \qquad (69)$$

subscript l denotes that the values of all the quantities refer to the lowest part of the hydrogen envelope. Let us note two circumstances which make it possible greatly to simplify equation (69).

Firstly, unless we are concerned with the dependence of T_l on time, extrapolation of the curve in Figure 4 causes no difficulty, inasmuch as approximately after model 69 relation $T_l(\rho_l)$ is of the form[13]

$$\lg T_l = -\lg \rho_l + C_l, \tag{70}$$

in which C_l = const. There is nothing surprising in this relation if we remember that variation in pressure P_l is determined by increase in the weight of the hydrogen envelope due to accretion, and at small values Δt, by virtue of $\Delta M = \dot{M}\Delta t \approx 0$ (see above) and r_l = const (see Figure 2), we have

$$P_l \cong 0, \tag{71}$$

for models 69-84 $\lg P_l \cong 18.8$ (see Appendix). Consequently, if the degeneration which is already insignificant in this region, is disregarded[14]

$$T_l = \frac{\mu P_l}{R} \cdot \frac{1}{\rho_l}, \tag{72}$$

from which relation (70) follows, in which the constant $C_l = \lg \frac{\mu P_l}{R}$ is a function of pressure P_l = const at the bottom of the hydrogen envelope. We note that such a simple unequivocal relationship between P_l and P_l is valid to the extent that we disregard the dynamic effects, that is, so long as the hydrogen envelope may be regarded as a kind of "piston" in quasistatic equilibrium under the influence of its own weight and pressure P_l. /23

Secondly, according to the results of precise calculations, in the last star models ratio $q = \frac{1}{\varepsilon_l}\left(\frac{\partial L_r}{\partial M_r}\right)_l$ differs very little from model to model, i.e. it is, almost constant. Quantity q, which characterizes the portion of specific heat removal relative to the specific intensity of thermonuclear energy release in the lowest layers of hydrogen, is calculated as follows:

$$q = \frac{1}{\varepsilon_l}\left(\frac{\partial L_r}{\partial M_r}\right)_l \cong \frac{L_r^+ - L_r^-}{\bar{\varepsilon}\Delta M}, \tag{73}$$

in which L_r^+ and L_r^- are the local luminosity values on the outside and the inside of a spherical envelope having a mass of $\Delta M = M_r^+ - M_r^-$ and enclosing the first three or four layers above the He-H boundary, and $\bar{\varepsilon}$ is the mean energy release energy in these layers. For models 50-82 the value of q calculated with (73) varies from ≈ 0.8 to ≈ 0.3, despite the fact that $\bar{\varepsilon}$ increases by more than 3 orders of magnitude during this time.

---

[13]The high accuracy of relation (70) may be verified by using the Appendix tables.

[14]It can easily be shown that the role of radiation pressure is quite negligible in this case, at least for $T_l \lesssim 10^8$°K.

For the sake of simplicity assuming the hydrogen to be entirely undegenerated ($E_l = c_v T_l$) and devoid of admixtures ($\mu = 1/2$), by means of (71) and (72) we obtain in place of (69) the equation

$$\varepsilon_l (1 - q) = 5R \frac{d}{dt} T_l \tag{74}$$

relative to function $T_l(t)$, the solution of which, on the condition that $q = \text{const}$, is reduced to squaring

$$t(T_l) = \frac{5R}{1 - q} \int_{T_0}^{T_l} \frac{dT_l}{\varepsilon_l(T_l, \rho_l)}, \tag{75}$$

since, according to (71) and (72), r_l is a function of T_l.

The results of the specific calculations performed with (75) are presented in Figure 5. The values of the integral in (75) were obtained by the numerical method on a Promin' computer. We selected as the initial temperature $\lg T_0 = 7.4528$ corresponding to model 72; energy release rate ε_l, which at $T_l \geqslant T_0$ is determined in effect only by reactions of the carbon-nitrogen cycle [21], was calculated with formulas (28)-(30) ($X = 0.996$, $X_n = 0.185 \cdot 10^{-3}$; the variation in chemical composition during hydrogen combustion is, as previously, disregarded); the constants in (72) were taken as equalling $\mu = 1/2$ and $P_l = 10^{18.8}$ dyne/cm^2. Since in models 72-78 the value of q is very near 50%, $q = 0.5$ was set. As may be seen from Figure 5, at $q = 0.5$ relation (75) agrees fairly closely with the results of precise calculation, which is represented in the figure by dots (the figures correspond to the model number), and the moment of runaway may be judged on the basis of curve $q = 0.5$. Curve $q = 0$ corresponding to "adiabatic" runaway is presented in the figure for the sake of comparison. The portion of heat removal q apparently must decrease over time; this is confirmed by calculations based on (73) and is clearly to be seen in Figure 5 (the points corresponding to the precise models shift from the region $q \geqslant 0.5$ to the region $0 < q < 0.5$). Hence the curve $q = 0.5$ gives only the upper limit for the moment of runaway, and the conclusion that we may draw on the basis of Figure 5 is that there apparently is no tendency toward stability and assumption A is very improbable[15].

To illustrate the role of the dynamic effect, there is shown in Figure 5 an additional curve corresponding to the "ultradynamic" limit, when the rate of the variations in the hydrogen combustion layer is so high that, if the analogy of the hydrogen envelope with a piston is continued, since the mass of the envelope piston is finite, the latter remains virtually stationary in the thermal /24

[15]Some doubt in this regard is admittedly caused by the rapid growth of the convective equilibrium zone in models 76-84, since convection can greatly increase the flow of energy toward the surface of the star.

runaway process. In this case we must assume $\dot{\rho}_l = 0$ (and, of course, $q = 0$), and in place of (69) we obtain the equation

$$\varepsilon_l = c_v \frac{d}{dt} T_l$$

the solution of which differs from (75) only in the different numerical coefficient in front of the integral.

As regards inclusion of ternary α particle collision reactions, definite conclusions regarding the value of $\varepsilon_{3\alpha}/\varepsilon_l$ in the last stages of the hydrogen flare may be drawn on the basis of the approximation $T_l = \text{const}$. Figure 6 illustrates the relation $\frac{\varepsilon_{3\alpha}}{\varepsilon_l}(T_l)$ on the assumption that T_l and ρ_l are connected by relation (72), where, as previously, $\mu = \mu_l = 1/2$ $P_l = 10^{18.8}$ dyne/cm^2. For the value of $\varepsilon_{3\alpha}$ use was made of the expression (10)

$$\varepsilon_{3\alpha} = 3.5 \cdot 10^{17} Y_1^3 \rho_1^2 \left(\frac{T_l}{10^6}\right)^{-3} f_\alpha \exp\left[-\frac{4{,}320 \cdot 10^6}{T_l}\right] \qquad (76)$$

with the screening coefficient [14] ($Z_1 Z_2 = 8$)

$$f_\alpha = \exp\left\{\frac{5\sqrt{2}e^{1/4}}{4k} \cdot \left(\frac{\pi m_e}{\hbar^2 m_l^2}\right)^{1/4} \cdot \frac{8\rho_1^{1/4}(1+X_1)^{1/4}}{T_l}\right\}, \qquad (77)$$

in which $X_1 = 0$, $Y_1 = 0.996$, and ρ_1 are parameters of the chemical composition and density on the inside of the He-H boundary. We note that ρ_1 is connected to ρ_l by

$$\frac{\rho_1}{\rho_l} = \frac{\mu_{He}}{\mu_H} = \frac{8}{3}.$$

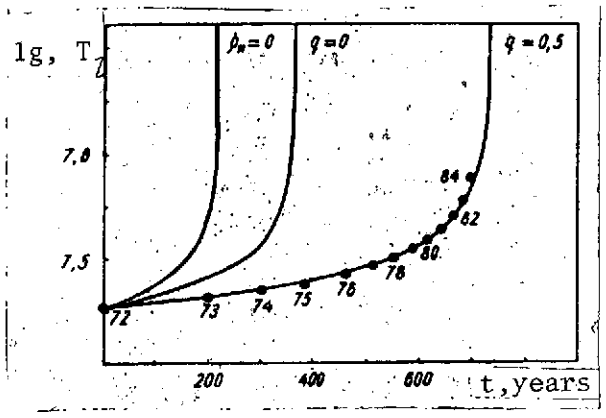

Figure 5.

As may be seen from Figure 6, when $T_l \lesssim 10^{8,0}$ K, the value of $\varepsilon_{3\alpha}$ is quite negligible in comparison to ε_l[16]. Thus we may draw the important conclusion that the three $He^4 \rightarrow C^{12}$ reactions begin to play an appreciable role at any rate no earlier than it becomes necessary to allow for the dynamic effects. In other words, within the framework of the customary quasistatic approach to the evolution of a white dwarf in the stage of accretion, it is basically impossible to reach the

/25

[16]It is curious that formal extension of relation $\varepsilon_{3\alpha}/\varepsilon_l (T_l)$ into the region $T_l > 10^{8}$°K (see Figure 6) indicates the existence of a maximum in which nevertheless $\varepsilon_{3\alpha}/\varepsilon_l \approx 10^{-3}$.

helium "ignition point." Allowance for the dynamic terms in the equilibrium equations of a star should lead to deflection of the track in Figure 4 upward from the line of (70), that is, to violation of the conditions P_l = const, something which greatly facilitates the helium combustion conditions (limiting case $\dot{\rho}_l = 0$ in Figure 5 apparently corresponds to the vertical track in Figure 4).

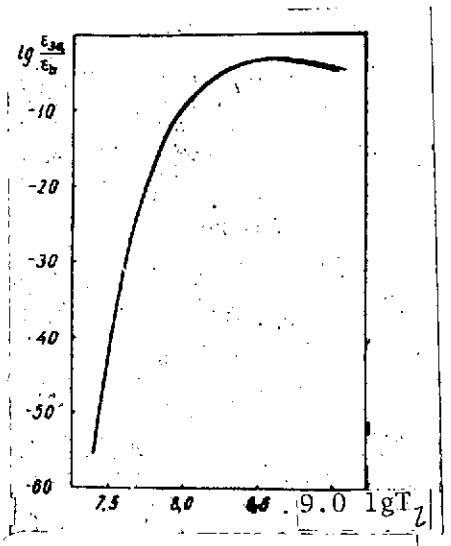

Figure 6.

The curve in Figure 4 obtained by us differs appreciably from the broken line corresponding to the results of Giannone and Weigert [4]. It is of interest to ascertain the extent to which this is due to difference in allowance for the screening (in our study and in [4]), and also the extent to which the screening effect in general determines the shape of curve T_l (ρ_l). Unfortunately, the role of this difference is difficult to isolate from that of the others — refinements in opacity, boundary conditions, rate of nuclear reactions, and so forth — but certain conclusions may nevertheless be drawn. As may be seen from Figure 4, the curve we have obtained is situated in its entirety above the line $f = f_{Salp}$, in which f corresponds to (28) [14], and f_{Salp} to the Salpeter expressions [15]. This means that for all the models obtained $f > f_{Salp}$, that is, when allowance is made for screening on the basis of (28), (30), we obtain shorter evolution times in comparison with the Salpeter formulas. This is also to be seen from Table 2, which presents the values of f and f_{Salp} at the bottom of the hydrogen envelope ($\rho = \rho_l$, $T = T_l$, $X = 0.996$). For models 1-31 the two coefficients differ very little from each other and are near unity — in this stage the role of screening (like that of thermonuclear reactions themselves) is negligible, and the disparity between these values and those of [4] is due to differences in the opacity and boundary conditions. After the formation of a shell energy source, f greatly exceeds f_{Salp} (with transition to reactions of the CN cycle the product of Z_1Z_2 increases), ratio f/f_{Salp} increasing. This possibly explains a certain difference in the shape of the curves in Figure 4 on transition to instability of the flare type ($\dot{\rho}_l \approx 0$). However, despite further increase in f/f_{Salp} (see Table 2), the difference between f and f_{Salp} soon becomes insignificant again, since after model 43 the shape of curve $T_l(\rho_l)$ is determined by relation (70) and is practically independent of the screening effect (until, of course, it is possible to disregard the dynamic effect, that is, until $P_l \cong$ const).

Consequently, it may be inferred that the form of function $T_l(\rho_l)$ on the whole changes only little when more precise allowance is made for the screening, with the possible exception of the flare period corresponding to $\rho_l \approx$ const. However, /26 the screening effect exerts an appreciable influence on the evolution time, that is, on the speed of "movement" along curve $T_l(\rho_l)$: the duration of the flare ($\dot{\rho}_l \approx 0$) is reduced more than twofold as a result of screening (Tables 1 and 2). The screening effect substantially reduces the evolution time in the "$P_l \cong$ $\cong$ const stage" as well; this is evident from Figure 7, which presents the results of calculation of relation (75) (with q = 0.5) in three different cases: 1, $f_N \equiv 1$, with no allowance for screening; 2, with allowance made for screening according to Salpeter [15]; 3, with allowance made for f_N in accordance with [14], that is, on the basis of [28] and [30].

TABLE 2.

Model no.	I	II Salp	III Salp	Comments
3	1,179	1,176	1,003	$Z_1Z_2=1$ (pp-cycle)
22	1,166	1,166	1,000	Same
31	1,154	1,151	1,003	" "
50	2,116	1,993	1,062	$Z_1Z_2=7$ (CN-cycle)
63	1,846	1,657	1,114	Same
76	1,603	1,394	1,149	" "
84	1,437	1,244	1,155	" "

Commas indicate decimal points.

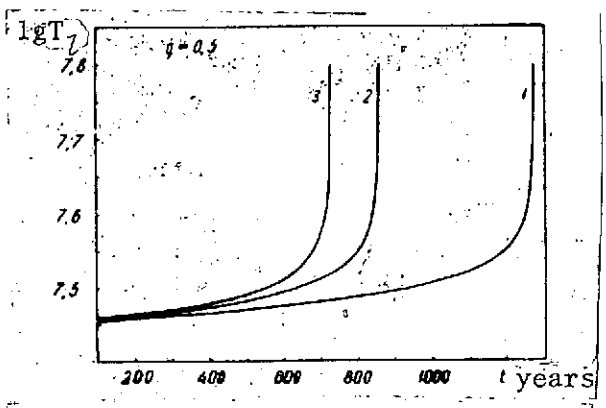

Figure 7.

Thus the results of calculations indicate the importance of precise allowance for the electron screening effect in thermonuclear reactions in studying thermal instability in the outer layers of a white dwarf.

Evolution at $\dot{M} \neq$ const

The results described in the foregoing were obtained on the condition $\dot{M}$ = const, the selection of which was dictated primarily by the simplicity of calculation. When $\dot{M} \neq$ const, calculation by the same process causes no basic difficulties, but at the present time it is difficult to give preference to any specific relation $\dot{M}(t)$. It may be assumed that function $\dot{M}(t)$ should be a decreasing one. This can be simulated the most simply by excluding accretion at any time and by studying the subsequent evolution of the star with M = const.

The results of calculation of additional branches of evolution originating in models 22, 31, and 50 are presented in Tables 3-5. As was to be expected, the corresponding tracks in Figure 4 satisfy the condition $P_z \cong \text{const}$; de- /27
partures from this law are noticeable only for the "earliest branch" (from model 22). This may be ascribed to a certain intensification of degeneration resulting from increase in parameter ψ_z (see Table 3). As may be seen from Table 5 and Figure 4, the evolution of the star in branch 50-50f leads to further increase in the intensity of the shell energy source and to the development of thermal instability (admittedly at a far slower pace than in the calculations with $\dot{M} = 10^{-9} M_\odot$ /year). In the case of 31-31d the initial growth of T_z is retarded to such an extent (see Table 4) that one can infer disappearance of the thermal instability and establishment of the stationary state[17].

TABLE 3.

Model no.	$t \cdot 10^{-6}$, years	$M/M_\odot$	$\lg T_z$	$\lg \rho_z$	ψ_z	$\lg T_e$
22	0,4994+ 0	0,5004994	7,2060	3,1419	1,887	4,4332
22a	+ 0,25	0,5004994	7,2027	3,1453	1,923	4,4005
22b	+ 2,25	0,5004994	7,2017	3,1463	1,935	4,3961
22c	+10,00	0,5004994	7,2007	3,1488	1,952	4,3846
22d	+12,00	0,5004994	7,2003	3,1494	1,957	4,3812
22e	+20,00	0,5004994	7,1999	3,1534	1,982	4,3829

Commas indicate decimal points.

TABLE 4.

Model no.	$t \cdot 10^{-6}$, years	$M/M_\odot$	$\lg T_z$	$\lg \rho_z$	ψ_z	$\lg T_e$
31	0,5994+ 0	0,5005994	7,2470	3,1853	1,809	4,4584
31a	+ 1,00	0,5005994	7,2566	3,1769	1,714	4,4413
31b	+ 3,00	0,5005994	7,2588	3,1748	1,692	4,4433
31c	+10,00	0,5005994	7,2594	3,1750	1,689	4,4440
31d	+12,00	0,5005994	7,2594	3,1753	1,690	4,4440

Commas indicate decimal points.

As regards models 22-22e, Table 3 shows that in this way the star is simply cooled, although very slowly, so that here as well it is possible to speak of attainment of a certain stationary state. Models 50f, 31d, and 22e are presented in Tables XI-XIII in the Appendix.

[17]We may note that formation of the temperature maximum in the external part of the star occurs between models 31 and 50 — in model 32.

TABLE 5.

Model no.	$t \cdot 10^{-6}$, years	$M/M_\odot$	$\lg T_z$	$\lg \rho_z$	ψ_z	$\lg T_e$
50	0,7369+0	0,5007369	7,3135	3,2124	1,512	4,5144
50a	+0,0800	0,5007369	7,3286	3,1989	1,370	4,5144
50b	+0,2021	0,5007369	7,3427	3,1855	1,240	4,5394
50c	+0,2521	0,5007369	7,3470	3,1809	1,199	4,5439
50d	+0,3521	0,5007369	7,3566	3,1709	1,110	4,5527
50e	+0,4000	0,5007369	7,3621	3,1652	1,060	4,5568
50f	+0,4300	0,5007369	7,3665	3,1605	1,020	4,5594

Commas indicate decimal points.

The calculations in the additional evolutionary branches were discontinued because at large values t (see Tables 3-5) the chemical composition may no longer be considered to be constant — allowance for this circumstance involves radical reorganization of the computer program. The results obtained nevertheless permit the conclusion that for the white helium dwarf considered ($M = 0.5\ M_\odot$; $L = 1.0337 \cdot 10^{32}$ erg/sec, $\lg T_e = 4.2805$) the occurrence of a thermally unstable hydrogen combustion layer is possible only on the condition that the mass accumulated as a result of accretion of the envelope at any rate exceeds the "critical" value

$$(M_z)_{cr} = 0{,}6 \cdot 10^{-3} M_\odot,$$

which corresponds approximately to model 31 (see Figure 4 and Table 1).

REFERENCES

1. Ledoux, P. and E. Sauvenier-Goffin, *Ap. J.*, Vol. 111, p. 611, 1950.
2. Lee, T. D., *Ap. J.*, Vol. 111, p. 625, 1950.
3. Mestel, L., *M.N.R.A.S.*, Vol. 112, p. 583, 1952.
4. Giannone, P. and A. Weigert, *Zschr. Astrophys.*, Vol. 67, p. 41, 1967.
5. Rose, W. K., *Ap. J.*, Vol. 152, p. 245, 1968.
6. Saslaw, W. C., *M.N.R.A.S.*, Vol. 138, No. 3, p. 337, 1968.
7. Hayakawa, S. and D. Sugimoto, *Astrophys. and Space Sci.*, Vol. 1, p. 2, 1968.
8. Secco, L., *Publ. Oss. Astr. di Padova*, p. 145, 1968.
9. Bahcall, J. N. and R. M. May; *Ap. J.*, Vol. 152, No. 1, 2, p. 17, 1968.
10. Landoll-Boernstein, *Num. Data and Functional Relations in Sci. and Techni. New ser.*, Gr. VI, Vol. 1, Berlin-Heidelberg, New York, 1965.
11. Cox, A. N. and Dzh. N. Stewart, *Nauchnyye Informatsii AS AN SSSR*, Vol. 15, Moscow, 1969.
12. Porfiriev, V. V. and Ju. N. Redcoborody, "The Effect of Electron Screening Thermonuclear Reactions under High Densities," Preprint, ITF-69-7, Kiev, 1969.
13. Porfir'ev, V. V. and Yu. N. Redkoborodyy, *Astrometriya i Astrofizika* [Astrometrics and Astrophysics], Vol. 8, "Naukova Dumka" Press, Kiev, 1969.
14. Porfir'ev, V. V. and Yu. N. Redkoborodyy, *Astrofizika*, Vol. 5, p. 39, 1969.
15. Salpeter, E., *Austral J. of Phys.*, Vol. 7, p. 373, 1954.
16. Cox, A. N., J. N. Stewart and D. D. Eilers, *Ap. J. Suppl. Ser.*, Vol. XI, Suppl. No. 94, 1965.
17. Baerentzen, J., *Ap. J.*, Vol. 151, No. 3, p. 2, 1968.
18. Bahcall, J. N. and R. M. May, *Ap. J.*, Vol. 152, No. 1, 2, p. 17, 1968.
19. Henyey, L. G., J. E. Forbes and N. L. Gould, *Ap. J.*, Vol. 139, p. 1, 1964.
20. Hofmeister, E., R. Kippenhahn and A. Weigert, in: *Methods of Computational Physics*, Vol. 7, New York-London, Academic Press, 1967.
21. Shvartsshil'd, M., *Stroyeniye i Evolyutsiya Zvezd* [Structure and Evolution of Stars], IL Press, Moscow, 1967.
22. Landay, L. D. and E. M. Lifshits, *Statisticheskaya Fizika* [Statistical Physics], "Nauka" Press, Moscow, 1964.
23. Mestel, L., in: *Stellar Structure*, Chicago University Press, 1965.
24. Clayton, D. C., *Principles of Stellar Evolution and Nucleosynthesis*, New York-St. Louis-San Francisco-Toronto-London-Sydney, 1968.
25. Kolesov, A. K., *Astron. Zhurn.*, Vol. 41, p. 2, 1964.
26. Sobolev, V. V., *Kurs Teoreticheskoy Astrofiziki* [A Course in Theoretical Astrophysics], "Nauka" Press, Moscow, 1967.
27. Allen, K. U., *Astrofizicheskiye Velichiny* [Astrophysical Quantities], IL Press, Moscow, 1960.
28. Gorbatskiy, V. G. and A. K. Kolesov, *Astrofizika*, No. 2, p. 3, 1966.
29. Giannone, P., K. Kohl and A. Weigert, *Zschr. Astrophys.*, Vol. 68, p. 107, 1968.
30. Kippenhahn, R., K. Kohl and A. Weigert, *Zschr. Astrophys.*, Vol. 66, p. 58, 1967.
31. Schwarzschild, M. and R. Haerm, *Ap. J.*, Vol. 142, p. 855, 1965.
32. Weigert, A., *Zschr. Astrophys.*, Vol. 64, p. 395, 1966.

33. Rose, W. K., *Ap. J.*, Vol. 146, p. 838, 1966.
34. Kraft, R., *Vzryvnyye Peremennyye Dvoynyye Zvezdy* [Explosive Variables as Binary Stars], "Mir" Press, Moscow, 1965.

APPENDIX

TABLE I. MODEL 0 (INITIAL MODEL)[18]

M_r/M	r, 10^9 cm	L_r, 10^{33} erg/sec	lg T	lg ρ	E, 10^{10} erg/g	lg P	ψ	ε, erg/g·sec	
0,0000000	0,0000	0,0000	7,3621	6,3097	$6,6270 \cdot 10^6$	22,898	132,27	0,0000	He
$0,9960155 \cdot 10^{-3}$	1,1946	0,1583	7,3613	6,2238	5,9063	22,766	116,14	0,0000	„
$0,4678055 \cdot 10^{-1}$	1,9605	0,5401	7,3598	6,1799	5,5662	22,699	108,93	0,0000	„
0,1649986	3,0475	1,7438	7,3568	6,0753	4,8285	22,538	93,42	0,0000	„
0,3161484	3,9839	3,4216	7,3533	5,9516	4,0748	22,345	77,90	0,0000	„
0,5099755	5,0159	5,5143	7,3478	5,7774	3,2014	22,072	60,38	0,0000	„
0,6927306	6,0219	7,4056	7,3401	5,5653	2,3813	21,736	44,37	0,0000	„
0,8427728	7,0404	8,8768	7,3286	5,2958	$1,6339 \cdot 10^6$	21,307	30,13	0,0000	„
0,9429983	8,0729	9,7843	7,3080	4,9315	$9,8827 \cdot 10^5$	20,724	18,06	0,0000	„
0,9768978	8,6889	10,058	7,2847	4,6177	6,3692	20,246	11,70	0,0000	„
0,9825876	8,8455	10,130	7,2764	4,5261	5,6391	20,101	10,34	0,0000	„
0,9882140	9,0359	10,200	7,2634	4,4011	4,7952	19,906	8,77	0,0000	„
0,9905001	9,1480	10,234	7,2538	4,3187	4,3208	19,778	7,88	0,0000	„
0,9949682	9,3689	10,285	7,2276	4,1307	3,4363	19,491	6,22	0,0000	„
0,9975063	9,5789	10,314	7,1903	3,9081	2,6621	19,157	4,74	0,0000	„
0,9989920	9,7881	10,330	7,1320	3,6194	1,9593	18,735	3,36	0,0000	„
0,9995835	9,9436	10,335	7,0649	3,3357	1,4824	18,331	2,37	0,0000	„
0,9998434	10,0751	10,337	6,9826	3,0186	$1,1101 \cdot 10^5$	17,888	1,52	0,0000	„
0,9999256	10,1540	10,337	6,9157	2,7756	$9,0018 \cdot 10^4$	17,554	0,99	0,0000	„
0,9999917	10,3149	10,337	6,7099	2,0471	50897	16,578	— 0,31	0,0000	„
0,9999982	10,3867	10,337	6,5675	1,5231	35390	15,896	— 1,13	0,0000	„
0,9999997	10,4493	10,337	6,3890	0,8363	23001	15,022	— 2,15	0,0000	„
0,9999999	10,5441	10,337	5,9283	—1,8396	7874,9	11,880	— 6,77	0,0000	„
0,9999999	10,5786	10,337	4,5040	—6,3212	789,21	6,399	—11,48	—	H
0,9999999	10,5802	10,337	4,2805	—7,0960	471,71	5,401	—12,49	—	„

Commas indicate decimal points.

[18] The number of decimal points in Tables I-XIII has been reduced by a factor of 3-4 in comparison to those used in the calculations.

TABLE II. MODEL 1 (t = 100,000 YEARS)

M_r/M	r, 10^8 cm	L_r, 10^{41} erg/sec	lg T	d $\mathfrak{B}_1$	E, 10^{15} erg/g	lg ρ	ψ	ε, erg/g·sec	
0,0000000	0,0000	0,0000	7,3619	6,3099	$6{,}6291 \cdot 10^6$	22,898	132,35	0,0000	He
$0{,}9958151 \cdot 10^{-2}$	1,1944	0,1571	7,3612	6,2241	5,9082	22,767	116,21	0,0000	„
$0{,}4877078 \cdot 10^{-1}$	1,9601	0,5377	7,3597	6,1801	5,5680	22,699	108,99	0,0000	„
0,1649656	3,0469	1,7340	7,3567	6,0756	4,8302	22,538	93,48	0,0000	„
0,3160852	3,9831	3,4028	7,3532	5,9519	4,0764	22,345	77,94	0,0000	„
0,5098736	5,0148	5,4763	7,3477	5,7777	3,2028	22,072	60,41	0,0000	„
0,6925921	6,0204	7,3405	7,3402	5,5657	2,3826	21,737	44,40	0,0000	„
0,8426043	7,0384	8,7610	7,3287	5,2963	$1{,}6352 \cdot 10^6$	21,308	30,14	0,0000	„
0,9428098	8,0696	9,5450	7,3086	4,9327	$9{,}8998 \cdot 10^5$	20,726	18,07	0,0000	„
0,9767025	8,6838	9,6944	7,2864	4,6202	6,3941	20,250	11,70	0,0000	„
0,9823911	8,8395	9,6625	7,2785	4,5294	5,6690	20,107	10,35	0,0000	„
0,9880164	9,0285	9,6287	7,2666	4,4058	4,8300	19,914	8,77	0,0000	„
0,9907020	9,1394	9,6253	7,2578	4,3246	4,3608	19,788	7,88	0,0000	„
0,9947692	9,3568	9,6227	7,2347	4,1411	3,4921	19,508	6,22	0,0000	„
0,9973068	9,5605	9,6752	7,2033	3,9285	2,7462	19,191	4,75	0,0000	„
0,9987923	9,7560	9,9562	7,1595	3,6677	2,0990	18,814	3,40	0,0000	„
0,9993836	9,8886	10,441	7,1190	3,4433	1,7061	18,499	2,50	0,0000	„
0,9996434	9,9808	11,080	7,0861	3,2538	1,4625	18,243	1,85	0,0000	„
0,9997256	10,0211	11,526	7,0712	3,1596	1,3666	18,119	1,55	0,0000	„
0,9997917	10,0614	12,264	7,0565	3,0573	1,2787	17,988	1,24	0,0000	„
0,9997982	10,0659	12,407	7,0548	3,0452	1,2696	17,973	1,21	0,0000	„
0,9997997	10,0670	12,450	7,0544	3,0425	1,2671	17,969	1,20	0,0000	„
0,9998000	10,0672	12,458	7,0544	3,0419	1,2670	17,969	1,20	0,0000	„
0,9998592	10,1395	12,458	7,0395	2,5053	2,9580	17,800	0,47	46,525	H
0,9998983	10,2477	12,604	7,0304	2,3674	2,8371	17,644	$0{,}88 \cdot 10^{-1}$	30,578	„
0,9999351	10,3926	12,688	7,0226	2,1724	2,7237	17,432	— 0,43	17,785	„
0,9999598	10,5430	12,721	7,0184	1,9620	2,6521	17,209	— 0,97	10,341	„
0,9999763	10,7052	12,733	7,0162	1,7315	2,6064	16,971	— 1,54	5,8608	„
0,9999850	10,8415	12,737	7,0153	1,5384	2,5848	16,775	— 2,01	3,6807	„
0,9999915	10,9994	12,739	7,0147	1,3174	2,5703	16,551	— 2,53	2,1755	„
0,9999963	11,1982	12,739	7,0144	1,0446	$2{,}5608 \cdot 10^5$	16,277	— 3,17	1,1432	„
0,9999999	12,6521	12,739	4,4878	—6,4050	760,32	6,299	—11,62	—	„
0,9999999	12,6543	12,739	4,2643	—7,2034	454,44	5,277	—12,68	—	„

Commas indicate decimal points.

TABLE III. MODEL 22 (t = 499,400 YEARS).

M_r/M	$r, 10^{9}$ cm	L_r, 10^{33} erg/sec	lg T	lg ρ	E, 10^{19} erg/g	lg P	ψ	ε, erg/g·sec
0,0000000	0,0000	0,0000	7.3630	6,3139	$6,6641 \cdot 10^{6}$	22,904	132,81	0,0000
$0,9949866 \cdot 10^{-2}$	1,1907	0,1453	7,3623	6,2280	5,9408	22,773	116,62	0,0000
$0,4873120 \cdot 10^{-1}$	1,9540	0,5285	7,3610	6,1843	5,5995	22,706	109,37	0,0000
0,1648322	3,0373	1,8351	7,3578	6,0794	4,8559	22,544	93,79	0,0000
0,3158297	3,9713	3,4847	7,3542	5,9554	4,0964	22,351	78,19	0,0000
0,5094615	5,0006	5,3915	7,3486	5,7808	3,2166	22,077	60,57	0,0000
0,6920324	6,0042	7,1482	7,3412	5,5688	2,3929	21,742	44,50	0,0000
0,8419234	7,0191	8,2101	7,3303	5,2998	$1,6434 \cdot 10^{6}$	21,313	30,20	0,0000
0,9420480	8,0446	8,3864	7,3123	4,9383	$9,9800 \cdot 10^{5}$	20,735	18,07	0,0000
0,9759133	8,6515	8,0111	7,2941	4,6305	6,4976	20,267	11,68	0,0000
0,9815973	8,8041	7,8506	7,2882	4,5423	5,7832	20,128	10,32	0,0000
0,9872181	8,9877	7,6659	7,2795	4,4237	4,9669	19,944	8,75	0,0000
0,9899015	9,0946	7,5711	7,2735	4,3468	4,5143	19,825	7,86	0,0000
0,9939654	9,2989	7,4042	7,2589	4,1793	3,7006	19,571	6,24	0,0000
0,9965010	9,4821	7,1928	7,2421	3,9981	3,0342	19,304	4,84	0,0000
0,9979853	9,6409	6,9038	7,2254	3,8066	2,5222	19,032	3,65	0,0000
0,9985761	9,7305	6,7155	7,2157	3,6800	2,2660	18,859	2,98	0,0000
0,9988358	9,7797	6,6540	7,2106	3,6033	2,1383	18,757	2,61	0,0000
0,9989179	9,7972	6,6468	7,2089	3,5748	2,0949	18,720	2,48	0,0000
0,9989839	9,8121	6,6437	7,2075	3,5500	2,0587	18,688	2,37	0,0000
0,9989904	9,8136	6,6436	7,2073	3,5474	2,0554	18,684	2,36	0,0000
0,9989919	9,8140	6,6436	7,2073	3,5470	2,0540	18,683	2,36	0,0000
0,9989921	9,8141	6,6436	7,2073	3,5469	2,0537	18,683	2,36	0,0000
0,9990513	9,8353	6,5943	7,2060	3,1419	4,8552	18,653	1,89	971,67
0,9990904	9,8788	10,294	7,2048	3,1241	4,8113	18,630	1,82	922,21
0,9991272	9,8817	13,617	7,2033	3,1069	4,7654	18,609	1,76	873,56
0,9993681	10,0550	30,667	7,1837	2,9760	4,3981	18,444	1,35	540,27
0,9995680	10,2452	39,613	7,1513	2,8297	3,9677	18,252	0,99	286,26
0,9997265	10,4540	44,565	7,1085	2,6569	3,5043	18,025	0,62	128,67
0,9998290	10,6480	48,048	7,0650	2,4812	3,0981	17,796	0,28	56,189
0,9998601	10,7257	49,390	7,0472	2,4042	2,9560	17,699	0,12	39,383
0,9998872	10,8060	50,803	7,0293	2,3216	2,8099	17,594	$-0,40 \cdot 10^{-1}$	27,110
0,9999046	10,8661	51,971	7,0164	2,2569	2,7094	17,514	— 0,17	20,482
0,9999239	10,9447	53,634	7,0006	2,1671	2,5971	17,406	— 0,36	14,065
0,9999349	10,9979	54,847	6,9908	2,1046	2,5249	17,331	— 0,49	10,963
0,9999385	11,0170	55,315	6,9875	2,0815	2,5005	17,303	— 0,54	10,024
0,9999472	11,0671	56,605	6,9791	2,0199	2,4409	17,231	— 0,66	7,9399
0,9999527	11,1026	57,573	6,9736	1,9743	2,4074	17,180	— 0,77	6,7271
0,9999568	11,1322	58,417	6,9693	1,9362	2,3767	17,136	— 0,85	5,8725
0,9999600	11,1564	59,139	6,9659	1,9049	2,3530	17,100	— 0,92	5,2596
0,9999672	11,2187	61,156	6,9579	1,8221	2,2987	17,007	— 1,09	3,9684
0,9999768	11,3253	65,346	6,9465	1,6751	2,2254	16,846	— 1,43	2,4802
0,9999838	11,4328	67,470	6,9381	1,5216	2,1716	16,682	— 1,77	1,5745
0,9999901	11,5750	67,470	6,9313	1,3137	2,1244	16,465	— 2,24	0,8945
0,9999926	11,6585	67,470	6,9289	1,1897	2,1101	16,338	— 2,53	0,6506
0,9999948	11,7560	67,470	6,9271	1,0454	2,0972	16,191	— 2,87	0,4541
0,9999968	11,8765	67,470	6,9258	0,8679	2,0881	16,012	— 3,28	0,2945
0,9999985	12,0414	67,470	6,9248	0,6284	$2,0799 \cdot 10^{5}$	15,770	— 3,82	0,1665
0,9999999	13,3802	67,472	4,6567	—6,3542	1121,6	6,518	—12,08	—
0,9999999	13,3831	67,472	4,4332	—6,9506	670,37	5,699	—12,68	—

Commas indicate decimal points.

TABLE IV. MODEL 31 (t = 599,400 YEARS)

M_r/M	r, 10^9 cm	L_r, 10^{33} erg/sec	lg T	lg ρ	E, 10^{10} erg/g	lg P	ψ	ε, erg/g·sec
0,0000000	0,0000	0,0000	7,3629	6,3141	$6,6659 \cdot 10^{6}$	22,904	132,89	0,0000
$0,9947787 \cdot 10^{-2}$	1,1905	0,1456	7,3622	6,2283	5,9425	22,773	116,69	0,0000
$0,4872138 \cdot 10^{-1}$	1,9536	0,5382	7,3608	6,1845	5,6011	22,706	109,44	0,0000
0,1647992	3,0369	1,8095	7,3577	6,0797	4,8574	22,544	93,85	0,0000
0,3157666	3,9707	3,4296	7,3541	5,9557	4,0977	22,351	78,23	0,0000
0,5093597	4,9996	5,3791	7,3486	5,7811	3,2179	22,078	60,61	0,0000
0,6918941	6,0029	7,0639	7,3412	5,5691	2,3940	21,742	44,52	0,0000
0,8417552	7,0173	8,0577	7,3305	5,3003	$1,6445 \cdot 10^{6}$	21,314	30,20	0,0000
0,9418598	8,0418	8,0717	7,3131	4,9393	$9,9949 \cdot 10^{5}$	20,737	18,06	0,0000
0,9757184	8,6471	7,5392	7,2959	4,6326	6,5196	20,271	11,66	0,0000
0,9814012	8,7991	7,2719	7,2905	4,5450	5,8083	20,133	10,31	0,0000
0,9870209	8,9817	6,8852	7,2828	4,4274	4,9974	19,950	8,73	0,0000
0,9897037	9,0877	6,5767	7,2777	4,3514	4,5492	19,833	7,84	0,0000
0,9937669	9,2898	5,6385	7,2663	4,1866	3,7483	19,584	6,20	0,0000
0,9963020	9,4695	4,0877	7,2560	4,0098	3,1059	19,326	4,77	0,0000
0,9977859	9,6234	2,3049	7,2497	3,8261	2,6302	19,070	3,54	0,0000
0,9983767	9,7086	1,3645	7,2478	3,7079	2,4054	18,913	2,87	0,0000
0,9986362	9,7547	0,8487	7,2472	3,6380	2,2966	18,823	2,51	0,0000
0,9987184	9,7709	0,6777	7,2471	3,6127	2,2603	18,791	2,39	0,0000
0,9987844	9,7846	0,5398	7,2470	3,5908	2,2302	18,763	2,28	0,0000
0,9987909	9,7860	0,5268	7,2470	3,5885	2,2275	18,760	2,27	0,0000
0,9987924	9,7863	0,5240	7,2470	3,5882	2,2260	18,760	2,27	0,0000
0,9987926	9,7864	0,5236	7,2470	3,5881	2,2259	18,759	2,27	0,0000
0,9988518	9,8057	0,2662	7,2470	3,1853	5,2951	18,733	1,81	1538,6
0,9988908	9,8271	5,8466	7,2467	3,1693	5,2686	18,715	1,74	1477,5
0,9989276	9,8479	10,871	7,2461	3,1545	5,2337	18,697	1,69	1418,0
0,9991685	10,0007	38,010	7,2338	3,0480	4,9292	18,565	1,34	987,20
0,9993683	10,1584	53,228	7,2121	2,9378	4,5859	18,423	1,05	628,98
0,9995268	10,3149	61,184	7,1854	2,8258	4,2294	18,276	0,80	382,43
0,9996292	10,4400	64,886	7,1616	2,7315	3,9571	18,153	0,61	248,10
0,9996875	10,5239	66,676	7,1447	2,6665	3,7728	18,067	0,48	182,92
0,9997388	10,6086	68,178	7,1272	2,5983	3,5909	17,977	0,35	132,76
0,9997840	10,6952	69,571	7,1089	2,5250	3,4218	17,883	0,21	94,329
0,9998440	10,8359	71,742	7,0793	2,3999	3,1551	17,722	$-0,30 \cdot 10^{-1}$	53,065
0,9998728	10,9198	73,173	7,0621	2,3207	3,0098	17,623	— 0,19	37,308
0,9999009	11,0157	74,947	7,0438	2,2239	2,8670	17,505	— 0,38	24,794
0,9999166	11,0853	76,356	7,0316	2,1511	2,7692	17,417	— 0,53	18,494
0,9999227	11,1139	76,991	7,0270	2,1202	2,7335	17,381	— 0,59	16,409
0,9999317	11,1605	78,088	7,0199	2,0689	2,6776	17,321	— 0,70	13,532
0,9999400	11,2082	79,276	7,0133	2,0138	2,6327	17,258	— 0,82	11,112
0,9999472	11,2550	80,508	7,0075	1,9598	2,5883	17,197	— 0,94	9,2187
0,9999527	11,2942	81,615	7,0031	1,9131	2,5545	17,144	— 1,04	7,8843
0,9999585	11,3413	83,016	6,9982	1,8564	2,5177	17,081	— 1,16	6,5582
0,9999638	11,3899	84,564	6,9937	1,7965	2,4868	17,016	— 1,30	5,4329
0,9999785	11,5711	91,691	6,9812	1,5677	2,3974	16,771	— 1,82	2,7781
0,9999926	11,9310	92,820	6,9709	1,1000	2,3197	16,289	— 2,89	0,8281
0,9999968	12,1887	92,820	6,9689	0,7696	2,3024	15,956	— 3,65	0,3734
0,9999985	12,3861	92,820	6,9682	0,5228	$2,2938 \cdot 10^{5}$	15,707	— 4,23	0,2082
0,9999999	13,9724	92,820	4,6819	—6,3605	1188,7	6,538	—12,19	—
0,9999999	13,9758	92,820	4,4584	—6,9331	710,45	5,741	—12,79	—

Commas indicate decimal points.

TABLE V. MODEL 50 (t = 736,900 YEARS)

/32

M_r/M	r, 10^9 cm	L_r, 10^{33} erg/sec	lg T	lg ρ	E_r, 10^{10} erg/g	LgP	ψ	ε, erg/g·sec
0,0000000	0,0000	0,0000	7,3628	6,3143	$6,6680 \cdot 10^6$	22,905	132,99	0,0000
$0,9944852 \cdot 10^{-2}$	1,1903	0,1499	7,3620	6,2286	5,9444	22,774	116,78	0,0000
$0,4870782 \cdot 10^{-1}$	1,9533	0,5422	7,3606	6,1848	5,6030	22,706	109,53	0,0000
0,1647538	3,0363	1,7768	7,3575	6,0799	4,8591	22,545	93,92	0,0000
0,3156798	3,9698	3,4016	7,3539	5,9560	4,0993	22,352	78,29	0,0000
0,5092197	4,9985	5,3375	7,3485	5,7814	3,2193	22,078	60,65	0,0000
0,6917041	6,0015	6,9613	7,3412	5,5695	2,3154	21,743	44,55	0,0000
0,8415241	7,0153	7,8138	7,3308	5,3009	1,6459	21,315	30,21	0,0000
0,9416012	8,0385	7,6023	7,3141	4,9405	$1,0012 \cdot 10^6$	20,738	18,05	0,0000
0,9754505	8,6421	6,5684	7,2987	4,6349	$6,5460 \cdot 10^5$	20,275	11,63	0,0000
0,9811318	8,7934	5,3148	7,2944	4,5479	5,8394	20,138	10,26	0,0000
0,9867498	8,9748	4,5889	7,2892	4,4313	5,0362	19,957	8,65	0,0000
0,9894320	9,0799	3,4444	7,2863	4,3561	4,5959	19,842	7,74	0,0000
0,9934940	9,2800	— 0,5628	7,2836	4,1931	3,8194	19,599	6,01	0,0000
0,9960284	9,4572	— 5,5879	7,2885	4,0182	3,2238	19,350	4,46	0,0000
0,9975120	9,6081	—11,056	7,2994	3,8383	2,8141	19,112	3,16	0,0000
0,9981025	9,6907	—14,014	7,3066	3,7260	2,6308	18,970	2,50	0,0000
0,9983620	9,7348	—15,664	7,3103	3,6617	2,5478	18,892	2,17	0,0000
0,9984442	9,7502	—16,150	7,3115	3,6390	2,5203	18,864	2,06	0,0000
0,9985101	9,7631	—16,553	7,3125	3,6194	2,4966	18,841	1,96	0,0000
0,9985166	9,7644	—16,593	7,3126	3,6174	2,4947	18,838	1,96	0,0000
0,9985181	9,7646	—16,601	7,3126	3,6171	2,4932	18,837	1,95	0,0000
0,9985184	9,7647	—16,602	7,3126	3,6170	2,4932	18,836	1,94	0,0000

Commas indicate decimal points.

TABLE V. CONT'D.

M/M_r	r, 10^8 cm	L_r, 10^{31} erg/sec	lg T	lg ρ	E, 10^{10} erg/g	LgP	ψ	ε, erg/g·sec
0,9985775	9,7830	—17,272	7,3135	3,2124	6,0148	18,815	1,51	3270,2
0,9986166	9,8031	— 5,4217	7,3139	3,1990	5,9904	18,800	1,46	3181,3
0,9986533	9,8225	+ 5,4015	7,3139	3,1864	5,9648	18,786	1,41	3085,0
0,9988942	9,9629	64,659	7,3067	3,0971	5,7308	18,679	1,11	2266,9
0,9990939	10,1012	99,095	7,2920	3,0129	5,4420	18,573	0,89	1565,1
0,9993548	10,3253	125,59	7,2607	2,8736	4,9625	18,393	0,58	826,94
0,9995425	10,5378	135,47	7,2262	2,7367	4,5024	18,214	0,31	440,43
0,9996781	10,7410	139,38	7,1912	2,5961	4,1007	18,033	$0,52\cdot10^{-1}$	233,03
0,9997691	10,9211	141,35	7,1601	2,4632	3,7672	17,863	— 0,19	129,50
0,9998453	11,1256	143,46	7,1279	2,2980	3,4587	17,661	— 0,52	65,488
0,9998751	11,2311	144,67	7,1134	2,2073	3,3209	17,552	— 0,71	46,259
0,9999100	11,3880	146,90	7,0958	2,0638	3,1645	17,388	— 1,01	27,958
0,9999251	11,4750	148,41	7,0882	1,9814	3,0949	17,296	— 1,18	21,409
0,9999446	11,6162	151,26	7,0784	1,8423	3,0097	17,145	— 1,56	14,043
0,9999581	11,7470	154,22	7,0718	1,7112	2,9526	17,005	— 1,86	9,6781
0,9999658	11,8423	156,61	7,0682	1,6144	2,9199	16,904	— 2,02	7,4421
0,9999691	11,8890	157,84	7,0668	1,5668	2,9074	16,854	— 2,13	6,5620
0,9999716	11,9300	158,94	7,0657	1,5254	2,8968	16,811	— 2,21	5,8691
0,9999745	11,9810	160,37	7,0644	1,4732	2,8877	16,758	— 2,35	5,1482
0,9999781	12,0516	162,42	7,0630	1,4013	2,8729	16,683	— 2,51	4,2882
0,9999800	12,0946	163,72	7,0623	1,3577	2,8673	16,639	— 2,60	3,8437
0,9999831	12,1771	166,33	7,0611	1,2742	2,8558	16,554	— 2,81	3,1248
0,9999870	12,3016	170,64	7,0598	1,1497	2,8438	16,427	— 3,08	2,3043
0,9999890	12,3851	173,94	7,0592	1,0667	2,8375	16,344	— 3,29	1,8860
0,9999990	13,5139	175,59	7,0569	$0,2954\cdot10^{-1}$	$2,8186\cdot10^5$	15,303	— 5,67	0,1643
0,9999999	15,9252	201,94	4,7379	—6,3879	1352,2	6,566	—12,44	—
0,9999999	15,9302	201,94	4,5144	—6,9121	808,19	5,818	—12,86	—

Commas indicate decimal points.

TABLE VI. MODEL 63 (t = 805,900 YEARS)

/34

M_r/M	r, 10^8 cm	L_r, 10^{31} erg/sec	lg T	lg ρ	E_i, 10^{16} erg/g	lg P	Ψ	ε, erg/g·sec
0,0000000	0,0000	0,0000	7,3627	6,3144	$6,6686 \cdot 10^6$	22,905	133,03	0,0000
$0,9943325 \cdot 10^{-3}$	1,1902	0,1511	7,3619	6,2287	5,9450	22,774	116,83	0,0000
$0,4870098 \cdot 10^{-1}$	1,9532	0,5434	7,3605	6,1848	5,6035	22,706	109,58	0,0000
0,1647310	3,0361	1,7694	7,3574	6,0800	4,8596	22,545	93,96	0,0000
0,3156363	3,9696	3,3986	7,3538	5,9560	4,0997	22,352	78,32	0,0000
0,5091495	4,9982	5,3226	7,3484	5,7815	3,2197	22,078	60,67	0,0000
0,6916088	6,0011	6,9042	7,3412	5,5696	2,3957	21,743	44,56	0,0000
0,8414082	7,0147	7,7381	7,3308	5,3011	1,6463	21,315	30,22	0,0000
0,9414714	8,0377	7,3429	7,3145	4,9408	$1,0017 \cdot 10^6$	20,739	18,04	0,0000
0,9753161	8,6408	5,6023	7,3003	4,6355	$6,5544 \cdot 10^5$	20,276	11,60	0,0000
0,9809966	8,7920	4,3052	7,2968	4,5485	5,8499	20,140	10,21	0,0000
0,9866139	8,9732	1,3862	7,2937	4,4319	5,0519	19,959	8,57	0,0000
0,9892956	9,0782	— 0,7695	7,2935	4,3566	4,6159	19,945	7,62	0,0000
0,9933571	9,2785	— 8,6156	7,3000	4,1922	3,8613	19,603	5,77	0,0000
0,9958912	9,4569	— 25,195	7,3221	4,0127	3,3156	19,357	4,05	0,0000
0,9973745	9,6111	— 54,414	7,3558	3,8235	2,9914	19,123	2,63	0,0000
0,9979650	9,6973	— 78,764	7,3752	3,7047	2,8715	18,987	1,93	0,0000
0,9982245	9,7437	— 94,130	7,3843	3,6372	2,8218	18,912	1,59	0,0000
0,9983066	9,7599	— 99,447	7,3873	3,6136	2,8042	18,885	1,47	0,0000
0,9983726	9,7736	—103,91	7,3896	3,5935	2,7907	18,863	1,38	0,0000
0,9983791	9,7749	—104,36	7,3898	3,5916	2,7888	18,861	1,37	0,0000
0.9983806	9,7752	—104,47	7,3899	3,5910	2,7874	18,860	1,37	0,0000

Commas indicate decimal points.

TABLE VI. CONT'D.

M_r/M	r, 10^8 cm	L_r, 10^{31} erg/sec	lg T	lg ρ	E, 10^{10} erg/g	lg P	ψ	ε, erg/g·sec
0,9983808	9,7753	—104,49	7,3899	3,5909	2,7870	18,859	1,37	0,0000
0,9984400	9,7948	—112,11	7,3921	3,1777	6,8833	18,839	0,94	$1,4694 \cdot 10^4$
0,9984790	9,8165	— 63,502	7,3933	3,1640	6,8743	18,825	0,89	1,4665
0,9985158	9,8376	— 18,377	7,3939	3,1514	6,8567	18,811	0,85	$1,4397 \cdot 10^4$
0,9987566	9,9884	207,60	7,3865	3,0667	6,6386	18,713	0,60	9442,1
0,9989562	10,1343	303,13	7,3689	2,9923	6,3085	18,616	0,45	5035,3
0,9992171	10,3624	337,67	7,3347	2,8751	5,7660	18,460	0,24	1942,1
0,9994048	10,5668	336,88	7,3017	2,7658	5,2921	18,313	$0,63 \cdot 10^{-1}$	961,88
0,9995404	10,7470	332,37	7,2712	2,6635	4,8912	18,177	$-0,99 \cdot 10^{-1}$	552,91
0,9997075	11,0430	324,97	7,2185	2,4858	4,2845	17,942	— 0,38	227,46
0,9998068	11,2894	321,11	7,1716	2,3247	3,8082	17,729	— 0,62	103,33
0,9998354	11,3790	320,29	7,1543	2,2622	3,6465	17,648	— 0,72	76,389
0,9998468	11,4183	320,03	7,1467	2,2333	3,5849	17,612	— 0,77	66,647
0,9999101	11,6952	319,78	7,0953	2,0210	3,1526	17,344	— 1,11	25,150
0,9999539	12,0134	322,47	7,0470	1,7414	2,7932	17,011	— 1,63	8,1600
0,9999700	12,2085	325,42	7,0261	1,5515	2,6508	16,799	— 2,01	4,2341
0,9999816	12,4273	329,79	7,0112	1,3270	2,5508	16,558	— 2,50	2,1472
0,9999900	12,6964	336,53	7,0020	1,0434	2,4890	16,263	— 3,13	1,0937
0,9999914	12,7658	338,50	7,0006	0,9698	2,4803	16,188	— 3,31	0,8329
0,9999927	12,8400	340,75	6,9995	0,8919	2,4713	16,109	— 3,50	0,6855
0,9999939	12,9192	343,38	6,9984	0,8091	2,4649	16,025	— 3,66	0,5589
0,9999957	13,0776	346,53	6,9970	0,6460	2,4505	15,859	— 4,05	0,3759
0,9999971	13,2503	346,53	6,9960	0,4700	2,4457	15,682	— 4,45	0,2467
0,9999983	13,4936	346,53	6,9952	0,2287	2,4456	15,440	— 5,00	0,1394
0,9999989	13,6700	346,53	6,9949	$0,5850 \cdot 10^{-1}$	2,4439	15,270	— 5,39	$0,9352 \cdot 10^{-1}$
0,9999994	13,9297	346,53	6,9947	—0,1854	$2,4424 \cdot 10^5$	15,025	— 5,95	$0,5290 \cdot 10^{-1}$
0,9999999	16,0974	346,53	4,7941	—6,3611	1539.2	6.6491	—12,57	—
0,9999999	16,1040	346,53	4,5706	—6,8420	919,98	5,9446	—12,91	—

Commas indicate decimal points.

TABLE VII. MODEL 76 (t= 812,380 YEARS)[19]

M_r/M	r, 10^9 cm	L_r, 10^{31} erg/sec	lg T	lg ρ	E, 10^{18} erg/g	lg P	ψ	ε, erg/g·sec
0,0000000	0,0000	0,0000	7,3626	6,3143	$6,6681 \cdot 10^6$	22,905	133,03	0,0000
$0,9943090 \cdot 10^{-2}$	1,1903	0,1528	7,3619	6,2286	5,9445	22,774	116,83	0,0000
$0,4870024 \cdot 10^{-1}$	1,9532	0,5425	7,3605	6,1848	5,6031	22,706	109,58	0,0000
0,1647288	3,0362	1,7791	7,3574	6,0799	4,8591	22,545	95,96	0,0000
0,3156323	3,9698	3,4176	7,3538	5,9560	4,0994	22,352	78,32	0,0000
0,5091430	4,9985	5,2087	7,3484	5,7814	3,2193	22,078	60,67	0,0000
0,6916000	6,0014	6,9505	7,3411	5,5695	2,3954	21,743	44,56	0,0000
0,8413974	7,0152	7,7920	7,3307	5,3009	$1,6459 \cdot 10^6$	21,315	30,21	0,0000
0,9414594	8,0384	7,1801	7,3144	4,9405	$1,0013 \cdot 10^6$	20,738	18,04	0,0000
0,9753036	8,6422	5,9543	7,3000	4,6348	$6,5480 \cdot 10^5$	20,275	11,60	0,0000
0,9809841	8,7935	3,7743	7,2965	4,5476	5,8428	20,138	10,21	0,0000
0,9866013	8,9751	2,0544	7,2934	4,4307	5,0436	19,957	8,56	0,0000
0,9892830	9,0804	— 1,1688	7,2930	4,3551	4,6066	19,842	7,61	0,0000
0,9933444	9,2815	— 9,6045	7,3006	4,1894	3,8517	19,599	5,73	0,0000
0,9958784	9,4615	— 32,808	7,3275	4,0065	3,3148	19,351	3,96	0,0000
0,9973618	9,6196	— 137,29	7,3797	3,8044	3,0539	19,113	2,35	0,0000
0,9979523	9,7115	— 430,49	7,4275	3,6635	3,0610	18,973	1,43	0,0000
0,9982117	9,7634	— 796,73	7,4558	3,5790	3,1164	18,897	0,96	0,0000
0,9982939	9,7820	— 967,64	7,4657	3,5490	3,1382	18,870	0,81	0,0000
0,9983598	9,7979	—1151,7	7,4738	3,5222	3,1673	18,847	0,68	0,0000
0,9983663	9,7995	—1169,4	7,4747	3,5193	3,1689	18,844	0,66	0,0000
0,9983678	9,7999	—1173,5	7,4749	3,5188	3,1713	18,844	0,66	0,0000
0,9983680	9,8000	—1174,2	7,4751	3,5186	3,1694	18,844	0,66	0,0000

Commas indicate decimal points.

[19]An asterisk (*) here and subsequently denotes the layers in which convective equilibrium is observed.

TABLE VII. CONT'D.

M_r/M	r, 10^8 cm	L_r, 10^{21} erg/sec	lg T	lg ρ	E, 10^{10} erg/g	lg P	ψ	ε, erg/g·sec
0,9984272	9,8232	—1524,7	7,4837	3,0891	8,1164	18,822	0,21	$2{,}2065 \cdot 10^5$
0,9984662	9,8498	—1007,1	7,4889	3,0712	8,1765	18,808	0,14	2,5161
0,9985030	9,8757	— 441,16	7,4916	3,0557	8,1993	18,793	$0{,}78 \cdot 10^{-1}$	2,6430
0,9987438	10,0612	1679,1	7,4775	2,9733	7,8632	18,693	$-0{,}99 \cdot 10^{-1}$	$1{,}3264 \cdot 10^5$
0,9989435	10,2360	1487,9	7,4391	2,9140	7,1953	18,595	— 0,10	$3{,}1403 \cdot 10^4$
0,9992044	10,4963	857,80	7,3764	2,8199	6,2272	18,438	— 0,10	3887,1
0,9993920	10,7196	669,59	7,3311	2,7211	5,5878	18,292	— 0,10	1263,4
0,9995276	10,9141	562,65	7,2944	2,6243	5,1190	18,157	— 0,31	633,38
0,9996948	11,2214	479,61	7,2369	2,4576	4,4440	17,929	— 0,53	249,69
0,9997940	11,4722	448,94	7,1883	2,3078	3,9421	17,727	— 0,73	114,94
0,9998973	11,8670	433,53	7,1077	2,0410	3,2430	17,376	— 1,11	29,622
0,9999906	12,8963	491,53	6,9041	1,0857	1,9904	16,209	— 2,68	0,3865
0,9999977	13,4132	517,82	6,8649	0,4363	1,8089	15,518	— 4,07	$0{,}5369 \cdot 10^{-1}$
0,9999986	13,5943	521,95	6,8607	0,2004	1,7919	15,278	— 4,60	0,2948
0,9999991	13,7628	524,42	6,8589	$-0{,}1619 \cdot 10^{-1}$	1,7868	15,059	— 5,09	0,1737
0,9999992	13,8076	524,91	6,8586	$-0{,}7330 \cdot 10^{-1}$	1,7854	15,001	— 5,22	0,1514
0,9999993	13,8588	525,40	6,8583	—0,1382	1,7840	14,936	— 5,67	0,1297
0,9999994	13,9234	525,94	6,8579	—0,2197	1,7826	14,854	— 5,56	$0{,}1068 \cdot 10^{-1}$
0,9999995	13,9990	526,47	6,8576	—0,3141	1,7814	14,760	— 5,78	$0{,}8539 \cdot 10^{-2}$
0,9999996	14,0942	527,01	6,8573	—0,4318	1,7802	14,642	— 6,04	0,6470
0,9999997	14,3042	527,82	6,8569	—0,6862	1,7786	14,387	— 6,63	0,3564
0,9999998	14,5595	527,82	6,8567	—0,9862	1,7777	14,087	— 7,31	0,1771
0,9999999	14,6607	527,82	6,85666	—1,1025	1,7775	13,970	— 7,69	$0{,}1352 \cdot 10^{-2}$
0,9999999	14,7960	527,82	6,8566	—1,2554	1,7773	13,817	— 7,94	$0{,}9476 \cdot 10^{-3}$
0,9999999	14,9983	527,82	6,8565	—1,4795	$1{,}7771 \cdot 10^5$	13,593	— 8,48	$0{,}5634 \cdot 10^{-3}$
0,9999999	16,6890	527,82	4,8320	—6,3542	1679,3	6,693	—12,69	—
0,9999999	16,6976	527,82	4,6085	—6,8093	1003,7	6,015	—12,96	—

Commas indicate decimal points.

TABLE VIII. MODEL 79 (t = 812,585 YEARS)

/38

M_r/M	r, 10^9 cm	L_r, 10^{33} erg/sec	$\lg T$	$\lg \rho$	E, 10^{20} erg/g	$\lg P$	Ψ	ε_r erg/g·sec
0,0000000	0,0000	0,0000	7,3626	6,3143	$6,6679 \cdot 10^{6}$	22,905	133,03	0,0000
$0,9943086 \cdot 10^{-2}$	1,1903	0,1530	7,3619	6,2286	5,9444	22,774	116,83	0,0000
$0,4870024 \cdot 10^{-1}$	1,9533	0,5364	7,3605	6,1848	5,6030	22,706	109,58	0,0000
0,1647288	3,0363	1,7492	7,3574	6,0799	4,8591	22,544	93,96	0,0000
0,3156323	3,9699	3,4493	7,3538	5,9560	4,0993	22,352	78,32	0,0000
0,5091430	4,9985	5,1164	7,3483	5,7814	3,2193	22,193	60,67	0,0000
0,6916000	6,0015	6,9332	7,3411	5,5695	2,3953	21,743	44,56	0,0000
0,8413974	7,0153	7,9825	7,3307	5,3009	1,6459	21,315	30,22	0,0000
0,9414594	8,0387	7,1923	7,3143	4,9404	$1,0012 \cdot 10^{6}$	20,738	18,04	0,0000
0,9753036	8,6424	5,9865	7,2999	4,6347	$6,5467 \cdot 10^{5}$	20,275	11,60	0,0000
0,9809841	8,7938	3,7906	7,2964	4,5475	5,8413	20,138	10,21	0,0000
0,9866013	8,9755	2,1304	7,2932	4,4304	5,0418	19,957	8,56	0,0000
0,9892830	9,0808	— 1,2168	7,2929	4,3548	4,6046	19,842	7,61	0,0000
0,9933444	9,2821	— 9,3245	7,3003	4,1890	3,8490	19,598	5,73	0,0000
0,9958784	9,4623	— 32,114	7,3271	4,0057	3,3113	19,350	3,95	0,0000
0,9973618	9,6209	— 142,75	7,3806	3,8024	3,0532	19,111	2,34	0,0000
0,9979523	9,7135	— 553,56	7,4339	3,6572	3,0864	18,971	1,37	0,0000
0,9982117	9,7664	—1240,4	7,4693	3,5671	3,1777	18,893	0,85	0,0000
0,9982939	9,7856	—1605,5	7,4822	3,5334	3,2279	18,866	0,67	0,0000
0,9983598	9,8021	—1967,2	7,4930	3,5051	3,2655	18,843	0,53	0,0000
0,9983663	9,8037	—2006,4	7,4941	3,5022	3,2703	18,841	0,52	0,0000
0,9983678	9,8041	—2015,6	7,4943	3,5018	3,2712	18,840	0,51	0,0000
0,9983680	9,8042	—2016,9	7,4943	3,5017	3,2714	18,840	0,51	0,0000

Commas indicate decimal points.

TABLE VIII. CONT'D.

M_r/M	r, 10^8 cm	L_r, 10^{31} erg/sec	lg T	lg ρ	E, 10^{10} erg/g	lg P	ψ	ε, erg/g·sec
0,9984272	9,8285	—2713,9	7,5060	3,0671	8,4660	18,819	$0,49\cdot10^{-1}$	$0,4185\cdot10^{6}$
0,9984662	9,8565	—1662,5	7,5128	3,0475	8,5564	18,804	$-0,38\cdot10^{-1}$	5,2747
0,9985030	9,8838	— 482,58	7,5156	3,0320	8,5882	18,790	$-0,95\cdot10^{-1}$	5,5806
0,9987438	10,0771	3404,5	7,4890	2,9592	8,0370	18,688	— 0,19	$1,8882\cdot10^{5}$ *
0,9989435	10,2570	3165,7	7,4498	2,9003	7,3423	18,590	— 0,19	$4,3167\cdot10^{4}$ *
0,9992044	10,5244	1181,5	7,3869	2,8061	6,3567	18,433	— 0,19	$4,9107\cdot10^{3}$
0,9993920	10,7508	658,08	7,3285	2,7186	5,5560	18,287	— 0,19	1207,7
0,9995276	10,9457	584,84	7,2945	2,6196	5,1176	18,153	— 0,32	627,30
0,9996948	11,2544	484,37	7,2362	2,4536	4,4345	17,924	— 0,54	245,86
0,9997940	11,5058	454,29	7,1873	2,3042	3,9312	17,723	— 0,74	112,94
0,9998973	11,9011	435,38	7,1060	2,0382	3,2305	17,371	— 1,11	28,957
0,9999906	12,9204	479,91	6,8905	1,0977	1,9301	16,207	— 2,61	0,3411
0,9999977	13,4138	501,23	6,8418	0,4620	1,7145	15,520	— 3,93	$0,4845\cdot10^{-1}$
0,9999986	13,5839	504,79	6,8364	0,2291	1,6932	15,282	— 4,45	0,2859
0,9999991	13,7416	506,92	6,8338	$0,1454\cdot10^{-1}$	1,6833	15,065	— 4,94	0,1385
0,9999992	13,7835	507,34	6,8333	$-0,4188\cdot10^{-1}$	1,6830	15,008	— 5,06	0,1207
0,9999993	13,8312	507,78	6,8329	—0,1062	1,6828	14,943	— 5,21	$0,1033\cdot10^{-1}$
0,9999994	13,8915	508,25	6,8324	—0,1870	1,6811	14,862	— 5,40	$0,8510\cdot10^{-2}$
0,9999995	13,9619	508,71	6,8320	—0,2805	1,6795	14,768	— 5,61	0,6807
0,9999996	14,0505	509,17	6,8316	—0,3972	1,6780	14,651	— 5,88	0,5162
0,9999997	14,2452	509,88	6,8311	—0,6494	1,6760	14,398	— 6,46	0,2852
0,9999998	14,4812	509,88	6,8309	—0,9465	1,6749	14,100	— 7,14	0,1425
0,9999999	14,5746	509,88	6,8308	—1,0615	1,6747	13,985	— 7,40	$0,1090\cdot10^{-2}$
0,9999999	14,6989	509,88	6,8307	—1,2125	1,6744	13,834	— 7,75	$0,7674\cdot10^{-3}$
0,9999999	14,8843	509,88	6,8306	—1,4336	$1,6742\cdot10^{5}$	13,613	— 8,26	$0,4594\cdot10^{-3}$
0,9999999	16,4467	509,88	4,8314	—6,3489	1677,1	6,699	—12,67	—
0,9999999	16,4551	509,88	4,6079	—6,8035	1002,4	6,020	—12,95	—

Commas indicate decimal points.

TABLE IX. MODEL 82 (t = 812,665 YEARS).

M_r/M	r, 10^9 cm	L_r, 10^{33} erg/sec	lg T	lg ρ	E, 10^{16} erg/g	lg P	ψ	ε, erg/g·sec
0,0000000	0,0000	0,0000	7,3626	6,3143	$6,6678 \cdot 10^{8}$	22,905	138,03	0,0000
$0,9943086 \cdot 10^{-8}$	1,1903	0,1538	7,3619	6,2285	5,9443	22,774	116,83	0,0000
$0,4870024 \cdot 10^{-1}$	1,9533	0,5390	7,3604	6,1847	5,6029	22,706	109,58	0,0000
0,1647288	3,0363	1,7733	7,3574	6,0799	4,8589	22,544	93,96	0,0000
0,3156323	3,9699	3,4333	7,3538	5,9559	4,0992	22,352	78,32	0,0000
0,5091430	4,9986	5,1144	7,3483	5,7814	3,2192	22,078	60,67	0,0000
0,6916000	6,0016	6,9223	7,3411	5,5695	2,3953	21,743	44,56	0,0000
0,8413974	7,0154	8,0913	7,3307	5,3008	1,6458	21,315	30,22	0,0000
0,9414594	8,0389	7,2861	7,3143	4,9403	$1,0011 \cdot 10^{8}$	20,738	18,04	0,0000
0,9753036	8,6428	5,8085	7,2998	4,6345	$6,5451 \cdot 10^{5}$	20,274	11,60	0,0000
0,9809841	8,7942	4,1013	7,2962	4,5473	5,8394	20,138	10,21	0,0000
0,9866013	8,9759	1,8469	7,2931	4,4302	5,0396	19,956	8,57	0,0000
0,9892830	9,0814	— 0,7727	7,2926	4,3544	4,6021	19,841	7,61	0,0000
0,9933444	9,2828	— 9,6211	7,2999	4,1884	3,8456	19,597	5,73	0,0000
0,9958784	9,4633	— 32,216	7,3265	4,0047	3,3067	19,348	3,95	0,0000
0,9973618	9,6223	— 147,06	7,3805	3,8003	3,0495	19,108	2,33	0,0000
0,9979523	9,7157	— 728,62	7,4405	3,6503	3,1108	18,967	1,31	0,0000
0,9982117	9,7699	—2129,1	7,4865	3,5506	3,2711	18,889	0,71	0,0000
0,9982939	9,7899	—2960,1	7,5041	3,5136	3,3421	18,862	0,51	0,0000
0,9983598	9,8072	—3785,6	7,5187	3,4821	3,4090	18,839	0,34	0,0000
0,9983663	9,8090	- 3875,7	7,5202	3,4791	3,4242	18,836	0,32	0,0000
0,9983678	9,8094	—3897,1	7,5205	3,4780	3,4166	18,836	0,32	0,0000
0,9983680	9,8096	-3900,4	7,5206	3,4781	3,4175	18,836	0,32	0,0000

Commas indicate decimal points.

TABLE IX. CONT'D.

M_r/M	r, 10^8 cm	L_r, 10^{31} erg/sec	lg T	lg ρ	E, 10^{10} erg/g	lg P	ψ	ε, erg/g·sec
0,9984272	9,8353	—5594,6	7,5365	3,0368	8,9769	18,814	— 0,17	$1,1332 \cdot 10^{6}$
0,9984662	9,8654	—2725,2	7,5451	3,0144	9,1313	18,799	— 0,27	1,4211
0,9985030	9,8948	483,45	7,5471	2,9991	9,1574	18,785	— 0,32	$1,4595 \cdot 10^{6}$
0,9987438	10,0981	6426,0	7,4978	2,9458	8,1908	18,683	— 0,27	$2,4485 \cdot 10^{6}$ *
0,9989435	10,2828	5917,1	7,4584	2,8867	7,4802	18,584	— 0,27	$5,5524 \cdot 10^{4}$ *
0,9992044	10,5573	3105,6	7,3951	2,7922	6,4682	18,427	— 0,27	5915,4 *
0,9993920	10,7895	1105,7	7,3367	2,7046	5,6538	18,281	— 0,27	1321,1 *
0,9995276	10,9867	480,23	7,2899	2,6176	5,0667	18,146	— 0,31	595,10
0,9996948	11,2956	463,25	7,2355	2,4483	4,4260	17,918	— 0,55	241,27
0,9997940	11,5479	455,69	7,1854	2,3000	3,9130	17,716	— 0,74	109,99
0,9998970	11,9439	432,29	7,1037	2,0346	3,2136	17,365	— 1,11	28,098
0,9999906	12,9587	468,86	6,8818	1,1025	1,8926	16,204	— 2,57	0,3124
0,9999977	13,4389	488,38	6,8264	0,4751	1,6575	15,518	— 3,83	$0,3726 \cdot 10^{-1}$
0,9999986	13,6029	491,71	6,8199	0,2450	1,6308	15,281	— 4,36	0,2008
0,9999991	13,7542	493,72	6,8167	$0,3191 \cdot 10^{-1}$	1,6183	15,065	— 4,84	0,1173
0,9999992	13,7944	494,13	6,8162	$-0,2442 \cdot 10^{-1}$	1,6167	15,008	— 4,97	$0,1022 \cdot 10^{-1}$
0,9999993	13,8402	494,54	6,8157	$-0,8819 \cdot 10^{-1}$	1,6161	14,944	— 5,12	$0,8749 \cdot 10^{-2}$
0,9999994	13,8979	494,99	6,8151	—0,1685	1,6155	14,863	— 5,29	0,7205
0,9999995	13,9653	495,42	6,8147	—0,2615	1,6136	14,769	— 5,51	0,5763
0,9999996	14,0500	495,87	6,8142	—0,3776	1,6119	14,653	— 5,77	0,4372
0,9999997	14,2359	496,54	6,8136	—0,6284	1,6096	14,401	— 6,34	0,2420
0,9999998	14,4608	496,54	6,8132	—0,9237	1,6084	14,106	— 7,03	$0,1212 \cdot 10^{-2}$
0,9999999	14,5496	496,54	6,8131	—1,0379	1,6081	13,991	— 7,29	$0,9290 \cdot 10^{-3}$
0,9999999	14,6677	496,54	6,8130	—1,1879	1,6078	13,841	— 7,63	0,6563
0,9999999	14,8433	496,54	6,8129	—1,4070	$1,6076 \cdot 10^{5}$	13,622	— 8,14	$0,3939 \cdot 10^{-3}$
0,9999999	16,3318	496,54	4,8300	—6,3469	$1,6719 \cdot 10^{8}$	6,699	—12,66	—
0,9999999	16,3400	496,54	4,6065	—6,8024	$9,9925 \cdot 10^{2}$	6,020	—12,94	—

Commas indicate decimal points.

TABLE X. MODEL 84 (t = 812,698 YEARS). /42

M_r/M	r, 10^9 cm	L_r, 10^{31} erg/sec	lg T	lg ρ	E, 10^{10} erg/g	lg P	ψ	ε, erg/g·sec
0,0000000	0,0000	0,0000	7,3626	6,3143	$6{,}6677 \cdot 10^6$	22,905	133,03	0,0000
$0{,}9943086 \cdot 10^{-2}$	1,1903	0,1540	7,3619	6,2286	5,9442	22,774	116,83	0,0000
$0{,}4870024 \cdot 10^{-1}$	1,9533	0,5384	7,3604	6,1847	5,6027	22,706	109,58	0,0000
0,1647288	3,0363	1,7663	7,3573	6,0799	4,8588	22,544	93,96	0,0000
0,3156323	3,9699	3,4616	7,3538	5,9559	4,0991	22,352	78,32	0,0000
0,5091430	4,9987	5,0646	7,3483	5,7814	3,2191	22,078	60,67	0,0000
0,6916000	6,0017	6,8766	7,3411	5,5695	2,3952	21,743	44,56	0,0000
0,8413974	7,0156	8,1385	7,3307	5,3008	1,6457	21,315	30,22	0,0000
0,9414594	8,0391	7,2817	7,3143	4,9403	$1{,}0010 \cdot 10^6$	20,738	18,04	0,0000
0,9753036	8,6431	5,9191	7,2997	4,6343	$6{,}5435 \cdot 10^5$	20,274	11,60	0,0000
0,9809841	8,7945	4,0652	7,2961	4,5471	5,8377	20,137	10,21	0,0000
0,9866013	8,9764	1,9853	7,2929	4,4299	5,0374	19,956	8,56	0,0000
0,9892830	9,0819	— 0,8201	7,2924	4,3541	4,5997	19,841	7,61	0,0000
0,9933444	9,2835	— 9,3011	7,2995	4,1878	3,8423	19,596	5,73	0,0000
0,9958784	9,4643	— 31,364	7,3259	4,0037	3,3021	19,346	3,95	0,0000
0,9973618	9,6237	— 152,36	7,3802	3,7985	3,0443	19,106	2,32	0,0000
0,9979523	9,7177	— 854,67	7,4441	3,6452	3,1234	18,964	1,27	0,0000
0,9982117	9,7731	— 3597,9	7,5025	3,5358	3,3547	18,885	0,58	0,0000
0,9982939	9,7939	— 5638,7	7,5266	3,4933	3,4704	18,858	0,36	0,0000
0,9983598	9,8122	— 8220,8	7,5475	3,4547	3,5952	18,834	0,12	0,0000
0,9983663	9,8141	— 8506,6	7,5496	3,4511	3,6056	18,832	0,10	0,0000
0,9983678	9,8145	— 8574,2	7,5501	3,4503	3,6102	18,832	$0{,}98 \cdot 10^{-1}$	0,0000

Commas indicate decimal points.

ORIGINAL PAGE IS
OF POOR QUALITY

TABLE X. CONT'D.

M_r/M	r, 10^8 cm	L_r, 10^{31} erg/sec	lg T	lg ρ	E, 10^{10} erg/g	lg P	ψ	ε, erg/g·sec
0,9983680	9,8146	— 8584,6	7,5502	3,4500	3,6089	18,831	$0,96 \cdot 10^{-1}$	0,0000
0,9984272	9,8423	—14461	7,5748	2,9981	9,7116	18,809	— 0,44	$3,5926 \cdot 10^{6}$
0,9984662	9,8753	— 5323,3	7,5871	2,9730	9,9417	18,794	— 0,55	5,0009
0,9985030	9,9075	5557,4	7,5870	2,9594	9,9233	18,780	— 0,69	$4,8151 \cdot 10^{6}$ *
0,9987438	10,122	9346,5	7,5026	2,9364	8,2687	18,678	— 0,31	$2,8117 \cdot 10^{5}$ *
0,9989435	10,310	8412,2	4,4631	2,8772	7,5499	18,579	— 0,31	63520 *
0,9992044	10,589	4755,0	7,4000	2,7826	6,5291	18,421	— 0,31	6634,0 *
0,9993920	10,825	2176,4	7,3415	2,6950	5,7065	18,275	— 0,31	1397,6 *
0,9995276	11,024	555,71	7,2876	2,6142	5,0404	18,141	— 0,31	576,67
0,9996948	11,333	415,07	7,2325	2,4456	4,3957	17,913	— 0,54	233,60
0,9997940	11,585	424,87	7,1839	2,2952	3,9084	17,711	— 0,75	107,36
0,9998973	11,982	428,27	7,1015	2,0315	3,1974	17,360	— 1,11	27,332
0,9999906	12,996	461,41	6,8771	1,1024	1,8729	16,199	— 2,55	0,2962
0,9999977	13,471	480,37	6,8188	0,4792	1,6287	15,515	— 3,80	$0,3430 \cdot 10^{-1}$
0,9999986	13,633	483,93	6,8117	0,2502	1,5999	15,278	— 4,32	0,1840
0,9999991	13,781	486,13	6,8083	$0,3772 \cdot 10^{-1}$	1,5874	15,062	— 4,80	$0,1073 \cdot 10^{-1}$
0,9999992	13,821	486,56	6,8077	$-0,1841 \cdot 10^{-1}$	1,5851	15,006	— 4,92	$0,9342 \cdot 10^{-2}$
0,9999993	13,866	487,03	6,8072	$-0,8201 \cdot 10^{-1}$	1,5846	14,941	— 5,07	0,7995
0,9999994	13,923	487,51	6,8066	—0,1621	1,5838	14,861	— 5,25	0,6582
0,9999995	13,989	487,98	6,8060	—0,2549	1,5819	14,767	— 5,46	0,5265
0,9999996	14,072	488,46	6,8055	—0,3707	1,5800	14,651	— 5,73	0,3994
0,9999997	14,254	489,19	6,8049	—0,6209	1,5776	14,400	— 6,30	0,2211
0,9999998	14,475	489,19	6,8045	—0,9154	1,5763	14,105	— 6,98	$0,1110 \cdot 10^{-2}$
0,9999999	14,561	489,19	6,8044	—1,0292	1,5760	13,991	— 7,24	$0,8509 \cdot 10^{-3}$
0,9999999	14,677	489,19	6,8043	—1,1787	1,5758	13,842	— 7,58	0,6008
0,9999999	14,849	489,19	6,8042	—1,3971	$1,5755 \cdot 10^{5}$	13,623	— 8,08	$0,3617 \cdot 10^{-3}$
0,9999999	16,307	489,19	4,8288	—6,3467	1666,9	6,6983	—12,66	—
0,9999999	16,315	489,19	4,6052	—6,8032	996,31	6,0181	—12,93	—

Commas indicate decimal points.

TABLE XI. MODEL 22e

M_r/M	r, 10^9 cm	L_r, 10^{31} erg/sec	lg T	lg ρ	E, 10^{10} erg/g	lg P	φ	ε_n, erg/g·sec
0,0000000	0,0000	0,0000	7,3300	6,3165	$6,6819 \cdot 10^6$	22,908	143,90	0,0000
$0,9949866 \cdot 10^{-2}$	1,1883	$0,9656 \cdot 10^{-1}$	7,3294	6,2307	5,9566	22,777	126,32	0,0000
$0,4873119 \cdot 10^{-1}$	1,9500	0,3305	7,3284	6,1869	5,6143	22,709	118,38	0,0000
0,1648322	3,0312	1,0586	7,3262	6,0821	4,8687	22,547	101,28	0,0000
0,3158297	3,9632	2,0853	7,3237	5,9582	4,1070	22,355	84,22	0,0000
0,5094615	4,9901	3,3678	7,3199	5,7836	3,2249	22,081	65,00	0,0000
0,6920323	5,9913	4,5518	7,3146	5,5717	2,3988	21,746	47,53	0,0000
0,8419233	7,0034	5,4785	7,3066	5,3031	1,6473	21,318	32,04	0,0000
0,9420480	8,0254	6,0587	7,2929	4,9421	$1,0004 \cdot 10^6$	20,740	19,00	0,0000
0,9759133	8,6265	6,0641	7,2781	4,6500	$6,7660 \cdot 10^5$	20,273	12,49	0,0000
0,9815973	8,7757	5,9780	7,2731	4,5477	5,7907	20,134	10,78	0,0000
0,9872181	8,9581	6,0269	7,2659	4,4294	4,9710	19,950	9,11	0,0000
0,9899015	9,0643	6,0499	7,2609	4,3527	4,6175	19,832	8,18	0,0000
0,9939654	9,2671	6,0784	7,2483	4,1857	3,7005	19,578	6,47	0,0000
0,9965010	9,4487	6,0958	7,2334	4,0052	3,0338	19,311	5,00	0,0000
0,9979853	9,6059	6,1060	7,2181	3,8147	2,5176	19,040	3,77	0,0000
0,9985761	9,6944	6,1091	7,2088	3,6888	2,2610	18,867	3,09	0,0000
0,9988358	9,7431	6,1104	7,2037	3,6128	2,1317	18,765	2,71	0,0000
0,9989179	9,7603	6,1107	7,2020	3,5844	2,0883	18,728	2,58	0,0000
0,9989839	9,7750	6,1110	7,2006	3,5599	2,0525	18,696	2,47	0,0000
0,9989904	9,7765	6,1110	7,2005	3,5574	2,0478	18,693	2,46	0,0000
0,9989919	9,7768	6,1110	7,2004	3,5567	2,0473	18,692	2,46	0,0000

Commas indicate decimal points.

TABLE XI. CONT'D.

M_r/M	$r, 10^8$ cm	L_r, 10^{31} erg/sec	lg T	lg ρ	E, 10^{10} erg/g	lg P	ψ	ε, erg/g·sec
0,9989921	9,7769	6,1110	7,2004	3,5566	2,0472	18,692	2,45	0,0000
0,9990513	9,7978	6,1115	7,1991	3,1534	4,8222	18,661	1,98	941,39
0,9990904	9,8208	9,6773	7,1979	3,1357	4,7787	18,639	1,91	893,37
0,9991272	9,8433	12,864	7,1963	3,1188	4,7306	18,618	1,85	846,39
0,9993681	10,0130	28,740	7,1758	2,9902	4,3565	18,453	1,45	520,76
0,9995680	10,1983	36,194	7,1412	2,8463	3,9124	18,263	1,10	272,25
0,9997265	10,4002	39,021	7,0950	2,6788	3,4235	18,037	0,76	119,62
0,9998290	10,5857	39,806	7,0474	2,5078	3,0058	17,810	0,44	50,513
0,9998601	10,6594	39,936	7,0277	2,4344	2,8478	17,713	0,30	34,962
0,9998872	10,7351	40,014	7,0078	2,3536	2,7031	17,609	0,15	23,606
0,9999046	10,7916	40,049	6,9933	2,2913	2,5963	17,530	$0,28 \cdot 10^{-1}$	17,554
0,9999239	10,8648	40,077	6,9750	2,2062	2,4673	17,422	— 0,14	11,864
0,9999349	10,9140	40,088	6,9632	2,1454	2,3930	17,348	— 0,26	9,0747
0,9999385	10,9316	40,092	6,9592	2,1233	2,3661	17,321	— 0,31	8,2463
0,9999472	10,9777	40,098	6,9490	2,0642	2,2999	17,250	— 0,43	6,4280
0,9999527	11,0102	40,101	6,9422	2,0214	2,2557	17,199	— 0,51	5,3994
0,9999568	11,0371	40,103	6,9369	1,9851	2,2217	17,156	— 0,59	4,6776
0,9999600	11,0591	40,105	6,9328	1,9549	2,1954	17,120	— 0,65	4,1629
0,9999672	11,1155	40,107	6,9230	1,8744	2,1381	17,028	— 0,83	3,0902
0,9999768	11,2112	40,110	6,9095	1,7326	2,0529	16,869	— 1,14	1,8993
0,9999838	11,3070	40,111	6,8998	1,5828	1,9956	16,707	— 1,48	1,1936
0,9999901	11,4328	40,111	6,8918	1,3791	1,9476	16,493	— 1,95	0,6736
0,9999926	11,5062	40,111	6,8890	1,2584	1,9278	16,367	— 2,22	0,4905
0,9999948	11,5914	40,111	6,8869	1,1168	1,9149	16,223	— 2,55	0,3426
0,9999968	11,6963	40,111	6,8853	0,9431	1,9041	16,047	— 2,96	0,2236
0,9999985	11,8387	40,111	6,8842	0,7091	$1,8958 \cdot 10^6$	15,811	— 3,50	0,1272
0,9999999	13,0045	40,111	4,6064	—6,3661	998,98	6,457	—11,94	—
0,9999999	13,0070	40,111	4,3829	—7,0142	597,08	5,585	—12,66	—

Commas indicate decimal points.

TABLE XII. MODEL 31d. /46

M_r/M	r, 10^9 cm	L_r, 10^{31} erg/sec	lg T	lg ρ	E, 10^{16} erg/g	lg P	Ψ	ε, erg/g·sec
0,0000000	0,0000	0,0000	7,3433	6,3153	$6,6735 \cdot 10^6$	22,906	139,30	0,0000
$0,9947787 \cdot 10^{-2}$	1,1894	$0,9355 \cdot 10^{-1}$	7,3428	6,2296	5,9491	22,775	122,26	0,0000
$0,4872138 \cdot 10^{-1}$	1,9518	0,3154	7,3419	6,1857	5,6073	22,708	114,52	0,0000
0,1647991	3,0340	0,9816	7,3399	6,0809	4,8626	22,546	97,95	0,0000
0,3157666	3,9670	1,8795	7,3378	5,9569	4,1020	22,353	81,37	0,0000
0,5093597	4,9950	2,9244	7,3346	5,7823	3,2210	22,079	62,71	0,0000
0,6918940	5,9974	3,7994	7,3304	5,5703	2,3963	21,744	45,73	0,0000
0,8417552	7,0111	4,3982	7,3244	5,3014	1,6460	21,316	30,68	0,0000
0,9418597	8,0352	4,7090	7,3145	4,9400	$1,0006 \cdot 10^6$	20,738	18,02	0,0000
0,9757184	8,6410	4,7929	7,3043	4,6323	$6,5356 \cdot 10^5$	20,271	11,43	0,0000
0,9814012	8,7934	4,8047	7,3009	4,5442	5,8273	20,134	10,05	0,0000
0,9870209	8,9766	4,8151	7,2960	4,4259	5,0192	19,950	8,44	0,0000
0,9897037	9,0831	4,8234	7,2926	4,3493	4,5740	19,833	7,54	0,0000
0,9937669	9,2868	4,8330	7,2846	4,1827	3,7806	19,584	5,90	0,0000
0,9963020	9,4687	4,8379	7,2757	4,0037	3,1449	19,325	4,49	0,0000
0,9977859	9,6249	4,8390	7,2675	3,8188	2,6682	19,069	3,33	0,0000
0,9983767	9,7117	4,8399	7,2633	3,6999	2,4413	18,911	2,70	0,0000
0,9986362	9,7586	4,8403	7,2612	3,6303	2,3296	18,821	2,37	0,0000
0,9987184	9,7750	4,8404	7,2605	3,6050	2,2929	18,789	2,25	0,0000
0,9987844	9,7890	4,8404	7,2600	3,5825	2,2643	18,761	2,15	0,0000
0,9987909	9,7904	4,8404	7,2599	3,5803	2,2602	18,758	2,14	0,0000
0,9987924	9,7907	4,8404	7,2599	3,5799	2,2600	18,758	2,14	0,0000

Commas indicate decimal points.

TABLE XII. CONT'D.

M_r/M	r, 10^8 cm	L_r, 10^{31} erg/sec	lg T	lg ρ	E, 10^{10} erg/g	lg P	ψ	ε, erg/g·sec
0,9987926	9,7908	4,8404	7,2599	3,5798	2,2599	18,758	2,14	0,0000
0,9988518	9,8105	4,8405	7,2594	3,1753	5,3966	18,731	1,69	1680,0
0,9988908	9,8324	11,240	7,2588	3,1600	5,3599	18,713	1,63	1611,5
0,9989276	9,8536	17,019	7,2579	3,1453	5,3227	18,695	1,58	1542,7
0,9991685	10,0095	47,559	7,2440	3,0386	5,0132	18,563	1,24	1054,6
0,9993683	10,1700	64,165	7,2206	2,9296	4,6497	18,421	0,98	663,86
0,9995268	10,3291	72,257	7,1921	2,8180	4,2844	18,274	0,74	398,07
0,9996292	10,4557	75,507	7,1666	2,7259	3,9902	18,151	0,56	255,94
0,9996875	10,5404	76,775	7,1484	2,6619	3,7966	18,065	0,45	187,01
0,9997388	10,6256	77,583	7,1293	2,5951	3,6048	17,976	0,33	134,32
0,9997840	10,7124	78,089	7,1092	2,5235	3,4245	17,882	0,20	94,199
0,9998440	10,8525	78,515	7,0758	2,4021	3,1334	17,722	$-0,88\cdot10^{-4}$	51,607
0,9998728	10,9356	78,637	7,0561	2,3254	2,9722	17,622	— 0,14	35,596
0,9999000	11,0296	78,715	7,0344	2,2326	2,8129	17,506	— 0,32	23,073
0,9999166	11,0975	78,748	7,0197	2,1622	2,7044	17,418	— 0,45	16,866
0,9999227	11,1253	78,758	7,0141	2,1324	2,6626	17,382	— 0,50	14,842
0,9999317	11,1704	78,770	7,0054	2,0831	2,5993	17,322	— 0,60	12,087
0,9999400	11,2163	78,779	6,9972	2,0310	2,5414	17,260	— 0,71	9,8219
0,9999472	11,2610	78,785	6,9899	1,9780	2,4937	17,199	— 0,82	8,0328
0,9999527	11,2990	78,789	6,9841	1,9330	2,4536	17,147	— 0,92	6,8010
0,9999589	11,3436	78,793	6,9777	1,8784	2,4098	17,084	— 1,03	5,5902
0,9999638	11,3897	78,795	6,9718	1,8211	2,3700	17,020	— 1,15	4,5856
0,9999785	11,5598	78,800	6,9553	1,5987	2,2617	16,777	— 1,64	2,2743
0,9999901	11,8030	78,802	6,9438	1,2645	2,1853	16,428	— 2,41	0,9124
0,9999968	12,1288	78,802	6,9391	0,8144	2,1518	15,971	— 3,45	0,3008
0,9999985	12,3080	78,802	6,9382	0,5724	$2,1403\cdot10^5$	15,727	— 4,01	0,1690
0,9999999	13,7564	78,802	4,6675	—6,3609	1149,9	6,523	—12,13	—
0,9999999	13,7596	78,802	4,4440	—6,9470	687,31	5,713	—12,71	—

Commas indicate decimal points.

TABLE XIII. MODEL 50f.

M_r/M	r, 10^8 cm	L_r, 10^{33} erg/sec	lg T	lg ρ	E, 10^{10} erg/g	lg P	Ψ	ε, erg/g sec
0,0000000	0,0000	0,0000	7,3618	6,3143	$6,6673 \cdot 10^6$	22,905	133,28	0,0000
$0,9944852 \cdot 10^{-2}$	1,1903	0,1549	7,3610	6,2285	5,9437	22,773	117,05	0,0000
$0,4870782 \cdot 10^{-1}$	1,9534	0,5408	7,3596	6,1847	5,6023	22,706	109,79	0,0000
0,1647538	3,0364	1,7312	7,3565	6,0799	4,8584	22,544	94,14	0,0000
0,3156798	3,9701	3,3493	7,3530	5,9559	4,0987	22,352	78,46	0,0000
0,5092197	4,9989	5,2278	7,3476	5,7813	3,2187	22,078	60,77	0,0000
0,6917041	6,0019	6,7259	7,3405	5,5694	2,3948	21,743	44,61	0,0000
0,8415241	7,0160	7,1028	7,3306	5,3006	1,6453	21,315	30,21	0,0000
0,9416012	8,0401	4,5191	7,3177	4,9397	$1,0007 \cdot 10^6$	20,737	17,89	0,0000
0,9754505	8,6464	$0,4503 \cdot 10^{-1}$	7,3123	4,6322	$6,5540 \cdot 10^5$	20,273	11,22	0,0000
0,9811318	8,7976	— 2,2061	7,3130	4,5441	5,8550	20,136	9,77	0,0000
0,9867498	8,9809	— 4,9268	7,3162	4,4252	5,0663	19,954	8,04	0,0000
0,9894320	9,0876	— 6,5027	7,3197	4,3479	4,6385	19,838	7,06	0,0000
0,9934940	9,2924	—10,228	7,3303	4,1784	3,8969	19,593	5,24	0,0000
0,9960284	9,4769	—13,721	7,3443	3,9942	3,3414	19,342	3,71	0,0000
0,9975120	9,6372	—16,824	7,3567	3,8051	2,9595	19,100	2,52	0,0000
0,9981025	9,7265	—18,418	7,3622	3,6871	2,7896	18,957	1,93	0,0000
0,9983620	9,7745	—19,195	7,3646	3,6199	2,7113	18,877	1,64	0,0000
0,9984442	9,7913	—19,456	7,3653	3,5959	2,6850	18,849	1,53	0,0000
0,9985101	9,8054	—19,673	7,3659	3,5756	2,6614	18,825	1,45	0,0000
0,9985166	9,8068	—19,694	7,3660	3,5736	2,6602	18,822	1,44	0,0000
0,9985181	9,8072	—19,699	7,3660	3,5730	2,6604	18,822	1,44	0,0000
0,9985184	9,8073	-19,700	7,3660	3,5730	2,6604	18,822	1,44	0,0000

Commas indicate decimal points.

TABLE XIII. CONT'D.

M_r/M	$r, 10^8$ cm	L_r, 10^{31} erg/sec	lg T	lg ρ	E, 10^{10} erg/g	lg P	ψ	ε, erg/g·sec
0,9985775	9,8274	—20,061	7,3665	3,1605	6,5290	18,799	1,02	7312,6
0,9986166	9,8499	—7,5400	7,3667	3,1467	6,5037	18,784	0,97	7078,8
0,9986533	9,8716	32,596	7,3663	3,1337	6,4747	18,769	0,93	6794,8
0,9988942	10,0285	159,99	7,3559	3,0430	6,2163	18,660	0,67	4312,7
0,9990939	10,1829	223,24	7,3375	2,9584	5,8818	18,552	0,49	2492,4
0,9993548	10,4323	263,37	7,3014	2,8192	5,3366	18,370	0,22	1090,2
0,9995425	10,6678	275,94	7,2631	2,6823	4,8224	18,189	$-0,11\cdot10^{-1}$	536,24
0,9996781	10,8911	280,05	7,2230	2,5452	4,3476	18,007	— 0,23	272,08
0,9997691	11,0873	281,15	7,1850	2,4159	3,9594	71,837	— 0,43	144,17
0,9998453	11,3060	281,30	7,1407	2,2625	3,5400	17,635	— 0,68	67,645
0,9998751	11,4155	281,22	7,1180	2,1791	3,3523	17,528	— 0,80	45,141
0,9999251	11,6602	280,93	7,0700	1,9780	2,9732	17,275	— 1,13	17,857
0,9999446	11,7962	280,75	7,0464	1,8548	2,8055	17,127	— 1,35	10,601
0,9999658	12,0036	280,51	7,0166	1,6518	2,5998	16,891	— 1,73	4,8743
0,9999716	12,0811	280,43	7,0079	1,5709	2,5448	16,800	— 1,91	3,6879
0,9999745	12,1258	280,39	7,0036	1,5235	2,5166	16,748	— 2,00	3,1543
0,9999781	12,1869	280,33	6,9984	1,4577	2,4821	16,676	— 2,14	2,5605
0,9999800	12,2237	280,30	6,9956	1,4173	2,4650	16,633	— 2,22	2,2627
0,9999831	12,2937	280,25	6,9911	1,3397	2,4370	16,550	— 2,40	1,7983
0,9999870	12,3980	280,18	6,9859	1,2230	2,4025	16,428	— 2,65	1,2939
0,9999890	12,4671	280,15	6,9832	1,1448	2,3878	16,346	— 2,83	1,0477
0,9999916	12,5735	280,13	6,9802	1,0244	2,3669	16,222	— 3,09	0,7651
0,9999945	12,7421	280,13	6,9772	0,8340	2,3478	16,029	— 3,53	0,4742
0,9999970	12,9700	280,13	6,9750	0,5812	2,3302	15,773	— 4,12	0,2564
0,9999990	13,3578	280,13	6,9735	0,1633	$2,3260\cdot10^5$	15,353	— 5,08	$0,9515\cdot10^{-1}$
0,9999999	15,2395	280,13	4,7830	—6,3438	1500,1	6,655	—12,49	—
0,9999999	15,2452	280,13	4,5594	—6,8328	896,59	5,943	—12,85	—

Commas indicate decimal points.

II. SOLAR PHYSICS /50

EFFECT OF A PROGRESSIVE SOUND WAVE ON THE PROFILES OF SPECTRAL LINES. II. ASYMMETRY OF FAINT FRAUNHOFER LINES

R. I. KOSTYK

ABSTRACT. The absorption coefficient profile is calculated for lines of different chemical elements in a medium with progressive sound waves. Calculations show that (1) the degree and direction of asymmetry depend on the atomic ionization potential and the potential of lower level excitation of the individual line; (2) the degree of asymmetry of a line decreases from the center toward the limb of the solar disc; (3) turbulent motions "suppress" the asymmetry.

At the present time two explanations are proposed for the asymmetry of Fraunhofer lines: the influence of convective motions and that of sound waves.

The asymmetry of Fraunhofer lines due to progressive sound waves is examined in the present paper.

Regions of elevated and lowered temperature appear when a progressive sound wave is propagated in the photosphere. All the "thickenings" are propagated in one direction and the "thinnings" in another, that is, the number of absorbing particles moving toward the observer and in the opposite direction are not the same, this resulting in asymmetry of the line.

The outline of the absorption coefficient for a medium with a progressive sound wave has been calculated by Eriksen and Maltby [1] and by Babiy and Al'tman [2].

For the profile of the line we have obtained an expression somewhat different from that in [1] and [2]. Calculations were performed for lines of different chemical elements. Turbulent motions were taken into account.

As we know, the absorption coefficient in the line is defined by the formula

$$\sigma(\nu) = \frac{\sqrt{\pi}\, e^2 N_{r,i}}{m_e c \Delta\nu_D} a\left(\frac{\nu - \nu_0'}{\Delta\nu_D}\right), \qquad (1)$$

in which $N_{r,i}$ is the number of particles of an r-times ionized atom in the ith state. The remaining notation is that universally employed.

In the photosphere, in which we assume progressive sound waves to be propagated, quantities $N_{r,i}$, $\Delta\nu_D$, ν_0' will depend on time t and altitude h, since temperature T and the directional velocities of the absorbing particles,

v, undergo variation as a wave is propagated in the photosphere. The problem consists of finding the law of variation in these quantities.

According to [3], the wave propagation process being assumed to be adiabatic, we have

$$T(h,t)=T^0\left[1+\frac{\gamma-1}{\gamma}\frac{\Delta p_m}{P_g^0}\sin(h-v_s t)\right], \tag{2}$$

in which γ is the adiabatic constant; Δp_m is the amplitude of pressure variation; v_s is the velocity of sound; and P_g^0, T_0 are the equilibrium values of pressure and temperature (in what follows all equilibrium values of the parameters will be designated by a superscript zero).

The number of absorbing particles can now easily be found from the Sach--Boltzmann equation:

$$\frac{N_{0,i}}{N_{0,i}^0}(h,t)=\frac{1+\frac{N_1}{N_0}(T^0)}{1+\frac{N_1}{N_0}(T)}\frac{B_0(T^0)}{B_0(T)}e^{\frac{\chi_{0,i}}{kT^0}-\frac{\chi_{0,i}}{kT}}, \tag{3}$$

$$\frac{N_{1,i}}{N_{1,i}^0}(h,t)=\frac{1+\frac{N_0}{N_1}(T^0)}{1+\frac{N_0}{N_1}(T)}\frac{B_1(T^0)}{B_1(T)}e^{\frac{\chi_{0,i}}{kT^0}-\frac{\chi_{0,i}}{kT}}, \tag{4}$$

in which

$$\frac{N_1}{N_0}(T)=\frac{(2\Pi m)^{3/2}(kT)^{5/2}}{P_e}\frac{2B_1(T)}{B_0(T)}e^{-\frac{\chi_0}{kT}}.$$

In these relations we have disregarded the second and higher stages of atomic ionization, which are insignificant in the photosphere of the Sun.

The Doppler half-width equals

$$\Delta\nu_D=\frac{\nu_0}{c}\sqrt{\frac{2RT}{A}+\xi^2}=\frac{\nu_0}{c}\sqrt{\frac{2RT^0}{A}\varkappa^{-2}(h,t)+\xi^2}. \tag{5}$$

In this equation

$$\varkappa(h,t)=\left[1+\frac{\gamma-1}{\gamma}\frac{\Delta p_m}{P_g^0}\sin(h-v_s t)\right]^{-1/2},$$

ξ being the turbulent velocity.

Lastly, central frequency ν_0' along the line of sight will vary in accordance with the law

$$\nu_0'=\nu_0+\nu_0\frac{v_m}{c}\sin(h-v_s t)\cos\Theta,$$

in which v_m is the amplitude of the particle velocity and Θ the angle between the line of sight and the direction of wave propagation.

Since the velocity of sound equals

$$v_s = \sqrt{\gamma \frac{2RT^0}{\bar{\mu}}},$$

$$a\left(\frac{\nu - \nu_0'}{\Delta\nu_D}\right) = a\left[x\frac{\eta^0(h,t)}{\eta(h,t)} - \left(\frac{RT^0}{\gamma\mu}\right)^{1/2}\frac{\Delta p_m}{P_g^0}\frac{1}{\eta(h,t)}\sin(h - v_s t)\cos\Theta\right], \quad (6)$$

in which the following notation has been introduced:

$$x = \frac{\nu - \nu_0}{\Delta\nu_D};\ \eta(h,t) = \left[\frac{2RT^0}{A}x^{-2}(h,t) + \xi^2\right]^{1/2},\ \eta^0(h,t) = \left[\frac{2RT^0}{A} + \xi^2\right]^{1/2}.$$

Inserting (3)-(6) in (1), we have

$$\sigma(x,h,t) = \frac{\sqrt{\Pi}e^2 f N_{r,i}^0}{m_e \nu_0}\frac{N_{r,i}}{N_{r,i}^0}\frac{1}{\eta(h,t)}a\left[x\frac{\eta^0(h,t)}{\eta(h,t)} - \left(\frac{RT^0}{\gamma\mu}\right)^{1/2}\frac{\Delta p_m}{P_g^0}\frac{1}{\eta(h,t)}\sin(h - v_s t)\cos\Theta\right].$$

From the foregoing we find

$$\frac{\sigma(x)}{\sigma(0)} = \left\{\int_0^{2\pi}\frac{N_{r,i}}{N_{r,i}^0}(h,t)\frac{1}{\eta(h,t)}a\left[-\left(\frac{RT^0}{\gamma\mu}\right)^{1/2}\frac{\Delta p_m}{P_g^0}\frac{1}{\eta(h,t)}\sin(h - v_s t)\cos\Theta\right]\times\right.$$

$$\left.\times\, d(h - v_s t)\right\}^{-1}\int_0^{2\pi}\frac{N_{r,i}}{N_{r,i}^0}(h,t)\frac{1}{\eta(h,t)}a\left[x\frac{\eta^0(h,t)}{\eta(h,t)} - \left(\frac{RT^0}{\gamma\mu}\right)^{1/2}\frac{\Delta p_m}{P_g^0}\frac{1}{\eta(h,t)}\sin(h - v_s t)\cos\Theta\right]d(h - v_s t). \quad (7)$$

In this equation

$$\sigma(0) = \frac{\sqrt{\Pi}e^2 f N_{r,i}^0}{m_e c}\int_0^{2\pi}\frac{N_{r,i}}{N_{r,i}^0}(h,t)\frac{1}{\eta(h,t)}a\left[-\left(\frac{RT^0}{\gamma\mu}\right)^{1/2}\times\right.$$

$$\left.\times\frac{\Delta p_m}{P_g^0}\frac{1}{\eta(h,t)}\sin(h - v_s t)\cos\Theta\right]d(h - v_s t).$$

This is the final formula with which the absorption coefficient profile was calculated. In the calculations we adopted the Doppler absorption coefficient and assumed the photosphere of the Sun to be isothermal, and γ = /54
= 5/3 and $\bar{\mu}$ = 1.33. The electron pressure versus temperature at an assigned gas pressure was taken from [4]. The equilibrium values of parameters P_g^0 and P_e^0 for temperature T^0 selected were found in accordance with the Bilderberg model of the solar atmosphere [5]. The results of the calculations have been presented in graphic form.

Figures 1 and 2 show the outline of the absorption coefficient plotted against the amplitude of variation in pressure, the equilibrium temperature, the position on the disc of the Sun, and the turbulent velocity value. The dimensionless frequency is plotted along the X-axis.

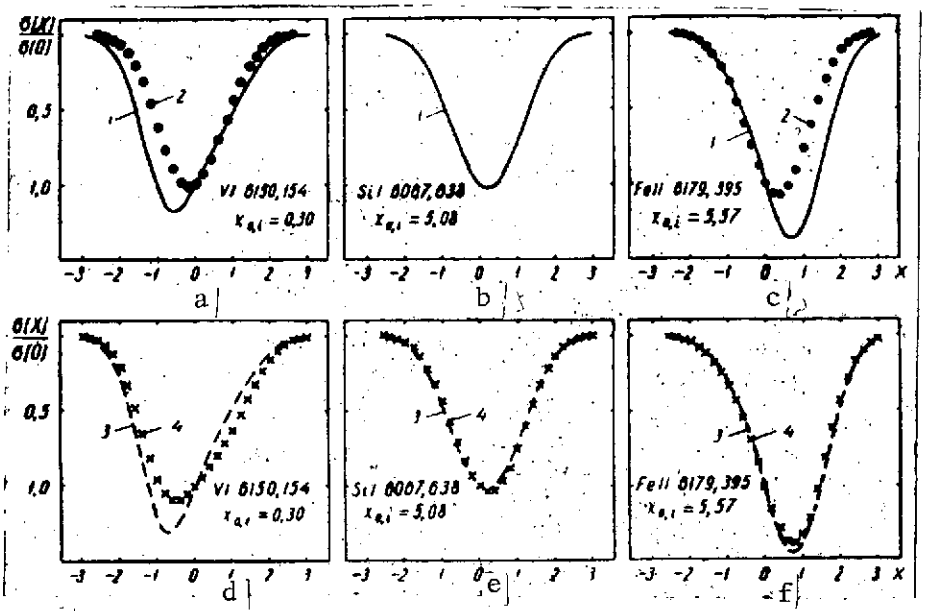

Figure 1. Outline of Absorption Coefficient Versus Variation in Pressure and Equilibrium Temperature (cos Θ = 1). a, b, c, at T^0 = 6,000° and ξ = 0.5 km/sec; d, e, f, at $\frac{\Delta p_m}{p_g^0}$ = 0.3 and ξ = 0.

1, $\frac{\Delta p_m}{p_g^0}$ = 0.3; 2, $\frac{\Delta p_m}{p_g^0}$ = 0.2; 3, T^0 = 5,700°; 4, T^0 = 6,300°.

/52

The axes of symmetry of the profiles of various chemical element lines are shown in Figures 3, 4. Milliangstroems are entered on the X-axis.

The following conclusions may be drawn on the basis of the calculations performed:

1. The magnitude and nature of the asymmetry depend on the atomic ionization potential and the excitation potential of the lower level of the absorption line under considertion.

2. The asymmetry decreases from the center toward the edge of the solar disc.

3. Turbulent motions "suppress" the asymmetry.

A comparison will be made between the calculated and the observed data in a future paper.

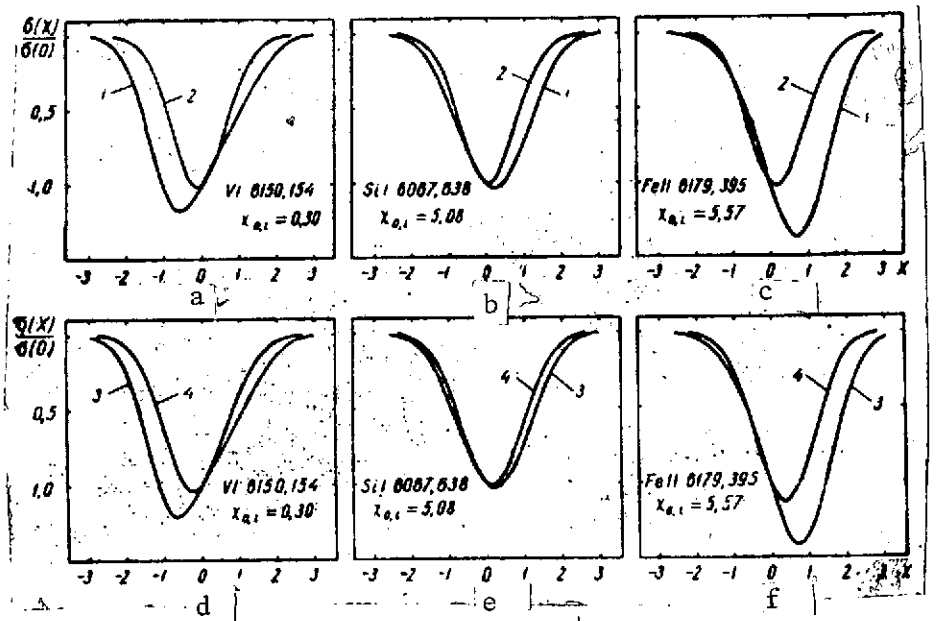

Figure 2. Outline of Absorption Coefficient Versus Angle Between Direction of Wave Propagation and Line of Sight and Versus Turbulent Velocity Value $\left(T^0 = 6{,}000°\ \frac{\Delta p_m}{p_g^0} = 0.3\right)$.

a, b, c, at $\xi = 0.5$; d, e, f, at $\cos\Theta = 1$; 1, $\cos\Theta = 1$; 2, $\cos\Theta = 0.28$; 3, $\xi = 0$; 4, $\xi = 2$ km/sec.

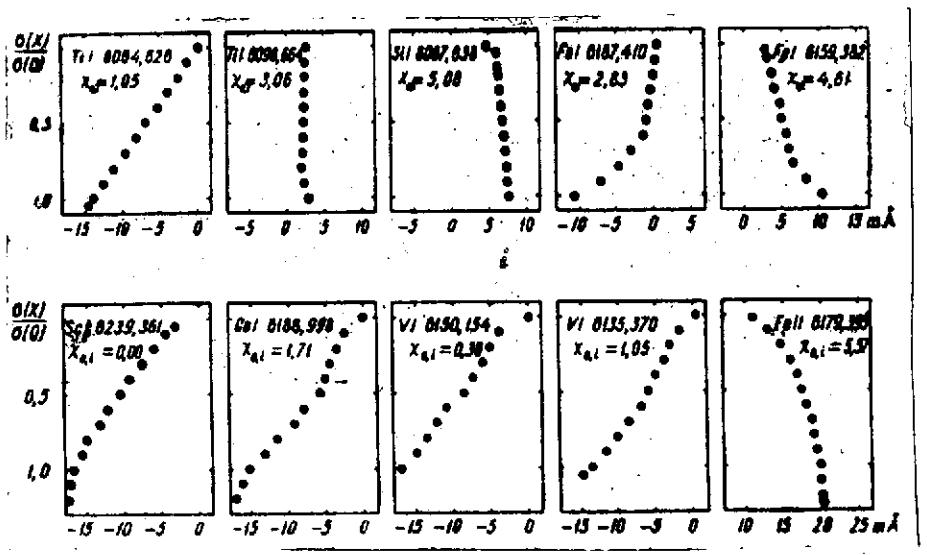

Figure 3. Axis of Symmetry of Absorption Coefficient Outline $\left(\frac{\Delta p_m}{p_g^0} = 0.3;\ \cos\Theta = 1;\ T^0 = 6{,}000°;\ \xi = 0.5\ \frac{\text{km}}{\text{sec}}\right)$.

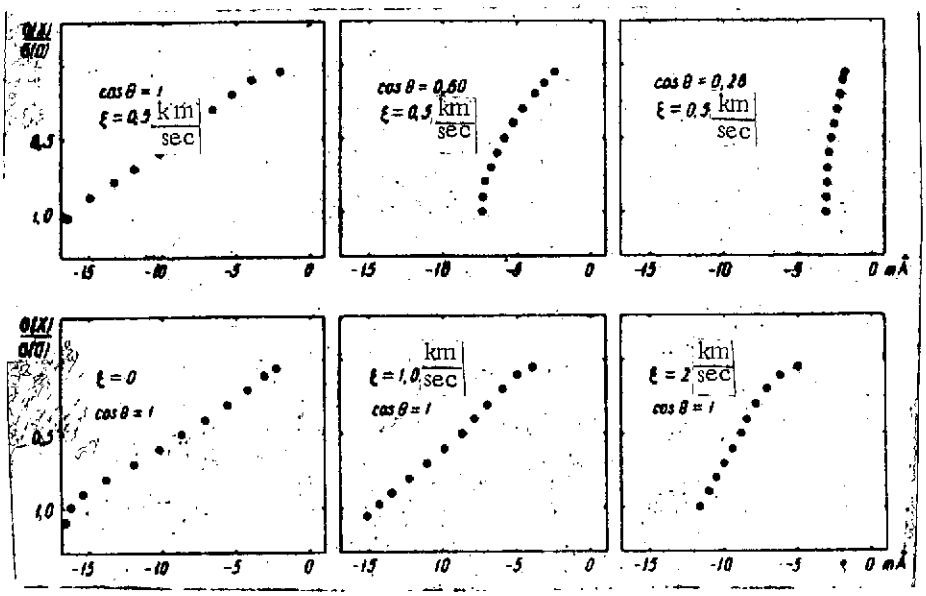

Figure 4. Axis of Symmetry of Absorption Coefficient Outline (VI 6,150,154; $X_{0.1}$ = 0.30; T^0 = 6,000°; $\frac{\Delta p_m}{p^0_g}$ = 0.3) for Various Positions on the Disc of the Sun (Top) and At Various Turbulent Velocities (Bottom).

REFERENCES

1. Eriksen, G. and P. Maltby, *Ap. J.*, Vol. 148, p. 833, 1967.
2. Babiy, B. T. and A. D. Al'tman, *Solnechnyye Dannyye* [Solar Data], Vol. 5, p. 103, 1969.
3. Landau, L. D. and E. M. Lifshits, *Mekhanika Sploshnykh Sred.* [Mechanics of Solids], Moscow, GITTL Press, 1951.
4. Grinsteyn, Dzh. L., *Zvezdnyye Atmosfery* [Stellar Atmospheres], IL Press, Moscow, 1963.
5. Quingerich, O. and C. de Yager, *Solar Phys.*, Vol. 3, p. 1, 1968.

N75 21167

EFFECT OF DEVIATION FROM LOCAL THERMODYNAMIC EQUILIBRIUM ON THE GOLDBERG-UNNO METHOD

/54

V. I. Troyan

ABSTRACT. The dependence of turbulent velocity ξ_t on depth $\tau^0_{(5000\ \text{Å})}$ was studied by use of the Goldberg-Unno method, with allowance made for the influence of deviation from the local thermodynamic equilibrium. It was found that allowance for deviation from local thermodynamic equilibrium displaces the curve of dependence of turbulent velocity ξ_t on $\tau^0_{(5000\ \text{Å})}$ both along the axis ξ_t ($\Delta\xi_t \simeq 1.5$ km/sec) and along the axis $\tau^0_{(5000\ \text{Å})}$ ($\Delta\tau^0 \simeq 0.05$).

The present article is a continuation of a project begun in the GAO of the Academy of Sciences of the Ukrainian SSR relating to study of the errors introduced by various distorting factors into the Goldberg-Unno method (determination of turbulent velocities in the solar photosphere). In the initial stage study was devoted to errors resulting from disregard of the instrument circuit effect and of radiation attenuation [1, 2]. The chief finding resulting from these studies is that allowance for the factors in question has no effect on the /55
nature of variation in turbulent velocity ξ_t with optical depth $\tau^0_{(5000\text{Å})}$, but in this instance the turbulent velocity value becomes smaller in value.

Formulation of the Problem. We had previosuly assumed that the assumptions underlying the Goldberg-Unno method are satisfied. These assumptions are the following [3]:

1) two lines of a multiplet have the same excitation temperature;

2) the source function does not depend on the frequency;

3) the absorption coefficient in the line does not depend on the optical depth.

The absorption coefficient for lines A and B may be assumed to be equal only when they refer to the same optical depth. Indeed this is emphasized by the first assumption. When the local thermodynamic equilibrium conditions are satisfied in the layers of the photosphere in which the absorption line is formed, this assumption is unquestionably satisfied; it is not apparent in the event of deviation from local thermodynamic equilibrium, and for this reason additional substantiation must be provided for it. Failure to satisfy this assumption may lead to considerable errors in determination of $\Delta\lambda_D$, since absorption coefficients referring to different depths are set to be equal. These errors can be allowed for if we are able to determine the value of T_{exc} for both lines and compare them. Whenever $T_{exp\ A} \neq T_{exc\ B}$, we must elaborate and apply a specific procedure enabling us to determine with relative ease and

speed the relationship between residual intensity r_λ and optical depth $\varepsilon_{0\lambda}$. When $T_{exc\ A} \neq T_{exc\ B}$ we can select the values of $r_{\lambda A}$ and $r_{\lambda B}$, and consequently of $\Delta\lambda_A$ and $\Delta\lambda_B$ corresponding to the same optical depth τ_λ^0.

We take the expression for source function S_λ obtained by theoretical calculations based on detailed study of radiation and absorption processes, with allowance made for collisions. Jeffries [4] concerned himself with study of these processes. In the case of coherent scattering, if it is assumed that the profiles of the absorption and radiation coefficients are equal, it follows from [4] that the source function may be represented by the Planck function at $T = T^*_{exc}$:

$$I_\lambda(\mu) \cong S_\lambda(\bar{t}_\lambda) \cong B_\lambda(T^*_{exc}) \text{ when } (\bar{t}_\lambda \simeq \mu = \cos\theta). \tag{1}$$

In this equation T^*_{exc} is the excitation temperature of the absorption line at the depth of occurrence of the effective layer responsible for emergent intensity $I_\lambda(\mu)$; t_λ is the total optical length in the line, which is defined by the relation

$$t_\lambda = \int_0^{\tau_\lambda^0} (1 + \eta_\lambda)\, d\tau_\lambda^0. \tag{2}$$

Relation (1) will be used in what follows as the first approximation for the source function.

From relation (1) we determine T_{exc} for a given section r_λ for both lines. It is clear that if $r_{\lambda A} = r_{\lambda B}$, from (1) we obtain $T^*_{exc\ A} = T^*_{exc\ B}$, but in the event of deviation from the local thermodynamic equilibrium, sections of the two lines with an assigned value r_λ may be formed in various layers. To verify this statement let us calculate η_λ by using photosphere model (BCA) [5], and also by introducing the factor of deviation from the local thermodynamic equilibrium, γ, by using the relation

$$T^*_{exc} = \gamma T, \tag{3}$$

in which T is assigned by the model. Factor γ is assumed to be invariable for all depths. This is acceptable in the first approximation for the assigned line profile section. γ will then characterize its mean value for the corresponding effective layer of the photosphere. The ratio of the absorption coefficient in the line to the absorption coefficient in the continuous spectrum may be written as follows [6]: /56

$$\eta_\lambda = \frac{\sigma_\lambda}{\varkappa_\lambda^0} = \frac{\sqrt{\pi}\, e^2 \lambda^2 (Ng) f}{m_e c^2 \Delta\lambda_D \varkappa_\lambda^0} \left[\frac{N_i}{(Ng)}\right] H(a,v). \tag{4}$$

We use the well-known relations of Boltzmann and Sach to estimate the number of atoms present on the lower excited level:

$$N_i = N_i \frac{g_i}{B_i(T)} e^{-\frac{\chi_i}{k \cdot T_{exc}}} \quad (5)$$

$$\lg \frac{N_{II}}{N_I} P_e = -\chi_r \frac{5040}{T_{ion}} + \frac{5}{2} \lg T_{ion} - 0{,}4772 + \lg \frac{2B_{II}(T)}{B_I(T)}. \quad (6)$$

With (5) and (6) taken into account we find

$$\frac{N_i}{Ng} = \frac{N_i}{N_1 g} \cdot \frac{1}{1 + \frac{N_{II}}{N_1}}, \quad (7)$$

assuming that the excitation temperature is assigned by relation (3), and that ionization temperature $T_{ion} = T$. The last-named assumption is, of course, an approximate one, but it is more important in our problem to know the relationship of N_i to T_{exc}; for this reason we retain it as the first approximation.

Now knowing the relationship between η_λ and τ_λ^0 for various values γ, we introduce it into equation (2). Since only observations for the center of the solar disc were used in the project, by integrating relation (2) up to values $t\lambda = 1.00$ we determine τ_λ^0, and as a result T_{exc} as well. The excitation temperature found in this manner should coincide with T^*_{exc} determined from observations on the basis of relation (1). Agreement between the result of calculations and the result of observations is achieved by varying factor γ. Thus, by allowing for the deviation from the local thermodynamic equilibrium it is possible to estimate the depth of occurrence of the effective layer responsible for the emergent intensity in the line over any section r_λ.

Analysis of Results. Such an estimate was made for one pair used in the work of Unno, which we had earlier examined in detail [1, 2]. This miltiplet, NaI λλ 6154, 2351 6160, 759 Å was corrected for the instrument circuit error.

Calculations of η_λ were performed for 6 sections in which half-width $\Delta\lambda$ equals 0.000; 0.025; 0.050; 0.075; 0.100; and 0.125 Å. The value of parameter a characterizing the attenuation of the radiation was taken from [2] and was assumed to be constant (a = 0.08). For the sake of convenience in calculation /57 and to achieve the necessary accuracy, all the physical parameters were assigned as a function of τ_λ^0 within the limits of 0.01-1.00 with a step of $\Delta\tau_\lambda^0 = 0.10$, as is shown in Table 1. The temperature, electron pressure, absorption coefficient in the continuous spectrum in the λ 6100 Å region, and the Doppler half-width $\Delta\lambda_D$ expressed in mÅ are entered respectively in the second, third, fourth, and fifth columns of the table. We may note that the variation in $\Delta\lambda_D$ with depth used in the calculations was found by the Goldberg-Unno method in [1] for this pair. The abundance value of Na, as well as the values of the absolute oscillator forces, were taken from [7]. These values are respectively $\lg N_{(Na)} = 6.18$; $\lg(qf)_{6160} = -1.27$; $\lg(qf)_{6154} = -1.57$. All other quantities

required were taken from [8]. Equation (2) was solved by numerical integration. In selection of interval $\Delta\tau_\lambda^0 = 0.1$ and the number of points dividing this interval (50 points), an effort was made to make certain that the accuracy in determination of τ_λ^0 would be no lower than $\Delta\tau_\lambda^0 = 0.01$.

TABLE 1.

τ_λ^0	T	P_e	$\varkappa_\lambda^0$	$\Delta\lambda_D$	τ_λ^0	T	P_e	$\varkappa_\lambda^0$	$\Delta\lambda_D$
0,00	4600	1,00	0,049	41,0	0,60	5960	22,00	0,412	62,0
0,10	5080	2,50	0,100	44,0	0,70	6070	28,00	0,490	66,0
0,20	5350	5,30	0,150	47,0	0,80	6160	34,50	0,577	69,0
0,30	5560	8,50	0,205	51,0	0,90	6250	41,50	0,668	73,0
0,40	5710	12,30	0,270	55,0	1,00	6330	50,00	0,756	75,0
0,50	5850	17,00	0,340	58,0					

Commas indicate decimal points.

All calculations were performed on a "Promin'" computer at the Main Astronomical Observatory of the Academy of Sciences of the UKrainian SSR. The results of the calculations are presented in Table 2 and in Figures 1 and 2.

TABLE 2.

Section no.	λ 6154,235 Å			λ 6160,759 Å		
	τ_λ^0	γ	r_λ	τ_λ^0	γ	r_λ
1	0,488	0,965	0,707	0,260	0,970	0,550
2	0,580	0,960	0,747	0,360	0,960	0,610
3	0,758	0,960	0,833	0,612	0,950	0,723
4	0,896	0,960	0,917	0,818	0,950	0,843
5	0,960	0,970	0,957	0,926	0,960	0,920
6	0,986	0,965	0,978	0,972	0,960	0,948

Commas indicate decimal points.

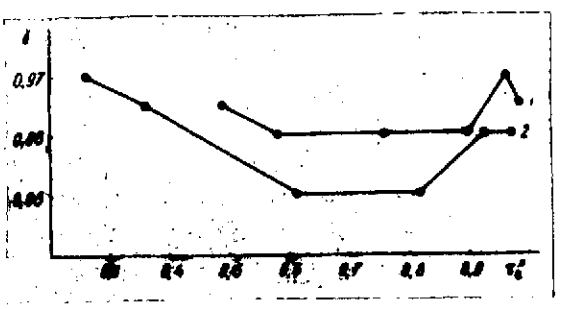

Figure 1. Factor γ Allowing for Deviation From Local Thermodynamic Equilibrium Versus Depth τ_λ^0 for Both Lines of Na I Multiplet; 1, λ 6154; 2, λ 6160.

Figure 1 shows factor γ (allowing for deviation from the local thermodynamic equilibrium) plotted against depth τ_λ^0. The purpose of plotting this graph is to show the general trend of variation in γ by using values of the latter derived for various sections in profiles for both multiplet lines. The stronger lines are known to be more greatly affected by deviation from the local thermodynamic equilibrium than are the weaker ones. The

method we applied leads to the same conclusion. On the whole the stronger line is characterized by smaller values of γ than the weaker ones.

The data of Table 2 were used to plot Figure 2, in which one can observe the relationships sought between residual intensity r_λ for both lines and depth τ^0_λ. The divergence of the curves of r_λ versus τ^0_λ is clearly evident; it is greater in magnitude in the interior of the lines than on the ends. This was to be expected, since these regions are formed in the higher layers, where the deviation from the local thermodynamic equilibrium is considerable. /58

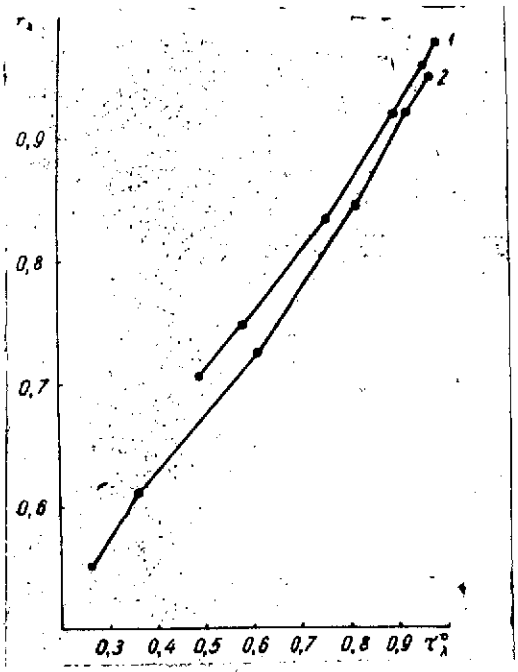

Figure 2. Residual Intensity r_λ for Na I Multiplet Lines Versus Depth τ^0_λ: 1, λ 6154; 2, λ 6160.

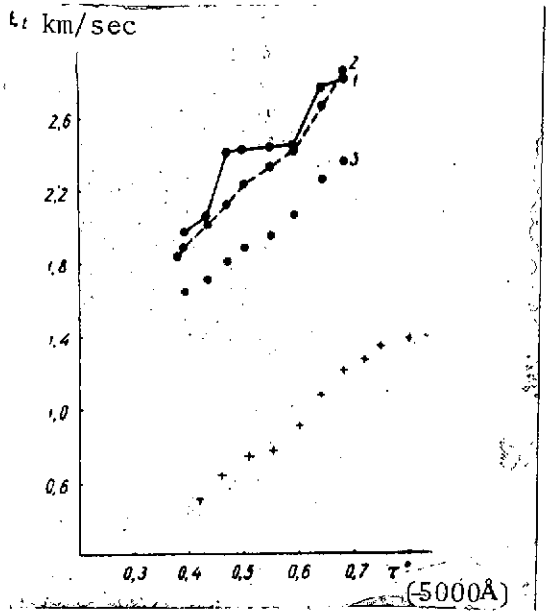

Figure 3. Turbulent Velocity ξ_t Versus Optical Depth $\tau^0_{(5000\ Å)}$: 1, Variation in ξ_t with $\tau^0_{(5000\ Å)}$ Before Correction of Line Profiles for Instrument Circuit Errors; 2, After Correction; 3, With Allowance Made for Effect of Radiation Attenuation; 4, With Allowance Made for Influence of Deviation from Local Thermodynamic Equilibrium.

We can now proceed directly to calculate $\Delta\lambda_D$. For this purpose we divide the weaker line of the pair into equal sections (starting from the values $1-r_\lambda = 0.075$) with a depth of $\Delta r_\lambda = 0.025$. On the basis of these values of r_λ we find r_λ from Figure 2, and then the corresponding residual intensity values for the weaker line. Subsequent values of $\Delta\lambda_D$ are found in the usual manner. In this project we applied the processing procedure discussed in [2], which permits allowance for the influence of radiation attenuation on results obtained by the Goldberg-Unno method.

The results of the processing are presented in Figure 3 and in Table 3. Crosses in Figure 3 designate turbulent velocity ξ_t as a function of depth $\tau^0_{(5000\ \text{Å})}$. The results of studies found in [1, 2] are presented for the sake of comparison. The important point is that, if allowance is made for the influence of deviation from the local thermodynamic equilibrium, the curve of ξ_t versus $\tau^0_{(5000\ \text{Å})}$ is displaced both along the axis ξ_t ($\Delta\xi_t \simeq 1.5$ km/sec) and along the axis $\tau^0_{(5000\ \text{Å})}$ ($\Delta\tau^0 \simeq 0.05$). It cannot be stated that the value of this (relatively large) displacement is realistic. The reason for this may be represented not so much by the assumptions we have adopted as by use of an "absolute" method of calculation involving the use of oscillators and with the element present in abundance. As is known, the content of the latter cannot be determined with precision. However, what is important is that the result obtained regarding the nature of increase with depth remained invariable.

It is to be noted that the variation found in $\Delta\lambda_D$, as well as in ξ_t, with increase in depth is only a first approximation. If the method employed is correct, the problem apparently may be considered to be solved only when the /59
assigned variation in $\Delta\lambda_D$ with τ^0_λ coincides entirely with the calculated variation. This can be accomplished by varying the initial turbulence model and solving the problem until the results coincide.

TABLE 3.

τ^0_λ	$1-r_{\lambda 8154}$	$1-r_{\lambda 8160}$	$\Delta\lambda_{8154}$	$\Delta\lambda_{8160}$	$\frac{\Delta\lambda_A}{\Delta\lambda_B}$	$\Delta\lambda_D$	ξ_t	$\tau^0_{(5000\ \text{Å})}$
0,91	0,075	0,093	39,5	46,0	1,165	52,0	1,37	0,80
0,87	0,100	0,122	34,4	41,7	1,215	51,6	1,34	0,75
0,83	0,125	0,150	30,5	38,3	1,255	50,7	1,27	0,72
0,79	0,150	0,176	27,3	35,5	1,300	49,8	1,21	0,68
0,74	0,175	0,202	24,0	32,5	1,355	48,5	1,08	0,64
0,69	0,200	0,232	20,5	29,3	1,430	46,7	0,90	0,60
0,64	0,225	0,262	16,9	26,3	1,560	45,6	0,77	0,55
0,59	0,250	0,288	13,0	23,7	1,820	45,1	0,73	0,51
0,53	0,275	0,313	8,1	21,0	2,60	44,3	0,63	0,46
0,49	0,293	0,332	0,0	19,0	—	43,4	0,50	0,42

Commas indicate decimal points.

REFERENCES

1. Troyan, V. I., in the book: *Astrometriya i Astrofizika* [Astrometrics and Astrophysics], "Naukova Dumka" Press, Kiev, Vol. 9, 1970.
2. Troyan, V. I., in the book: *Astrometriya i Astrofizika* [Astrometrics and Astrophysics], :Naukova Dumka" Press, Kiev, Vol. 12, 1971.
3. Goldberg, L., *Ap. J.*, Vol. 127, p. 328, 1958.
4. Jefferies, J. T., *Spectral Line Formation*, Blaisdell Publishing Co., Chapter 3, 1968.
5. Gingerich, O. and C. de Jager, *Solar Physics*, Vol. 3, p. 5, 1968.
6. Unzol'd, A., *Fizika Zvezdnykh Atmosfer* [Physics of Stellar Atmospheres], Chapter VIII, Moscow, 1949.
7. Lambert, D. L. and B. Warner, *Mon. Not. R.A.S.*, Vol. 138, p. 181, 1968.
8. Allen, K. U., *Astrofizicheskiye Velichiny* [Astrophysical Qauntities], Moscow, 1960.

LUMINOSITY CONDITIONS OF Cr IX AND Fe XI IN THE CORONA

K. V. Alikayeva and Z. M. Bikchantayeva

ABSTRACT. Coronal lines λ 4566 Å Cr IX and λ 3986 Å Fe XI have been studied. The electron temperature in the corona is found to be 10^{6}°K and the electron density ~ $0.8 \cdot 10^{9}$ cm^{-3}. Calculations have been performed for Cr IX ion populations of levels.

The present paper is a continuation of a study begun in [1] of the spectral corona obtained during the total solar eclipse of 1970 in Mexico [2]. The subject of study is this time represented by lines I of the class λ 3986 Å Fe XI and λ 4566 Å Cr IX. Both ions belong to one isoelectron series S I and have similar ionization potentials. In addition, the lines in question are formed as a result of the same forbidden transition $^{1}D_{2}$-$^{3}P_{1}$. This justifies the assumption that these lines are formed under identical conditions.

As was pointed out in [1], analysis of the Doppler widths points to the conclusion that coronal lines of the first and the second classes shine in parts of the corona characterized by different physical conditions. The values /60 found for the electron temperature and concentration for ion lines having an ionization potential of ≈ 300 ev equal respectively 2.7-2.1·10^{6}°K and 3.5-0.7·10^{9} cm^{-3}. T_e and N_e may be found in similar fashion for lines of the first class having an ionization potential of approximately 200 ev.

Spectrogram Processing Data

Lines λλ 3986 Å Fe XI and λ 4566 Å Cr IX were scanned photometrically within the limits of altitudes of 48,000-110,000 km. The values of the total energy emitted in the E_λ line were determined for all the photometric sections. This makes it possible to find the quantity of excited ions in the line of sight N'. The required values of the spontaneous transition probabilities were taken from [3]. By solving the Abel equation

$$N'(h) = 2\int_{h}^{\infty} \frac{n'(r)\,r\,dr}{\sqrt{r^2 - h^2}},$$

we found the concentration of excited ions n' at various levels in the corona (Table 1). These values of n' were subsequently used in determination of T_e and n_e.

As in [1], the electron temperature and concentration were found by comparing the degree of ionization of Fe XI and Cr IX.

$$\varkappa = -\lg \frac{n_{\text{Fe XI}}}{n_{\text{Fe}}} + \lg \frac{n_{\text{Cr IX}}}{n_{\text{Cr}}} = \lg \frac{n_{\text{Fe}}}{n_{\text{Cr}}} - \lg n_{\text{Fe XI}} + \lg n_{\text{Cr IX}} =$$

$$= \lg \frac{A_{\text{Fe}}}{A_{\text{Cr}}} - (\lg n'_{\text{Fe}} - \lg n'_{\text{Cr}}) + \left(\lg \frac{n'_{\text{Fe XI}}}{n_{\text{Fe XI}}} - \lg \frac{n'_{\text{Cr IX}}}{n_{\text{Cr IX}}}\right).$$

The first term of this relation is determined by the chemical composition of the corona. According to [4], $\lg A_{Cr} = 5.30$ and $\lg A_{Fe} = 7.30$. The second term may be found from Table 1. The third term represents the difference in logarithms of relative level populations $^1D_2$ Fe XI and Cr IX. As Zirker [5] has shown, the relative populations of the coronal ions depend chiefly on the electron density, and the dependence on temperature may be disregarded. The degree of ionization, on the other hand, is a function of T_e alone. Once $\varkappa$ has been calculated, one can determine the electron temperature and concentration. The method of finding T_e and n_e is described in greater detail in [1].

Ionization Balance and Steadiness Equations

Since radiation ionization processes play no appreciable role in the ionization balance of coronal ions at high electron temperatures, the degree of ionization depends on T_e alone and is entirely independent of n_e. Ionization balance calculations for a large group of elements, including Fe and Cr, were performed by House [6]. In these calculations allowance was made on the one hand for the impact ionization, and on the other for the photorecombination and impact recombination. Burgess and Seaton [7] subsequently pointed out the necessity of allowing also for dielectronic recombinations and autoionization. Jordan calculated the degree of ionization of a number of elements over a broad temperature range, making allowance for these processes as well [8]. Comparison of the tables given in [8] with the results obtained by House shows that allowance for dielectronic recombination and autoionization more than doubles the electron temperature value. Unfortunately, in his paper Jordan failed to perform calculations of the degree of Cr ionization, and for this reason we were forced to use the earlier calculations of House.

Calculations of Fe XI excitation were performed by Zirker [5] for three values $n_e = 10^8$, 10^9, 10^{10} and $T_e = 1.5 \cdot 10^6$°K. Similar calculations were not performed for Cr IX. We calculated the distribution of Cr IX ions over the excited levels. In the calculations allowance was made for the ^3P, ^1D, and ^1S levels of the basic s^2p^4 configurations. In addition, the transitions between the basic configuration levels and the displaced terms of the sp^5 and s^2p^3d configurations were taken into account. The numbering adopted in the project for

/61

the levels included in the calculations and their excitation potentials are shown in Table 2.

TABLE 1.

h, km	$n'_{Fe\ XI}$	h, km	$n'_{Cr\ IX}$
43500	10,7	48200	0,235
58700	14,3	53400	0,240
66700	9,8	58500	0,254
77200	8,8	63700	0,238
87500	5,3	68900	0,233
98000	5,0	79400	0,225
		84500	0,204

Commas indicate decimal points.

TABLE 2.

Level No.	Configuration	Level	Excitation Energy
1	$3s^23p^4$	$^3P_2$	0
2		$^3P_1$	0,975
3		$^3P_0$	1,19
4		$^1D_2$	3,76
5		$^1S_0$	8,29
6	$3s3p^5$	$^3P_2$	30,0
7		$^3P_1$	30,0
8		$^3P_0$	30,0
9		$^1P_1$	37,4
10	$3s^23p^33d$	$^3D_3$	56,4
11		$^3D_2$	56,4
12		$^3D_1$	56,4

Commas indicate decimal points.

The steadiness equation of the i level is written as follows in the general case:

$$\sum_{k \neq i} n_k (A_{ki} + Z_{ki} n_e) = n_i \sum_{k \neq i} (A_{ik} + Z_{ik} n_e).$$

In this equation A_{ki}, A_{ik} are the probabilities of radiation transitions and Z_{ki}, Z_{ik} are the coefficients of transitions under the influence of electron impacts. Equations of this type were prepared for levels 2-5. Owing to the slight degree of population of the displaced terms, the transitions between the latter and the basic configuration levels may be disregarded. Hence no steadiness equations were prepared for these levels. For the sake of uniformity of the calculations, we use the same data and formulas as were used in [5].

I. Spontaneous transition probabilities. The theoretical values of the probabilities of forbidden transitions accompanied by the emission of quanta for the basic Cr IX configuration have been calculated in [9].

II. Radiation excitation. The photoexcitation probabilities were estimated with the formula

$$A_{ki} = \frac{1}{2} \frac{g_i}{g_k} A_{ik} [e^{h\nu/kT} - 1]^{-1}.$$

The temperature of the exciting radiation was assumed in accordance with [5] to be $T_r = 6{,}000°$. The values of A_{ki} are given in Table 3.

III. Transitions under the influence of electron impact. The probabilities of impact excitation of forbidden transitions between the basic configuration levels were calculated with the following formula taken from [10]:

$$Z_{ik} = 8{,}54 \cdot 10^{-6} \Omega g_i^{-1} T_e^{-1/2} e^{-h\nu/kT_e};$$

Ω is the impact force. The values of these quantities are given in [11]. The probabilities of impact transitions between levels belonging to different configurations were calculated with the following formula given in [5]:

$$Z_{ik} = 5{,}1 \cdot 10^{-4} E^{-1} T^{-1/2} f_{ik} e^{-h\nu/kT}.$$

f_{ik} – the oscillator forces for transitions between levels of different configurations – were calculated by Zirker [5] for Fe XI and extended to other elements of this isoelectron series. We have used them for Cr IX as well in this paper. /62

The reverse transition probabilities were calculated on the basis of the well-known ratio of the transition coefficients under the influence of impacts of the first and second kinds.

The calculated values of the impact excitation coefficients are given in Tables 3 and 4.

TABLE 3.

Transition	Z_{ki} $T_e = 1 \cdot 10^6$	Z_{ki} $T_e = 1{,}5 \cdot 10^6$	A_{ki}	Transition	Z_{ki} $T_e = 1 \cdot 10^6$	Z_{ki} $T_e = 1{,}5 \cdot 10^6$	A_{ki}
1—2	$0{,}618 \cdot 10^{-9}$	$0{,}505 \cdot 10^{-9}$	0,51	3—4	$0{,}304 \cdot 10^{-9}$	$0{,}633 \cdot 10^{-9}$	0
1—3	$0{,}194 \cdot 10^{-9}$	$0{,}158 \cdot 10^{-9}$	0	1—5	$0{,}340 \cdot 10^{-10}$	$0{,}287 \cdot 10^{-10}$	0
2—3	$0{,}230 \cdot 10^{-9}$	$0{,}192 \cdot 10^{-9}$	0,094	2—5	$0{,}343 \cdot 10^{-10}$	$0{,}288 \cdot 10^{-10}$	0
1—4	$0{,}304 \cdot 10^{-9}$	$0{,}252 \cdot 10^{-9}$	0	3—5	$0{,}344 \cdot 10^{-10}$	$0{,}289 \cdot 10^{-10}$	0
2—4	$0{,}307 \cdot 10^{-9}$	$0{,}254 \cdot 10^{-9}$	0	4—5	$0{,}738 \cdot 10^{-9}$	$0{,}622 \cdot 10^{-9}$	0

Commas indicate decimal points.

TABLE 4.

Transition	Z_{ki} $T_e = 1 \cdot 10^6$	Z_{ki} $T_e = 1{,}5 \cdot 10^6$	Transition	Z_{ki} $T_e = 1 \cdot 10^6$	Z_{ki} $T_e = 1{,}5 \cdot 10^6$
1—6	$0{,}322 \cdot 10^{-8}$	$0{,}293 \cdot 10^{-8}$	4— 9	$0{,}450 \cdot 10^{-8}$	$0{,}417 \cdot 10^{-8}$
2—6	$0{,}188 \cdot 10^{-8}$	$0{,}171 \cdot 10^{-8}$	5— 9	$0{,}414 \cdot 10^{-8}$	$0{,}377 \cdot 10^{-8}$
4—6	$0{,}143 \cdot 10^{-11}$	$0{,}129 \cdot 10^{-11}$	1—10	$0{,}517 \cdot 10^{-8}$	$0{,}523 \cdot 10^{-8}$
1—7	$0{,}109 \cdot 10^{-8}$	$0{,}100 \cdot 10^{-8}$	4—10	$0{,}105 \cdot 10^{-8}$	$0{,}108 \cdot 10^{-8}$
2—7	$0{,}115 \cdot 10^{-8}$	$0{,}104 \cdot 10^{-8}$	1—11	$0{,}940 \cdot 10^{-9}$	$0{,}955 \cdot 10^{-9}$
3—7	$0{,}469 \cdot 10^{-8}$	$0{,}425 \cdot 10^{-8}$	2—11	$0{,}435 \cdot 10^{-9}$	$0{,}437 \cdot 10^{-9}$
4—7	$0{,}143 \cdot 10^{-10}$	$0{,}129 \cdot 10^{-10}$	4—11	$0{,}370 \cdot 10^{-9}$	$0{,}368 \cdot 10^{-9}$
5—7	$0{,}182 \cdot 10^{-10}$	$0{,}162 \cdot 10^{-10}$	1—12	$0{,}469 \cdot 10^{-11}$	$0{,}475 \cdot 10^{-11}$
2—8	$0{,}150 \cdot 10^{-8}$	$0{,}136 \cdot 10^{-8}$	2—12	$0{,}481 \cdot 10^{-9}$	$0{,}486 \cdot 10^{-9}$
1—9	$0{,}142 \cdot 10^{-8}$	$0{,}133 \cdot 10^{-8}$	3—12	$0{,}702 \cdot 10^{-8}$	$0{,}689 \cdot 10^{-8}$
2—9	$0{,}277 \cdot 10^{-9}$	$0{,}260 \cdot 10^{-9}$	4—12	$0{,}526 \cdot 10^{-12}$	$0{,}526 \cdot 10^{-12}$
3—9	$0{,}278 \cdot 10^{-8}$	$0{,}260 \cdot 10^{-8}$	5—12	$0{,}969 \cdot 10^{-10}$	$0{,}945 \cdot 10^{-10}$

Commas indicate decimal points.

The system of four steadiness equations was solved for the unknowns $\frac{n_2}{n_1}$, $\frac{n_3}{n_1}$, $\frac{n_4}{n_1}$, and $\frac{n_5}{n_1}$ for three electron concentration values: 10^8, 10^9, 10^{10}, and for $T_e = 1.0 \cdot 10^6$ and $1.5 \cdot 10^6$°K. The populations of the levels in relation

to the total Cr IX content – $\frac{n_i}{n_{Gr\ IX}}$ – are given in Table 5. The table shows that in reality the relative populations depend only slightly on T_e.

TABLE 5.

Levels	$n_e = 10^8$		$n_e = 10^9$		$n_e = 10^{10}$	
	$T_e = 1 \cdot 10^6$	$T_e = 1{,}5 \cdot 10^6$	$T_e = 1 \cdot 10^6$	$T_e = 1{,}5 \cdot 10^6$	$T_e = 1 \cdot 10^6$	$T_e = 1{,}5 \cdot 10^6$
1	9,42(—1)	9,58(—1)	9,46(—1)	9,30(—1)	9,20(—1)	9,15(—1)
2	4,75(—2)	4,64(—2)	4,16(—2)	4,80(—2)	5,00(—2)	4,70(—2)
3	9,32(—3)	1,12(—2)	1,15(—2)	1,02(—2)	1,13(—2)	9,80(—3)
4	1,13(—3)	1,11(—3)	8,20(—3)	1,21(—2)	2,78(—2)	2,56(—2)
5	7,83(—6)	8,00(—6)	9,50(—5)	1,00(—4)	1,38(—3)	1,10(—3)

Commas indicate decimal points.

The excited levels are populated chiefly from the ground state, electron impact playing the chief role when $n_e \geqslant 10^9$. At low densities escape from the excited levels is accomplished mostly through radiation, and almost entirely through electron impacts for $n_e \geqslant 10^9$. /63

Electron Concentration and Temperature in the Corona

The condition of equality of the values adopted for n_e and hydrogen concentration n_H was used in determining the temperature and concentration of electrons in the corona, as was also done in [1]. The hydrogen concentration was determined on the basis of the chemical composition of the corona.

The variation in n_e and T_e with variation in altitude is shown in the drawing. The temperature values obtained (~ 400,000°K) are much lower than for lines of the second class. These values are approximately doubled if allowance is made for the dielectronic recombinations and autoionization in the ionization balance equation. Thus it is to be assumed that the actual electron temperature is near 10^{6}°K in the luminosity region of the Cr IX and Fe XI lines. However, it is substantially lower than the temperature obtained on the basis of the Fe XIV and Ni XII lines. Consequently, actual division of the luminosity regions of the lines of various classes takes place.

As may be seen from the illustration, the temperature and electron density of the luminosity regions of the Cr IX and Fe XI lines scarcely change with altitude. These lines probably shine in the relatively narrow surface layer of the corona.

It is interesting to note that the λ 4566 Å line is not always observed. For example, this line does not appear in [12], although the Fe XI line is similar in intensity to the observed values used in this paper. The presence of the Cr IX line in the coronal spectrum possibly indicates increased density of matter in this particular region. However, this matter calls for further study.

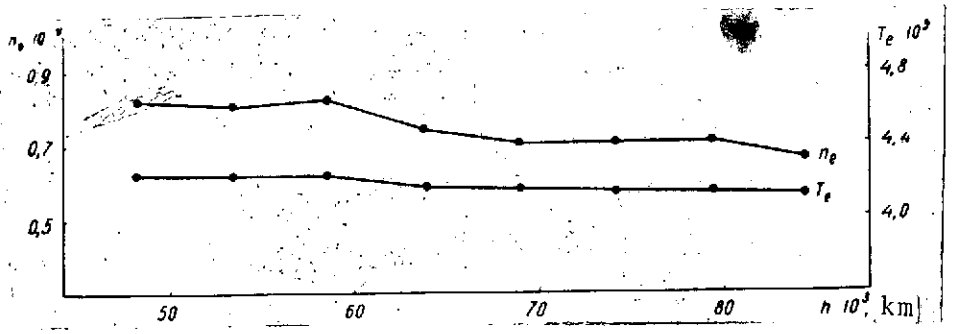

Variation of Electron Temperature and Concentration in the Corona.

REFERENCES

1. Gurtovenko, E. A. and K. V. Alikayeva, in the book: *Astrometriya i Astrofizika* [Astrometrics and Astrophysics], "Naukova Dumka" Press, Vol. 15, Kiev, 1971.
2. Gurtovenko, E. A. and K. E. Skorik, *ATS.*, Vol. 580, p. 1, 1970.
3. Jefferies, J. T., F. Q. Orrall and J. B. Zirker, *Les Transitions Interdites dans les Spectres des Astres* [Forbidden Transitions in the Spectra of Stars], Belgium, p. 235, 1969.
4. Ivanov-Kholodnyy, G. S. and G. M. Nikol'skiy, in the book: *Solntse i ionosfera* [The Sun and the Ionosphere], "Naukova Dumka" Press, Moscow, 1969.
5. Zirker, J. B., *Solar Phys.*, Vol. 11, p. 68, 1970.
6. House, L. L., *Aph. J.*, Suppl., Vol. 8, p. 81, 1964.
7. Burgess, A. and M. J. Seaton, *MN*, Vol. 127, p. 355, 1964.
8. Jordan, C., *MN*, Vol. 142, p. 501, 1969.
9. Krueger, T. K. and S. J. Czyzak, *Aph. J.*, Vol. 144, p. 1194, 1966.
10. Menzel, D. H., *Les Transitions Interdites dans les Spectres des Astres* [Forbidden Transitions in the Spectra of Stars], Belgium, p. 113, 1969.
11. Krueger, T. K. and S. J. Cayzak, *Proc. Roy. Soc.*, London, Vol. A318, p. 531, 1970.
12. Falchi, A., R. Falciani and M. Rigutti, *Z. f. Aph.*, Vol. 67, p. 115, 1967.

SPECTROPHOTOMETRY OF PROMINENCES IN THE PHASE PRECEDING DECAY

A. S. Rakhubovskiy

ABSTRACT. The results are presented of spectrophotometric processing of prominence spectra in both the quiet and the decay phases. A catalogue is compiled of equivalent widths, central intensities, Doppler half-widths, and half-widths of emission lines. The reduced Doppler half-widths of D_3 and of the H, K Ca^+ lines obtained in a prominence active phase are much larger than those obtained during a quiet phase. Comparison of the equivalent widths and central intensities of H_α, H_β hydrogen and D_3 helium lines shows that the values increase in the active phase for the D_3 lines and decrease for the H_α, H_β lines.

Observations and Processing

The purpose of the present project was to study prominences in the process of development and to compare the quantitative spectral characteristics (central densities, equivalent widths, Doppler half-widths) in the quiet phase of development and at the time of decay of a prominence. For this purpose the spectra of all the prominences on the limb of the Sun were photographed regularly from 1965 to 1970; the photographing of the spectra was repeated if the weather conditions permitted this. The faint prominences were photographed in the hydrogen lines from H_α to H_9, in the D_3, λ 3889, λ 4471 helium lines, and in the H, K ionized calcium lines, and the relatively bright prominences were photographed in the hydrogen lines from H_α to the limit of the Balmer series in the helium lines, and in the lines of metals.

The design of the spectrograph [1, 2, 3] does not permit simultaneous photographing of various spectral sections, and so the spectral lines were photographed in succession. The process itself of photographing all the lines of a faint prominence took 5-7 minutes, and 10-15 minutes for a relatively bright prominence. Standardization and calibration were accomplished by printing in the center of the solar disc through a step reducer and neutral filter. The regions of lines H_α, H_β, and D_3 were photographed in the second sequence on Rot rapid ORWO photographic plates, and the He λ 4471 line on Blau rapid emulsion; the remaining hydrogen lines and the He λ 3889 line in the third sequence on Blau rapid ORWO photographic plates. The exposure time for the various lines ranged from 1.5 sec to 25 sec. Photographing of the prominence spectrum was accompanied by simultaneous observation through an AFR-2 telescope by means of a motion picture camera with a frame speed of 1-2 per minute.

Photometric scanning of the spectral lines of a prominence was accomplished with an MF-4 microphotometer additionally equipped with a special attachment for recording darkening events on the paper tape of an EPP-09 potentiometer. To eliminate scattered light, after the photometric scanning of the prominence lines the sections of the same region of the spectrum above the prominence were subjected to photometric scanning. As a result of processing of the recordings outlines of the spectral lines were constructed, on the basis of which the equivalent widths, central intensities, and half-widths of the lines and the Doppler half-widths were determined. The Doppler half-widths $\Delta\lambda_D$ were determined on the basis of inclination of the distant wings of the logarithmic outline [1]. The outlines were plotted in fractions of the intensity of the continuous spectrum of the center of the solar disc. The intrument outline was not taken into account, since in the second and third sequences it equalled 0.07 Å.

Description of Prominences /65

In selecting the spectral material we proceeded on the assumption that the prominences (filaments) may be divided into three major groups. The first group is represented by prominences observed in the high latitudes (polar zone), the second in the spot-forming zone in the area of the active regions, and the third also in the spot-forming zone, but not associated with the apparent active region. Basically we selected the spectra of prominences observed in the high latitudes (polar zone) and decaying in one or two days. Several spectrograms obtained at the time of the decay of a prominence were also processed. In addition, the spectra were selected of prominences which should have been observed on the limb on the following day but were not detected by our observations through the AFR-2 telescope or in the charts of the Fraunhofer Institute [4], that is, they decayed during the 12-hour period following the last observation. Unfortunately, we were unable to process all the prominence spectra selected in the brief time interval and confined ourselves to processing individual prominences for 1965-1966 and 1968-1929 observed in the northern and southern hemispheres at a latitude above 40°. All these prominences are characterized by relatively weak emission in the H_α line (the central intensity in H_α did not exceed 0.09 of the luminosity of the spectrum in the center of the solar disc). On the average the central intensity in the H_α line for them is 0.05-0.07.

Prominence 163 + 45 NE (Figure 1) was observed with the AFR-2 from 18 to 23 August 1965. From 21 August onward the prominence was observed on the limb and part of it, in the form of a filament, on the solar disc. The prominence and the filament decayed during the period from 23 to 24 August. The spectral observations were conducted from 18 to 22 August, that is, a day before the disappearance.

Prominence 178 + 55 NW (Figure 2f) was observed from 21 to 23 September 1965. Spectral observations were conducted on 23 September. The filament of this prominence was observed starting on 16 September in the form of individual

small filaments, one of them being observed on the limb in the form of a prominence. It was not present on the following day.

Prominence 184 + 32 NW (Figure 2a, b, c) was observed on 29 September 1965 in the corona, and another part in the form of a filament on the disc. Spectral observations of the prominence were conducted from 0723 hours to 0800 hours UT (the time of observation given here is in each instance universal time). Only the spectrograms of the coronal prominence obtained over the 0750-0800 hour period were processed. Ascent and decay were observed after 0830 hours. At 0925 hours it broke up into three parts and disappeared in a short time. The filament remained unchanged on the disc.

Prominence 185 - 45 SE was observed on 2 October 1965. It was in the form of a very high arc, but neither the filament nor the prominence was present on the following day.

Prominence 202 + 50 NW (Figure 2i) was observed from 7 to 12 June 1966. Before it emerged to the edge of the disc this formation was observed as a filament from 1 to 6 June. The filament changed in dimensions and shape. Spectral observations were conducted on 9 and 11 June.

Prominence 213 + 45 NE (Figure 2d, e) was observed on 19 and 20 June 1966. The prominence was a high one. At 0500 hours on 21 June it was not present on the limb, and there was no filament on the disc, although on 20 June it had been observed up to 1410 hours in the form of two filaments gradually decreasing and becoming thinner and simultaneously diminishing in luminosity. Spectral observations were conducted on 19 and 20 June.

Prominence 226 + 57 NE (Figure 2g, h) was observed from 5 to 7 July 1966. Spectral observations were conducted on 6 and 7 July, and neither the filament nor the prominence was present on 8 July.

Prominence 231 - 50 SE (Figure 3a, b) was observed from 7 to 10 July 1966. /66 Neither the prominence nor the filament was present on 11 July. Spectral observations were conducted on 9 and 10 July. The prominence changed in dimensions and shape.

Prominence 261 + 45 NE was observed from 7 to 12 August 1966. Starting on 10 August part of it was projected onto the disc in the form of a filament. On 12 August the prominence decayed and part of it, which on 10 August had been observed as a filament, decayed on 13 August. Spectral observations of the parts of the prominence which decayed on 13 August were conducted on 8 August, and observations of the second part of the prominence, which decayed on 12 August, on 9 and 10 August.

Prominence 281 + 58 NE (Figure 3c) was observed from 7 to 11 September 1966. Spectral observations were conducted from 7 to 10 September. Neither the prominence nor a filament was observed on 12 September.

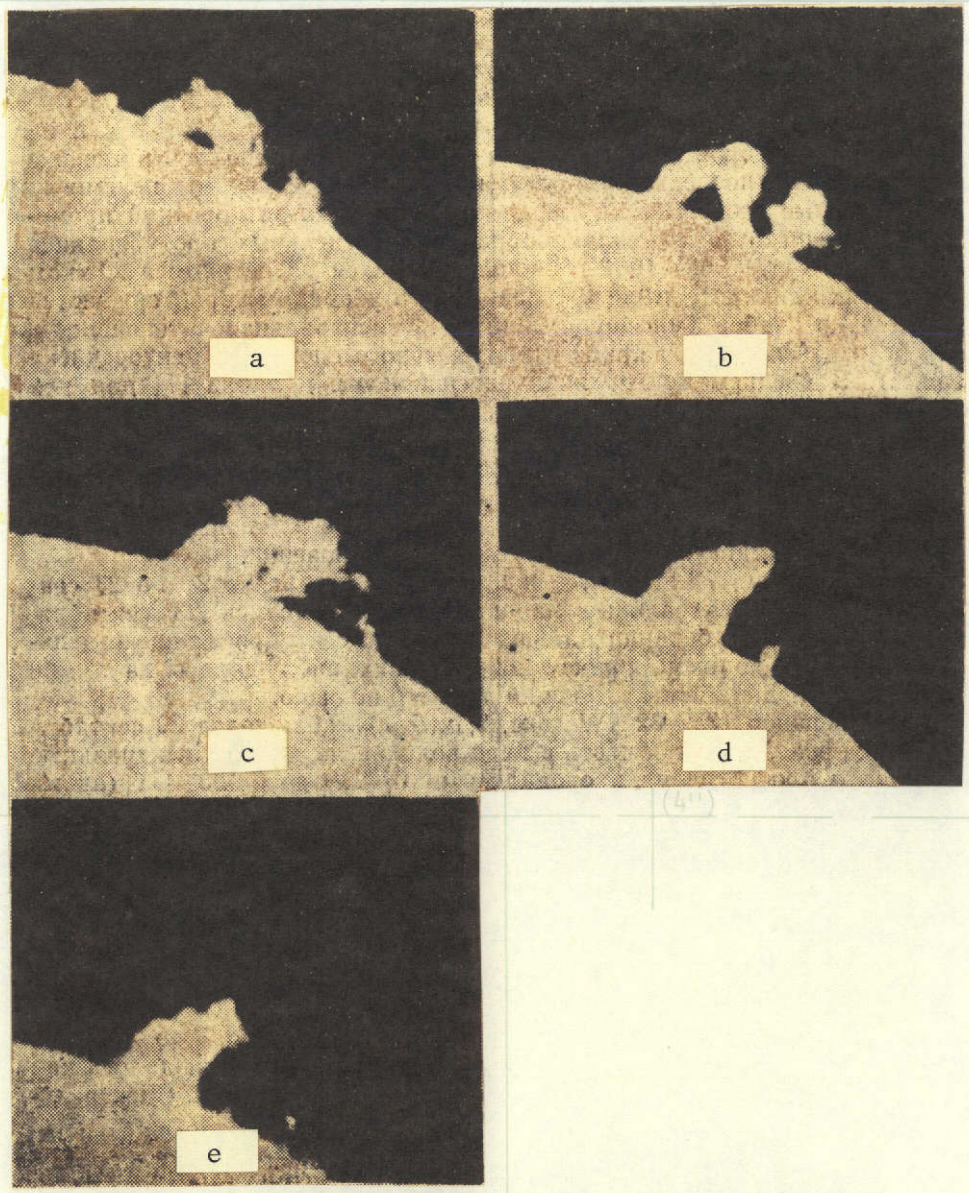

Figure 1. Phases of Development of Prominence 163.
a, 19 August, 0540 hours; b, 20 August, 1135 hours;
c, 21 August, 0720 hours; d, 22 August, 0835 hours;
e, 22 August, 1240 hours.

Prominence 320 + 55 NW (Figure 3d, e) was observed on 5 October 1966. A /67
filament of this prominence was observed starting on 23 September and part of it emerged in the form of a prominence onto the NE edge of the limb. The filament constantly changed in dimensions and outline. On 5 October a filament was observed on the western edge of the disc and part of it in the form of a prominence on the limb. The prominence consisted of two parts. One part of the prominence was observed in the corona and the other above the chromosphere. Spectral observations of the part of the prominence situated in the corona were

conducted at 1015 hours (Section 1a, 1b, 1c). At 1210 hours the spectra of the coronal part (Section 2c, 2d) were photographed, as well as parts of the prominence situated above the chromosphere (Section 2a, 2b). On 6 October there was neither a filament nor a prominence on the limb. The D_3 helium line at the coronal part of the prominence was relatively bright in comparison to the H_α hydrogen line.

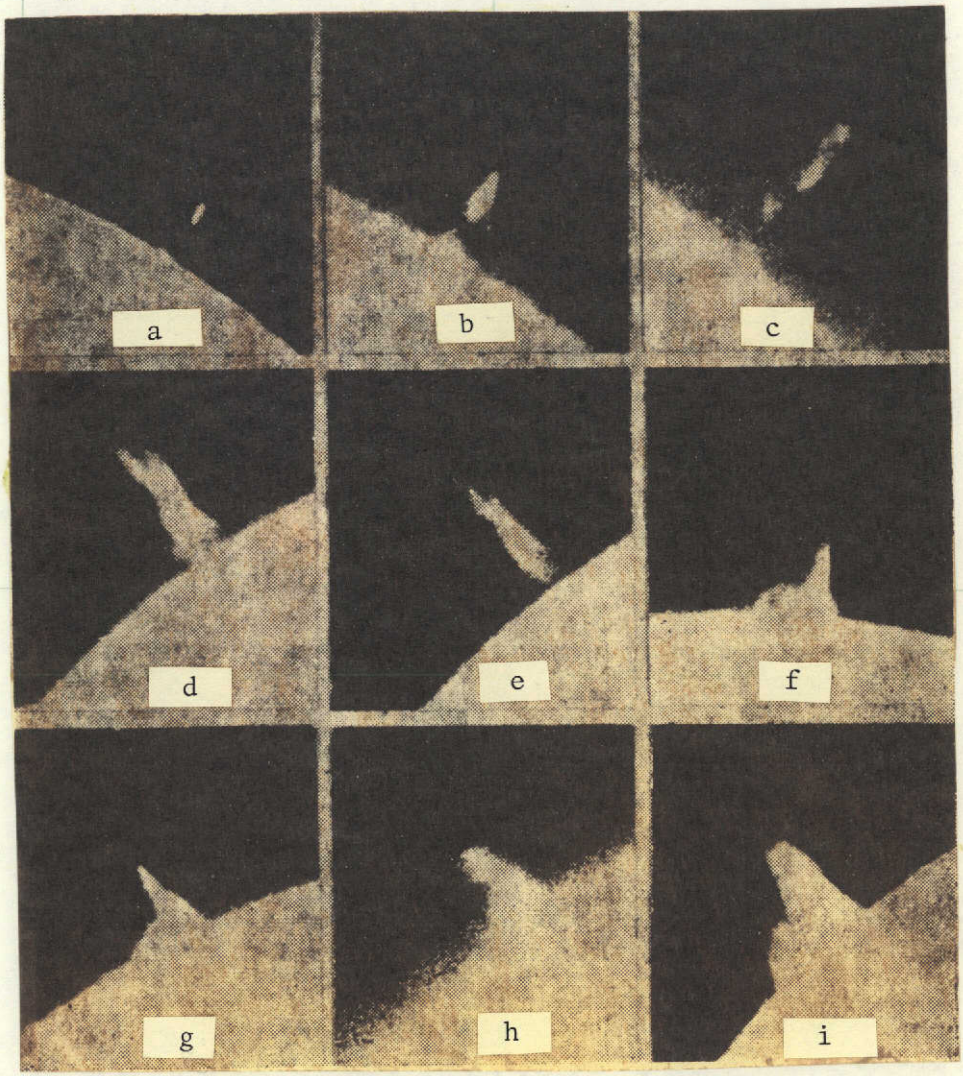

Figure 2. Phases of Development of Prominences. Prominence 184: a, 29 September, 0700 hours; b, 29 September, 0855 hours; c, 29 September, 0925 hours; prominence 213: d, 20 June, 1115 hours; e, 20 June, 1249 hours; prominence 178: f, 23 September, 0558 hours; prominence 226: g, 6 July, 1100 hours; h, 7 July, 0539 hours; prominence 202: i, 11 June, 0852 hours.

Prominence 327 + 25 NE (Figure 3e) was observed on 10 October 1966 in the corona. Spectral observations were conducted at 0800 hours. It had decayed by 1000 hours. The D_3 helium line is bright. /68

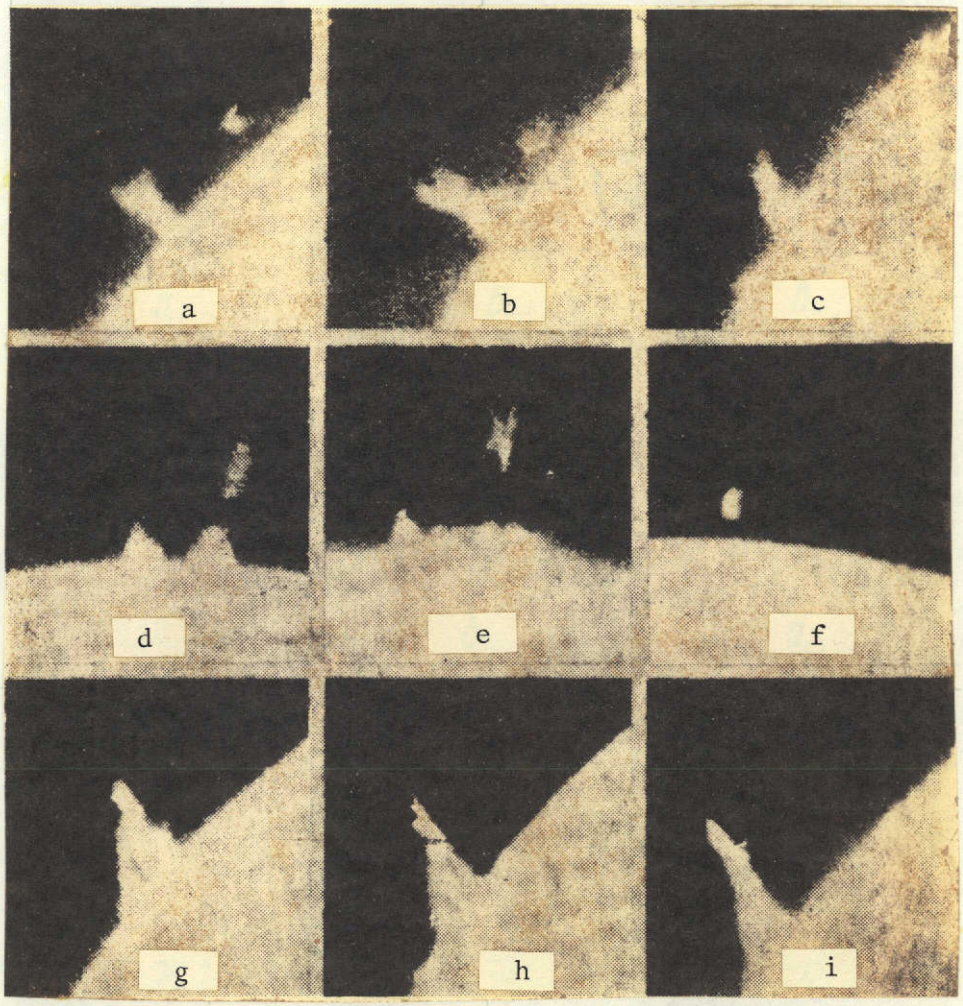

Figure 3. Phases of Development of Prominences. Prominence 231: a, 9 July, 1322 hours; b, 10 July, 0736 hours; prominence 281: c, 9 September, 1105 hours; prominence 320: d, 5 October, 0855 hours; e, 5 October, 1140 hours; prominence 327: f, 10 October, 0550 hours; prominence 1027: g, 11 October, 0635 hours; h, 11 October, 1320 hours; i, 11 October-14 October, 1400 hours.

Prominence 713 - 60 SE (Figure 4c) was observed from 20 to 28 June 1968 on the eastern edge of the limb and then in the form of an elongated filament on the disc of the Sun. On 4 July part of the filament emerged to the western edge of the disc and a prominence, which we have numbered 736, was observed up to 9 July. Spectral observations of prominence 713 were conducted on the eastern edge on 20, 21, 26, 27, and 28 June and on the western edge from 5 to 9

July. Spectrograms of prominence 713 for 26, 27 and 28 July and spectrograms of prominence 736 for 5, 6, 8, and 9 July were processed. Part of prominence 736 the spectra of which were observed on 8 July (Figure 4d), began to decay on 9 July after 0700 hours (Figure 4e, f).

Prominence 824 - 60 SW (Figure 4a, b) was observed from 12 to 15 August 1968. At 0520 hours on 16 August it was also observed in the corona — not in the form of a cloud. Spectral observations were conducted on 15 August.

Prominence 981 + 42 NW (Figure 5) was observed from 6 to 8 August 1969. /69
From 26 July to 5 August a filament was observed which on 6 August was present on the western edge of the disc and was photographed as a prominence. On 8 August the prominence was in the form of a high column (Figure 5a, b, c), and after 0900 hours it began to expand and decompose into individual units. The decay was observed up to 1130 hours (Figure 5d, e, f, g, h, i). Spectral observations were conducted from 0600 hours to 0932 hours.

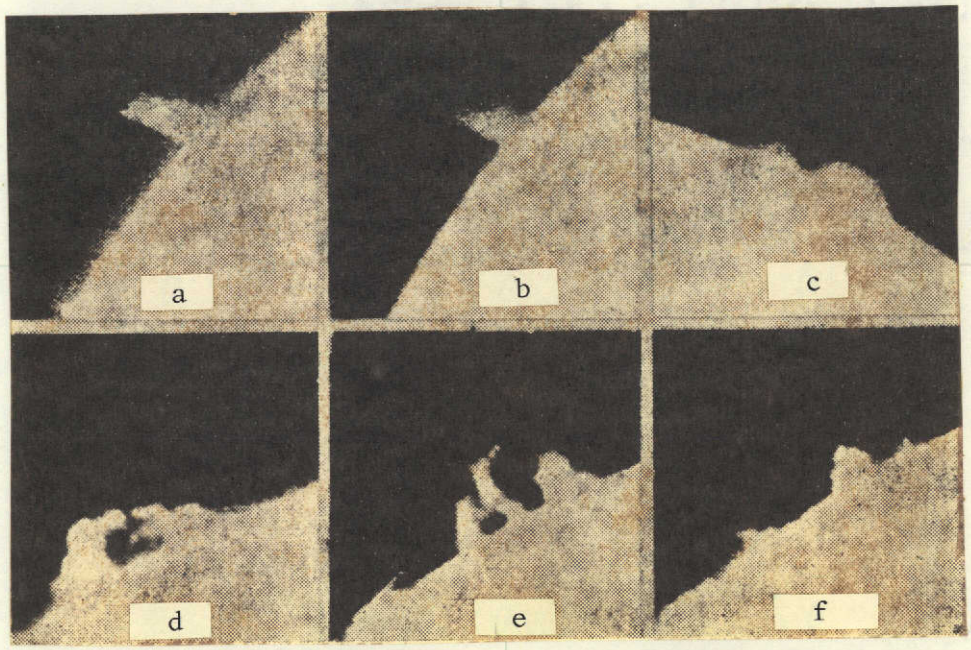

Figure 4. Phases of Development of Prominences. Prominence 824: a, 15 August, 0911 hours; b, 15 August, 1325 hours; prominence 713: c, 27 June, 0810 hours; prominence 736: d, 8 July, 1047 hours; e, 9 July, 0540 hours; f, 9 July, 1053 hours.

Prominence 1027 + 50 NE (Figure 3g, h, i) was observed from 8 to 11 September 1969. On the following day nothing was detected at the place where a filament should have been observed on the disc of the Sun. Spectral observations were conducted on 9, 10 and 11 September. The dimensions of the prominence increased during 11 September. Spectral observations were conducted from 0620 hours to 0650 hours and from 1310 hours to 1325 hours.

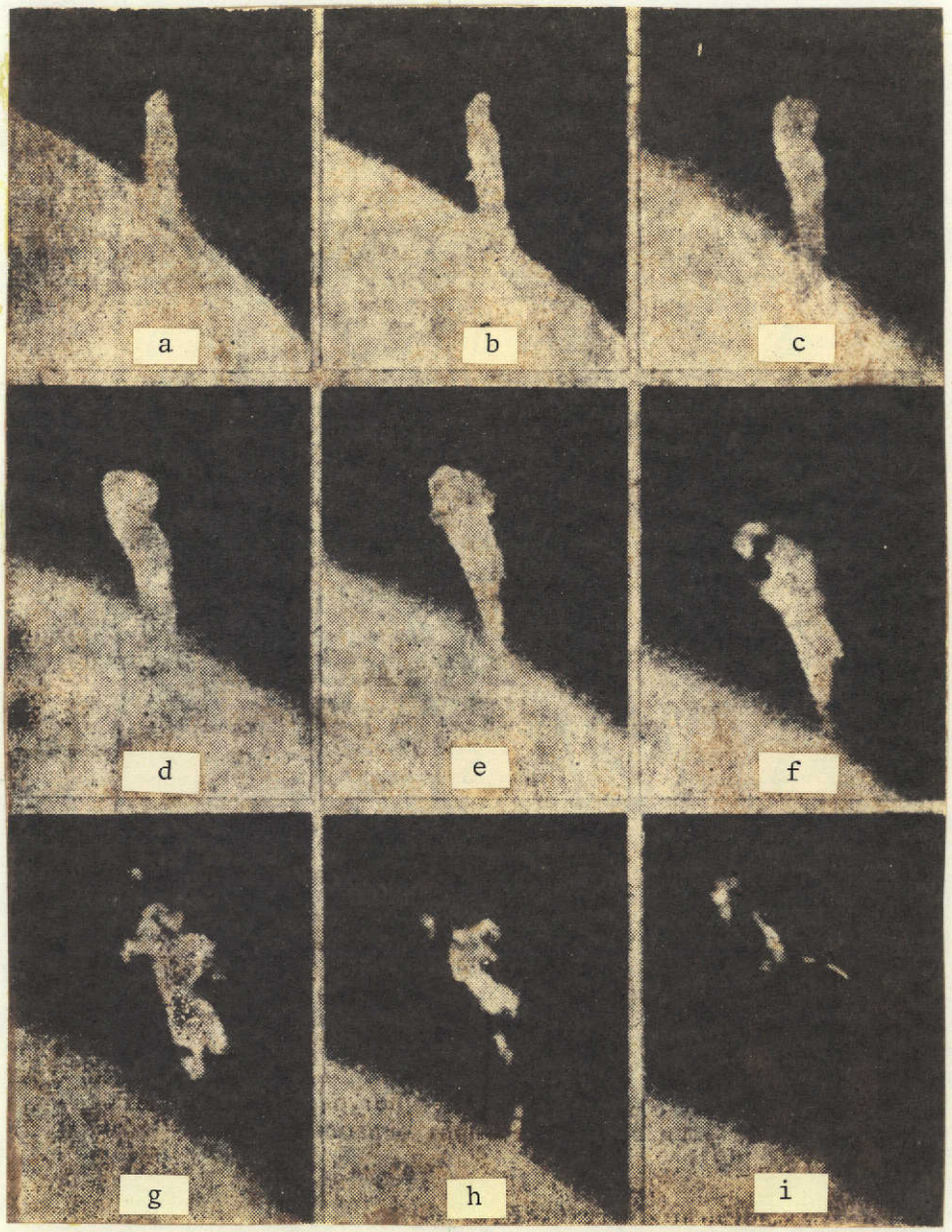

Figure 5. Phases of Development of Prominence 981. a, 0600 hours; b, 0716 hours; c, 0855 hours; d, 0910 hours; e, 0928 hours; f, 0953 hours; g, 1018 hours; h, 1030 hours; i, 1059 hours.

As can be seen from the description, spectral observations of a number of prominences were conducted immediately before decay or at the time of decay (prominence 184, 320, 327, 981). Certain prominences were observed 2-3 days in advance of decay (prominences 261, 281), but the majority of them a day or less in advance of decay (prominences 163, 178, 185, 202, 213, 226, 231, 736, 1027).

Results of Photometric Processing

Let us consider the Doppler half-widths given for the line, values which are presented in the catalogue in units of $\frac{\Delta\lambda_D}{\lambda} \cdot 10^5$. According to the formula $\frac{\Delta\lambda_D}{\lambda} = \frac{1.665}{\lambda} \cdot \Delta\lambda_D = \frac{1.665}{c}\sqrt{\frac{2RT}{\mu} + V_t^2}$, ratios $\frac{\Delta\lambda_D}{\lambda}$ should be the same for all the lines of one chemical element. The catalogue shows that the Doppler half-width given for the hydrogen lines is subject to variation. It is much larger /70 for the H_α lines than for the lines of the higher terms in the Balmer series, and it is much larger for the H_β lines than for the H_γ-H_8 lines. The Doppler half-width given for the H_δ lines is larger than for the H, KCa^+ lines for the periods during which the prominence is in a relatively quiet phase. If a prominence is in the active phase, that is, in the phase of decay, the Doppler half-width of the H, KCa^+ lines is the same, and sometimes becomes larger than for the H_δ lines (Figure 6). In the active phase there is also an increase in the Doppler half-widths given for the D_3 helium lines. Comparison of the values of $\frac{\Delta\lambda_D}{\lambda}$ for helium lines D_3, λ 3889, and λ 4471 shows that the Doppler /71 half-widths given for the D_3 lines is on the average larger than for the λ 3889 lines (Figure 6). Line λ 4471 occupies an intermediate position between them. The data for the λ 4471 lines is less dependable, since the intensity of the lines in the prominences is relatively weak and the accuracy of plotting the outline is low.

The materials obtained from processing of the spectral observations were divided as follows to ascertain the manner of variation in the central intensities $\frac{I_c}{I_\odot}$ and in the equivalent widths W of the hydrogen, helium, and calcium lines in the process of development of a prominence. The mean values of the central intensities and equivalent widths of the outlines of the hydrogen, helium, and calcium lines 1-2 days in advance of the active phase were assigned to one group and the observations at an earlier period to another. Tables were compiled of the mean values of the central intensities and equivalent widths for prominences 163, 261, 281, 713, and 736 (Tables 1, 2, 3, and 4). For prominences 713, 736 the mean values of the values indicated for observations in the east and in the west were taken separately, as were also the mean values of the quantities for 8 August, that is, for the part of prominence 736

which decayed during the subsequent 24 hours. The tables show that the central intensities of hydrogen lines H_α, H_β and the equivalent widths of these lines decrease as the active phase, that is, the phase of decay, approaches. The opposite picture is observed for the D_3 helium lines. Central intensity $\frac{I_c}{I_\odot}$ and equivalent width W increase, and the nearer is the time of decay the closer /72 is the value of these quantities for the helium lines to the value of the quantities for the H_β line. The intensity of the lines and the equivalent widths decrease on the average for the H and K calcium lines. However, we observe no pronounced decrease in the values for prominences in a state near decay or in the active phase. A similar picture is observed for prominences 981, 1027, and 327 (Tables 5, 6), which were observed at the time of decay. In the units of prominences 327, 320, and 981 (Section 3) and 1027 (Section 3), which were situated high above the chromosphere, the equivalent width and intensity of the D_3 helium lines were much greater than for H_β hydrogen lines.

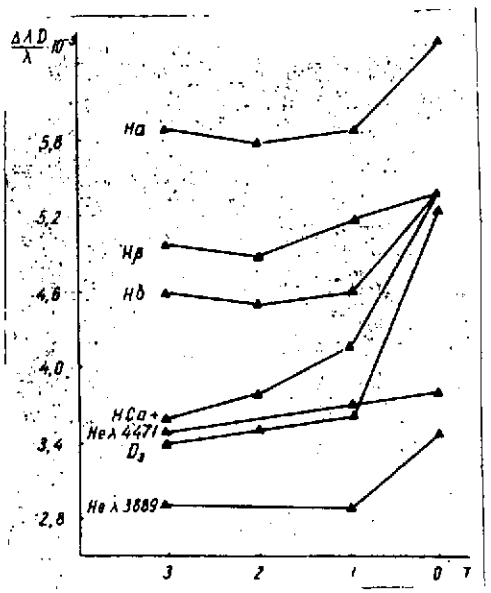

Figure 6. Variation in Given Doppler Half-Width in Time. Numerals 1, 2, and 3 designate the time intervals in days up to the active phase, that is, the phase of decay, and numeral 0 the time of decay of a prominence.

The equivalent widths and intensities of the H_ε lines for prominence 713, 736 are greater than for the H_8 lines, and for the active phase (prominences 163, 178, 226, 824, 981, 1027, and 736 on 8 July) the equivalent widths and intensities of the H_8 lines are greater than for H_ε. Comparison of the equivalent widths and intensities of the H_8 and He λ 3889 lines shows that for the relatively quiet phase (prominences 713, 736) the equivalent widths of the H_8 lines are greater than for the He λ 3889 lines. The central intensity of the H_8 lines is almost equal to the central intensity of the He λ 3889 lines. For the prominences in the active phase I_c of the He λ 3889 lines increases considerably in comparison to the H_8 /74 lines. The central intensity of the helium λ 3889 lines begins to increase approximately 1-2 days in advance of decay (prominences 163, 178, 185, 202, 213, 226, and 231). /73

Hence it may be assumed that the equivalent widths and intensities of the H_ε, H_8 hydrogen lines and λ 3889 helium lines depend on the degree of prominence activity. According to the classification of Newkirk [5], prominences

in which the central intensity ratio He λ 3889/H_8 ≥ 0.7 belong to the class of highly excited prominences. All the prominences selected by us for processing have He λ 3889 lines with central intensities greater than or equal to the central intensity of the H_8 hydrogen line and are highly excited ones.

TABLE 1. PROMINENCE 163

Lines	18-20 August 1965			21-22 August 1965		
	$W \cdot 10^{-4}$ Å	$\frac{I_c}{I_\odot} \cdot 10^{-4}$	$\frac{\Delta\lambda_D}{\lambda}$	$W \cdot 10^{-4}$ Å	$\frac{I_c}{I_\odot} \cdot 10^{-4}$	$\frac{\Delta\lambda_D}{\lambda}$
H_α	500	630	5,7	400	510	5,7
H_β	104	250	4,9	92	215	5,2
H_γ	36	76	4,4	37	98	4,5
H_δ	18	59	4,4	15	51	4,5
H_ε	7,3	28	4,0	5,5	20	4,3
H_8	8	32	3,7	7,8	28	4,5
D_3	38	131	2,8	66	198	3,1
He λ 3889	6,4	36	2,9	9,2	50	3,1
He λ 4471	2	9	3,3	3,9	17	3,3
H Ca+	32	155	2,6	34	119	3,6
K Ca+	33	147	2,9	40	128	3,9

Commas indicate decimal points.

TABLE 2.

Lines	8 June 1966			9 June 1966			10 June 1966		
	$W \cdot 10^{-4}$ Å	$\frac{I_c}{I_\odot} \cdot 10^{-4}$	$\frac{\Delta\lambda_D}{\lambda}$	$W \cdot 10^{-4}$ Å	$\frac{I_c}{I_\odot} \cdot 10^{-4}$	$\frac{\Delta\lambda_D}{\lambda}$	$W \cdot 10^{-4}$ Å	$\frac{I_c}{I_\odot} \cdot 10^{-4}$	$\frac{\Delta\lambda_D}{\lambda}$
H_α	415	552	5,9	281	390	5,8	184	240	5,8
H_β	69	155	5,2	61	137	5,1	53	133	5,0
D_3	28	62	3,7	29	75	3,9	41	103	3,8
H Ca+	63	200	3,7	52	160	3,9	50	170	3,3
K Ca+	75	243	4,2	61	160	4,5	49	210	3,8

Commas indicate decimal points.

TABLE 3. PROMINENCE 281.

Lines	9 September 1966			10 September 1966		
	$W \cdot 10^{-4}$ Å	$\frac{I_c}{I_\odot} \cdot 10^{-4}$	$\frac{\Delta\lambda_D}{\lambda}$	$W \cdot 10^{-4}$ Å	$\frac{I_c}{I_\odot} \cdot 10^{-4}$	$\frac{\Delta\lambda_D}{\lambda}$
H_α	306	470	5,7	283	440	5,8
H_β	26	78	4,2	32	80	4,9
D_3	16	48	3,4	28	66	3,8
H Ca+	28	158	2,6	32	180	3,0
K Ca+	34	171	2,9	46	205	3,1

Commas indicate decimal points.

TABLE 4. PROMINENCES 713, 736

Lines	713			736			736 on 8 August 1968		
	$W \cdot 10^{-4}$ Å	$\frac{I_C}{I_\odot} \cdot 10^{-4}$	$\frac{\Delta\lambda_D}{\lambda}$	$W \cdot 10^{-4}$ Å	$\frac{I_H}{I_\odot} \cdot 10^{-4}$	$\frac{\Delta\lambda_D}{\lambda}$	$W \cdot 10^{-4}$ Å	$\frac{I_H}{I_\odot} \cdot 10^{-4}$	$\frac{\Delta\lambda_D}{\lambda}$
H_α	515	670	5,9	442	500	6,2	533	640	5,8
H_β	82	180	5,2	72	150	5,2	66	160	4,9
H_γ	18	53	4,0	21	62	4,6	18	58	4,4
H_δ	10	34	4,6	13	41	4,6	13	47	4,2
H_ε	9	30	4,9	8	26	4,8	7,5	27	4,5
H_8	6,3	22	4,6	5	22	4,4	8,5	36	4,2
D_3	30	77	3,8	40	115	3,3	39	120	2,9
He λ 3889	4,4	26	3,1	4,1	27	2,9	6,2	38	3,1
He λ 4471	3,1	11	3,8	3	12	3,4	3,1	11	4,2
H Ca+	34	135	3,9	35	125	3,9	34	135	3,5
K Ca+	45	155	4,3	40	115	4,2	41	140	3,6

Commas indicate decimal points.

TABLE 5. PROMINENCE 981

Lines	Section 1			Section 2		
	$W \cdot 10^{-4}$ Å	$\frac{I_C}{I_\odot} \cdot 10^{-4}$	$\frac{\Delta\lambda_D}{\lambda}$	$W \cdot 10^{-4}$ Å	$\frac{I_C}{I_\odot} \cdot 10^{-4}$	$\frac{\Delta\lambda_D}{\lambda}$
H_α	756	810	7,3	524	565	7,0
H_β	128	240	6,3	93	185	5,8
H_γ	32	72	5,8	28	68	5,8
H_δ	16	42	5,6	13	38	5,4
H_ε	9	31	4,6	6,4	23	4,6
H_8	7	24	4,6	10	32	5,4
D_3	90	180	4,3	88	170	4,4
He λ 3889	8	40	3,2	11,4	53	3,3
He λ 4471	8	29	3,8	9	29	4,2
H Ca+	75	165	6,1	40	100	5,6
K Ca+	90	175	7,1	39	105	6,1

Commas indicate decimal points.

TABLE 5. CONT'D.

Lines	Sections 3, 4			Section 5		
	$W \cdot 10^{-4}$ Å	$\frac{I_C}{I_\odot} \cdot 10^{-4}$	$\frac{\Delta\lambda_D}{\lambda}$	$W \cdot 10^{-4}$ Å	$\frac{I_C}{I_\odot} \cdot 10^{-4}$	$\frac{\Delta\lambda_D}{\lambda}$
H_α	505	580	7,6	329	475	6,6
H_β	45	85	6,3	23	55	5,3
H_γ	12	30	5,9	7	20	5,1
H_δ						
H_ε						
H_8	1,3	7	3,2			
D_3	52	90	5,3	21	55	4,0
He λ 3889	2,2	14	2,8			
He λ 4471						
H Ca+	41	90	5,6	40	110	5,0
K Ca+	51	112	6,3	61	150	5,2

Commas indicate decimal points.

TABLE 6. PROMINENCE 1027

Lines	Section 1			Section 3		
	$W \cdot 10^{-4}$ Å	$\frac{I_C}{I_\odot} \cdot 10^{-4}$	$\frac{\Delta\lambda_D}{\lambda}$	$W \cdot 10^{-4}$ Å	$\frac{I_C}{I_\odot} \cdot 10^{-4}$	$\frac{\Delta\lambda_D}{\lambda}$
H_α	500	580	5,2	434	565	6,3
H_β	80	200	4,8	69	160	5,2
H_γ	19	60	4,5	15	44	5,3
H_δ	9,2	32	4,6	10,5	30	5,1
H_ε	8	26	5,0	6	18	5,1
H_8	4	19	3,2	9,5	32	5,2
D_3	56	145	3,4	84	180	4,7
He λ 3889	4	24	2,7	21,5	99	3,2
He λ 4471	6	27	3,2	19	59	4,4
H Ca+	43	145	4,1	63	160	4,8
K Ca+	55	175	4,4	71	155	5,4

Commas indicate decimal points.

REFERENCES

1. Rakubovskiy, A. S., in the book: *Astrometriya i Astrofizika* [Astrometrics and Astrophysics], (Investigation of the Sun and the Stars), Vol. 9, "Naukova Dumka" Press, Kiev, 1970.
2. Gurtovenko, E. A. and E. I. Didychenko, *Izv. GAO AN USSR*, Vol. 3, No. 2, p. 138, 1961.
3. Gurtovenko, E. A. and N. N. Semenova, *Izv. GAO AN USSR*, Vol. 4, No. 1, p. 39, 1961.
4. *Fraunhofer Institute Map of the Sun*, 1965-1969.
5. Newkirk, G., *Astron. j.*, Vol. 59, p. 330, 1954.

APPENDIX

CATALOGUE OF EQUIVALENT WIDTHS AND LINE INTENSITIES OF PROMINENCES IN THE PHASE PRECEDING DECAY

Sequential number	Item No.	Date, Co-ordinates, and time of observation	Lines	$W \cdot 10^4$ Å	$I_c/I_\odot \cdot 10^{-4}$	$\Delta\lambda/2$ Å	$\Delta\lambda_D$ Å	$\frac{\Delta\lambda_D}{\lambda} \cdot 10^{-5}$
	163	18 August 1965	H_α	550	700	0,390	0,385	5,9
		+45 NE	H_β	80	185	0,220	0,255	5.2
		06h,9 UT	H_γ	27	90	0,150	0,175	4,0
			H_δ	19	60	0,150	0,175	4,3
			D_3	65	190	0,160	0,195	3,3
			H Ca+	37	180	0,115	0,110	2,8
			K Ca+	37	160	0,125	0,115	2,9
			H_ε	10	38	0,130	0,160	4,0
			H_8	8	36	0,115	0,140	3,6
			He_{3889}	8	42	0,090	0,110	2,8
			He_{4471}	3	13	0,140	0,170	3,8
2	163	19 August	H_α	620	840	0,370	0,355	5,4
		+45 NE	H_β	100	235	0,190	0,225	4,6
		06h,4 UT	H_γ	28	85	0,140	0,165	3,8
		Section a	H_δ	11,5	42	0,140	0,175	4,3
			D_3	35	120	0,125	0,155	2,6
			H Ca+	43	225	0,085	0,090	2,3
			K Ca+	41	205	0,100	0,095	2,4
			H_ε	6	22	0,130	0,160	4,0
			H_8	6	25	0,140	0,160	4,1
			He_{3889}	3,5	22	0,090	0,110	2,8
			He_{4471}	2	8	0,140	0,170	3,8
3	163	19 August 1965	H_α	570	700	0,410	0,355	5,4
		+45 NE	H_β	108	265	0,205	0,235	4,8
		Section b	H_γ	35	105	0,155	0,180	4,1
			H_δ	17	54	0,150	0,180	4,4
			D_3	46	160	0,130	0,160	2,7
			H Ca+	35	190	0,095	0,095	2,4
			K Ca+	52	170	0,155	0,130	3,3
			H_ε	6	23	0,135	0,160	4,0
			H_8	6	31	0,115	0,135	3,5
			He_{3889}	4,5	28	0,085	0,120	3,1
			He_{4471}	1,5	7	0,110	0,130	2,9
4	163	19 August	H_α	542	680	0,400	0,370	5,6
		+45 NE	H_β	94	235	0,200	0,240	4,9
		Section c	H_γ	28	80	0,160	0,190	4,4
			H_δ	9	36	0,130	0,170	4,1
			D_3	33	130	0,135	0,160	2,7
			H Ca+	35	180	0,105	0,130	3,3
			K Ca+	36	165	0,115	0,120	3,1
			H_ε	5,5	22	0,135	0,140	3,5
			H_8	4	16	0,130	0,130	3,3
			He_{3889}	2,5	18	0,075	0,090	2,3
5	163	20 August	H_α	422	525	0,380	0,380	5,9
		+45 NE	H_β	119	270	0,210	0,240	4,9
		07h,1 UT	H_γ	38	100	0,180	0,210	4,8
		Section a	H_δ	24	80	0,150	0,180	4,4

Commas indicate decimal points.

Sequential number	Item No.	Date, Co-ordinates, and time of observation	Lines	$W \cdot 10^4$ Å	$I_c/I_\odot \cdot 10^{-4}$	$\Delta\lambda/2$ Å	$\Delta\lambda_D$ Å	$\frac{\Delta\lambda_D}{\lambda} \cdot 10^{-5}$
			D_3	30	95	0,135	0,170	
			H Ca+	23	115	0,105	0,100	
			K Ca+	26	125	0,115	0,110	
			H_ε	4	14	0,170	0,170	4,3
			H_8	10	40	0,135	0,160	4,1
			He_{3889}	9	50	0,090	0,135	3,5
			He_{4471}	0,8	4	0,120	0,145	3,2
6	163	20 August 1965 +45 NE Section b	H_α	492	570	0,440	0,415	6,3
			H_β	159	380	0,200	0,240	4,9
			H_γ	43	110	0,180	0,195	4,5
			H_δ	31	100	0,145	0,180	4,4
			D_3	59	176	0,160	0,190	3,2
			H Ca+	31	110	0,110	0,095	2,4
			K Ca+	26	110	0,135	0,135	3,4
			H_ε	12	53	0,125	0,155	3,9
			H_8	12	48	0,125	0,140	3,6
			He_{3889}	11	54	0,110	0,120	3,1
			He_{4471}	3	14	0,115	0,140	3,1
7	163	20 August +45 NE Section c	H_α	302	400	0,375	0,370	5,6
			H_β	65	170	0,200	0,240	4,9
			H_γ	22	60	0,160	0,195	4,5
			H_δ	15	40	0,165	0,200	4,9
			D_3	11	45	0,110	0,130	2,2
			H Ca+	17	85	0,090	0,085	2,1
			K Ca+	15	85	0,100	0,100	2,5
			H_ε	7	26	0,135	0,175	4,4
			H_8	7	31	0,120	0,140	3,6
			He_{3889}	6,5	40	0,090	0,105	2,7
			He_{4471}	2	9	0,110	0,130	2,9
8	163	21 August 1965 +45 NE 07h,9 UT	H_α	454	630	0,360	0,390	6,9
			H_β	73	200	0,190	0,250	5,1
			H_γ	18	45	0,170	0,200	4,6
			H_δ	15	45	0,170	0,200	4,4
			D_3	38	130	0,125	0,155	4,0
			H Ca+	36	135	0,140	0,180	4,6
			K Ca+	47	125	0,195	0,220	5,6
			H_ε	7	28	0,125	0,165	4,2
			He_{4471}	6	28	0,120	0,140	3,1
9	163	22 August 1965 +45 NE 06h,3 UT Section a	H_α	380	430	0,430	0,375	5,7
			H_β	114	235	0,235	0,285	5,8
			H_γ	50	150	0,180	0,210	4,8
			H_δ	15	52	0,155	0,200	4,9
			D_3	92	260	0,150	0,200	3,4
			H Ca+	33	105	0,140	0,130	3,3
			K Ca+	38	110	0,155	0,125	3,2
			H_ε	5,5	18	0,150	0,170	4,3
			H_8	8,5	30	0,145	0,180	4,6
			He_{3889}	11	51	0,105	0,130	3,3
			He_{4471}	3,5	15	0,120	0,150	3,3

Commas indicate decimal points.

Sequential number	Item No.	Date, Co-ordinates, and time of observation	Lines	$W \cdot 10^4$ Å	$I_c/I_\odot \cdot 10^{-5}$	$\Delta\lambda/2$ Å	$\Delta\lambda_D$ Å	$\frac{\Delta\lambda_D}{\lambda} \cdot 10^{-4}$
10	163	22 August	H_α	314	490	0,320	0,325	5,0
		+45 NE	H_β	65	165	0,205	0,230	4,7
		Section b	H_γ	22	62	0,155	0,180	4,1
			H_δ	8	30	0,135	0,160	3,9
			D_3	44	135	0,160	0,195	3,3
			H Ca+	28	115	0,130	0,125	3,2
			K Ca+	34	132	0,135	0,135	3,4
			H_ε	2,5	9	0,140	0,170	4,3
			H_8	6	21	0,160	0,155	4,0
			He_{3889}	5,5	34	0,090	0,105	2,7
			He_{4471}	1,5	5	0,150	0,180	4,0
11	163	22 August	H_α	450	500	0,450	0,375	5,7
		+45 NE	H_β	117	260	0,230	0,255	5,2
		Section c	H_γ	57	135	0,160	0,200	4,6
			H_δ	22	78	0,135	0,175	4,3
			D_3	90	260	0,150	0,175	3,0
			H Ca+	37	120	0,140	0,140	3,5
			K Ca+	41	145	0,140	0,130	3,3
			H_ε	7	25	0,145	0,170	4,3
			H_8	9	34	0,155	0,190	4,9
			He_{3889}	12	64	0,090	0,125	3,2
		23 September 1965	He_{4471}	4,5	22	0,115	0,135	3,0
12	178		H_α	462	640	0,350	0,415	6,3
		+55 NW	H_β	50	140	0,200	0,260	5,3
		08h,8 UT	H_γ	16	46	0,200	0,240	5,5
		Section a	D_3	48	95	0,200	0,245	4,2
			H Ca+	49	175	0,110	0,135	3,4
			K Ca+	76	260	0,120	0,150	3,8
			H_ε	3,5	16	0,120	0,150	3,8
			H_8	6	18	0,185	0,220	5,7
			He_{3889}	6,5	38	0,085	0,105	2,7
		23 September 1965	He_{4471}	3	14	0,130	0,160	3,6
13	178		H_α	374	480	0,400	0,435	6,7
		+55 NW	H_β	43	105	0,210	0,245	5,0
		Section b	H_γ	17	45	0,200	0,240	5,5
			D_3	49	115	0,200	0,240	4,1
			H Ca+	32	85	0,205	0,245	6,2
			K Ca+	42	105	0,215	0,245	6,2
			H_ε	2,5	9	0,155	0,190	4,8
			H_8	5,5	17	0,190	0,225	5,8
			He_{3889}	6	38	0,085	0,105	2,7
		29 September 1965	He_{4471}	1,5	9	0,100	0,120	2,7
14	184		H_α	700	650	0,570	0,590	9,0
		+32 NW	H_β	113	210	0,285	0,300	6,2
		07h,9 UT	H_γ	31	70	0,215	0,255	5,8
			H_δ	23	63	0,195	0,240	5,8
			D_3	92	190	0,220	0,270	4,6
			H Ca+	91	160	0,240	0,250	6,3
			K Ca+	118	215	0,270	0,270	6,9

Commas indicate decimal points.

Sequential number	Item No.	Date, Coordinates, and time of observation	Lines	$W \cdot 10^4$ Å	$I_c/I_\odot \cdot 10^{-4}$	$\Delta\lambda/2$ Å	$\Delta\lambda_D$ Å	$\frac{\Delta\lambda_D}{\lambda} \cdot 10^{-5}$
			H_ε	10	30	0,195	0,230	5,8
			H_8	4	12	0,185	0,225	5,5
			He_{3889}	5,5	18	0,155	0,185	4,8
			He_{4471}	3	14	0,125	0,130	2,9
15	185	2 October 1965	H_α	404	500	0,400	0,390	5,9
		—42 SE	H_β	80	215	0,200	0,230	4,7
		11h,2 UT	H_γ	22	65	0,190	0,230	5,3
			H_δ	12	44	0,160	0,200	4,9
			D_3	40	105	0,160	0,205	3,5
			H Ca+	56	180	0,150	0,185	4,7
			K Ca+	60	175	0,175	0,190	4,8
			H_ε	8	22	0,180	0,230	5,8
			H_8	3,5	14	0,140	0,170	4,4
			He_{3889}	6	33	0,115	0,140	3,5
			He_{4471}	6,5	21	0,170	0,180	4,0
16	202	11 June 1966	H_α	526	800	0,340	0,360	5,5
		+58 NW	H_β	71	190	0,200	0,245	5,0
		06h,4 UT	H_γ	20	60	0,175	0,210	4,8
		Section 1a	D_3	42	135	0,145	0,175	3,0
			H Ca+	58	245	0,115	0,140	3,5
			K Ca+	76	255	0,140	0,150	3,9
17	202	11 June	H_α	440	710	0,290	0,325	4,9
		+58 NW	H_β	64	160	0,205	0,240	4,9
		Section 1b	H_γ	14	45	0,160	0,200	4,6
			D_3	32	105	0,140	0,170	2,9
			H Ca+	25	180	0,075	0,090	2,2
			K Ca+	49	235	0,095	0,115	2,9
18	202	11 June	H_α	360	530	0,340	0,380	5,8
		+58 NW	H_β	50	122	0,225	0,250	5,1
		Section 1c	H_γ	10	32	0,180	0,220	5,0
			D_3	43	115	0,175	0,210	3,5
			H Ca+	61	145	0,200	0,205	5,2
			K Ca+	87	150	0,220	0,230	5,9
19	202	11 June 1966	H_α	390	550	0,365	0,395	6,0
		+58 NW	H_β	68	165	0,210	0,225	4,6
		06h,8 UT	D_3	68	140	0,220	0,260	4,4
		Section 2a	H Ca+	30	115	0,115	0,140	3,5
			K Ca+	30	135	0,110	0,135	3,4
			H_8	2,5	12	0,125	0,155	4,0
			He_{3889}	3,0	16	0,110	0,135	3,5
20	202	11 June 1966	H_α	320	440	0,365	,0395	6,0
		+58 NW	H_β	38	105	0,170	0,220	4,5
		Section 2b	D_3	28	70	0,170	0,200	3,4
			H Ca+	24	130	0,085	0,105	2,6
			K Ca+	29	150	0,095	0,110	2,8
			H_8	2	9	0,115	0,140	3,6
			He_{3889}	2	15	0,090	0,110	28,

Commas indicate decimal points.

Sequential number	Item No.	Date, Coordinates, and time of observation	Lines	W·10⁴ Å	$I_C/I_\odot \cdot 10^{-4}$	$\Delta\lambda/2$ Å	$\Delta\lambda_D$ Å	$\frac{\Delta\lambda_D}{\lambda} \cdot 10^{-5}$
21	213	20 June 1966 +45 NE 05h,9 UT Section 1a	H_α	514	680	0,375	0,375	5,7
			H_β	80	190	0,205	0,245	5,0
			H_γ	22	63	0,185	0,225	5,2
			H_δ	5	20	0,145	0,180	4,4
			D_3	59	165	0,175	0,220	3,7
			H Ca+	47	180	0,135	0,140	3,5
			K Ca+	58	200	0,140	0,150	3,8
			H_8	5	18	0,140	0,170	4,4
			He_{3889}	7	48	0,080	0,100	2,6
			He_{4471}	4	20	0,120	0,145	3,2
22	213	20 June +45 NE Section 1b	H_α	498	710	0,350	0,360	5,5
			H_β	66	170	0,195	0,235	4,8
			H_γ	15	53	0,140	0,170	3,9
			H_δ	8	24	0,175	0,200	4,9
			D_3	68	145	0,230	0,260	4,4
			H Ca+	49	165	0,150	0,160	4,0
			K Ca+	60	170	0,170	0,180	4,6
			H_8	4	14	0,150	0,180	4,6
			He_{3889}	7	48	0,070	0,090	2,3
			He_{4471}	4	20	0,110	0,135	3,0
23	213	20 June 1966 +45 NE 12h,2 UT Section 2a	H_α	370	465	0,390	0,465	7,1
			H_β	49	110	0,230	0,275	5,6
			H_γ	11	35	0,180	0,220	5,0
			H_δ	3	16	0,130	0,160	3,9
			D_3	54	100	0,280	0,345	5,9
			H Ca+	71	175	0,195	0,235	5,9
			K Ca+	82	195	0,205	0,245	6,2
			H_8	5	18	0,130	0,160	4,1
			He_{3889}	8	38	0,110	0,135	3,5
			He_{4471}	6	28	0,125	0,150	3,4
24	213	20 June +45 NE Section 2b	H_α	305	420	0,360	0,430	6,5
			H_β	32	65	0,255	0,310	6,4
			D_3	49	90	0,280	0,345	5,9
			H Ca+	60	155	0,180	0,225	5,7
			K Ca+	75	175	0,205	0,245	6,2
			H_8	5	22	0,110	0,135	3,5
			He_{3889}	10	40	0,130	0,160	4,1
			He_{4471}	8	32	0,155	0,185	4,1
25	226	6 July 1966 +57 NE 06h,1 UT Section a	H_α	568	720	0,390	0,330	5,0
			H_β	84	205	0,190	0,240	4,9
			H_γ	19	58	0,170	0,210	4,8
			H_δ	10	33	0,160	0,195	4,7
			D_3	42	105	0,155	0,190	3,2
			H Ca+	35	165	0,080	0,095	2,4
			K Ca+	50	200	0,095	0,115	2,9
			H_ε	6	20	0,165	0,195	4,9
			H_8	7	30	0,145	0,170	4,4
			He_{3889}	4	31	0,080	0,095	2,4
			He_{4471}	4,5	18	0,120	0,150	3,4

Commas indicate decimal points.

Sequential number	Item No.	Date, Coordinates, and time of observation	Lines	$W \cdot 10^4$ Å	$I_c/I_\odot \cdot 10^{-4}$	$\Delta\lambda/2$ Å	$\Delta\lambda_D$ Å	$\frac{\Delta\lambda_D}{\lambda} \cdot 10^{-5}$
26	226	6 July 1966	H_α	492	610	0,410	0,395	6,0
		+57 NE	H_β	67	170	0,195	0,240	4,9
		Section b	H_γ	22	65	0,170	0,205	4,7
			H_δ	7	32	0,130	0,160	3,9
			D_3	34	80	0,180	0,220	3,7
			H Ca+	36	120	0,150	0,165	4,2
			K Ca+	45	130	0,170	0,180	4,6
			H_ε	7	23	0,155	0,185	4,7
			H_8	5	20	0,135	0,160	4,1
			He_{3889}	3	22	0,080	0,095	2,4
			He_{4471}	2	8	0,130	0,155	3,5
27	226	7 July 1966	H_α	510	625	0,400	0,415	6,3
		+57 NE	H_β	77	195	0,190	0,230	4,7
		05h,7 UT	H_γ	30	90	0,160	0,200	4,6
			H_δ	16	55	0,155	0,190	4,6
			D_3	27	70	0,195	0,250	4,2
			H Ca+	43	165	0,115	0,125	3,2
			K Ca+	47	180	0,120	0,140	3,6
			H_ε	6	23	0,125	0,150	3,8
			H_8	8,5	26	0,165	0,195	5,0
			He_{3889}	8	44	0,100	0,125	3,2
			He_{4471}	3	14	0,115	0,140	3,1
28	231	9 July 1966	H_α	538	580	0,455	0,510	7,8
		—50 SE	H_β	106	265	0,195	0,225	4,6
		13h,4 UT	H_γ	25	75	0,170	0,190	4,4
		Section a	H_δ	17	55	0,155	0,180	4,4
			D_3	92	255	0,150	0,185	3,2
			H Ca+	65	170	0,190	0,195	4,0
			K Ca+	72	180	0,195	0,190	4,8
			H_ε	5	18	0,140	0,170	4,3
			H_8	2,5	11	0,140	0,170	4,4
			He_{3889}	5	26	0,105	0,130	3,4
			He_{4471}	8	27	0,170	0,205	4,6
29	231	9 July	H_α	440	480	0,440	0,485	7,4
		—50 SE	H_β	89	210	0,215	0,250	5,1
		Section b	H_γ	22	70	0,165	0,180	4,1
			D_3	83	222	0,150	0,175	3,0
			H Ca+	50	155	0,170	0,185	4,7
			K Ca+	64	165	0,200	0,210	5,3
			H_ε	8	27	0,150	0,180	4,6
			H_8	3	11	0,145	0,175	4,5
			He_{3889}	6	32	0,100	0,120	3,1
			He_{4471}	5	26	0,115	0,140	3,1
30	231	10 July 1966	H_α	226	345	0,325	0,390	5,9
		—50 SE	H_β	32	83	0,210	0,255	5,2
		07h,5 UT	D_3	20	55	0,160	0,195	3,3
		Section a	H Ca+	58	150	0,165	0,200	5,0
			H_8	5	22	0,120	0,145	3,7
			He_{3889}	5	27	0,095	0,115	3,0

Commas indicate decimal points.

Sequential number	Item No.	Date, Coordinates, and time of observation	Lines	W·10⁴ Å	$I_c/I_\odot \cdot 10^{-4}$	$\Delta\lambda/2$ Å	$\Delta\lambda_D$ Å	$\frac{\Delta\lambda_D}{\lambda} \cdot 10^{-5}$
31	231	10 July	H_α	230	350	0,325	0,365	5,6
		—50 SE	H_β	39	95	0,210	0,255	5,2
		Section b	H_γ	14	48	0,160	0,190	4,4
			D_3	25	70	0,165	0,200	3,4
			H Ca+	33	130	0,125	0,150	3,8
			K Ca+	45	145	0,135	0,160	4,1
			H_δ	3	12	0,135	0,160	4,1
			He_{3889}	4	22	0,105	0,125	3,2
32	231	10 July 1966	H_α	154	230	0,335	0,365	5,6
		—50 SE	H_β	26	60	0,230	0,275	5,7
		Section c	D_3	24	50	0,230	0,290	4,9
			H Ca+	22	90	0,130	0,155	3,9
			K Ca+	28	95	0,150	0,180	4,6
			H_8	4,5	16	0,150	0,180	4,6
			He_{3889}	5	25	0,110	0,135	3,5
33	261	8 August 1966	H_α	588	715	0,340	0,375	5,7
		+45 NE	H_β	90	180	0,220	0,265	5,4
		13h,1 UT	H_γ	32	90	0,170	0,210	4,9
		Section a	H_δ	22	65	0,195	0,230	5,6
			D_3	41	85	0,225	0,270	4,6
			H Ca+	98	260	0,145	0,165	4,2
			K Ca+	104	280	0,165	0,195	5,0
			H_ε	26	70	0,185	0,220	5,5
34	261	8 August	H_α	390	560	0,340	0,375	5,7
		+45 NE	H_β	64	155	0,215	0,260	5,3
		Section b	H_γ	26	70	0,185	0,225	5,2
			H_δ	13	35	0,170	0,210	5,1
			D_3	20	65	0,135	0,160	2,7
			H Ca+	53	210	0,120	0,135	3,4
			K Ca+	68	240	0,140	0,160	4,1
			H_ε	12	45	0,150	0,175	4,4
35	261	8 August	H_α	266	380	0,350	0,400	6,1
		+45 NE	H_β	54	135	0,210	0,245	5,0
		Section c	H_γ	12	30	0,195	0,240	5,5
			H_δ	6	18	0,175	0,215	5,2
			D_3	13	35	0,180	0,230	3,9
			H Ca+	39	165	0,110	0,135	3,4
			K Ca+	54	210	0,125	0,145	3,7
			H_ε	5,5	27	0,110	0,135	3,4
36	261	9 August 1966	H_α	416	550	0,385	0,360	5,5
		+45 NE	H_β	105	240	0,225	0,270	5,7
		08h,8 UT	D_3	35	100	0,145	0,175	3,0
		Section a	H Ca+	55	190	0,115	0,115	2,9
			H_ε	22	75	0,175	0,215	5,4
37	261	9 August	H_α	244	340	0,365	0,410	6,2
		+45 NE	H_β	38	100	0,200	0,240	4,9
		Section b	D_3	26	62	0,195	0,235	4,0
			H Ca+	53	150	0,175	0,180	4,5
			K Ca+	59	145	0,195	0,195	5,0

Commas indicate decimal points.

Sequential number	Item No.	Date, Coordinates, and time of observation	Lines	$W \cdot 10^4$ Å	$I_C/I_\odot \cdot 10^{-4}$	$\Delta\lambda/2$ Å	$\Delta\lambda_D$ Å	$\frac{\Delta\lambda_D}{\lambda} \cdot 10^{-5}$
38	261	9 August	H_α	184	280	0,320	0,375	5,7
		+45 NE	H_β	39	70	0,240	0,240	4,9
		Section c	D_3	27	63	0,220	0,270	4,6
			H Ca+	49	140	0,180	0,185	4,7
			K Ca+	63	175	0,185	0,185	4,7
39	261	10 August 1966	H_α	216	310	0,325	0,400	6,1
		+45 NE	H_β	58	150	0,195	0,225	4,6
		06h,6 UT	D_3	41	93	0,190	0,230	3,9
		Section a	H Ca+	48	170	0,090	0,115	2,9
			K Ca+	67	210	0,110	0,130	3,3
40	261	10 August	H_α	180	300	0,300	0,355	5,4
		+45 NE	H_β	55	140	0,190	0,230	4,7
		Section b	D_3	41	105	0,205	0,250	4,3
			H Ca+	57	180	0,115	0,145	3,7
			K Ca+	78	240	0,125	0,160	4,1
41	261	10 August 1966	H_α	155	225	0,350	0,420	6,4
		+45 NE	H_β	46	110	0,220	0,270	5,5
		Section c	D_3	40	115	0,170	0,200	3,4
			H Ca+	44	160	0,120	0,155	3,9
		9 September 1966	K Ca+	50	190	0,120	0,155	4,0
42	281		H_α	334	525	0,320	0,370	5,6
		+58 NE	H_β	32	95	0,170	0,185	3,8
		06h,2 UT	H_γ	6	18	0,170	0,210	4,8
		Section a	D_3	18	60	0,150	0,180	3,1
			H Ca+	26	175	0,070	0,085	2,1
			K Ca+	37	210	0,075	0,090	2,3
43	281	9 September	H_α	326	520	0,310	0,370	5,6
		+58 NE	H_β	30	85	0,175	0,175	3,6
		Section b	H_γ	3	15	0,115	0,140	3,2
			D_3	18	15	0,165	0,195	3,3
			H Ca+	27	170	0,080	0,095	2,4
			K Ca+	32	185	0,090	0,110	2,8
44	281	9 September	H_α	346	520	0,320	0,380	5,8
		+58 NE	H_β	38	96	0,200	0,240	4,9
		Section c	H_γ	7	20	0,185	0,210	4,8
			D_3	21	55	0,165	0,200	3,4
			H Ca+	33	160	0,100	0,120	3,0
			K Ca+	37	175	0,110	0,125	3,2
45	281	9 September	H_α	216	310	0,325	0,390	5,9
		+58 NE	H_β	14	38	0,170	0,215	4,4
		Section d	D_3	7	20	0,180	0,220	3,7
			H Ca+	25	125	0,100	0,120	3,0
			K Ca+	27	115	0,105	0,125	3,2
		10 September 1966	H_α	158	250	0,295	0,320	4,9
46	281		D_3	11	32	0,185	0,220	3,7
		+58 NE	H Ca+	24	130	0,100	0,120	3,0
		06h,1 UT	K Ca+	34	150	0,115	0,130	3,3
		Section a						

Commas indicate decimal points.

Sequential number	Item No.	Date, Coordinates, and time of observation	Lines	$W \cdot 10^4$ Å	$I_C/I_\odot \cdot 10^{-4}$	$\Delta\lambda/2$ Å	$\Delta\lambda_D$ Å	$\frac{\Delta\lambda_D}{\lambda} \cdot 10^{-5}$
47	281	10 September	H_α	298	440	0,340	0,400	6,1
		+58 NE	H_β	35	80	0,215	0,250	5,1
		Section b	H_γ	6	25	0,140	0,165	3,8
			D_3	26	62	0,185	0,220	3,7
			H Ca+	28	170	0,085	0,100	2,5
			K Ca+	38	210	0,085	0,100	2,6
	281	10 September	H_α	268	440	0,300	0,355	5,4
		+58 NE	H_β	30	80	0,185	0,230	4,7
		Section c	H_γ	4	16	0,135	0,160	3,7
			D_3	31	70	0,190	0,230	3,9
			H Ca+	36	190	0,120	0,135	3,4
			K Ca+	54	205	0,120	0,150	3,8
49	320	5 October 1966	H_α	294	340	0,420	0,480	7,3
		+55 NW	D_3	21	32	0,350	0,440	7,5
		10h,3 UT	H Ca+	57	145	0,200	0,245	6,2
		Section 1a	K Ca+	75	155	0,240	0,285	7,3
50	320	5 October	H_α	176	320	0,265	0,305	4,6
		+55 NW	D_3	18	42	0,210	0,255	4,3
		Section 1b	H Ca+	32	115	0,120	0,140	3,5
			K Ca+	31	115	0,140	0,170	4,3
51	320	5 October	H_α	180	300	0,280	0,300	4,6
		+55 NW	D_3	17	34	0,270	0,315	5,4
		Section 1c	H Ca+	22	115	0,090	0,110	2,8
		5 October 1966	K Ca+	24	125	0,100	0,115	2,9
	320		H_α	254	330	0,370	0,420	6,4
		+55 NW	H_β	110	190	0,255	0,305	6,3
		12h,2 UT	D_3	35	60	0,285	0,340	5,8
		Section 2a	H Ca+	64	140	0,220	0,265	6,7
			K Ca+	82	185	0,210	0,260	6,6
52	320	5 October	H_α	224	310	0,350	0,415	6,3
		+55 NW	H_β	65	115	0,260	0,305	6,3
		Section 2b	D_3	27	45	0,290	0,340	5,8
			H Ca+	53	100	0,235	0,265	6,7
			K Ca+	67	135	0,265	0,315	8,0
54	321	5 October	H_α	78	155	0,260	0,275	4,2
		+55 NW	D_3	22	40	0,290	0,340	5,8
		Section 2c	H Ca+	17	90	0,075	0,095	2,4
			K Ca+	22	105	0,105	0,125	3,2
55	321	5 October	H_α	72	150	0,225	0,245	3,7
		+55 NW	D_3	11	35	0,160	0,190	3,2
		Section 2d	H Ca+	17	95	0,075	0,100	2,5
		10 October 1966	K Ca+	22	95	0,120	0,130	3,3
56	327		H_α	324	450	0,365	0,420	6,4
		−25 NE	H_β	25	70	0,175	0,200	4,1
		08h,0 UT	D_3	56	115	0,225	0,275	4,7
			H Ca+	67	230	0,120	0,150	3,8
			K Ca+	75	250	0,135	0,165	4,2
			He_{3889}	3	21	0,090	0,105	7,2
			He_{4471}	6	28	0,115	0,140	3,1

Commas indicate decimal points.

Sequential number	Item No.	Date, Co-ordinates, and time of observation	Lines	W 10^4 Å	$I_{c\gamma}/I_\odot \cdot 10^{-4}$	$\Delta\lambda/2$ Å	$\Delta\lambda_D$ Å	$V_T \cdot 10^{-5}$ / λ
57	713	26 June 1968	H_α	750	840	0,435	0,410	6,3
		—60 SE	H_β	92	170	0,245	0,255	5,2
		$10^h,6$ UT	H_γ	20	55	0,190	0,230	5,3
		Section a	D_3	41	120	0,140	0,170	2,9
			H Ca+	29	105	0,130	0,135	3,4
			K Ca+	61	210	0,130	0,140	3,6
			H_ε	16	62	0,135	0,160	4,0
			H_8	12	35	0,175	0,210	5,4
			He_{3889}	6	32	0,100	0,120	3,1
			He_{4471}	3	10	0,160	0,180	4,0
58	713	26 June	H_α	640	740	0,415	0,405	6,2
		—60 SE	H_β	82	175	0,220	0,245	5,0
		Section b	H_γ	16	45	0,195	0,225	5,2
			H_δ	25	80	0,150	0,175	4,3
			D_3	31	100	0,125	0,150	2,6
			H Ca+	32	105	0,145	0,160	4,0
			K Ca+	62	210	0,145	0,175	4,5
			H_ε	15	50	0,150	0,180	4,5
			H_8	8,5	27	0,155	0,195	5,0
			He_{3889}	5	32	0,085	0,105	2,7
			He_{4471}	2	8	0,130	0,155	3,5
59	713	26 June	H_α	350	440	0,380	0,430	6,5
		—60 SE	H_β	30	60	0,260	0,320	6,6
		Section c	H_γ	12	35	0,185	0,215	5,0
			H_δ	5	18	0,170	0,205	5,0
			D_3	14	28	0,250	0,296	5,0
			H Ca+	22	55	0,200	0,250	6,3
			K Ca+	43	90	0,230	0,275	7,0
			H_ε	6	15	0,195	0,215	5,4
60	713	27 June 1968	H_α	750	960	0,355	0,355	5,4
		—60 SE	H_β	128	290	0,200	0,235	4,8
		$05^h,4$ UT	H_γ	28	85	0,135	0,180	4,1
		Section 1a	H_δ	16	55	0,140	0,170	4,1
			D_3	60	170	0,160	0,180	3,1
			H Ca+	35	180	0,095	0,120	3,0
			K Ca+	37	145	0,115	0,110	2,8
			H_ε	10	35	0,155	0,190	4,8
			H_8	8	32	0,125	0,150	3,9
			He_{3889}	6	35	0,059	0,115	3,0
			He_{4471}	6,5	18	0,180	0,190	4,2
61	713	27 June	H_α	620	800	0,385	0,410	6,2
		—60 SE	H_β	106	235	0,210	0,245	5,0
		Section 1b	H_γ	27	85	0,165	0,195	4,5
			H_δ	15	55	0,145	0,185	4,5
			D_3	37	110	0,140	0,175	3,0
			H Ca+	30	160	0,090	0,110	2,8
			K Ca+	27	145	0,090	0,105	2,7
			H_ε	10	34	0,165	0,200	5,0
			H_8	5,0	22	0,120	0,150	3,9

Commas indicate decimal points.

Sequential number	Item No.	Date, Co-ordinates, and time of observation	Lines	W·10⁴ Å	I_C/I_⊙·10⁻⁴	Δλ/2 Å	Δλ_D Å	Δλ_D/λ ·10⁻⁵
			He_{3888}	3,0	23	0,075	0,105	2,7
			He_{4471}	3,0	10	0,150	0,160	3,6
	713	27 June	H_α	475	700	0,340	0,400	6,1
		—60 SE	H_β	80	170	0,210	0,245	5,0
		Section 1c	H_γ	20	52	0,195	0,240	5,5
			D_3	29	60	0,225	0,270	4,6
			H Ca+	34	107	0,160	0,190	4,8
			K Ca+	39	125	0,155	0,200	5,1
			H_ε	9	26	0,180	0,220	5,5
			H_8	8	26	0,160	0,190	4,9
			He_{3889}	5	28	0,095	0,120	3,1
63	713	27 June	H_α	540	700	0,390	0,390	5,9
		06h,3 UT	H_β	117	270	0,200	0,230	4,7
		Section 2a	H_γ	27	85	0,155	0,185	4,3
			H_δ	11	35	0,155	0,185	4,5
			D_3	40	100	0,160	0,190	3,2
			H Ca+	40	195	0,100	0,120	3,0
			K Ca+	43	190	0,105	0,130	3,3
			H_ε	11	35	0,165	0,200	5,0
			H_8	8	28	0,155	0,185	4,8
			He_{3889}	6	41	0,085	0,100	2,6
			He_{4471}	2	8	0,135	0,160	3,6
64	713	27 June	H_α	440	600	0,365	0,375	5,7
		—60 SE	H_β	110	245	0,210	0,250	5,1
		Section 2b	H_γ	20	65	0,155	0,200	4,6
			H_δ	8,5	30	0,145	0,185	4,5
			D_3	26	62	0,200	0,240	4,1
			H Ca+	29	150	0,100	0,120	3,0
			K Ca+	32	140	0,110	0,130	3,3
			H_ε	9	30	0,170	0,200	5,0
			H_8	6	21	0,150	0,180	4,6
			He_{3889}	5,5	28	0,095	0,120	3,1
			He_{4471}	3	15	0,130	0,155	3,5
65	713	27 June 1968	H_α	395	495	0,405	0,450	6,9
		—60 SE	H_β	66	140	0,215	0,260	5,3
		Section 2c	H_γ	11	33	0,170	0,205	4,7
			H_δ	4,5	14	0,170	0,210	5,1
			D_3	24	58	0,195	0,245	4,2
			H Ca+	32	110	0,150	0,190	4,8
			K Ca+	41	110	0,175	0,215	5,5
			H_ε	5	18	0,165	0,205	5,2
			H_8	3	11	0,140	0,170	4,4
			He_{3889}	3,5	25	0,080	0,100	2,6
66	713	28 June 1968	H_α	522	750	0,330	0,350	5,3
		—60 SE	H_β	67	150	0,210	0,240	4,9
		06h,4 UT	H_γ	12	37	0,160	0,210	4,8
		Section 1a	H_δ	10,5	35	0,160	0,200	4,9
			D_3	25	53	0,230	0,275	4,7
			H Ca+	40	160	0,115	0,150	3,8

Commas indicate decimal points.

Sequential number	Item No.	Date, Coordinates, and time of observation	Lines	$W \cdot 10^4$ Å	$I_c/I_\odot \cdot 10^{-4}$	$\Delta\lambda/2$ Å	$\Delta\lambda_D$ Å	$\frac{\Delta\lambda_D}{\lambda} \cdot 10^{-5}$
			K Ca+	58	170	0,155	0,180	4 6
			H_ε	8	25	0,165	0,190	4 8
			H_8	5,5	17	0,170	0,200	1
			He_{3889}	4	20	0,110	0,135	,5
			He_{4471}	1	4	—	—	—
67	713	28 June —60 SE Section 1b	H_α	286	430	0,330	0,355	5,4
			H_β	43	100	0,210	0,250	5,1
			H_γ	7	20	0,165	0,220	5,
			H_δ	5	17	0,165	0,215	5 2
			D_3	16	46	0,190	0,230	3 4
			H Ca+	37	120	0,135	0,175	4,4
			K Ca+	48	145	0,160	0,190	4,8
			H_ε	4	17	0,160	0,190	4 8
			H_8	2	8	0,140	0,170	4,4
			He_{3889}	2,5	17	0,080	0,100	2,6
			He_{4471}	1	4	—	—	—
68	713	28 June —60 SE 07h,5 UT Section 2a	H_α	500	700	0,345	0,340	5,2
			H_β	82	185	0,210	0,250	5,1
			H_γ	18	53	0,165	0,200	4,6
			H_δ	5	18	0,160	0,195	4,8
			D_3	24	60	0,195	0,240	4,
			H Ca+	38	165	0,110	0,135	3,4
			K Ca+	43	170	0,115	0,145	3,
			H_ε	6	16	0,200	0,220	5,
			H_8	6	22	0,145	0,175	4,
			He_{3889}	4	16	0,135	0,160	4,
			He_{4471}	3	10	0,165	0,200	4,
69	713	28 June —60 SE Section 2b	H_α	430	580	0,365	0,375	5,
			H_β	66	135	0,240	0,290	6,
			H_γ	15	43	0,165	0,200	4,6
			H_δ	4	15	0,140	0,180	4,4
			D_3	21	50	0,190	0,215	3,7
			H Ca+	47	165	0,140	0,170	4,3
			K Ca+	45	160	0,145	0,180	4,6
			H_ε	4	16	0,130	0,155	3,9
			H_8	4	18	0,135	0,155	4,0
			He_{3889}	3	17	0,115	0,140	,6
			He_{4471}	2,5	10	0,140	0,170	,8
70	736	5 July 1968 —60 SW 07h,5 UT Section a	H_α	300	380	0,405	0,420	6 4
			H_β	85	165	0,225	0,260	5 1
			H_γ	28	85	0,155	0,190	4 4
			H_δ	20	65	0,150	0,170	4,1
			D_3	48	145	0,150	0,180	3,1
			H Ca+	36	150	0,115	0,120	3,0
			K Ca+	37	145	0,115	0,125	3,2
			H_ε	11	40	0,135	0,165	4,2
			H_8	6	23	0,160	0,195	5,0
			He_{3889}	4	25	0,085	0,105	2,7
			He_{4471}	3	14	0,115	0,140	3,1

Commas indicate decimal points.

Sequential number	Item No.	Date, Co-ordinates, and time of observation	Lines	W·10⁴ Å	$I_c/I_\odot \cdot 10^{-4}$	Δλ/2 Å	$\Delta\lambda_D$ Å	$\frac{\Delta\lambda_D}{\lambda} \cdot 10^{-5}$
7	736	5 July	H_α	380	440	0,435	0,395	6,0
		—60 SW	H_β	75	165	0,215	0,220	4,5
		Section b	H_γ	43	140	0,145	0,155	3,6
			H_δ	25	85	0,135	0,155	3,8
			D_3	31	100	0,155	0,190	3,2
			H Ca+	38	150	0,125	0,125	3,1
			K Ca+	36	150	0,120	0,130	3,3
			H_ε	12	40	0,145	0,175	4,4
			H_8	7	23	0,155	0,185	4,8
			He_{3889}	4	26	0,095	0,125	3,2
			He_{4471}	2	8	0,110	0,135	3,0
	736	5 July 1968	H_α	288	370	0,390	0,380	5,8
		—60 SW	H_β	45	100	0,235	0,250	5,2
		Section c	H_γ	20	70	0,135	0,165	3,8
			H_δ	16	52	0,155	0,160	3,9
			D_3	23	75	0,145	0,205	3,5
			H Ca+	37	150	0,130	0,125	3,1
			K Ca+	48	150	0,155	0,140	3,6
			H_ε	9	30	0,140	0,175	4,4
			H_8	4	15	0,150	0,190	4,9
			He_{3889}	3	16	0,095	0,120	3,1
	736	5 July	H Ca+	25	100	0,125	0,150	3,8
		—60 SW	K Ca+	27	100	0,135	0,160	4,1
		Section d	H_ε	3,5	13	0,155	0,185	4,7
			H_8	2,5	10	0,135	0,165	4,2
			He_{3889}	2	10	0,100	0,120	3,1
	736	6 July 1968	H_α	532	600	0,450	0,400	6,1
		—60 SW	H_β	86	180	0,240	0,210	4,3
		05h,9 UT	H_γ	29	85	0,160	0,185	4,3
		Section 1a	H_δ	15	52	0,145	0,175	4,3
			D_3	57	180	0,140	0,170	2,9
			H Ca+	34	135	0,125	0,125	3,1
			K Ca+	44	150	0,140	0,140	3,6
			H_ε	10	33	0,140	0,175	4,4
			H_8	4,5	16	0,140	0,170	4,4
			He_{3889}	4	38	0,070	0,095	2,4
			He_{4471}	2,5	12	0,120	0,145	3,2
	736	6 July	H_α	455	535	0,425	0,385	5,9
		—60 SW	H_β	67	175	0,190	0,225	4,6
		Section 1b	H_γ	21	70	0,155	0,190	4,4
			H_δ	11	35	0,165	0,190	4,6
			D_3	55	155	0,135	0,165	2,8
			H Ca+	34	130	0,140	0,140	3,5
			K Ca+	40	140	0,150	0,150	3,8
			H_ε	8	23	0,175	0,225	5,7
			H_8	3	14	0,130	0,160	4,1
			He_{3889}	5,5	38	0,080	0,095	2,4
			He_{4471}	2,5	13	0,110	0,135	3,0

Commas indicate decimal points.

Sequential number	Item No.	Date, Coordinates, and time of observation	Lines	$W \cdot 10^4$ Å	$I_{c}/I_{\odot} \cdot 10^{-4}$	$\Delta\lambda/2$ Å	$\Delta\lambda_D$ Å	$\frac{\Delta\lambda_D}{\lambda} \cdot 10^{-5}$
76	736	6 July 1968	H_α	310	420	0,370	0,[illegible]0	5,9
		—60 SW	H_β	70	160	0,215	0,240	4,9
		05h,7 UT	H_γ	14	40	0,170	0,210	4,8
		Section 2a	H_δ	7	25	0,155	0,1[illegible]0	4,6
			D_3	35	100	0,160	0,1[illegible]	3,3
			H Ca+	34	150	0,110	0,135	3,4
			K Ca+	48	150	0,140	0,16[illegible]	4,2
			H_ε	4	12	0,140	0,16[illegible]	4,2
			H_8	3	12	0,135	0,16[illegible]	4,1
			He_{3888}	2	15	0,070	0,10[illegible]	2,6
			He_{4471}	2,5	8	0,145	0,170	3,8
77	736	6 July	H_α	350	475	0,380	0,380	5,8
		—60 SW	H_β	95	200	0,210	0,225	4,6
		Section 2b	H_γ	11	35	0,165	0,195	4,5
			H_δ	7	25	0,155	0,185	4,5
			D_3	45	135	0,150	0,180	4,1
			H Ca+	59	170	0,160	0,145	3,7
			K Ca+	55	180	0,145	0,160	4,1
			H_ε	4,5	14	0,160	0,190	4,8
			H_8	4	13	0,140	0,165	4,2
			He_{3888}	3,5	20	0,090	0,105	2,7
			He_{4471}	2,5	10	0,140	0,170	3,8
78	736	6 July 1968	H_α	390	475	0,420	0,425	6,5
		—60 SW	H_β	87	180	0,235	0,240	4,9
		Section 2c	H_γ	19	60	0,150	0,185	4,3
			H_δ	7	22	0,170	0,200	4,0
			D_3	50	155	0,150	0,180	3,1
			H Ca+	50	170	0,145	0,145	3,7
			K Ca+	51	175	0,145	0,160	4,1
			H_ε	4	20	0,150	0,185	4,7
			H_8	4	20	0,135	0,160	4,1
			He_{3888}	3,5	28	0,085	0,105	2,7
			He_{4471}	3	12	0,130	0,155	3,5
79	736	6 July	H_α	290	330	0,460	0,410	6,2
		—60 SW	H_β	36	95	0,195	0,235	4,8
		Section 2d	H_γ	5	20	0,155	0,190	4,4
			H_δ	6	21	0,150	0,180	4,4
			D_3	22	65	0,165	0,200	3,4
			H Ca+	34	130	0,125	0,150	3,8
			K Ca+	40	133	0,145	0,160	4,1
			H_ε	3,5	12	0,140	0,170	4,3
			H_8	2	10	0,115	0,140	3,6
			He_{3888}	2	13	0,090	0,110	2,8
			He_{4471}	3	18	0,100	0,120	2,7
80	736	8 July 1968	H_α	502	590	0,440	0,395	6,0
		—60 SW	H_β	71	190	0,185	0,235	4,8
		10h,0 UT	H_γ	19	53	0,175	0,205	4,7
		Section a	H_δ	15	50	0,140	0,175	4,3
			D_3	48	145	0,140	0,175	3,0

Commas indicate decimal points.

Sequential number	Item No.	Date, Co-ordinates, and time of observation	Lines	W·10⁴ Å	I C//⊙·10⁻⁴	Δλ/2 Å	Δλ_D Å	Δλ_D/λ ·10⁻⁵
			H Ca+	37	130	0,125	0,150	3,8
			K Ca+	55	175	0,135	0,150	3,8
			H_ε	12	42	0,145	0,175	4,4
			H_8	3,5	17	0,135	0,185	4,6
			He_{3888}	2	16	0,100	0,130	3,4
			He_{4471}	3	8	0,180	0,215	4,8
	736	8 July 1968	H_α	616	700	0,440	0,395	6,0
		—60 SW	H_β	78	175	0,215	0,255	5,2
		Section b	H_γ	21	68	0,160	0,195	4,5
			H_δ	15	57	0,145	0,175	4,3
			D_3	42	125	0,135	0,170	2,9
			H Ca+	38	160	0,115	0,130	3,3
			K Ca+	36	135	0,130	0,135	3,4
			H_ε	7	28	0,145	0,175	4,4
			H_8	12,5	50	0,125	0,150	3,9
			He_{3888}	9	50	0,095	0,120	3,1
			He_{4471}	3	10	0,150	0,180	4,0
83	736	8 July	H_α	480	620	0,405	0,360	5,5
		—60 SW	H_β	48	120	0,190	0,230	4,7
		Section c	H_γ	15	54	0,150	0,180	4,1
			H_δ	9	33	0,135	0,170	4,1
			D_3	26	88	0,130	0,170	2,9
			H Ca+	26	118	0,115	0,135	3,4
			K Ca+	31	116	0,130	0,140	3,6
			H_ε	3,5	12	0,155	0,185	4,7
			H_8	10	40	0,130	0,160	4,1
			He_{3888}	7,5	48	0,085	0,110	2,8
			He_{4471}	3,5	14	0,140	0,170	3,8
84	736	9 July 1968	H_α	502	510	0,500	0,415	6,3
		—60 SW	H_β	68	130	0,255	0,295	6,1
		06h0 UT	H_γ	15	40	0,195	0,235	5,4
		Section a	H_δ	8	26	0,170	0,210	5,1
			D_3	17	50	0,180	0,225	3,8
			H Ca+	16	55	0,160	0,180	4,5
			K Ca+	18	52	0,170	0,185	4,7
			H_ε	7	18	0,195	0,235	5,9
84	736	9 July 1968	H_α	606	520	0,595	0,490	7,5
		—60 SW	H_β	93	155	0,300	0,315	6,5
		Section b	H_γ	25	62	0,200	0,230	5,3
			H_δ	15	41	0,175	0,220	5,4
			D_3	51	115	0,190	0,230	3,9
			H Ca+	27	70	0,205	0,210	5,3
			K Ca+	35	80	0,215	0,205	5,2
			H_ε	12	33	0,220	0,230	5,8
85	736	9 July	H_α	624	525	0,610	0,455	6,9
		—60 SW	H_β	90	140	0,320	0,335	6,9
		Section c	H_γ	29	70	0,205	0,240	5,5
			H_δ	15	45	0,180	0,215	5,2
			D_3	62	135	0,210	0,255	4,3

Commas indicate decimal points.

Sequential number	Item No.	Date, Coordinates, and time of observation	Lines	$W \cdot 10^4$ Å	$I_c/I_\odot \cdot 10^{-4}$	$\Delta\lambda/2$ Å	$\Delta\lambda_D$ Å	$\frac{\Delta\lambda_D}{\lambda} \cdot 10^{-5}$
			H Ca+	29	62	0,240	0,210	5,1
			K Ca+	32	65	0,260	0,240	6,1
			H_ε	12,5	36	0,180	0,220	5,5
			H_8	7	25	0,155	0,195	5,0
			He_{3889}	5	23	0,115	0,135	3,5
			He_{4471}	4,5	13	0,185	0,220	4,9
86	736	9 July	H_α	472	470	0,510	0,440	6,7
		—60 SW	H_β	52	100	0,265	0,295	6,1
		Section d	H_γ	18	44	0,200	0,240	5,5
			H_δ	8	25	0,180	0,225	5,5
			D_3	36	78	0,200	0,255	4,3
			H Ca+	27	60	0,235	0,230	5,8
			K Ca+	35	60	0,285	0,280	7,1
			H_ε	7	24	0,180	0,210	5,3
			H_8	4	17	0,155	0,185	4,8
			He_{3889}	3	19	0,105	0,125	3,2
			He_{4471}	3,5	12	0,155	0,190	4,2
87	736	9 July	H_β	33	68	0,240	0,300	6,2
		—60 SW	H_γ	7	21	0,170	0,205	4,7
		Section e	H_δ	3,5	12	0,160	0,195	4,7
			H Ca+	19	50	0,200	0,235	5,9
			K Ca+	26	50	0,280	0,270	6,9
			H_ε	4	14	0,150	0,180	4,5
			H_8	4	12	0,170	0,200	5,1
			He_{3889}	2,5	15	0,095	0,115	3,0
88	824	15 August 1968	H_α	450	490	0,420	0,480	7,3
		—60 SW	H_β	61	125	0,230	0,265	5,4
		09h,0 UT	H_γ	16	50	0,175	0,215	5,0
		Section a	H_δ	11	32	0,170	0,200	4,9
			D_3	47	80	0,290	0,360	6,1
			H Ca+	101	220	0,165	0,200	5,0
			K Ca+	118	240	0,185	0,225	5,7
			H_ε	7	22	0,160	0,195	4,9
			H_8	10	28	0,195	0,215	5,5
			He_{3889}	8	45	0,100	0,130	3,3
			He_{4471}	3	11	0,155	0,180	4,0
89	824	15 August	H_α	340	450	0,375	0,425	6,5
		—60 SW	H_β	53	120	0,205	0,220	4,5
		Section b	H_γ	14	40	0,160	0,200	4,6
			H_δ	9	30	0,160	0,195	4,8
			D_3	33	70	0,230	0,280	4,8
			H Ca+	46	170	0,125	0,160	4,0
			K Ca+	52	200	0,125	0,150	3,8
			H_ε	5	15	0,155	0,190	4,8
			H_8	8	23	0,205	0,250	6,4
			He_{3889}	6	31	0,105	0,120	3,1
90	824	15 August	H_α	324	350	0,445	0,525	8,0
		—60 SW	H_β	44	100	0,225	0,295	6,1
		Section c	H_γ	12	30	0,205	0,250	5,8

Commas indicate decimal points.

Sequential number	Item No.	Date, Coordinates, and time of observation	Lines	$W \cdot 10^4$ Å	$I_c/I_\odot \cdot 10^{-4}$	$\Delta\lambda/2$ Å	$\Delta\lambda_D$ Å	$\frac{\Delta\lambda_D}{\lambda} \cdot 10^{-5}$
			H_δ	6	20	0,165	0,205	5,0
			D_3	30	50	0,310	0,395	6,7
			H Ca+	61	150	0,195	0,240	6,0
			K Ca+	68	155	0,215	0,270	6,9
			H_ε	4	12	0,170	0,205	5,2
			H_8	7,5	18	0,210	0,250	6,4
			He_{3888}	5,5	30	0,105	0,130	3,3
981		8 August 1969 +42 NW 06h,0 UT Section 1a	H_α	880	940	0,465	0,485	7,4
			H_β	129	250	0,265	0,305	6,3
			H_γ	20	40	0,250	0,260	6,0
			H_δ	13	35	0,185	0,225	5,5
			D_3	84	160	0,225	0,270	4,6
			H Ca+	58	165	0,180	0,225	5,7
			K Ca+	78	185	0,205	0,250	6,4
			H_ε	8	28	0,155	0,195	4,9
			H_8	5	18	0,150	0,180	4,6
			He_{3889}	4	25	0,090	0,100	2,6
			He_{4471}	6	25	0,120	0,150	3,4
981		8 August 1969 +42 NW Section 1b	H_α	772	860	0,445	0,450	6,9
			H_β	128	260	0,240	0,290	5,9
			H_γ	29	60	0,220	0,260	6,0
			H_δ	13	40	0,170	0,205	5,0
			D_3	96	200	0,200	0,245	4,2
			H Ca+	77	165	0,215	0,235	5,9
			K Ca+	78	168	0,230	0,255	6,5
			H_ε	7	28	0,130	0,160	4,0
			H_8	7,5	25	0,160	0,185	4,8
			He_{3889}	7	40	0,100	0,110	2,8
			He_{4471}	6,5	26	0,135	0,160	3,6
981		8 August +42 NW Section 1c	H_α	728	800	0,455	0,480	7,3
			H_β	138	250	0,270	0,320	6,6
			H_γ	38	90	0,200	0,255	5,9
			H_δ	19	48	0,200	0,245	6,0
			D_3	103	200	0,210	0,255	4,3
			H Ca+	86	170	0,225	0,240	6,0
			K Ca+	106	175	0,280	0,335	8,5
			H_ε	10	31	0,160	0,190	4,8
			H_8	7	23	0,150	0,180	4,6
			He_{3889}	9,5	48	0,110	0,130	3,3
			He_{4471}	10,5	32	0,165	0,195	4,4
94	981	8 August 1969 +42 NW Section 1d	H_α	646	650	0,500	0,505	7,7
			H_β	112	210	0,270	0,310	6,4
			H_γ	42	100	0,195	0,235	5,4
			H_δ	21	55	0,200	0,240	5,8
			D_3	77	160	0,200	0,245	4,2
			H Ca+	78	158	0,235	0,275	6,9
			K Ca+	97	175	0,255	0,280	7,1
			H_ε	12	38	0,175	0,195	4,9
			H_8	8	28	0,165	0,170	4,4

Commas indicate decimal points.

Sequential number	Item No.	Date, Coordinates, and time of observation	Lines	$W \cdot 10^4$ Å	$I_c/I_\odot \cdot 10^{-4}$	$\Delta\lambda/2$Å	$\Delta\lambda_D$ Å	$\frac{\Delta\lambda_D}{\lambda} \cdot 10^{-5}$
			He_{3889}	11	48	0,130	0,160	4,1
			He_{4471}	9,5	32	0,150	0,175	3,9
95	981	8 August	H_α	438	530	0,440	0,405	6,2
		+42 NW	H_β	73	135	0,270	0,295	6,1
		Section 1e	H_γ	35	80	0,200	0,250	5,8
			H_δ	12	40	0,170	0,205	5,0
			H Ca+	47	125	0,190	0,230	5,8
			K Ca+	55	120	0,220	0,270	6,9
			H_ε	8	28	0,140	0,175	4,4
			H_8	4	17	0,140	0,170	4,4
			He_{3889}	6	28	0,105	0,130	3,4
			He_{4471}	4	18	0,115	0,140	3,1
96	981	8 August	H_α	422	490	0,440	0,460	7,0
		+42 NW	H_β	47	105	0,230	0,210	4,3
		06h,3 UT	H_γ	28	57	0,250	0,300	6,9
		Section 2a	H_δ	9	27	0,170	0,215	5,2
			D_3	59	105	0,245	0,280	4,8
			H Ca+	40	100	0,195	0,240	6,0
			K Ca+	48	117	0,210	0,250	6,4
			H_ε	5	16	0,170	0,195	4,9
			H_8	10	28	0,190	0,235	6,0
			He_{3889}	9,5	45	0,115	0,145	3,7
			He_{4471}	9	30	0,165	0,190	4,2
97	981	8 August 1969	H_α	666	690	0,485	0,480	7,3
		+42 NW	H_β	117	220	0,265	0,315	6,5
		Section 2b	H_γ	40	95	0,190	0,245	5,6
			H_δ	20	56	0,185	0,225	5,5
			D_3	116	240	0,185	0,240	4,1
			H Ca+	51	125	0,200	0,225	5,7
			K Ca+	60	130	0,235	0,250	6,4
			H_ε	9	35	0,150	0,155	3,9
			H_8	11	38	0,150	0,180	4,6
			He_{3889}	14	66	0,110	0,140	3,6
			He_{4471}	11,5	35	0,175	0,225	5,0
98	981	8 August	H_α	618	625	0,500	0,475	7,2
		+42 NW	H_β	134	255	0,260	0,315	6,5
		Section 2c	H_γ	25	64	0,180	0,230	5,3
			H_δ	12	37	0,185	0,230	5,6
			D_3	117	230	0,195	0,230	3,9
			H Ca+	40	102	0,195	0,210	5,3
			K Ca+	53	116	0,220	0,240	6,1
			H_ε	7,5	30	0,140	0,170	4,3
			H_8	14	39	0,205	0,250	6,4
			He_{3889}	14	64	0,110	0,135	3,5
			He_{4471}	11	31	0,175	0,215	4,8
99	981	8 August 1969	H_α	392	460	0,430	0,430	6,6
		+42 NW	H_β	74	152	0,250	0,275	5,6
		Section 2d	H_γ	20	57	0,185	0,235	5,3

Commas indicate decimal points.

Sequential number	Item No.	Date, Coordinates, and time of observation	Lines	W·10⁴ Å	$I_C/I_\odot \cdot 10^{-4}$	Δλ/2 Å	Δλ_D Å	$\frac{\Delta\lambda_D}{\lambda} \cdot 10^{-5}$
			H_δ	10	32	0,170	0,210	5,1
			D_3	58	100	0,235	0,280	4,8
			H Ca+	27	78	0,175	0,205	5,2
			K Ca+	34	90	0,180	0,225	5,7
			H_ε	4	11	0,170	0,205	5,2
			H_8	7	25	0,145	0,170	4,4
			He_{3889}	8	37	0,100	0,100	2,6
			He_{4471}	4,5	21	0,105	0,130	2,9
100	981	8 August +42 NW Section 3a	H_α	625	600	0,540	0,570	8,7
			H_β	55	80	0,340	0,385	7,9
			H_γ	17	34	0,275	0,330	7,6
			H_δ	7	16	0,245	0,300	7,3
			D_3	90	110	0,380	0,395	6,7
			H Ca+	68	115	0,280	0,320	8,1
			K Ca+	73	125	0,290	0,320	8,2
			H_8 / He_{3889}	9	20	—	—	—
101	981	8 August +42 NW Section 3b	H_α	508	560	0,435	0,510	7,8
			H_β	39	80	0,240	0,285	5,9
			H_γ	9,5	26	0,200	0,240	5,5
			D_3	45	85	0,260	0,315	5,4
			H Ca+	33	77	0,225	0,270	6,8
			K Ca+	47	105	0,225	0,270	6,9
			H_8	1,5	8	0,100	0,120	3,1
			He_{3889}	2,5	15	0,100	0,125	3,2
102	981	8 August 1969 +42 NW 09h,4 UT Section 4a	H_α	524	650	0,395	0,470	7,2
			H_β	50	102	0,250	0,300	6,2
			H_γ	13	30	0,230	0,270	6,2
			H_δ	5	12	0,220	0,265	6,4
			D_3	43	88	0,240	0,295	5,0
			H Ca+	45	115	0,155	0,190	4,8
			K Ca+	60	130	0,180	0,210	5,3
			H_8	1	5	0,105	0,125	3,2
			He_{3889}	2	15	0,085	0,100	2,6
103	981	8 August +42 NW Section 4b	H_α	362	510	0,360	0,435	6,6
			H_β	34	82	0,215	0,265	5,4
			H_γ	8	28	0,155	0,180	4,2
			D_3	30	70	0,215	0,255	4,3
			H Ca+	19	70	0,130	0,160	4,0
			K Ca+	24	90	0,150	0,190	4,8
			H_8	1,5	8	0,105	0,125	3,2
			He_{3889}	2	13	0,085	0,100	2,6
104	981	8 August +42 NW 09h,5 UT Section 5a	H_α	356	480	0,370	0,425	6,5
			H_β	26	60	0,215	0,250	5,1
			H_γ	9	25	0,220	0,260	6,0
			D_3	25	60	0,215	0,265	4,5
			H Ca+	50	125	0,150	0,190	4,8
			K Ca+	76	165	0,165	0,200	5,1

Commas indicate decimal points.

Sequential number	Item No.	Date, Coordinates, and time of observation	Lines	$W \cdot 10^4$ Å	$I_C/I_\odot \cdot 10^{-4}$	$\Delta\lambda/2$ Å	$\Delta\lambda_D$ Å	$\frac{\Delta\lambda_D}{\lambda} \cdot 10^{-5}$
105	981	8 August	H_α	340	470	0,370	0,445	6,8
		+42 NW	H_β	28	60	0,240	0,300	6,2
		Section 5b	H_γ	6	23	0,145	0,180	4,2
			D_3	23	60	0,190	0,230	3,9
			H Ca+	44	120	0,160	0,200	5,0
			K Ca+	68	165	0,175	0,220	5,6
106	981	8 August 1969	H_α	290	380	0,375	0,440	6,7
		+42 NW	H_β	16	45	0,190	0,230	4,7
		Section 5c	H_γ	5	16	0,180	0,220	5,1
			D_3	14	40	0,170	0,210	3,6
			H Ca+	27	85	0,160	0,205	5,2
		11 September 1969	K Ca+	39	125	0,155	0,200	5,1
107	1027		H_α	500	600	0,420	0,375	5,7
		+50 NE	H_β	125	315	0,195	0,240	4,9
		06h,3 UT	H_γ	32	100	0,160	0,200	4,6
		Section 1a	H_δ	14	54	0,140	0,170	4,2
			D_3	60	166	0,140	0,175	3,0
			H Ca+	36	120	0,160	0,155	3,9
			K Ca+	51	160	0,180	0,160	4,1
			H_ε	10	35	0,160	0,165	4,2
			H_8	8	34	0,120	0,145	3,7
			He_{3889}	6	34	0,085	0,100	2,6
			He_{4471}	7	24	0,160	0,185	4,1
108	1027	11 September	H_α	416	630	0,355	0,340	5,2
		+50 NE	H_β	69	167	0,210	0,250	5,1
		Section 1b	H_γ	15	50	0,160	0,190	4,4
			H_δ	8,5	26	0,150	0,180	4,4
			D_3	69	173	0,160	0,200	3,4
			H Ca+	40	170	0,120	0,155	3,9
			K Ca+	59	190	0,150	0,175	4,5
			H_ε	6	16	0,210	0,230	5,8
			H_8	2	13	0,105	0,115	3,0
			He_{3889}	4	20	0,105	0,115	3,0
		11 September 1969	He_{4471}	7	28	0,130	0,155	3,5
109	1027		H_α	336	520	0,340	0,300	4,6
		+42 NE	H_β	45	115	0,195	0,220	4,5
		Section 1c	H_γ	9	28	0,155	0,190	4,4
			H_δ	5	16	0,165	0,205	5,0
			D_3	39	95	0,175	0,215	3,7
			H Ca+	54	150	0,170	0,175	4,4
			K Ca+	55	170	0,165	0,180	4,6
			H_8	2	11	0,105	0,115	3,0
			He_{3889}	2,5	18	0,085	0,100	2,6
		11 September 1969	He_{4471}	5	22	0,130	0,160	3,6
110	1027		H_α	214	460	0,305	0,335	5,1
		+42 NE	H_β	24	65	0,190	0,230	4,7
		12h,4 UT	D_3	27	70	0,170	0,225	3,8
		Section 3a	H Ca+	48	162	0,155	0,160	4,0

Commas indicate decimal points.

Sequential number	Item No.	Date, Coordinates, and time of observation	Lines	W·10⁴ A	$I_c/I_\odot \cdot 10^{-4}$	Δλ/2 A	$\Delta\lambda_D$ A	$\frac{\Delta\lambda_D}{\lambda} \cdot 10^{-5}$
			K Ca+	61	173	0,175	0,185	4,7
			H_ε	2	6	0,125	0,150	3,8
111	1027	8 August	H_α	302	490	0,330	0,365	5,6
		+42 NE	H_β	34	85	0,190	0,225	4,6
		Section 3b	H_γ	3	13	0,130	0,150	3,5
			D_3	33	80	0,170	0,220	3,8
			H Ca+	59	175	0,160	0,190	4,8
			K Ca+	63	170	0,180	0,205	5,2
			H_ε	2,5	8	0,140	0,170	4,3
112	1027	11 September	H_α	456	580	0,400	0,415	6,3
		+42 NE	H_β	68	165	0,210	0,245	5,0
		Section 3c	H_γ	16	46	0,180	0,225	5,2
	1027	11 September	H_δ	11	32	0,180	0,205	5,0
		+42 NE	D_3	78	185	0,185	0,240	4,1
		Section 3d	H Ca+	66	148	0,220	0,200	5,0
			K Ca+	72	155	0,240	0,220	5,6
			H_ε	6,5	19	0,170	0,205	5,2
			H_8	10	35	0,150	0,195	5,0
			He_{3889}	22	103	0,105	0,120	3,1
			He_{4471}	22	68	0,160	0,195	4,4
113	1027	11 September	H_α	414	550	0,380	0,415	6,3
		+42 NE	H_β	70	150	0,225	0,265	5,4
		Section 3e	H_γ	14	41	0,190	0,235	5,4
			H_δ	10	28	0,195	0,215	5,2
			D_3	90	170	0,260	0,310	5,3
			H Ca+	60	155	0,185	0,185	4,7
			K Ca+	70	155	0,230	0,205	5,2
			H_ε	5,5	16	0,175	0,200	5,0
			H_8	9	30	0,160	0,210	5,4
			He_{3889}	21	95	0,105	0,125	3,2
			He_{4471}	16	50	0,175	0,195	4,4
14	1027	11 September	H_ε	7,5	20	0,200	0,240	6,1
		+42 NE	H_8	5	18	0,155	0,185	4,8
		14h,2 UT	He_{3889}	12	53	0,110	0,135	3,5
		Section 2a	He_{4471}	3,5	15	0,135	0,165	3,7
	1027	11 September	H_ε	6	19	0,160	0,195	4,9
		+42 NE 1969	H_8	4	13	0,155	0,185	4,8
		Section 2b	He_{3889}	10	42	0,125	0,150	3,9
			He_{4471}	3	12	0,145	0,175	3,9

Commas indicate decimal points.

DETERMINATION OF ASTRONOMICAL REFRACTION NEAR THE HORIZON IN DIFFERENT SEASONS OF THE YEAR

N. A. Vasilenko

ABSTRACT. The results are presented of astronomical refraction measurements for zenith distances of 80-90° performed by the author in different seasons with a two inch universal instrument. The differences between observed and calculated refraction were found to exhibit seasonal variations. The results were compared with data of atmospheric aerologic soundings. The great departures in observed refraction from that calculated with the Pulkovo tables are to be ascribed chiefly to temperature gradient changes within the ground kilometer layer of atmosphere.

This project is a continuation of similar studies conducted in 1965-1966 in the Goloseyevskiy Forest in the territory of the Main Astronomical Observatory of the Academy of Sciences of the Ukrainian SSR [1]. Its purpose is determination of astronomic refraction on the basis of observations of bright celestial objects at great zenith distances (80-90°) and comparison of the measured refraction values with values calculated both with the tables of the Pulkovo Observatory and on the basis of the theory of refraction using aerologic data obtained by sounding of the atmosphere to high altitudes.

To obtain the astronomic refraction on the basis of observations of the Sun, planets, and certain bright stars the zenith distances of these bodies measured at a certain point in time were compared with the ephemeral zenith distances z.

The observations were conducted during the summer, autumn, and winter seasons of 1968-1970 by means of a UV 2"/2" universal instrument. The zenith distances of rising and setting celestial bodies were measured.

The instrument was mounted outside the building on a special brick pillar 8 m high and shielded from the influence of the wind and solar rays by plywood shields. The altitude of the observation point above sea level was 367 m. In all 1580 zenith distances of celestial bodies were measured, 430 in summer, 350 in winter, and 800 in autumn. The observations were conducted under the following weather conditions:

	Temperature, °C		Pressure, mm	
1968, September	from +4	to +18	from 728	to 738
1968, October	−2	+10	736	743
1969, July	+18	+27	721	728
1969, August	+18	+25	728	729
1969, December	−8	−1	737	743
1970, February	−15	−2	736	750
1970, June	+10	+22	728	736

In measurement of the zenith distance there was recorded on the tape of the printing chronograph the time of passage of a body through the central horizontal filament of the telescope, which corresponds to the almucantar of the zenith distance being measured. The thermometer and barometer readings were entered in a log at the same time. The mean errors in measurement of the time of sighting on a celestial body $\sigma_s = \sigma_t = \pm 0.1$ sec, temperature $\sigma_T = \pm 0.3°$ C, and atmospheric pressure was around 1 mm Hg. At intervals of two hours during the observations the position of the zenith on the vertical circle of the instrument was determined on the basis of observations of the North Star with the circle in both positions. By means of a shortwave receiver and a pulse attachment exact time second signals were recorded on the chronograph tape at approximately the same time intervals, that is, before the beginning and at the end of observations of a particular body.

Possible Accuracy of Astronomical Refraction Determination /97

Since astronomical refraction is expressed as the difference between the true and the measured zenith distances,

$$r = z - \zeta, \quad (1)$$

the results of its determination by measuring zenith distances are affected by (1) the instrument errors and (2) the errors in calculation of the true zenith distance.

Given below are the estimated root mean square instrument errors of the two-second universal instrument:

Sighting on distant fixed point.....	±1.0"
Readings of four microscopes and level.....	1.2
Error in allowance for cube curvature.....	1.0
Determination of zenith location on interpolation to observation time.....	2.0

Errors in the position of celestial bodies due to vibration of the image depend on the zenith distance. They may be estimated in approximation with the formula obtained by I. G. Kolchinskiy for Goloseyev [2]:

$$\sigma_d \approx \pm 0,''31 (\sec z)^{0,5}. \quad (2)$$

We obtain 0.7; 1.7; 2.4; 3.3; and 5.4" for ζ = 80; 85; 88; 89.5; and 89.8° respectively.

To reduce the influence of atmospheric dispersion the instrument was stopped down so that the clearest diffraction picture was obtained and the spectrum brightness was considerably diminished. Then for the same zenith distances we have the following root mean square errors caused by atmospheric dispersion: 1.2"; 1.4"; 2.0"; 2.6"; and 3.5".

Thus by adding up the influence of all the sources of errors we obtain the root mean square value of the anticipated instrument error in measurement of the zenith distance of a celestial body as follows:

ζ	80°	85°	88°	89°	89.5°	89.8°
σ	±3.0"	±3.1"	±3.4"	±3.8"	±4.5"	±6.0"

Errors in calculation of the true zenith distance result from error Δt in determining the time of observation, errors in the values adopted for the latitude of the observation site φ and longitude λ, and celestial body coordinate errors.

On the basis of the formula

$$\Delta z = 15 \cos\varphi \sin A \Delta t, \quad (3)$$

when $\Delta t \approx 0.1$ sec we obtain $\Delta z = \pm 1''$ if azimuth A falls within the range 45-90°. An error in latitude determination of $\sigma_\varphi = \pm 0.3''$ on the basis of the formula

$$\cos z = \sin\varphi \sin\delta + \cos\varphi \cos\delta \cos t \quad (4)$$

may introduce an error of around 0.5" on the average into z. An error in declination of the celestial body of $\sigma_\delta \approx 0.1''$ in accordance with (4) may also result in an error in the calculated value of z not exceeding 0.5".

Thus the root mean square value of the anticipated errors in calculation of z will be around 1.2". The total effect of the measurement and calculation errors on determination of the actual astronomical refraction errors by the particular instrument and method will, in accordance with (1), be:

ζ	80°	85°	88°	89°	89.5°	89.8°
σ_r ...	3.1"	3.3"	3.6"	4.0"	4.7"	6.1"

Errors of two types occur in calculation of astronomical refraction with the tables of Pulkovo Observatory. /98

1. Errors due to measurement of air temperature, pressure, and humidity, which are due to errors in reading, error in the instruments themselves, and incorrect selection of the site for mounting them.

2. Errors due to failure of the visually effective wavelengths of the bodies observed at the horizon to match the wavelength for which the refraction tables were compiled.

The first error may be considered to be approximately proportional to the expression

$$\operatorname{tg}\zeta \frac{\rho}{\rho_0} = \operatorname{tg}\zeta \frac{PT_0}{P_0 T}. \quad (5)$$

In this equation ρ and ρ_0 are the error densities at temperatures T and T_0 and pressures P and P_0. Hence the error in calculating refraction with the Pulkovo Observatory tables may be estimated in approximation from the formula

$$\Delta r \approx r_0\left(1-\frac{P_0+\Delta P_0}{P_0}\cdot\frac{T_0}{T_0+\Delta T_0}\right), \tag{6}$$

in which r_0 is the refraction with the initial temperature and pressure values adopted.

Assuming $\Delta T_{0\pi} = \pm 0.3°C$ and $\Delta P_0 = \pm 1$ mbar, and the air temperature and pressure to be the mean seasonal values (for summer $T_0 = 293.2°$, $P_0 = 971$ mbar; for autumn $T_0 = 273.2°$, $P_0 = 981.5$ mbar; and for winter $T_0 = 258.2°$, $P_0 = 988.5$ mbar), we calculate the errors in the calculated refraction due to erroneous air temperature and pressure. These errors, Δr_{TP}, are shown in Table 1 for the mean seasonal stratification of the atmosphere.

TABLE 1.

ζ	Δr_{TP}			Δr_h	Δr_λ	Root mean square error of refraction calculation with Pulkovo Observatory tables		
	Summer	Autumn	Winter			Summer	Autumn	Winter
80°	±0,6	±0,7	±0,7	±0,1	±0,5	±0,8	±0,9	±0,9
85	1,1	1,3	1,4	0,1	0,9	1,4	1,6	1,7
88	2,0	2,4	2,7	0,2	1,8	2,7	3,0	3,3
89	2,6	3,1	3,6	0,4	2,4	3,6	3,9	4,3
89,5	3,0	3,7	4,3	0,5	2,8	4,1	4,6	5,1
89,8	3,6	4,5	5,4	0,7	3,5	5,1	5,7	6,5

Commas indicate decimal points.

The refraction calculation error due to an erroneous air humidity value is insignificant. It may be estimated in approximation with the formula

$$\Delta r_h \approx \pm 0'',012\, P_h K, \tag{7}$$

in which P_h is the absolute air humidity in millibars; K is the ratio of the refraction value at a given zenith distance to its value for $\zeta = 45°$. Assuming the error in determination of humidity $\Delta P_h = \pm 0.5$ mbar, representing around 10% of the mean humidity value in this particular region, from (7) we find that the error at the horizon will be around 0.7". The refraction calculation error due to discrepancy in the visually effective wavelength for the body observed and the system adopted in compiling the refraction tables may be estimated with the approximate formula

$$\Delta r_\lambda \approx (\mu_{600}-\mu_{575})K, \tag{8}$$

in which μ_{600} and μ_{575} are the air refraction coefficients for visually effective wavelengths of 600 and 575 μ. The estimates obtained for the errors in question are given in Table 1.

On the basis of the measurement and calculation errors obtained we can make an approximate estimate of the anticipated deviation of measured refraction from its tabulated values for different seasons of the year. These estimates, which were obtained with the expression

/99

$$\Delta r = z - \zeta - r_{pulk} = r_{meas} - r_{pulk} \quad (9)$$

are given in Table 2 for summer, autumn and winter.

TABLE 2.

ζ	Root mean square error of difference in measured and calculated refraction		
	Summer	Autumn	Winter
80°	±3,2	±3,2	±3,2
85	3,6	3,7	3,7
88	4,5	4,7	4,9
89	5,4	5,6	5,9
89,5	6,3	6,6	7,0
89,8	8,0	8,4	9,0

Commas indicate decimal points.

The root mean square errors of the deviations of measured refraction from its values as calculated on the basis of Pulkovo Observatory tables, which are presented in Table 2, represent the characteristic accuracy only of this particular method and instrument. Unlike the estimates by F. Bessel [3], these errors are not estimates of the probable deviations of the actual astronomic refraction from the tabulated values.

According to the estimates of Bessel, the refraction may differ as follows from the tabulated values:

ζ	80°	85°	88°	89°	89.5°
σ_r....	±0.9"	±1.7"	±7.7"	±16.8"	±20.0"

In reality, however, as we know from the survey in [4], anomalies in astronomic refraction at the horizon may exceed 2-3' when the atmosphere is in a certain condition.

Results of Comparison of Measured and Tabulated Refraction

The results of the observations, which are understood to mean deviations in the measured refraction from the values calculated on the basis of the Pulkovo Observatory tables (measured minus calculated value), were broken down by seasons into three groups: "summer", "autumn", and "winter." The mean deviation results are given in Table 3 for summer, in Table 4 for winter, and in Table 5 for autumn, in which ζ is the zenith distance, n the number of observations, $\overline{\Delta r}$ is the mean deviation of the measured refraction from the calculated value, σ is the root mean square error of the arithmetic mean, and m is the root mean square error of the individual deviation in measured refraction from the tabulated value.

It follows from Table 3 that during the summer season the actual refraction is smaller than the calculated over the entire zenith distance range of 80-90°. The maximum deviations of the actual refraction from the calculated values indicate the possible value of the errors when allowance is made for refraction at given zenith distances, if use is made of the Pulkovo Observatory refraction tables.

When $\zeta < 87°$ quantity m apparently represents the root mean square error of a single measurement to a greater extent. When $\zeta > 87°$ a substantial contribution to m is made by variation in the refraction value.

Examination of Table 4 reveals that the actual refraction during the winter season is at this particular point larger than the tabulated values over the 80-89.8° zenith distance interval. As with the summer season, the maximum deviation values indicate possible refraction errors when allowance is made for refraction on the basis of the Pulkovo tables.

The autumn observation period is characterized by the fact that both the negative and the positive values of maximum deviation Δr are of the same order of magnitude for corresponding values ζ for all zenith distances from 80° to 89°. On the whole the mean deviations of actual refraction $\overline{\Delta r}$ from the calculated values for the autumn observation period are comparable to the mean measurement errors, at least up to $\zeta = 89°$. In our observations positive maximum deviations Δr predominated over the 89°-90° zenith distance interval; this affected the values of mean deviations $\overline{\Delta r}$, which were found to equal 28" and 47" for $\zeta = 89.5°$ and 89.8°. The maximum deviations at the horizon ($\zeta = 89.5°$, 89.8°) for the autumn period occupy an intermediate position between the summer and winter periods. /100

TABLE 3. SUMMER

ζ	n	$\overline{\Delta r}$	σ	Δr_{max} From	Δr_{max} To	m
80°	15	— 1,5	±0,6	— 4,3	+ 1,9	± 2,2
81	6	— 1,6	1,5	— 6,8	+ 3,2	3,6
82	28	— 3,2	0,3	— 6,0	+ 1,2	1,8
83	9	— 2,0	0,7	— 4,5	+ 2,9	2,2
84	30	— 3,7	0,4	— 8,4	+ 0,2	2,3
85	18	— 2,3	0,8	— 10,0	+ 3,6	3,3
86	47	— 4,3	0,5	— 14,1	+ 3,8	3,7
87	47	— 6,7	0,9	— 17,8	+ 6,2	6,2
88	54	—12,5	1,3	— 38,6	+ 2,9	9,4
89	42	—21,6	2,4	— 68,5	+ 2,0	15,7
89,5	7	—33,3	5,7	— 46,1	— 6,3	15,0
89,8	13	—73,7	8,8	—116,0	—29,7	31,7

Commas indicate decimal points.

For the sake of the fullest possible illustration of the deviations obtained in actual astronomic refraction from its values calculated on the basis of the Pulkovo Observatory tables, we present a composite table (Table 6) for zenith distances 87-90°. It is supplemented by the relative values of Δr_{max}

and m, which were obtained by division of their absolute values by the refraction value at a given zenith distance. The data in Table 6 indicate that the actual astronomic refraction at the horizon may, under certain meteorological conditions, in summer be 6% smaller and in winter 10% larger than the tabular value. Examination of the tables together confirms once again the fact that the values of $\overline{\Delta r}$, σ, Δr_{max}, and m are much larger than the same values during the summer season for the autumn and winter observation seasons.

TABLE 4. WINTER

ζ	n	$\overline{\Delta r}$	σ	Δr_{max} From	Δr_{max} To	m
80°	22	+ 0,3	± 0,6	— 4,4	+ 4,9	± 2,7
81	23	+ 1,7	0,6	— 5,0	+ 6,1	2,7
82	29	+ 1,4	0,4	— 4,4	+ 5,6	2,4
83	28	+ 1,1	0,5	— 3,8	+ 6,2	2,8
84	28	+ 1,2	0,6	— 6,5	+ 6,8	3,1
85	33	+ 1,5	0,6	— 5,9	+ 10,0	3,6
86	33	+ 1,9	0,5	— 5,7	+ 6,3	3,1
87	42	+ 3,3	0,9	— 9,4	+ 16,8	6,0
88	36	+ 9,0	1,2	— 8,0	+ 24,2	7,4
88,5	6	+ 19,5	3,7	+ 7,8	+ 30,9	9,1
89	23	+ 46,1	3,8	+ 8,6	+ 74,2	18,5
89,5	7	+103,3	23,0	+27,4	+188,9	60,9

Commas indicate decimal points.

This phenomenon may be ascribed in part to the influence of the mean inclination of the layers of air of uniform density at altitudes of 1-5 km. In view of the results of studies by N. A. Belyayev [5] and M. S. Zverev [6], /101 it may be assumed that the maximum air layer inclination values are reached during the periods of stable anticyclones. It must be supposed that the mean inclination values do not exceed one minute, as is customarily assumed for the European territory of the USSR.

On the basis of such an assumption we could explain the mean deviations $\overline{\Delta r}$ for the summer and winter seasons of the year, at least up to $\zeta = 88°$, and for the autumn season up to $\zeta = 89°$. However, if these deviations are caused by the mean inclinations of layers of uniform density, i.e., by displacement of the "refraction zenith," they should have different signs for the stars the azimuths of which differ by 180° (for the same evening of observation). This circumstance was not confirmed on the whole when we familiarized ourselves with the results. Instances of different refraction deviation signs in opposite azimuths are very rare. The explanation for the great deviations of the measured from the calculated refraction is possibly to be sought in special conditions in the ground kilometer layer. As a matter of fact, in the majority of cases such substantial refraction deviations at the horizon have been observed when the meteorological data of atmospheric sounding have revealed the presence of temperature inversion up to altitudes of 300 m above the surface of the Earth. In some cases the inversion depth reached 0.6, 1.0, and even 1.5 km, and the inversion gradient 3-4° per 100 m. The assumption that the large

refraction anomalies for zenith distances of 88-90° may be ascribed to the influence of temperature inversion is confirmed by the refraction deviations during the autumn observation season, for which we have the data of several soundings of the atmosphere.

TABLE 5. AUTUMN

ζ	n	$\overline{\Delta r}$	σ	Δr_{max} From	Δr_{max} To	m
		"	"	"	"	"
80°	19	+ 0,4	± 0,4	— 2,1	+ 3,1	± 1,6
80,5	11	+ 0,4	0,4	— 1,5	+ 2,9	1,2
81	25	— 0,1	0,4	— 4,9	+ 5,3	2,1
81,5	21	— 0,1	0,4	— 5,0	+ 2,3	2,0
82	27	+ 0,6	0,4	— 2,6	+ 5,1	2,1
82,5	21	+ 0,1	0,5	— 5,0	+ 5,6	2,4
83	27	+ 0,1	0,6	— 7,0	+ 6,2	2,9
83,5	29	+ 0,2	0,6	— 5,1	+ 7,9	3,0
84	32	— 0,4	0,5	— 5,6	+ 6,0	2,8
84,5	36	— 0,1	0,4	— 5,4	+ 5,7	2,5
85	41	— 0,5	0,5	— 8,3	+ 6,9	3,5
85,5	42	— 0,9	0,6	— 8,8	+ 10,3	3,6
86	44	— 0,7	0,6	— 7,2	+ 10,1	4,0
86,5	39	— 1,1	0,6	— 7,6	+ 8,2	3,7
87	42	— 1,2	0,8	—12,7	+ 9,8	5,4
87,5	41	— 2,6	1,1	—14,5	+ 13,4	6,7
88	38	— 1,9	1,2	—14,9	+ 15,3	7,2
88,5	37	— 4,9	2,9	—50,7	+ 65,3	17,6
89	39	— 3,5	3,9	—88,8	+ 60,0	24,2
89,5	13	+27,5	9,9	—23,2	+ 86,9	35,7
89,8	12	+47,0	23,2	—70,2	+167,0	80,6

Commas indicate decimal points.

Another explanation is possible, namely that in calculation both of the Pulkovo and of the other refraction tables the temperature gradient for the 10-km layer of the atmosphere was considered to be constant, something which on the whole does not correspond to the actual conditions. This is also the reason for certain restrictions in use of the refraction tables at large zenith distances. In particular, our studies show that at an accuracy of 5" the Pulkovo Observatory tables may be used only up to $\zeta < 85°$. In the general case, /102 however, the large astronomic refraction deviations from the tabulated values may be caused by a large number of factors. For example, calculations show that at an average inclination of uniform density layers of 1, 2, and 3" at altitudes of 1-5 km the refraction angle at the horizon may vary by 13, 26, and 40". However, this matter requires additional study.

Comparison of Measured Refraction Deviations with Temperature Gradient Variations in the Ground Layer of the Atmosphere

To compare the deviations of refraction from its tabulated values with the temperature gradients in the ground kilometer layer of the atmosphere, we made use of the data of aerologic sounding of the atmosphere of two nearby weather stations (at distances of 3 and 25 km). The station situated 3 km from the astronomic observation point may for practical purposes be assumed to be combined with it. In the autumn of 1968 we had the meteorological data of 26 radiosonde

launchings performed at the nearest weather station, 14 of which were carried out no more than 1 hour before or after the astronomic observations. At the more distant weather station (25 km) the radiosonde launching program enabled us from the viewpoint of time to use the results of only 9 soundings (4 in autumn, 2 in summer, and 3 in winter).

From 7 to 14 October 1968 sounding of the atmosphere was carried out at intervals of 2-3 hours, and for this reason its results may give some idea of the variability of the temperature gradients in the ground layer of atmosphere during nighttime observations. Certain results are presented in Table 7, which show that in the majority of cases deep and extensive inversions and isothermal conditions predominate at night at the point of observation.

According to the theory of refraction, temperature inversion in the ground layer of air increases refraction. As a matter of fact, by examining the refraction deviations obtained at the times of sounding we note that in the case /103
of moderate and extensive inversion the measured refraction is always greater than the tabulated value, and conversely, when there is little or no inversion the refraction deviations are insignificant. I. G. Kolchinskiy derived a formula by means of which it is possible to estimate the increase in refraction if the inversion characteristic at the time of observation is known [7]:

$$r - r^* \approx \frac{(\mu - 1)(\mu^* - 1)(a_T - a_{TH})(H - H_0)}{T_0} \operatorname{tg} \zeta \sec^2 \zeta. \qquad (10)$$

In this formula T_0 is the temperature at the surface of the Earth; a_T is the /104
mean temperature gradient in the ground layer of air, expressed in degrees per 100 m. For the standard atmosphere it is assumed to equal 0.65°; a_{TH} is the temperature gradient on inversion; μ and μ^* are the values of the air refraction coefficients at temperatures T_0 and T^* and the corresponding pressures at altitudes H_0 and H; r and r^* is the astronomic refraction respectively without and with allowance for the inversion. Formula (10), with no allowance made for terms of the second order of smallness, was derived for plane-parallel layers of standard air and for the inversion atmosphere. The corrections found with the aid of this formula in [7] agree closely with the results of T. A. Banakhevich [8] at $\zeta < 88°$.

We used (10) to calculate corrections for the Pulkovo Observatory tables and compared them with deviations Δr of the measured refraction from the tabulated values. The initial data and the results of calculations are presented in Table 8. For zenith distances greater than 88°, in formula (10) tg ζ is replaced by the ratio of the refraction value at a given zenith distance to its value for $\zeta = 45°$. This table shows that:

(1) A large part of the deviation in measured refraction from the tabulated value may be ascribed to the effect of temperature inversion in the ground layer of air;

TABLE 6.

ζ	n	$\overline{\Delta r}$	σ	Δr_{max} Absolute	Δr_{max} Relative	m Absolute	m Relative
			Summer				
87°	47	— 6,7	± 0,9	— 17,8	0,023	± 6,2	0,008
88	54	— 12,5	1,3	— 38,6	36	9,4	9
89	42	— 21,6	2,4	— 68,5	49	15,7	11
89,5	7	— 33,3	5,7	— 46,1	31	15,0	10
89,8	13	— 73,7	8,8	—116,0	63	31,7	17
			Winter				
87	42	+ 3,3	0,9	+ 16,8	0,019	6,0	0,007
88	36	+ 9,0	1,2	+ 24,2	21	7,4	6
89	23	+ 41,6	3,8	+ 74,2	46	18,5	11
89,5	7	+103,3	23,0	+188,9	96	60,9	31
89,8	3	+145,2	48,0	+239,1	104	82,0	36
			Autumn				
87	43	— 0,9	0,8	— 12,7	0,016	5,4	0,007
88	38	— 1,9	1,2	+ 15,3	15	7,2	7
89	39	— 3,5	3,9	— 88,8	62	24,2	17
89,5	13	+ 27,5	9,9	+ 86,9	51	35,7	21
89,8	12	+ 47,0	23,2	+167,0	81	80,6	39

Commas indicate decimal points.

(2) formula (10) may be used for approximate estimation of the effect of inversion on refraction up to a zenith distance of 89.5°. It is necessary in this instance to have the inversion characteristics at the time of observation itself;

(3) to refine formula (10) it is necessary to have more precise temperature values at different levels of the ground layer of air for the times of observation, values which may be obtained by means of a special meteorological mast or captive balloon.

Comparison of Measured Refraction with Values Calculated on the Basis of Meteorological Atmospheric Sounding Data

In accordance with the method employed in [9], to obtain the refraction on the basis of aerologic data numerical integration was performed of the expression

$$r = -C_\lambda \int_{R_0}^{R_0+H} \frac{\operatorname{tg} i}{1 + C_\lambda \rho} \frac{d\rho}{dH} dH, \qquad (11)$$

in which C_λ is a constant corresponding to a wavelength of λ = 575 μ and the air /105 temperature and pressure values at the observation point; i is the angle between the normal and tangent to the line of site at a point at altitude H; ρ is the air density in relation to the density at the observation point; $(1 + C_\lambda \rho)$ is the refraction coefficient; and r_0 is the radius of the Earth. Numerical

integration of refraction equation (11) was carried out with a constant step of dH = 0.5 km up to an altitude of H = 60 km; the atmosphere was subdivided into 120 uniform layers having densities ρ_i referred to the middle of the layer.

TABLE 7.

Date	Sonde launch time (local)	Inversion gradient, deg/100 m	Inversion altitude, m	Inversion depth, m	Isothermal conditions at altitudes of
		Sounding at observation point			
	h m	°			
7.10 1968	04 20	0,5	0	100	—
	21 00	1,5	0	100	—
	23 00	1,1	0	300	—
8.10 1968	02 04	—	—	—	100—400 m
	05 04	—	—	—	—
	20 10	—	—	—	—
9.10 1968	23 00	0,25	0	400	—
10.10 1968	02 00	1,5	0	600	—
	05 00	—	—	—	0—400 m
	07 10	2,0	0	400	—
	21 00	0,7	0	400	—
	23 30	4,5	0	100	100—300 m
11.10 1968	02 14	7,9	0	100	—
	02 14	0,3	100	100	—
	05 09	0,2	0	100	—
	05 09	4,4	100	100	—
	05 09	2,4	200	100	—
	07 35	7,0	0	100	—
	07 35	4,2	100	100	—
12.10 1968	04 00	2,0	0	300	—
	04 00	0,4	300	100	—
12.10 1968	07 00	2,8	0	100	—
	07 00	1,4	100	300	—
12.10 1968	21 00	4,9	0	100	—
	23 00	5,5	0	100	100—300 m
13.10 1968	02 25	3,8	0	200	—
	02 25	0,7	200	100	—
	05 00	3,0	0	100	—
	05 00	6,4	100	100	—
	05 00	0,6	200	100	—
	07 09	3,8	0	300	—
	20 05	2,8	0	200	—
	23 15	3,0	0	200	200—300 m
14.10 1968	02 00	3,0	0	200	—
	02 00	0,5	200	100	—
	05 00	3,2	0	200	—
	05 00	1,3	200	100	—
		Sounding at point 25 km distant			
	h m	°			
28.09 1968	06 00	0,5	0	1000	—
29.09 1968	06 00	2,9	0	300	—
08.10 1968	06 00	0,9	0	300	—
09.10 1968	06 00	—	—	—	300—2000 m
03.12 1969	06 00	1,6	0	900	—
05.12 1969	06 00	0,5	300	1500	—
06.12 1969	06 00	0,4	0	600	—
	06 00	2,1	600	300	—
05.06 1970	06 00	0,8	0	300	—
	06 00	—	—	—	300—600 m
06.06 1970	06 00	0,5	0	600	—

Commas indicate decimal points.

TABLE 8.

Date	Observation time	Sonde launching time	Inversion gradient per 100 m	Inversion depth, m	T_0	ζ	$r - r^*$	$\Delta r = r_{meas} - r_{calc}$
	h	h	°		°	°	"	"
29.09 1968	7,2	6,0	2,9	300	278,2	89,0	— 46	+60
11.10 1968	7,3	7,6	5,6	200	271,7	89,3	—135	+80
11.10 1968	7,4	7,6	5,6	200	271,4	88,6	— 28	+65
11.10 1968	7,5	7,6	5,6	200	271,0	88,0	— 11	+23
12.10 1968	19,6	21,0	4,9	100	280,2	89,4	— 80	+87
13.10 1968	7,4	7,2	3,8	300	273,2	89,4	—197	+72
13.10 1968	7,4	7,2	3,8	300	273,2	88,8	— 41	+39
13.10 1968	7,5	7,2	3,8	300	273,2	88,1	— 13	+15

Commas indicate decimal points.

Since as a star approaches the horizon i at the initial point of the beam trajectory tends towards 90°, and tg i increases without limit, the error in calculation of the integral will also increase. To reduce this error it would be necessary in the lower layers of the atmosphere to reduce the integration step, something which in turn requires more detailed sounding of the atmosphere. Such sounding is also necessary to allow for the inversion effect in the lower layers of the atmosphere. Since in the program previously employed to calculate the integral of (11) the integration step was 0.5 km, when the results of numerical integration are compared with the observational data more or less dependable conclusions may be drawn only at zenith distances which in any event do not exceed 89°. This follows from the circumstance that, as is pointed out in [7], the numerical integration error at a given step will reach several seconds of arc even at z = 88°, and at ζ = 89° it may reach 10-15", this representing about 0.5% of the refraction value.

For zenith distances greater than 85° it is also necessary to take into account the fact that the meteorological conditions at the observation point may differ from the conditions at distant points on the beam trajectory. In Table 9 we present the distances (in km) taken from [7] from the observation point at which the light beam intersects the interface of layers situated at altitude H equalling 1, 2, and 10 km.

According to M. V. Zavarina [10], with an extrapolation error of 2° the radius of action of temperature sounding of the atmosphere at these altitudes is assumed to equal 200 km. The paper by Ye. S. Selezneva [11] gives the characteristics of temperature variation with time. According to these data, in a two-hour period at an altitude of 1-2 km the root mean square variation in temperature is 0.8°, and 1.1° C at an altitude of 4 km. These estimates do not, of course, apply to the ground kilometer layer, which is the most greatly subject to temperature variations both in time and in space. This layer causes considerable variation in the refraction value at the horizon. On the whole it may be assumed that in the region in question the inversion depth reaches 500 m above the surface of the Earth. The light beam enters this layer 50 km from

the observation point, if the zenith distance equals 89° 30". Within a radius of 50 km the underlying surface in this region could be assumed to be uniform (hilly, rocky steppe) if the observation point were not adjoined on the east (1 km) by an extensive water surface. It is known from aerologic studies that temperature inversions are generally insignificant above a water surface. It seems to us to be interesting to confirm this by determining the differences in observed refraction for western and eastern bodies. The refraction measured on the basis of rising stars should in our case be on the average smaller than the refraction obtained from observations of setting stars. Unfortunately, it was rather seldom possible to conduct simultaneous observations of setting and rising stars, owing to the small number of bright bodies. However, there were 47 /106 stars observed in pairs at zenith distances of 88-89° during the two-hour observation interval in the autumn-summer season.

TABLE 9.

ζ	H=1 km	H=2 km	H=10 km
80°	8	10	55
85	12	23	105
88	30	52	205
89	45	90	275
89,5	93	140	325

Commas indicate decimal points.

Table 10 gives the mean values of refraction deviations $\overline{\Delta r}$ (the measured value minus the value calculated with the Pulkovo Observatory tables), as well as their root mean square errors σ for both setting and rising stars.

Despite the absence of data on the inversion picture at the times of observation both for land and for the water surface, root mean square deviations $\overline{\Delta r}$ in Table 10 indicate increase in refraction for setting stars, the beams of which pass over land. As was to be expected, this increase is slight for $\zeta = 88°$, while for $\zeta = 89°$ the refraction increased on the average by 27.5", with a root mean square error in the mean value difference of ±7.8".

It would also be interesting to verify this effect, first confirmed by way of experiment, by the use of data of aerologic sounding of the atmosphere. According to our assumptions, the refraction calculated on the basis of data of sounding above land should, owing to the effect of inversion, be greater than the refraction obtained from observations of bodies the beams from which passed over the surface of water. To verify this assumption we used the aerologic data of the 8 sondes of the weather station situated 25 km from the observation point, the launching times of which coincided within the limits of an hour with the time of the astronomical observation. The astronomical refraction was calculated for 8 series of observations by numerical integration of expression (11). Table 11 gives, for zenith distances of 85-89°, the differences between the measured refraction values and those calculated on the basis of data of aerologic sounding of the atmosphere, $\Delta r = r_{meas} - r_{cal}$, as well as their mean values for all series. The data of Table 11 confirm the assumption advanced in the foregoing.

For observations of the Sun at $\zeta = 89°$ we have a large dispersion of the /107 refraction measurement results, which is typical of the transitional period between stratification of the "nighttime" atmosphere and the "daytime"

stratification, when rapid distortions of the inversion picture take place. In contrast to Table 10, in Table 11 we have a smaller number of measurements one-half of which refer to observations of the Sun. In both instances the mean refraction differences confirm statistically the decrease in the inversion effect when beams from celestial bodies pass over an extensive water surface.

TABLE 10.

ζ	Setting			Rising			Difference	
	n	$\overline{\Delta r}$	σ	n	$\overline{\Delta r}$	σ	$\overline{\Delta r_w}-\overline{\Delta r_0}$	Root mean square difference error
88°	16	+ 1,1	±2,0	15	— 4,2	±1,5	5,3	±2,5
89°	9	+12,4	±5,9	7	—15,1	±5,2	27,5	±7,8

Commas indicate decimal points.

TABLE 11.

Series No.	Body	85°	86°	87°	88°	89°
1	Sun	+2,0	—5,0	—13,5	— 3,5	+20,0
2	Jupiter	+4,0	+2,0	— 2,0	— 9,9	—
3	Sun	—	—1,0	+ 3,4	— 5,3	—54,0
4	Jupiter	—1,2	+0,9	— 7,8	—12,6	—
5	Jupiter	+1,8	+3,1	+ 4,1	+ 3,1	+ 5,5
6	Jupiter	—1,6	—7,8	—22,5	—18,2	—
7	Sun	—4,9	—5,8	— 5,0	—19,2	—27,0
8	Sun	—3,4	—2,9	— 6,5	—17,8	—23,1
	Mean	—0,5	—2,1	— 6,2	—10,4	—15,7
	σ	±1,2	±1,4	± 3,1	± 2,9	±13,2

Commas indicate decimal points.

Similar comparison of the measured refraction with that calculated on the basis of aerologic data was made by use of the data of atmospheric sounding at the point of observation on the basis of 8 series of observations in the autumn of 1968. It was found in this instance as well that the refraction obtained from observations of rising stars is smaller than the values calculated on the basis of data of atmospheric sounding of the atmosphere at the observation point. The mean values of deviations $\overline{\Delta r}$ and their errors σ prove to be of the same order of magnitude as in Tables 10 and 11.

It should be noted that the dependence of astronomic refraction deviations at the horizon on temperature inversion in the ground layer of air have been confirmed experimentally for the first time. This applies equally to the seasonal fluctuations in the refraction values.

Findings

1. The differences in the observed and the tabulated refraction are subject to seasonal fluctuations. On the basis of the mean values of this distance the value of measured refraction at the horizon was found in summer to be 4% smaller and in winter 6% larger than that calculated on the basis of tables. The maximum differences observed at the temperatures measured reached -6% and +10% respectively.

2. The large deviations of the actual refraction from its tabulated values for zenith distances of 88-90° may be ascribed chiefly to variations in the temperature gradient in the ground kilometer layer of the atmosphere.

3. Use of the Pulkovo Observatory tables with an observation accuracy of 5" is possible for zenith distances not exceeding 85°.

4. When the observation point is situated on the shore of an extensive water surface the effect of temperature inversion on refraction at the horizon is greatly weakened for bodies beams from which pass above the surface of the water.

REFERENCES

1. Vasilenko, N. A., in the book: *Astrometriya i Astrofizika* [Astrometrics and Astrophysics], Vol. 5, (Questions of Atmospheric Optics), "Naukova Dumka", Kiev, 1969.
2. Kolchinskiy, I. G., *Izv. GAO AN USSR*, Vol. 3, p. 2, Kiev, 1961.
3. Fogel', R., *Kurs sfericheskoy astronomii* [A Course in Spherical Astronomy], Kiev, 1910.
4. Kolchinskiy, I. G., *Refraktsiya sveta v zemnoy atmosfere (obzor)* [Refraction of Light in the Earth's Atmosphere (A Survey)], "Naukova Dumka", Kiev, 1969.
5. Belyeyev, N. A., *AZh.*, Vol. 31, p. 3, 1954.
6. Zverev, M. S., *AZh.*, Vol. 23, p. 2, 1946.
7. Kolchinskiy, I. G., *Issledovaniye refraktsii sveta v zemnoy atmosfere* [Study of Light Refraction in the Earth's Atmosphere] Doctoral Dissertation, Part 1, Kiev, 1968.
8. Banakhevich, T. A., *Tri eskiza po teorii refraktsii* [Three Discourses on Refraction Theory], Kazan', 1915.
9. Kolchinskiy, I. G. et al., in the book: *Astrometriya i Astrofizika* [Astrometrics and Astrophysics], Vol. 5, (Questions of Atmospheric Optics), "Naukova Dumka", Kiev, 1969.
10. Zavarina, M. V., *Trudy NIU GUGMS*, Series 1, p. 21, 1946.
11. Selezneva, E. S., *Trudy NIU GUGMS*, Series 1, p. 21, 1946.

N75 21171

SCINTILLATION SPECTRA OF STARS AND PLANETS AND DEPENDENCE OF THEIR CHARACTERISTICS ON METEOROLOGICAL CONDITIONS

Yu. K. Filippov

ABSTRACT. 839 scintillation spectra of stars and 102 scintillation spectra of planets were obtained at Goloseyevo. Study was made of the dependence of the scintillation spectral density and of the amplitude and frequency characteristics on zenith distances and aerological parameters. The differences in the scintillation spectra amplitude characteristics for "white" and "red" stars were found. Examination was also made of increase in the limiting frequency of the planet scintillation spectrum as the wind becomes stronger and of the dependence of spectral characteristics on wind and star azimuth differences.

Observations of the scintillation spectra of stars and planets have been conducted regularly at the Main Astronomical Observatory of the Academy of Sciences of the Ukrainian SSR since 1965. The experimental equipment consists of an AZT-7 telescope (lens diameter 20 cm), a photomultiplier, a direct-current amplifier, a sequential action spectral analyzer, and a recording instrument [1].

The spectra are recorded in the 0.5-75 Hz frequency range. This range is of interest from the viewpoint of establishment of the dependence of scintillation parameters on meteorological characteristics. The filter band width is constant over the entire range and equals 0.5 Hz, and the analysis time 7.5 minutes. However, the differences in the characteristics of 2-3 consecutive spectral recordings do not exceed the instrument error.

Over the 1965-1968 period around 2000 recordings were made of the scintillation spectra of stars and planets. Observations were conducted during 128 nights. Study was made of the spectra of 13 bright stars (8 "white" stars of spectral classes B-G and 5 "red" stars of spectral classes K-M) and of 4 planets. The number of measured scintillation spectra of these stars and planets are given below:

"White" stars		"Red" stars		Planets	
Vega	268	Arcturus	154	Venus	44
Altair	153	Betelgeuse	13	Jupiter	36
Capella	94	Antares	9	Mars	17
Sirius	33	Aldebaran	4	Saturn	5
Deneb	32	Pollux	4		
Spica	32	Total	184	Total	102
Procyon	22				
Rigel	21				
Total	655				

Use was made for the measurements of the data of 117 nighttime observations, which included 839 star scintillation spectra and 102 planet scintillation spectra, with allowance for averaging over 2-3 consecutive recordings. In the course of 11 nights the recordings contained very small signal amplitude values (ones falling within the measurement error limit). Of the total number of nights of observations there were 5, 47, 55, and 21 respectively in the winter, spring, /109 summer, and autumn periods. Thus the average number of spectra obtained in a night is around 7.

The scintillation of the stars was observed at zenith distances z = 10-85°, and that of the planets at z = 5-75°. To eliminate the influence of z, in the processing all the spectra were divided into 3 groups covering the following ranges: z_1 = 10-40°, z_2 = 41-60°, and z_3 = 61-85°.

The results of the observations were compared with the data of aerological sounding in the 0.2-15 km layer obtained at times near the times of observation. The data on temperature, relative humidity, and wind speed and direction were averaged over the 0.2-0.5, 1-3, 4-7, 8-11, and 12-15 km layers. The mean wind speed characteristic in the 3-km layers was adopted as the basic characteristic of the atmospheric conditions. The mean wind speed in these layers over the 1965-1968 period was 8-16 m/sec; wind speed values from 2-4 to 46-53 m/sec were observed experimentally.

Scintillation Spectra Characteristics

The scintillation spectra studied by us are characterized by the following quantities.

1. a_f — the variable component amplitude. This quantity is determined on measurement of the spectral recording on the recording instrument tape. In practice a_f is proportional to the analyzer output voltage U_{out}, which in turn is defined by the formula

$$\overline{U_{out}} = k\sqrt{F(\omega)\Delta\omega}, \quad (1)$$

in which $f(\omega)$ is the scintillation spectral density and k a constant allowing for the amplification factor of the system and the analyzer frequency characteristic. Hence quantity a_f^2, which is proportional to $f(\omega)$, may be used as the basic characteristic of the scintillation spectrum. In addition, the instrument records constant signal component a_0.

2. K_f — the ratio of the variable component amplitude at a given frequency to the variable component amplitude at a frequency of 0.5 Hz (lower analysis limit). In practice subscript f is assigned by two values 1 and 2 corresponding to frequencies of 9 Hz (K_1) and 30 Hz (K_2).

3. m_f — The ratio of variable component amplitude a_f to constant component amplitude a_0. In this instance subscript f assumes values 1, 2, 3, corresponding

to frequencies of 0.5, 9, and 30 Hz. This quantity permits determination of the scintillation intensity modulation depth.

4. $F(\omega)$ – the spectral density of scintillation. This quantity was used to plot $F(\omega)$ against frequency ω in logarithmic coordinates.

5. $\overline{f}$ – the mean spectral density. This quantity is defined by the formula

$$\overline{f} = \frac{\sum_i a_i f_i}{\sum_i a_i}, \qquad (2)$$

in which a_i is the mean variable component amplitude over a rather small frequency interval Δf_i. The mean frequency values over the Δf_i range of 2, 6, 12, 20, 30, 42, and 60 Hz correspond to subscript f_i.

6. f_{lim} – the scintillation spectrum limiting frequency. It is defined as the maximum spectral frequency at which the signal amplitude decreases to 10% of the maximum, i.e., in effect to the noise level.

Dependence of Scintillation on Zenith Distance /110

The amplitude characteristics are shown in Figure 1 plotted against the zenith distance. The graphs were obtained as a result of averaging over all the star scintillation spectra during 117 nights.

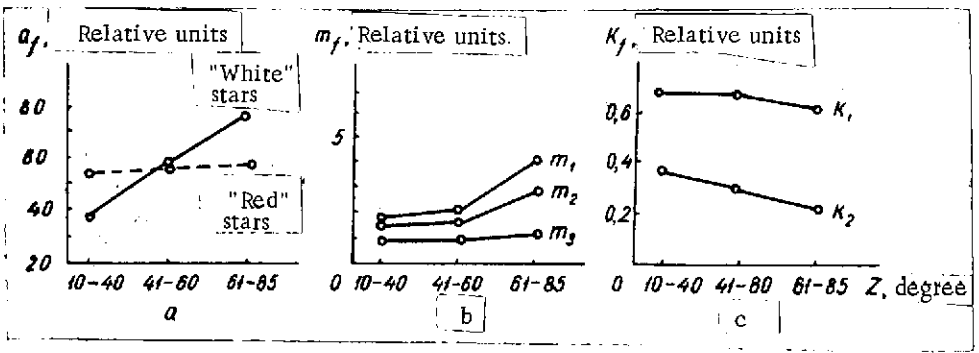

Figure 1. Scintillation Spectra Amplitude Characteristics Versus Zenith Distance.

1. The mean values of a_f increase with increase in the zenith distance. This dependence is more pronounced for the "white" stars, while the scintillation intensity of the "red" stars depends very little on z (Figure 1a). This was known earlier only from the data of very simple visual observations.

2. The modulation depth defined by quantity m_f increases with the zenith distance, this dependence being less pronounced at higher frequencies (Figure 1b).

3. Quantity K_f decreases with increase in z. Consequently, the contribution of the low frequencies increases at large values z (Figure 1c). On the whole this finding is in agreement with the results of previous studies [1, 5, 6].

Analysis of Results of Observations and Comparison of Results with Aerologic Data

1. According to our observations, an indeterminate relationship exists between the scintillation characteristics and the vertical temperature gradient and relative humidity values. Hence the conclusion drawn earlier [1] that there is a relationship between K_f and U has not been confirmed. At the same time, the results of comparisons between K_f and the values of mean wind speed v in different atmospheric layers are more definite and have been investigated in detail.

2. Figure 2 shows K_f plotted against wind speed $\bar{v}$ in the 12-15 km layer. These data were obtained as a result of averaging over all the spectra during 117 nights in the range of zenith distances z_2 (41-60°). The blank circles designate the values of K_1 and the solid circles those of K_2. Despite the considerable scattering of the points, this relationship is definitely established: the value of K_f increases with increase in the wind speed. The picture is similar in the other atmospheric layers and ranges (z_1, z_3). Thus, with increase in the rate of transfer of optical heterogeneities in the 0.2-15 km layers the contribution of the latter to the high frequency portion of the spectrum increases. This conclusion is also in agreement with the results of earlier works [1, 5]. /111

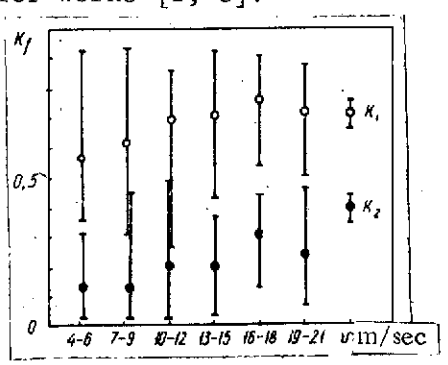

Figure 2. Amplitude Characteristics of Scintillation Spectra (K_f) Versus Wind Speed (v) in the 12-15 Layer at Zenith Disatnces of 41-60°.

The relationship of spectral density $F(\omega)$ to frequency ω is nonlinear and is characterized by abrupt decrease in the high-frequency region of the spectrum.

Figures 3a-c show the averaged relationships of $F(\omega)$ to ω obtained in 117 nights of observation. These observations are represented by three groups to which mean wind speed value $\bar{v}$ in the 0.2-15 km layers correspond:

first group (33 nights) — $\bar{v} < 10$ m/sec,
second group (53 nights) — $10 < \bar{v} < 20$ m/sec,

3rd group (31 nights) — $\bar{v}$ > 20 m/sec.

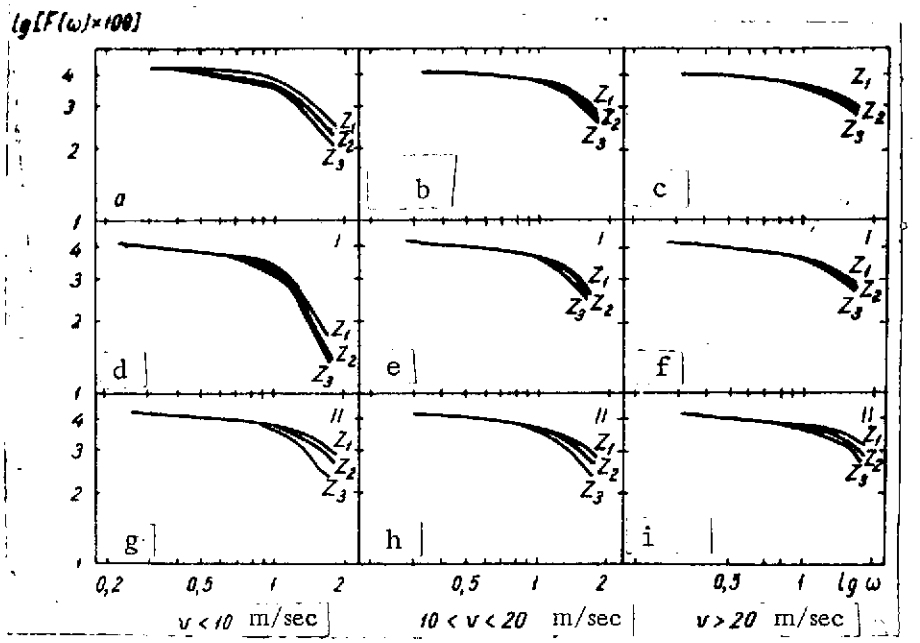

Figure 3. Spectral Density of Scintillation F(ω) Versus Frequency ω in Logarithmic Coordinates.

In this instance the steepness of the high-frequency region of the spectrum and the corresponding values of $\bar{f}$ increase with increase in zenith distance z in each group and with decrease in wind speed v. Each group of nights has 3 spectra in the ranges z_1, z_2, and z_3 corresponding to it.

4. Spectra with steepness of varying nature are observed, in turn, in each group in the region of the high frequencies. This provides a basis for dividing the nights of observations in each group into two types:

Nights of the first type (Figure 3d-f) are characterized by very similar values $\bar{f}$ in all ranges of z. The form of the spectrum is determined by the condition

$$\bar{f}_{z_1} = \bar{f}_{z_2} = \bar{f}_{z_3}, \tag{3}$$

in which $\bar{f}_z$ are the mean frequency values in a given range z.

Nights of the second type (Figure 3g-i) are characterized by spectra exhibiting considerable difference in the steepness of the high-frequency portions in the z_1-z_3 ranges. The form of the spectrum is in this instance defined by the condition

$$\bar{f}_{z_1} > \bar{f}_{z_2} > \bar{f}_{z_3}. \tag{4}$$

The number of nights are distributed as follows by types within each group: /11

first group (first type 19 nights, second type 14 nights),
second group (first type 13 nights, second type, 40 nights),
third group (first type 12 nights, second type 19 nights).

Thus the number of observation nights of the second type represent 62% of the total number of nights.

5. Analysis of the materials obtained showed that the form of the spectrum varies from night to night, i.e., transitions are observed from a night of one type to a night of the other type and vice versa.

Series of spectra obtained during specific observation cycles were studied to ascertain the possible relationships of such transitions to meteorological conditions. Each such cycle consists of a sequence of clear nights.

One of these cycles (5-11 August 1967) is shown in Figure 4. All the nights of this cycle are characterized by a mean wind speed characteristic in the 0.2-15 km layer of $\bar{v} > 20$ m/sec.

The passage of an atmospheric front during the 5-7 August period coincided with transition from a night of the first type (5 August) to a night of the second type (8 August). However, no apparent changes took place in the meteorological situation during the following two days. Anticyclonic weather was established in the area of the point. A change in the form of the spectrum (transition to a night of the first type) is observed again on the night of 11 August. This transition cannot be directly associated with change in the meteorological conditions, since the weather remains stable at the observation point. Two circumstances must be taken into account in study of the dependence of scintillation characteristics on meteorological conditions.

Firstly, there is the change in the value and direction of wind speed in the tropospheric layers. This change may be associated with change in the weather (for example, the passage of a front). The folklore about the association of scintillation intensity with variation in the weather apparently is fairly well-founded. Confirmation of such an association by the data of objective (photoelectric) analysis is of interest.

Secondly, the scintillation spectrum characteristics are determined by the position of the telescope tube, or rather by the azimuth of the star. This follows from theoretical considerations [2]. When a light wave of length λ is propagated in a turbulent medium the rate of transfer of optical heterogeneities in a layer of thickness L_0 is determined basically by the mean wind speed component, which is perpendicular to the direction of the beam, v_n. In this case, as has been demonstrated in [3] in particular, the scintillation frequency is determined by the formula

$$f = \frac{v_n}{\sqrt{\lambda L_0 \sec z}}. \qquad (5)$$

If the wind blows at an angle to the vertical plane in which the telescope tube /113 is situated, then

$$v_n = \bar{v}\sqrt{1 - \sin^2 z \cos^2 \varphi}, \quad (6)$$

in which φ is the angle between the planes in which the azimuths of the wind A_w and of the star A are situated:

$$\varphi = A_w - A. \quad (7)$$

It follows that at large values z the scintillation frequency should be greatly decreased if vector $\vec{v}_n$ is in the vertical plane of the telescope (φ = 0 and 180°). In this case $\bar{f}_z$ decreases, and the low frequencies predominate in the spectrum. If vector $\vec{v}_n$ is perpendicular to the vertical plane of the instrument (φ = 90° or 270°), $\bar{f}_z$ increases and the high frequencies predominate in the spectrum. At small values z the form of the spectrum is determined substantially by the values of $\bar{v}$, since $v_n \approx \bar{v}$.

Thus the type of night is determined chiefly by the value of $\bar{f}_{z_3}$, and to a lesser extent by $\bar{f}_{z_2}$ and $\bar{f}_{z_1}$ (at a given value $\bar{v}$).

Let us consider the series of spectra in Figure 4 from this viewpoint. The observation conditions on different nights of the cycle are reflected in the vector diagrams, which show the variation in the wind and star azimuths. The position of a_w and A on 5 August has corresponding to it a mean value of φ near 90°. In this instance $\bar{f}_{z_3}$ assumes its maximum value and approaches the value of $\bar{f}_{z_2}$ and $\bar{f}_{z_1}$. Hence condition (3) corresponding to a night of the first type is satisfied.

On the night of 8 August A_w rotates 90°. Since the spectra were recorded for the same stars and at approximately the same times as on the night of 5 August, the position of A remained unchanged. The value of φ in this case approaches zero, this leading to decrease in $\bar{f}_{z_3}$. $\bar{f}_{z_1}$ undergoes hardly any change at the same value of $\bar{v}$. This corresponds to condition (4), i.e., to a night of the second type. This change in the form of a spectrum may possibly be due to the approach of a front, since there is change in the wind direction. But the change in the value of φ may also be caused by rotation of A. A situation such as this was observed on the night of 10 to 11 August, when the observation program was changed. In the first instance rotation of A does not result in change in the form of the spectrum, since A_w rotated at the same time. In this instance φ assumes a value of around 180°. Condition (4) is preserved (night of the second type). Only A changes in the second case. Thus on the

night of 11 August we observed a spectrum corresponding to a night of the first type, but this transition is not associated with change in the weather. In reality, the values of A_w and A may vary over a wide range. For this reason the division of the observation nights into two types is somewhat conditional in nature. It is this which explains in particular the predominance of the nights of the second type, since they include the greater part of the spectra having different values $\overline{f}_z$. Condition (3) is not satisfied as often, although on individual nights the conditions of observation are such that the greater part of the spectra may have similar values $\overline{f}_z$ over all ranges z.

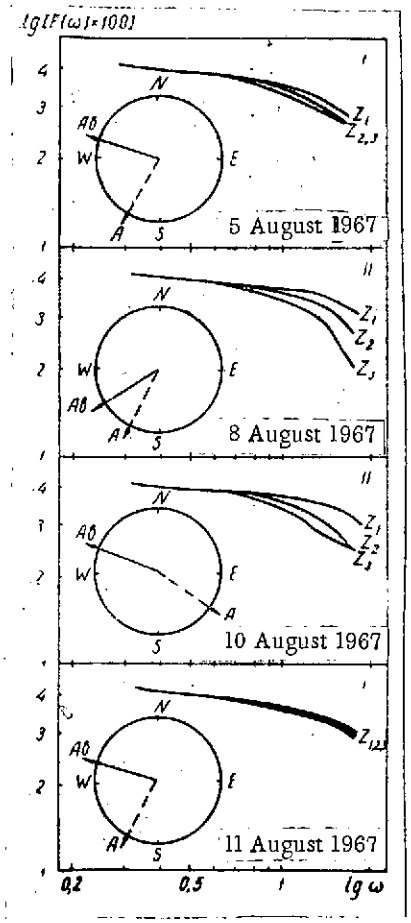

Figure 4. Scintillation Parameters Versus Wind Speed Direction and Star Azimuth.

In this paper we have not analyzed the relationship between the scintillation characteristics and the vertical wind and temperature speed profiles in detail. Such relationships are apparently less pronounced than the relationships with the position of the telescope tube (values of A and z) and the mean wind direction and speed values in all the layers of the troposphere. A clearcut relationship between the characteristics of the scintillation spectra and the meteorological conditions can probably be established if the position of the instrument is kept unchanged in the process of observation. There should in this case be a sufficiently rigid observation program. In other /114 words, the recordings of the spectra should be made for the same stars and at closely spaced points in time throughout the cycle. It is extremely difficult to meet such requirements with conventional instruments with the clockwork mechanism in operation. It would be more advisable to conduct observations of the scintillation of the North Star with a polar monitor. The position of the instrument remains virtually unchanged at all times, A and z are constant, and influence by the latter is eliminated.

Planetary Scintillation Spectra

Planetary scintillation spectra were recorded at the Main Astronomic Observatory of the Academy of Sciences of the Ukrainian SSR in 1967-1968. The observations were conducted for 24 nights. Typical planetary scintillation spectra are shown in Figure 5a. For the sake of comparison the scintillation spectra of a star (Capella) is shown here as well. The spectra were obtained at z = 50-70°. It may be seen that the planetary scintillation spectrum is concentrated in the region of the lower frequencies in comparison to the stellar scintillation spectra. The spectra obtained by us are similar to those given in the work by Young [4] for a telescope with an aperture of around 23 cm.

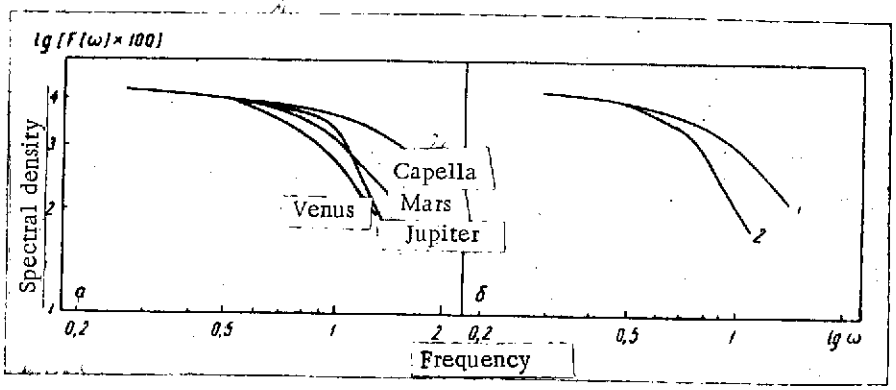

Figure 5. Planetary Scintillation Spectra Versus v and z: a, 27-28 April 1967; b, 23--24 May with v = 17 m/sec (1) and 25-26 May 1967 with v = 6 m/sec (2).

Comparison of the scintillation spectra of Venus with the data on the mean wind speed in the 0.2-15 m layer permits the conclusion that intensification of the wind results in increase in the boundary frequency of the spectrum, i.e., in relative increase in the share of the high frequencies (Figure 5b). The corresponding values of v and f_z (z = 70°) were on 24 May 1967 17 m/sec and 16 Hz and on 25 May 1967 6 m/sec and 9 Hz. These results are in agreement with the data we obtained during observation of the stars.

Comparative characteristics of the scintillation spectra of the stars and planets are given in the table. These data were obtained as a result of averaging over all the spectra. The upper limit of the scintillation spectra of the stars is adopted here on the basis of the data in [5, 6].

Analysis of the results of the present project point to the following conclusions:

1. The low frequencies predominate in the scintillation spectrum of the stars with increase in the zenith distance, the relative value of the scintillation amplitude of the "white" stars increasing more intensively than the corresponding values for the "red" stars. /115

COMPARATIVE CHARACTERISTICS OF STELLAR AND PLANETARY SCINTILLATION SPECTRA

Spectral characteristics	Stars	Planets
Limiting spectral frequencies, f_{lim}, Hz:		
minimum	10-15	3-6
maximum	500-1000	
mean (for all spectra)	35	12
f, Hz	11	9
K_1	0.60	0.19
K_2	0.19	0

2. Relative increase in the share of the high frequencies is observed in the scintillation spectra of the stars and planets with increase in mean wind speed $\bar{v}$ in the 0.2-15 km layers of the atmosphere (the limiting frequency of the spectrum increases).

3. The relationship of spectral density $F(\omega)$ to frequency ω in logarithmic coordinates is nonlinear. The form of the spectrum is in this instance determined by the zenith distance and the azimuth of the star, and by the value and direction of the wind speed. At a given value of v and z the form of the spectrum depends basically on the difference in the azimuths of the wind and the star.

4. The scintillation spectra of the planets have a much lower frequency than do the spectra of the stars.

5. To ascertain a more clearcut relationship between the scintillation parameters and the meteorological characteristics, it is advisable to conduct regular observations of the scintillation of the North Star.

REFERENCES

1. Diamant, E. M., I. G. Kolchinskiy and Yu. K. Filippov, in the book: *Voprosy Atmosfernoy Optiki* [Questions of Atmospheric Optics], "Naukova Dumka", Kiev, Vol. 5, pp. 110-117, 1969.
2. Tatarskiy, V. I., *Teoriya Fluktuatsionnykh Yavleniy pri Rasprostranenii Voln v Turbulentnoy Srede* [Theory of Fluctuation Phenomena in the Propagation of Waves in a Turbulent Medium], Izd-vo AN SSSR Press, Moscow, 1959.
3. Kolchinskiy, I. G., *Opticheskaya Nestabil'nost Zemnoy Atmosfery po Nablyudeniyam Zvezd.* [The Optical Instability of the Earth's Atmosphere According to Observations of the Stars], "Naukova Dumka", Kiev, 1967.
4. Young, A. T., *Appl. Optics*, Vol. 8, p. 5, 1969.
5. Mikesell, A. H., *Publ. of the US Naval Observatory*, II ser., XVII, Part IV, Washington, 1955.
6. Protheroe, W. M., *Cont. Perkins Observatory*, II ser., p. 4, 1955.

N75 21172

THE LAW OF DISTRIBUTION OF LIGHT BEAM DIRECTION FLUCTUATIONS IN TELESCOPES

M. L. Divinskiy and I. G. Kolchinskiy

ABSTRACT. The distribution of deviations from mean star trail directions was studied on the basis of 105 star trails. It was found that about 93% of the trails yield a distribution in agreement with the normal law. About 4% of the star trails agree with the Charlier distribution.

It follows from the general theory of the propagation of electromagnetic waves in media characterized by random density fluctuations that the distribution of fluctuations in the direction of light beams passing through the atmosphere should be Gaussian [1]. Considerable interest attaches to experimental verification of this consequence.

On the other hand, knowledge of the various statistical properties of fluctuations in the direction of light beams, and especially the laws governing their distribution, is necessary for study of the influence of these fluctuations /116 on the position of star images and the dimensions and internal structure of the latter.

We may cite in particular the work of Gyldenkaerne [2] and Morel [3] as examples of use of these laws. In both of these papers it is assumed that the deviation of the instantaneous center of the photographic image from a certain mean position in the focal plane obeys the normal law.

In 1957 it was demonstrated in a paper by one of the authors of this article [4], as a result of processing of trail observations and direct calculation of the numbers of deviations from the mean trail direction falling within assigned limits, that the law of distribution of the deviations may be assumed to be Gaussian. This result was subsequently confirmed in [5]. It is noted in the last named paper that the normal law is fulfilled basically for trails observed at zenith distances smaller than 70°. For the remaining trails the distribution of the deviation was asymmetric and resembled the Charlier distribution.

It must be pointed out that in all the papers mentioned measurement was made of segments of trails corresponding to time intervals of around 10 sec. It follows from the method itself of obtaining the deviations that the possible frequencies of the fluctuations were approximately in the 0.2-5 Hz range. Since the results of all previous studies were based on the data of measurements of no more than 20 trails, we believed it to be advisable to take up the question of the distribution law again, this time using a much larger number of trails.

In the present paper the distribution of fluctuations from the mean direction of a trail was investigated on the basis of 105 star trails obtained

with a 400-mm astrograph (F = 5.5 m) in 1955 and an AZT-7 200-mm telescope (F = 10 m) in 1964. Both instruments were mounted at the Main Astronomic Observatory of the Academy of Sciences of the Ukrainian SSR in Goloseyevo.

The method of conducting the observations and measurements for the trails obtained with the astrograph is described in [4]. It is basically similar for the trails obtained with the AZT-7, with certain modifications indicated in [6]. The fluctuation sequences for the 1955 trails consist of 4 series with 100 points in each series. The measurement intervals for the trails on the astrograph equalled 50 μ, this corresponding to 0.12 sec for an equatorial star. In the trails obtained with the AZT-7, 200 points, each measured at intervals of 50 μ, were adopted for processing.

The fluctuations for the trails were grouped according to intervals with a step equalling 0.01 micrometer rotation, the centers of which are represented by values of 0, 10, -10, 20, -20, and so forth. One-thousandth of a micrometer rotation in the case of the trail measurements obtained with the astrograph corresponded to 0.018", and in the case of the AZT-7 to 0.013". For two trails (Plate 25, trail 1 and Plate 7, trail 2) the number of measured points equalled 300. Of the 1964 trails 20 each contained 400 points, and the remaining 4 a somewhat smaller number. A theoretical curve of the normal distribution with a mathematical expectation $m_x = 0$ and a root mean square deviation σ equalling the statistical one was constructed for each statistical sequence.

The degree of matching of the statistical and the theoretical frequency distributions was determined by Pearson's criterion χ^2 [7], [8], and by the rule of V. I. Romanovskiy [9], which consists of working out the value

$$R = \frac{|\chi^2 - r|}{\sqrt{2r}},$$

in which r is the number of degrees of freedom.

In the case of random divergence of the theoretical (m_i') and statistical (m_i) frequencies $R < 3$.

According to Pearson's criterion, the frequency over the interval may be no smaller than 5-10 (8). Whenever necessary the intervals of the sequences described were combined so that $m_i' > 5.0$, and $m_i \geqslant 8$. The independent conditions (s) imposed on the statistical probabilities $\left(p_i' = \frac{m_i}{n}\right)$ are in our case determined by two requirements: /117

1) $\sum_{i}^{k} p_i' = 1,$

in which n and k are the number of measurements and classes respectively,

2) coincidence of the theoretical (D_x') and statistical (D_x) dispersions

$$D_x = D_x' = \sigma^2,$$

thus, s = 2 and the number of degrees of freedom

$$r = k - 2.$$

It was assumed that the hypothesis of a normal law of distribution of the vibration values does not contradict the observed distribution of the frequencies over the intervals $(m_i - x_i)$ at probability P(g) for the χ^2 criterion

$$P(g) \geq 0.010 \text{ and } R < 3.$$

The results obtained on matching of the statistical and theoretical frequency sequences for the 1955 and 1964 star trails are presented in Tables 1 and 2.

TABLE 1. 1955

Date	Plate and trail no.	Star	z°	χ^2	r	$P(g)$	R
January 16/17	Plate 1, trail 1	γ Gem	34,°2	23,84	16	0,093	1,39
January 24/25	Plate 5, trail 2	α Lep	68,3	6,84	9	0,691	0,59
January 26/27	Plate 6, trail 4	α Hya	65,9	9,04	11	0,618	0,42
January 26/27	Plate 7, trail 2	β Gem	24,4	15,95	7	0,026	2,39
January 26/27	Plate 8, trail 2	δ Ori	69,8	8,17	10	0,612	0,41
January 30/31	Plate 9, trail 1	β CMa	69,6	17,95	12	0,117	1,21
January 30/31	Plate 9, trail 5	β CMa	68,7	37,27	13	≪0,010	4,76
February 12/13	Plate 10, trail 5	α Hya	59,3	6,46	9	0,693	0,60
February 16/17	Plate 11, trail 1	η CMa	80,4	17,00	18	0,523	0,17
February 16/17	Plate 12, trail 1	ε CMa	82,1	12,91	13	0,455	0,02
February 19/20	Plate 13, trail 1	β CMa	69,3	14,38	7	0,045	1,97
February 26/27	Plate 15, trail 1	α Hya	59,2	18,23	12	0,109	1,27
February 26/27	Plate 16, trail 1	α Vir	70,4	22,34	15	0,100	1,34
February 28/March 1	Plate 17, trail 1	α CMa	83,3	10,14	14	0,752	0,73
February 28/March 1	Plate 18, trail 1	α Vir	69,5	23,18	12	0,026	2,28
March 12	Plate 20, trail 1	α Hya	60,4	12,59	15	0,634	0,44
March 13/14	Plate 21, trail 3	α Vir	67,6	12,72	11	0,313	0,37
March 15/16	Plate 22, trail 1	α Vir	66,9	8,55	9	0,481	0,11
March 28/29	Plate 23, trail 3	σ Sgr	81,8	9,36	13	0,745	0,71
April 7/8	Plate 24, trail 1	α CMa	76,2	18,32	9	0,032	2,20
April 14/15	Plate 25, trail 1	ζ Ori	80,0	21,92	12	0,039	2,02
April 19/20	Plate 26, trail 1	α Hya	60,5	10,72	7	0,153	0,99
April 20/21	Plate 28, trail 1	α Vir	61,5	11,47	6	0,076	1,58
April 22/23	Plate 30, trail 1	α Hya	63,3	12,73	11	0,312	0,37
April 28/29	Plate 32, trail 1	α CMi	72,1	2,97	7	0,887	1,08
June 7/8	Plate 34, trail 1	α Sco	77,3	65,77	13	≪0,010	10,35
July 10/11	Plate 41, trail 1	α Boo	64,1	8,56	10	0,575	0,32
July 13/14	Plate 43, trail 1	α Oph	52,7	13,97	7	0,052	1,86
July 14/15	Plate 44, trail 1	σ Sgr	77,2	20,94	8	0,007	3,24
July 16/17	Plate 46, trail 1	α PsA	83,4	6,82	8	0,557	0,30
July 18/19	Plate 47, trail 1	α Oph	41,1	12,66	10	0,245	0,60
July 20/21	Plate 48, trail 1	α Oph	45,8	27,65	9	≪0,010	4,40
July 28/29	Plate 53, trail 1	σ Sgr	79,4	10,74	11	0,466	0,06
July 28/29	Plate 53, trail 2	σ Sgr	80,0	16,97	11	0,109	1,27
July 28/29	Plate 53, trail 3	σ Sgr	80,7	22,46	18	0,213	0,74
July 28/29	Plate 53, trail 4	σ Sgr	81,4	2,60	10	0,987	1,66
July 28/29	Plate 53, trail 5	σ Sgr	82,3	20,11	14	0,127	1,16

Commas indicate decimal points.

TABLE 1. CONT'D.

Date	Plate and trail no.	Star	z°	χ^2	r	$P(g)$	?
July 28/29	Plate 54, trail 2	θ Aql	55,2	8,18	8	0,417	0,05
August 16/17	Plate 56, trail 1	α Oph	52,2	2,67	6	0,845	0,96
August 20/21	Plate 57, trail 1	β Cet	69,5	22,36	13	0,051	1,84
August 20/21	Plate 57, trail 2	β Cet	≈69°	10,47	9	0,315	0,35
August 21/22	Plate 58, trail 1	α CrB	49,8	7,76	8	0,458	0,06
August 21/22	Plate 59, trail 1	α CrB	57,4	4,86	7	0,677	0,57
August 24/25	Plate 60, trail 1	α CrB	63,3	12,60	5	0,028	2,41
August 24/25	Plate 61, trail 1	α CrB	68,6	8,22	7	0,315	0,33
August 27/28	Plate 62, trail 1	β Cet	68,7	4,92	5	0,427	0,03
August 27/28	Plate 62, trail 3	β Cet	69,0	6,20	6	0,403	0,06
September 17/18	Plate 66, trail 1	α PsA	81,5	15,76	18	0,609	0,37
October 15/16	Plate 71, trail 1	α Oph	54,2	13,25	6	0,040	2,09
October 15/16	Plate 71, trail 2	α Oph	62,4	15,52	7	0,030	2,28
October 15/16	Plate 71, trail 3	α Oph	66,7	12,11	10	0,278	0,47
October 16/17	Plate 72, trail 1	α Oph	77,8	22,56	15	0,095	1,38
November 4/5	Plate 74, trail 1	β Cet	69,9	8,67	10	0,564	0,30
November 4/5	Plate 74, trail 2	β Cet	68,9	36,94	12	≪0,010	5,09
November 10/11	Plate 75, trail 1	α Oph	65,2	9,22	9	0,418	0,05
November 10/11	Plate 76, trail 1	α PsA	80,5	19,75	14	0,139	1,09
November 10/11	Plate 77, trail 1	β Cet	74,5	18,17	10	0,053	1,83
November 10/11	Plate 78, trail 1	β Cet	70,4	7,54	11	0,753	0,74
November 15/16	Plate 79, trail 1	α Oph	71,7	17,83	15	0,272	0,52
November 15/16	Plate 80, trail 1	β Aur	62,5	15,24	15	0,435	0,04
November 15/16	Plate 80, trail 2	β Aur	60,6	8,98	13	0,774	0,79
November 15/16	Plate 81, trail 1	β Cet	68,5	13,82	13	0,387	0,16
November 15/16	Plate 81, trail 2	β Cet	68,7	14,67	11	0,199	0,78
November 15/16	Plate 82, trail 1	α Lyr	65,1	9,23	11	0,601	0,38
November 19/20	Plate 83, trail 1	α PsA	80,8	14,91	16	0,531	0,19
November 19/20	Plate 83, trail 2	α PsA	80,9	24,69	18	0,134	1,12
November 19/20	Plate 84, trail 1	β Aur	56,5	5,03	7	0,656	0,53
November 19/20	Plate 84, trail 2	β Aur	56,1	18,80	15	0,224	0,69
December 8/9	Plate 85, trail 1	ζ Ori	72,5	21,59	11	0,028	2,26
December 8/9	Plate 85, trail 2	ζ Ori	71,1	20,28	13	0,089	1,43
December 14/15	Plate 86, trail 1	α PsA	81,3	29,22	15	0,015	2,60
December 14/15	Plate 87, trail 1	α Aql	73,7	11,60	8	0,171	0,90
December 14/15	Plate 87, trail 2	α Aql	74,0	6,08	9	0,732	0,69
December 19/20	Plate 88, trail 1	β Cet	68,7	10,13	9	0,341	0,27
December 19/20	Plate 88, trail 2	β Cet	68,7	4,04	8	0,849	0,98
December 19/20	Plate 89, trail 1	ε Ori	72,6	18,68	9	0,028	2,28
December 19/20	Plate 89, trail 2	ε Ori	≈73°	12,71	10	0,242	0,61
December 19/20	Plate 90, trail 1	β CMa	70,7	8,49	10	0,581	0,34
December 19/20	Plate 90, trail 2	β CMa	71,2	20,80	12	0,054	1,80
December 19/20	Plate 91, trail 1	δ CMa	77,3	22,63	14	0,067	1,63
December 19/20	Plate 91, trail 2	δ CMa	78,0	11,15	15	0,742	0,70

Commas indicate decimal points.

For trails which did not satisfy the normal law of vibration value distribution, coefficients of asymmetry S_k and excess E_x were calculated in the conventional manner, and then with the values obtained for S_k and E_x a theoretical sequence of Charlier distribution frequencies was constructed on the basis of the equation /118

$$m_i' = \frac{nh}{\sigma' \sqrt{2\pi}} e^{-\frac{t^2}{2}} \left[1 + \frac{S_k}{6}(t^3 - 3t) - \frac{E_x}{24}(t^4 - 6t^2 + 3)\right],$$

in which m_i'' is the theoretical value of the Charlier distribution frequency for the ith interval with term x_i, h is the interval step, and σ' is the new standard value with the statistical mean m_x', $t = \frac{x_i - m_x'}{\sigma'}$. The number of conditions imposed on the frequencies equals 4 in this instance; consequently,

$$r = k - 4.$$

Matching of the theoretical curves obtained with the observed curves was determined by the criteria χ^2 and R. The results of the calculations are summarized in Table 3, in which data are also given for one trail (plate 18, trail 1, α, Vir) with a small P(g) value for the χ^2 criterion in accordance with the normal law hypothesis (P(g) = 0.026). Adjustment on the basis of the Charlier distribution yields a higher degree of probability (P(ch) = 0.484). /119

TABLE 2. 1964.

Date	Plate and trail no.	Star	z^o	χ^2	r	P(g)	R
June 10/11	Plate 120, trail 8	ζ Her	19,6	4,59	9	0,866	1,04
	Plate 120, trail 11	α UMa	43,2	2,94	7	0,890	1,09
	Plate 120, trail 14	ε UMa	35,0	12,28	8	0,140	1,07
	Plate 120, trail 17	η UMa	30,1	9,93	7	0,193	0,78
	Plate 120, trail 20	α Boo	45,6	15,77	11	0,151	1,02
	Plate 120, trail 23	ε Boo	36,2	16,58	12	0,167	0,93
	Plate 120, trail 26	α CrB	30,2	10,73	10	0,380	0,16
	Plate 121, trail 8	ε Cyg	38,9	8,57	9	0,479	0,10
	Plate 121, trail 11	α Cyg	28,0	19,55	9	0,021	2,49
	Plate 121, trail 17	α Aql	49,7	11,80	11	0,379	0,17
	Plate 121, trail 20	α Lyr	16,1	16,68	9	0,055	1,81
	Plate 121, trail 23	η Oph	66,2	12,95	13	0,452	0,01
	Plate 121, trail 26	α Oph	37,8	8,91	10	0,541	0,24
June 17/18	Plate 122, trail 5	α Boo	55,8	13,38	10	0,204	0,76
	Plate 122, trail 8	ε Boo	46,1	5,66	7	0,581	0,36
	Plate 122, trail 11	α CrB	39,3	7,63	9	0,572	0,32
	Plate 122, trail 14	η UMa	43,2	16,99	9	0,049	1,88
	Plate 122, trail 17	ε UMa	47,9	6,13	7	0,525	0,23
	Plate 122, trail 20	γ UMa	56,9	5,16	6	0,525	0,24
	Plate 122, trail 23	α Lyr	12,0	26,19	9	<0,010	4,05
	Plate 122, trail 26	α Oph	41,4	8,03	9	0,531	0,23
	Plate 123, trail 5	α And	53,2	15,40	17	0,567	0,27
	Plate 123, trail 8	β Peg	44,4	5,01	9	0,833	0,94
	Plate 123, trail 11	α Cyg	12,4	>100	11	≪0,010	>20

Commas indicate decimal points.

Four of the seven trails not obeying the Gaussian distribution of vibration values are described well by the Charlier distribution. The others do not match the asymmetric frequency distribution. However, it should be noted that direct comparison of the frequencies of trail 1, plate 34 (α Sco), from $x_1 = -110$ to $x_1 = 80$ reveals satisfactory agreement with the theoretical distribution and influence chiefly by the intervals $80 < x_i < 120$ on deviation from the Charlier distribution.

The number of trails observed for various vibration value distributions is shown in Table 4. In the majority of the star images (93.3%), as in shown by the 1965 and 1964 observations, the vibration value distribution does not contradict the normal law. /120

TABLE 3.

Plate and trail no.	Star	S_k	E_x	χ^2	k	P(ch)	R(ch)
Plate 122, trail 23	α Lyr	—0,68984	1,79857	12,92	5	0,0243	2,51
Plate 123, trail 11	α Cyg	0,40590	—0,13572	9,06	9	0,4320	0,01
Plate 9, trail 5	β CMa	—0,51051	0,13304	15,11	10	0,1285	1,14
Plate 34, trail 1	α Sco	0,54441	0,71763	25,25	11	<0,010	3,04
Plate 44, trail 1	σ Sgr	—0,44930	—0,05634	8,75	6	0,1897	0,79
Plate 48, trail 1	α Oph	0,25206	0,30063	20,04	8	0,010	3,01
Plate 74, trail 2	β Cet	—0,33301	0,21241	26,32	10	<0,010	3,65
Plate 18, trail 1	α Vir	—0,44500	0,18553	9,53	10	0,4836	0,11

Commas indicate decimal points.

TABLE 4.

Year	Total no. of trails	Normal distribution	Not obeying normal distribution	Charlier distribution
1955	81	76	5	2
1964	24	22	2	2
Total	105	98	7	4

Only 2.9% of the total number of trails failed to conform to the Gaussian or Charlier distributions. The remaining 3.8% of the trails are adjusted well by the Charlier distribution. Trails conforming to the normal law of vibration value distributions are encountered at virtually all zenith distances.

As a result of processing the observational data we found that in 94.1% of the trails obtained at $z > 60°$ the distribution of the fluctuations does not contradict the normal law. As we see, the percentage in this case proved to be even higher than the mean for all the trails. The numbers of observed star images for various distributions over the zenith distances are shown in Table 5.

The trails not satisfying the Gaussian fluctuation distribution represent 8.1% of all the trails over the $0° < z < 60°$ interval. This number is somewhat smaller (5.9%) at $z > 60°$.

TABLE 5.

z Intervals	Normal vibration value distribution	Vibration value distribution not conforming to normal law	Total
0—30°	4	2	6
30—60	30	1	31
60—90	64	4	68
Total	98	7	105

By way of example the theoretical and the observed frequency values of 3 trails with normal distribution are compared in Figure 1. A similar comparison of 2 trails which do not contradict the Charlier distribution is presented in Figure 2. It is understandable why in some instances the fluctuation distribution law differs from the normal law. In [10] attention is called to the fact that the total deviation of an image at the point of observation may be regarded as the sum of a large number of individual deviations a_i, each of which arises in a small volume of the air mass along the path of the beam, i.e., $\alpha = \Sigma\alpha_i$. If deviations α_i in the individual volumes may be assumed to be independent quantities, based on the A. M. Lyapunov limit theorem, the distribution of α will tend toward normal with unlimited increase in the number of terms in the sum. There may be any law of distribution of values α_i, but an essential restriction imposed on α_i is that each of them exerts only a small influence on the sum [11], i.e., there may be in the sum no terms which can assume values comparable in order of magnitude to the entire sum. It is pointed out in [12] that the number of air density heterogeneities along the path of the beam will probably be fairly large. If a small deviation occurs in each of the elementary air volumes, it is to be expected that the law of distribution of total deviation α will be normal. /121
However, under actual conditions it is not to be expected that the deviation will be sufficiently small in comparison to the total deviation in each of these elementary volumes. Violations of this rule may occur, for example, on the interfaces of two air masses of different temperature and density. Of course, corresponding deviations from the normal law also take place in this instance. This possibly explains the deviations of the values of the exponent from 0.5 in the law expressing the dependence of the root mean square deviations on the zenith distance [13].

It is of interest to note in connection with the foregoing that the trails in which the deviation from the normal law is substantial ($P(g) < 0.010$, $R > 3$) or is even not determined with great certainty ($0.050 \geqslant P(g) > 0.010$), in the majority of cases were obtained under poor meteorological conditions (fog, haze, /122 wind, low atmospheric pressure, etc.).

The trails obtained under good meteorological conditions are characterized by a distribution that does not contradict the Gaussian, at both small and large values z.

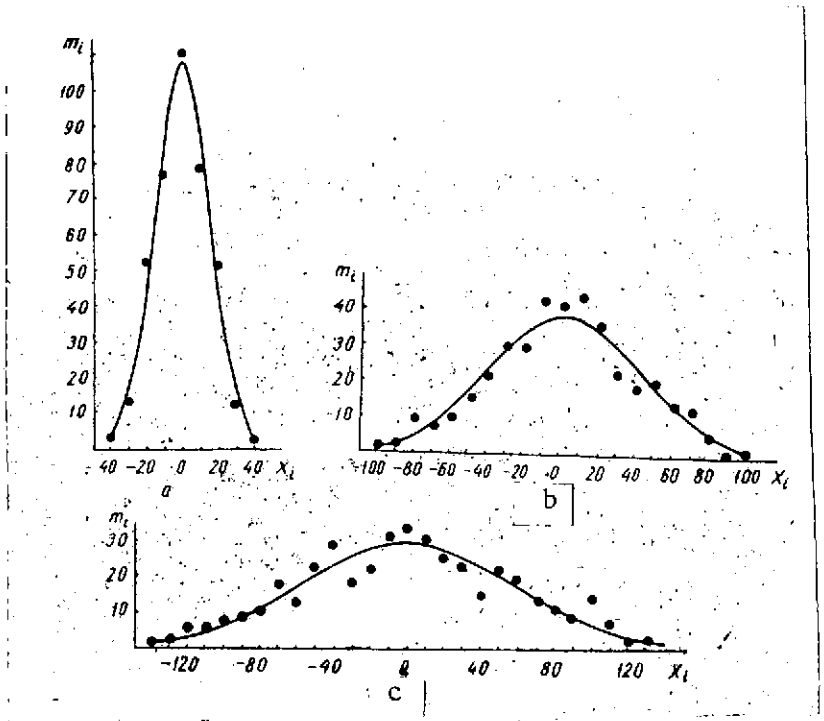

Figure 1. Observed Distribution (Dots) and Theoretical Normal Distribution (Line): a, Plate 62, Trail 1, β Cet; b, Plate 17, Trail 1, α GMa; c, Plate 66, Trail 1, α PsA.

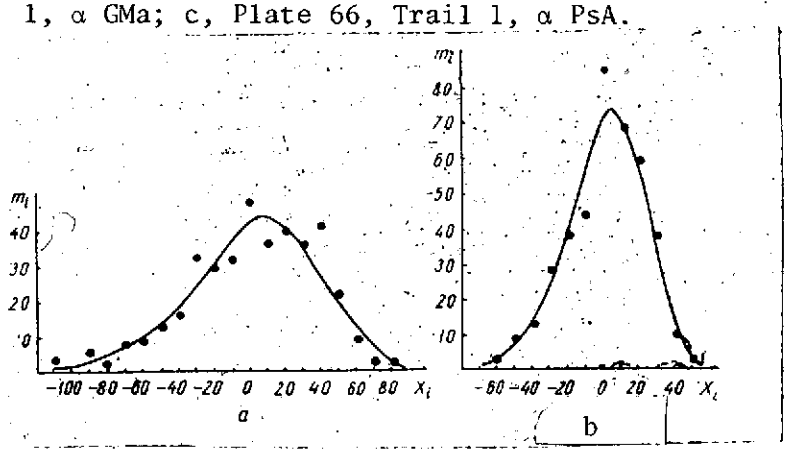

Figure 2. Observed Distributions (Dots) and Theoretical Charlier Distribution (Line): a, Plate 9, Trail 5, β CMa; b, Plate 44, Trail 1, σ Sgr.

REFERENCES

1. Monin, A. S. and A. M. Yaglom, *Statisticheskaya Gidromekhanika* [Statistical Hydromechanics], "Nauka" Press, 2nd edition, Moscow, p. 2, 1967.
2. Gyldenkaerne, K., *Ann. d'Astr.*, Vol. 13, p. 97, 1950.
3. Morel, P. T., *Astron. and Astroph.*, Vol. 6, No. 3, pp. 10, 441-452, 1970.
4. Kolchinskiy, I. G., *AZh.*, Vol. XXXIV, No. 4, pp. 638-651, 1957.
5. Kuznetsova, L. Kh., in the book: *Ob Astroklimate Sibiri* [The Astroclimate of Siberia], "Nauka" Press, Siberian division, Novosirbsk, pp. 35-42, 1967.
6. Esikov, N. P., L. Kh. Kuznetsova and T. S. Troitskaya, in the book: *Ob Astroklimate Sibiri* [The Astroclimate of Siberia], "Nauka" Press, Siberian Division, Novosirbsk, pp. 5-24, 1967.
7. Venttsel', E. S., *Teoriya Veroyatnostey* [Probability Theory], Moscow, Fitmatgiz Press, 1958.
8. Mills, F., *Statisticheskiye Metody* [Statistical Methods], Gosstatizdat, Moscow, 1958.
9. Romanovskiy, V. I., *Primeneniye Matematicheskoy Statistiki v Opytnom Dele.* [Use of Mathematical Statistics in Experimentation], OGIZ-Gostekhizdat, 1947.
10. Kolchinskiy, I. G., *Opticheskaya Nestabil'nost' Zemnoy Atmosfery po Nablyudeniyam Zdezd.* [The Optical Instability of the Earth's Atmosphere on the Basis of Observations of Stars], "Naukova Dumka", Kiev, 1967.
11. Gnedenko, B. V., *Kurs Teorii Veroyatnostey* [A Course in Probability Theory], GTTI Press, Moscow, 1954.
12. Kolchinskiy, I. G., in the book: *Atmosfernaya Optika* [Atmospheric Optics], "Nauka" Press, Moscow, 1968.
13. Kolchinskiy, I. G., in the book: *Astrometriya i Astrofizika* [Astrometrics and Astrophysics], "Naukova Dumka" Press, Kiev, No. 10, 1970.

ESTIMATIONS OF THE SMOOTHING OPERATOR RESPONSE CHARACTERISTICS

Ya. S. Yatskiv

ABSTRACT. An attempt is made to estimate the "mean response characteristic" of the graphical smoothing method. The method is illustrated by analysis of latitude observations at Washington from 1915.9 to 1941.0.

Various smoothing methods, such as the graphic, Whittaker's numerical method, and so forth, are employed in processing the results of astronomical observations.

In the general case one can write the following basic equation, which links the initial observed process x(t) to the smoothed process y(t):

$$y(t) = Lx(t), \tag{1}$$

in which L is the smoothing operator selected. In the frequency region, in place of (1) we have

$$S_y(\omega) = |f(\omega)|^2 S_x(\omega), \tag{2}$$

in which $S(\omega)$ is the spectral density, and $f(\omega)$ the frequency characteristic describing the spectral properties of operator L.

The most important advantage of the numerical smoothing method as compared to the graphic method is the possibility of precise determination of frequency characteristic $f(\omega)$. Consequently, if $S_y(\omega)$ is known, it is always possible to find $S_x(\omega)$ from formula (2), and vice versa. The term "response characteristic" loses its strict mathematical meaning in the case of graphic smoothing, and the relationship between the spectra of the initial and the converted processes depends on the individual qualities and the experience of the person performing the operation. This results in subjective and often contradictory scientific results and conclusions.

Cases are possible in practice in which spectra $S_x(\omega)$ and $S_y(\omega)$ are known. Formula (2) may then be used to find the response characteristic of the smoothing operator employed. We have used precisely this method to estimate the "mean response characteristics" of graphic smoothing of Washington latitude observations. We had available to us latitude observations for the period from 1915.9 to 1941.0 processed by two different methods: graphic (publications by American astronomers in the Astrn. Journ.) and numerical (that employed at the Main Astronomical Observatory of the Academy of Sciences of the Ukrainian SSR).

Let $\varphi(t)$ be the initial latitude values, $\varphi_I(t)$ values plotted for every 20th part of a year with a manually smoothed curve of latitude variation, $\varphi_{II}(t)$ values obtained by the numerical method for the same fractions of a year, L_I and L_{II} the operators of the graphic and the numerical smoothing methods respectively, and B the A. Ya. Orlov filtration operator. Smoothed values $\varphi_I(t)$ and $\varphi_{II}(t)$ are related to initial values $\varphi(t)$ by the following relations:

$$\begin{aligned} \varphi_I(t) &= (1-B)L_I\varphi(t), \\ \varphi_{II}(t) &= (1-B)L_{II}\varphi(t). \end{aligned} \tag{3}$$

We rewrite (3) in spectral form:

$$\begin{aligned} S_I(\omega) &= [1-f_B^2(\omega)]f_I^2(\omega)S(\omega), \\ S_{II}(\omega) &= [1-f_B^2(\omega)]f_{II}^2(\omega)S(\omega). \end{aligned} \tag{4}$$

From (4) we find

$$f_I^2(\omega) = \frac{S_I(\omega)f_{II}^2(\omega)}{S_{II}(\omega)}. \tag{5}$$

/124

At the Main Astronomic Observatory of the Academy of Sciences of the Ukrainian SSR, the processing was carried out in such a way as not to distort fluctuations with periods of 0.5 to 1.3 years, to which frequencies of 2.0 to 0.6 cycle per year correspond. For this reason the value of the degree of smoothing was selected so that $f_{II}(\omega) \approx 1$ in the frequency region indicated. Thus in place of (5) we write the working formula for determining the "mean response characteristic" of graphic smoothing in the frequency region of 0.6 to 2.0 cycles per year:

$$f_I^2(\omega) = \frac{S_I(\omega)}{S_{II}(\omega)}. \tag{6}$$

Estimates of spectra of an intensity of $S_I(\omega)$ and $S_{II}(\omega)$ were found with the Tyuki formula, with a resolving power of 0.2 and 0.1 cycle per year (N = 502, m = 50, m = 100). The results are presented in Tables 1 and 2 respectively in units of $(0.01'')^2$ and are illustrated in the drawing. As may be seen, the values of the graphic smoothing "mean response characteristic" differ considerably from unity in the frequency region of 1.4-1.8 cycles per year. A noteworthy aspect is represented by the increase in $f_I(\omega)$ at a semi-annual fluctuation frequency of ω = 2.0 cycles per year. In this case it is as if the researcher tries to keep the semi-annual polar motion component undistorted.

The extent to which our estimates are realistic may be judged from the following calculations:

1. Verification of significance of differences in spectral density estimates $S_I(\omega)$ and $S_{II}(\omega)$.

TABLE 1.

Frequency	$S_I(\omega)$	$S_{II}(\omega)$	$f_I^2(\omega)$
0,6	7,595	7,938	0,957
0,8	25,840	26,373	0,980
1,0	25,969	26,443	0,982
1,2	8,121	8,366	0,971
1,4	0,708	1,112	0,637
1,6	0,547	1,089	0,502
1,8	0,329	0,531	0,619
2,0	0,522	0,556	0,939

Commas indicate decimal points.

We know that $S(\omega)$ has χ^2 distribution with ν degrees of freedom. In our case

$$\nu = \frac{2N - m/2}{m} \approx 20.$$

Let us assume that $S_{II}(\omega)$ is the true spectral density value (see Table 1) and let us determine the lower 10% confidence limit of spectral density

$$S^{l}(\omega) = \frac{\chi^2_{0,90}}{\nu} S_{II}(\omega) \approx 0,62\, S_{II}(\omega).$$

In the frequency region 1.6 cycle/year $\leqslant \omega \leqslant$ 1.8 cycle/year the values $S_I(\omega) \leqslant S^{l}(\omega)$. Hence it may be stated that, with a probability of only 10%, the differences in the estimates of $S_{II}(\omega)$ and $S_I(\omega)$ in the frequency region in question may be ascribed to random sampling errors.

Let us consider another example. Let us now assume that $S_I(1.8) = 0.329$, /125 the true spectral density value. Let us determine the probability that sampling may yield an estimate of $S_{II}(1.8) \geqslant 0.531$. For this purpose we find

$$\chi^2 = \frac{S_{II}(1.8)\,\nu}{S_I(1.8)} = 32,32,$$

to which probability P = 0.04 corresponds [2]. Thus the differences in the estimates of $S_I(1.8)$ and $S_{II}(1.8)$ are significant in the frequency region in question.

TABLE 2.

Frequency	$S_I(\omega)$	$S_{II}(\omega)$	$f_I^2(\omega)$	Frequency	$S_I(\omega)$	$S_{II}(\omega)$	$f_I^2(\omega)$
0,6	0,471	0,512	0,919	1,4	0,551	0,740	0,744
0,7	4,216	4,443	0,950	1,5	0,247	0,620	0,399
0,8	17,016	17,383	0,979	1,6	0,189	0,589	0,321
0,9	23,156	23,422	0,989	1,7	0,128	0,349	0,368
1,0	15,118	15,470	0,977	1,8	0,129	0,148	0,871
1,1	5,623	5,768	0,975	1,9	0,253	0,218	1,161
1,2	1,030	1,023	1,008	2,0	0,317	0,302	1,051
1,3	0,549	0,627	0,876				

Commas indicate decimal points.

2. Estimation of accuracy of $f_I(\omega)$.

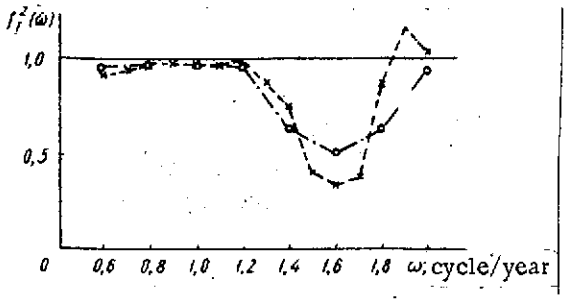

Graphic Smoothing "Mean Response Characteristic".

For dispersions of estimates $f^2(\omega)$ and $f_I(\omega)$ we have

$$D[f_I^2(\omega)] = \frac{S_{II}^2(\omega) D_I(S)}{S_{II}^4(\omega)} + \frac{S_I^2(\omega) D_{II}(S)}{S_{II}^4(\omega)},$$

$$D[f_I(\omega)] = \frac{D[f_I^2(\omega)]}{4 f_I^2(\omega)},$$

in which D(S) is the dispersion of the spectral density estimate. Since

$$D_I(S) \approx D_{II}(S),$$
$$S_{II}(\omega) \approx S_I(\omega),$$
$$D(S)/S^2(\omega) \approx \nu^{-1},$$

we find

$$D[f_I^2(\omega)] \approx 2/\nu \approx 0{,}10,$$
$$D[f_I(\omega)] \approx \frac{1}{2\nu} f_I^2(\omega). \qquad (7)$$

For example, for the estimate $f_I(1.6) = 0.71$ from formula (7) we calculate

$$D[f(\omega)] \approx 0{,}05, \quad \sigma_f = \sqrt{D[f(\omega)]} = \pm 0{,}22.$$

Let us assume that $f_I(\omega)$ in the frequency region with which we are concerned approximately obeys the normal law of distribution with parameters of $\overline{f(\omega)} = 1.00$, σ_f equals ±0.22. The probability that sampling may yield an estimate of $f_I(1.6) = 0.71$ is found on the basis of the standard deviation value $\frac{1.00 - 0.71}{0.22} = 1.32$. It is found to be less than 0.10. Thus it may be concluded that the departure of the graphic smoothing "response characteristic" from unity at a frequency of 1.6 cycle/year cannot be ascribed to random errors.

REFERENCES

1. Bol'shev, N. L. and N. V. Smirnov, *Tablitsy Matematicheskoy Statistiki* [Mathematical Statistical Tables], "Nauka" Press, Moscow, 1965.

Translated for the National Aeronautics and Space Adminstration under Contract No. NASw-2485 by Techtran Corporation, P.O. Box 729, Glen Burnie, Maryland, 21061, translator, William L. Hutcheson.